

Supporting Information

Metal-Silicon Triple Bonds:

Reactivity of the Silylidyne Complexes $[\text{Cp}^*(\text{CO})_2\text{M}\equiv\text{Si}-\text{Tbb}]$ (M = Cr – W)

*Kanishk Tomer, Gregor Schnakenburg, Ujjal Das and Alexander C. Filippou**

Institut für Anorganische Chemie, Universität Bonn, Gerhard-Domagk-Str. 1, 53121 Bonn, Germany;

E-mail: filippou@uni-bonn.de

Table of Contents

1	Experimental Section – General Procedures.....	2
2	Syntheses, analytical data, IR and NMR spectra of compounds 1-Cr – 5-Mo	5
2.1	$[\text{Mo}(\text{Cp}^*)(\text{CO})_2(\text{SiTbb})]$ (1-Mo)	5
2.1.1	Synthesis from (<i>E</i>)-Tbb(Br)Si=Si(Br)Tbb and $\text{Li}[\text{Cp}^*\text{Mo}(\text{CO})_3]$	5
2.1.2	Synthesis from (<i>E</i>)-Tbb(Br)Si=Si(Br)Tbb and $\text{Li}[\text{Cp}^*\text{Mo}(\text{CO})_2(\text{PMe}_3)]$	10
2.2	$[\text{Cr}(\text{Cp}^*)(\text{CO})_2(\text{SiTbb})]$ (1-Cr).....	11
2.3	$[\text{W}(\text{Cp}^*)(\text{CO})_2(\text{SiTbb})]$ (1-W).....	16
2.4	$[\text{Mo}(\text{Cp}^*)(\text{CO})_2(\text{CNMes})\{\text{Si}(\text{Tbb})(\kappa^2\text{O},\text{O}'\text{-O}_2\text{CNMes})\}]$ (2-Mo)	21
2.5	$[\text{W}(\text{Cp}^*)(\text{CO})_2(\text{CNMes})\{\text{Si}(\text{Tbb})(\kappa^2\text{O},\text{O}'\text{-O}_2\text{CNMes})\}]$ (2-W).....	34
2.6	$[\text{Mo}(\text{Cp}^*)(\text{H})(\text{CO})_2\{\text{Si}(\text{Tbb})(\text{OCH}=\text{CH}\text{Et})\}]$ (3-Mo)	40
2.7	$[\text{Mo}(\text{Cp}^*)(\text{CO})_2\{\kappa^2\text{N},\text{N}'\text{-}(\text{N}_2\text{CHSiMe}_3)_2\text{Si}(\text{Tbb})\}]$ (4-Mo).....	46
2.8	$[\text{Mo}(\text{Cp}^*)(\text{CO})_2\{\eta^2\text{-Si}(\text{Tbb})\text{N}(\text{Mes})\}]$ (5-Mo)	53
3	Crystal structure determination of 1-Cr – 5-Mo	60
3.1	Crystal data and structure refinement parameters of 1-Cr – 5-Mo	60
3.2	Molecular structures of 1-Cr – 5-Mo with selected bonding parameters	66
4	Electronic structure calculations.....	70
4.1	General methodology.....	70
4.2	Quantum chemical and experimental studies of the stereoisomerism and dynamics of 3-Mo	71
4.2.1	Stereoisomerization pathways of 3-Mo	81

1 Experimental Section – General Procedures

All experiments were carried out under strict exclusion of air and moisture in an atmosphere of purified argon using Schlenk or glovebox techniques. Argon was commercially received with a purity of $\geq 99.998\%$ and was further purified by passing through a gas purification system composed of two consecutive columns to remove traces of O_2 and H_2O . The first column was filled with the BTS copper catalyst R3-11G from BASF and heated with an electrical heating coil at ca. $80\text{ }^\circ\text{C}$ and the second column with 4 \AA molecular sieves. All glassware was dried in an oven at approximately $110\text{ }^\circ\text{C}$ and baked with a heat gun at ca. $500\text{ }^\circ\text{C}$ under fine vacuum ($0.01 - 0.005\text{ mbar}$) prior to use. Stainless steel transfer- and filter-cannulas ($\varnothing = 1\text{ mm}$ and 2 mm) were used for the transfer of liquids and filtrations through Glass Microfibre Whatman™ filters, respectively.

Commercially available solvents were rigorously dried, degassed and freed from stabilizers prior to use. Toluene and *n*-hexane were dried using a MBraun SPS800 solvent purification system. *n*-pentane was dried in solvent stills upon refluxing over a Na-wire ($\varnothing = 2\text{ mm}$), purged several times with argon during reflux and distilled under argon. All solvents were degassed after collection by two freeze-pump-thaw cycles and stored inside the glove box in 500 mL SCHOTT DURAN® laboratory glass bottles. The residual H_2O content of the dried solvents (except fluorobenzene) was determined by a Metrohm 831 KF Coulometer. A constant drift of the order of $\leq 3\text{ }\mu\text{g}$ of H_2O/min was ensured before and during the titration. The automatic drift correction was applied to the determined H_2O content following the manual. The H_2O content was found to be less than 5.0 ppm in all solvents.

The C, H, N analyses were carried out in triplicate for each sample using an Elementar Vario Micro elemental analyzer. Samples were weighed up in a micro-analytical balance located inside a glove box. The individual C, H and N values did not differ by more than $\pm 0.3\%$. The mean C, H and N values are given below for each compound.

Melting points were determined in triplicate for each compound in vacuum sealed capillaries on a Büchi M-560 melting point apparatus. Internal temperature correction was done by using the recommended pharmacopoeia melting point standards: 4-nitrotoluene ($52.5 \pm 0.2\text{ }^\circ\text{C}$ at $0.5\text{ }^\circ\text{C}/\text{min}$), diphenylacetic acid ($148 \pm 0.2\text{ }^\circ\text{C}$ at $0.5\text{ }^\circ\text{C}/\text{min}$), caffeine ($237 \pm 0.2\text{ }^\circ\text{C}$ at $0.5\text{ }^\circ\text{C}/\text{min}$) and potassium nitrate ($335\text{ }^\circ\text{C}$). The samples were sealed in glass capillaries under vacuum and heated once with a gradient of $5\text{ }^\circ\text{C}/\text{min}$ for a rough determination of the melting point or temperature of starting decomposition. Heating of the second and third sample was then repeated with a gradient of $2\text{ }^\circ\text{C}/\text{min}$ starting $20\text{ }^\circ\text{C}$ below the temperature of melting or decomposition determined in the first experiment. The pharmacopoeia melting points of the samples are given without any correction for the temperature gradient. The thermally treated samples were cooled to room temperature and studied by ^1H NMR spectroscopy to confirm whether decomposition had occurred upon heating.

The FT-IR spectra of solutions were recorded at room temperature on a Nicolet 380 FT-IR spectrometer using a stainless-steel cell of NaCl or CaF₂ windows, which were separated by a teflon spacer with a cell thickness of 0.20 mm. The solution IR spectra were background corrected for the solvent absorptions. The IR spectra of solids were recorded in the spectral range of 4000 – 400 cm⁻¹ on a Bruker Alpha FT-IR spectrometer inside a glove box using a platinum single reflection diamond ATR module. The following abbreviations were used for the relative intensities and shape of the IR absorption bands: vs (very strong), s (strong), m (medium), w (weak), vw (very weak), sh (shoulder).

The NMR spectra were recorded on a Bruker AV I-300 or Bruker AV III HD Prodigy-500 NMR spectrometer in dry, deoxygenated (D₆)benzene, or (D₈)THF using 5 mm NMR tubes equipped with J. Young valves. The deuterated solvents were dried by stirring over Na/K alloy, then degassed, and finally trap-to-trap condensed and stored over 4 Å molecular sieves. The ¹H and ¹³C{¹H} NMR spectra were calibrated, respectively, against the residual proton and natural abundance ¹³C resonances of the deuterated solvent relative to tetramethylsilane set at δ = 0 ppm ((D₆)benzene: δ_H = 7.15 ppm and δ_C = 128.0 ppm; (D₈)THF: δ_H = 1.73 ppm and δ_C = 25.3 ppm; (D₈)toluene: δ_H = 2.09 ppm and δ_C = 20.4 ppm). The ²⁹Si NMR spectra were calibrated using the ²H frequency of the deuterated solvent (lock frequency) and the frequency ratio value $\Xi(^{29}\text{Si}) = 19.867187$ recommended by IUPAC for SiMe₄ as external reference ($\varphi = 1\%$ in chloroform).^[S1] All lock frequencies were calibrated internally against the ¹H signals of solutions of tetramethylsilane (δ_H = 0 ppm) with a volume fraction of $\varphi \leq 1\%$ in the corresponding degassed deuterated solvent. The following abbreviations were used for the multiplicities and forms of the NMR signals: s = singlet, d = doublet, t = triplet, dt = doublet of triplets, quintd = quintet of doublets, br = broad.^[S2] All coupling constants are given as absolute values in Hz regardless of their signs. The ¹H, ¹³C and ²⁹Si NMR signals of compounds **1-Cr** – **5-Mo** were assigned after a detailed analysis of the ¹H-¹H COSY, ¹H-¹³C HSQC, ¹H-¹³C HMBC and ¹H-²⁹Si HMBC spectra.

The starting materials Li[Cp**M*(CO)₃] (*M* = Cr – W; Cp* = η⁵-pentamethylcyclopentadienyl),^[S3] *E*-(Tbb)BrSi=SiBr(Tbb) (Tbb = 2,6-bis[bis(trimethylsilyl)methyl]-4-*tert*-butylphenyl),^[S4] Li[Cp**Mo*(CO)₂(PMe₃)]^[S5] and mesityl azide^[S6] were prepared following published procedures. The NMR spectroscopic data of *E*-(Tbb)BrSi=SiBr(Tbb) in (D₆)benzene and (D₈)tetrahydrofuran

[S1] R. K. Harris, E. D. Becker, S. M. Cabral de Menezes, P. Granger, R. E. Hoffman, K. W. Zilm, *Pure Appl. Chem.* **2008**, *80*, 59.

[S2] The parameter Δv_{1/2} denotes the full width at half maximum of broad signals.

[S3] O. Chernov, *Novel Molecular Si(II) Precursors for Synthesis of the First Compounds with Metal-Silicon Triple Bonds*, Dissertation, University of Bonn, **2012**.

[S4] T. Agou, N. Hayakawa, T. Sasamori, T. Matsuo, D. Hashizume, N. Tokitoh, *Chem. Eur. J.* **2014**, *20*, 9246.

[S5] W. Malisch, R. Lankat, S. Schmitzer, R. Pikel, U. Posset, W. Kiefer, *Organometallics* **1995**, *14*, 5622.

[S6] P. A. S. Smith, C. D. Rowe, L. B. Bruner, *J. Org. Chem.* **1969**, *34*, 11.

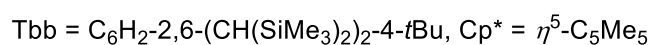
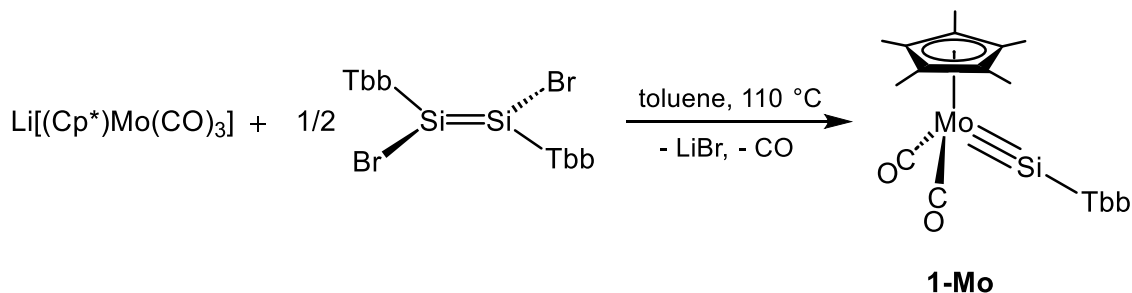
are given in reference S7 (Supporting information). Mesityl isocyanate (98%, Alfa Aesar) was purified by sublimation prior to use, trimethylsilyldiazomethane (2.0 M in *n*-hexane, Acros Organics™) and ethyloxirane (99%, TCI Chemicals) were used as received.

[S7] S. Kumar, L. R. Maurer, G. Schnakenburg, U. Das, A. C. Filippou, *Angew. Chem. Int. Ed* **2024**, e202400227.

2 Syntheses, analytical data, IR and NMR spectra of compounds 1-Cr – 5-Mo

2.1 [Mo(Cp*)(CO)₂(SiTbb)] (1-Mo)

2.1.1 Synthesis from (*E*)-Tbb(Br)Si=Si(Br)Tbb and Li[Cp*Mo(CO)₃]



A mixture of (*E*)-Tbb(Br)Si=Si(Br)Tbb (1.50 g, 1.34 mmol, 1.00 equiv.) and Li[Cp*Mo(CO)₃] (866 mg, 2.69 mmol, 2.00 equiv.) was suspended in 75 mL of toluene and the resulting yellow suspension was heated at 110 °C under static vacuum for 4 hours. During this time all disilene dissolved and the color of the solution changed to orange-red. ¹H NMR spectroscopic analysis of an aliquot of the reaction mixture showed a complete conversion of the starting materials and the selective formation of **1-Mo**. The reaction mixture was evaporated to dryness under reduced pressure at 50 °C and the red-brown, sticky residue obtained was extracted with *n*-hexane (2 × 10 mL). The combined extracts were concentrated to approximately 3 mL under reduced pressure and stored at –30 °C for 24 hours. The crystallized red solid was isolated after filtration at –30 °C and dried in a fine vacuum at 50 °C for 30 minutes. Yield: 1.40 g (1.83 mmol, 68% from *E*-(Tbb)BrSi=SiBr(Tbb)).

Elemental analysis calcd (%) for C₃₆H₆₄MoO₂Si₅ (765.26 g/mol): C 56.50, H 8.43; found: C 56.21, H 8.67%.

Complex **1-Mo** is a highly air sensitive, orange-red solid that melts at 174 °C. It is sparingly soluble in acetonitrile and highly soluble in *n*-pentane, diethyl ether, benzene and toluene.

Spectroscopy:

ATR-IR (solid, 298 K, *Figure S1* and *Figure S2*): $\tilde{\nu}$ (cm⁻¹) = 2951 (m), 2902 (w), 2865 (vw), 1914 (vs) [$\nu(\text{CO})$], 1848 (vs) [$\nu(\text{CO})$], 1581 (w), 1528 (w), 1476 (vw), 1462 (vw), 1425 (vw), 1396 (w), 1383 (w), 1362 (vw), 1260 (m, sh), 1248 (s), 1173 (m), 1141 (vw), 1048 (vw), 1016 (m), 960 (m), 934 (w), 890 (m), 838 (vs), 772 (w), 762 (w), 743 (w), 724 (w), 688 (m), 657 (w), 646 (w), 620 (vw), 611 (w), 597 (w), 561 (w), 545 (w), 521 (w), 512 (w), 474 (m), 459 (w), 439 (vw), 416 (m).

IR (toluene, 298 K, *Figure S3*): $\tilde{\nu}$ (cm⁻¹) = 1916 (s) [$\nu(\text{CO})$], 1854 (vs) [$\nu(\text{CO})$], 1583 (w) and 1527 (w) [$\nu(\text{C}=\text{C})_{\text{Tbb}}$].

IR (*n*-hexane, 298 K, *Figure S4*): $\tilde{\nu}$ (cm⁻¹) = 1924 (s) [$\nu(\text{CO})$], 1863 (vs) [$\nu(\text{CO})$], 1583 (w) and 1528 (w) [$\nu(\text{C}=\text{C})_{\text{Tbb}}$].

¹H NMR (300.1 MHz, (D₆)benzene, 298 K, *Figure S5*): δ (ppm) = 0.26 (s, $^2J(^{29}\text{Si}, ^1\text{H}) = 6.4$ Hz, 36H, C^{2,6}-CH(SiMe₃)₂), 1.20 (s, 9H, C⁴-CMe₃), 2.06 (s, 15H, C₅Me₅), 3.21 (s, $^2J(^{29}\text{Si}, ^1\text{H}) = 9.6$ Hz, 2H, C^{2,6}-CH(SiMe₃)₂), 6.79 (s, 2H, C^{3,5}-H).

¹³C{¹H} NMR (125.8 MHz, (D₆)benzene, 298 K, *Figure S6*): δ (ppm) = 0.39 (s, $^1J(^{29}\text{Si}, ^{13}\text{C}) = 51.6$ Hz, 12C, C^{2,6}-CH(SiMe₃)₂), 12.3 (s, 5C, C₅Me₅), 30.9 (s, 3C, C⁴-CMe₃), 31.8 (s, $^1J(^{29}\text{Si}, ^{13}\text{C}) = 41.2$ Hz, 2C, C^{2,6}-CH(SiMe₃)₂), 34.9 (s, 1C, C⁴-CMe₃), 103.4 (s, 5C, C₅Me₅), 121.4 (s, 2C, C^{3,5}-H), 148.2 (s, 1C, Si-C¹), 149.5 (s, 2C, C^{2,6}-CH(SiMe₃)₂), 154.8 (s, 1C, C⁴-CMe₃), 234.7 (s, 2C, 2 × CO).

²⁹Si{¹H} NMR (99.36 MHz, (D₆)benzene, 298 K, *Figure S7*): δ (ppm) = 2.4 (s, $^1J(^{29}\text{Si}, ^{13}\text{C}) = 51.6$ Hz, 4Si, C^{2,6}-CH(SiMe₃)₂), 308.9 (s, 1Si, Mo≡Si).

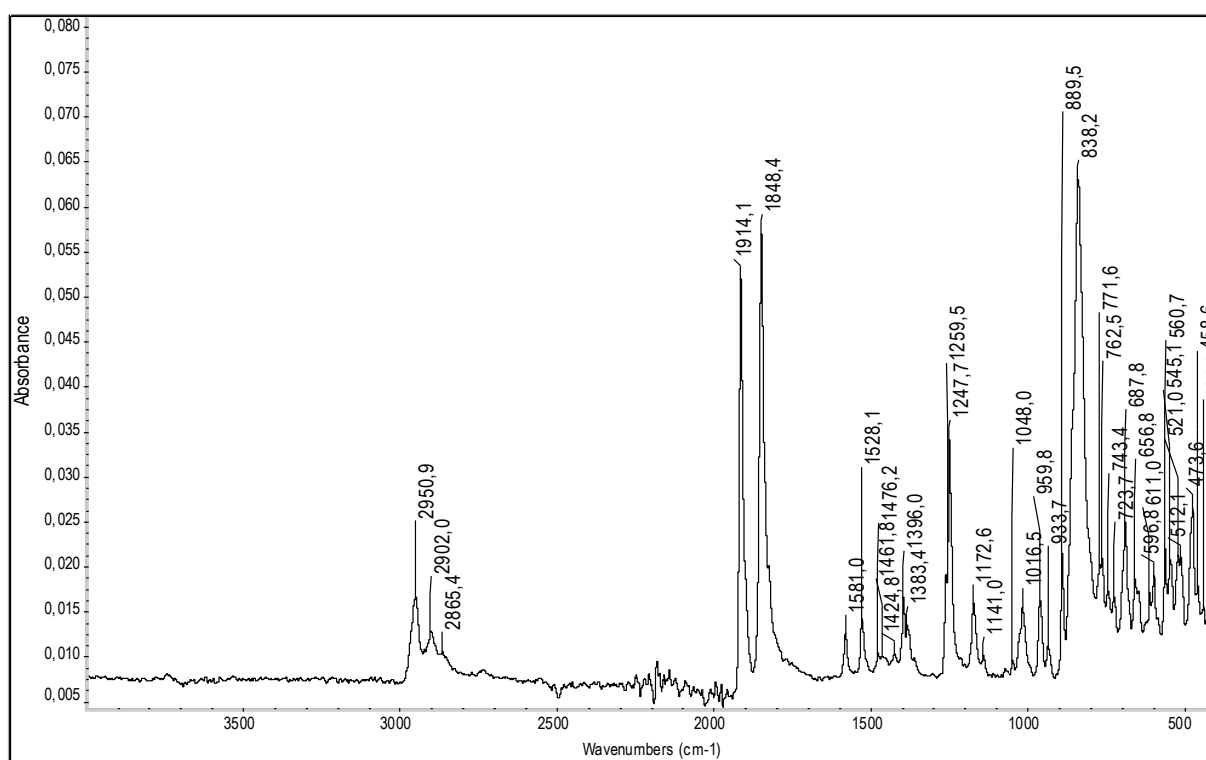


Figure S1. ATR-IR spectrum of **1-Mo** in the solid state in the spectral range of 4000 - 400 cm⁻¹.

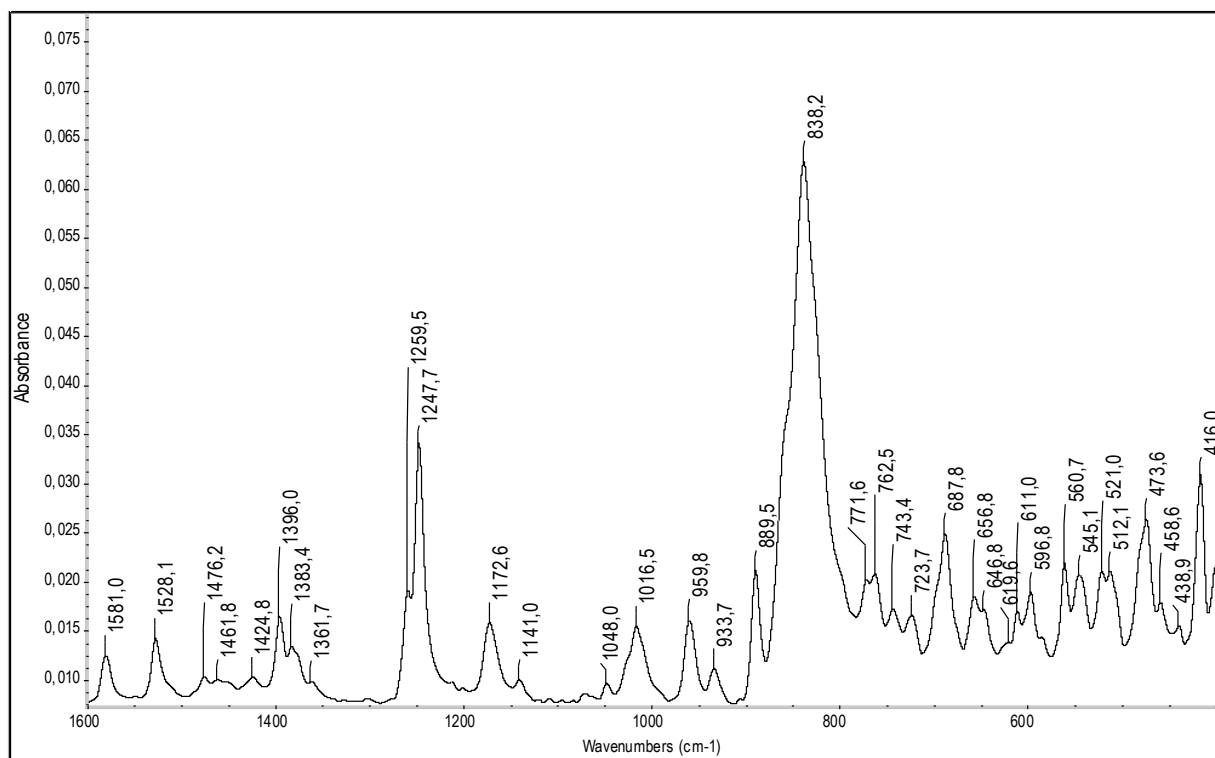


Figure S2. Excerpt of the ATR-IR spectrum of **1-Mo** in the solid state (spectral range: 1600 - 400 cm⁻¹).

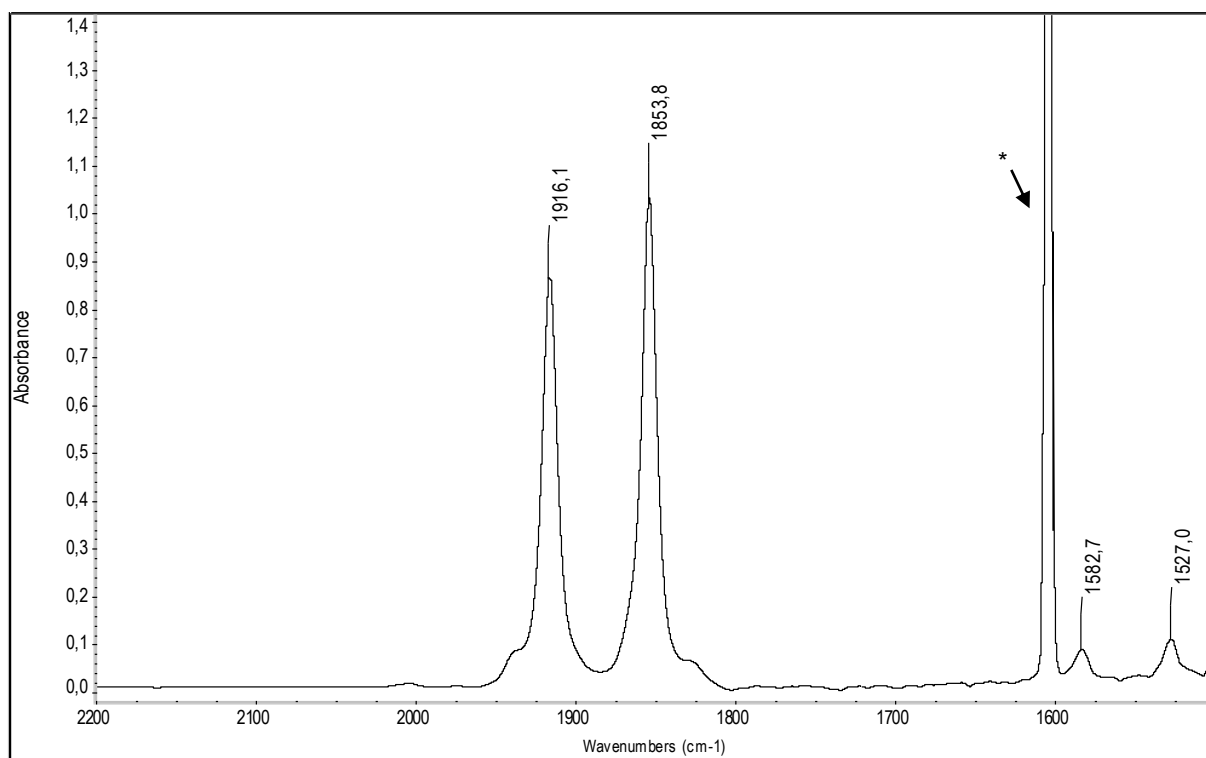


Figure S3. FT-IR spectrum of **1-Mo** in toluene in the spectral range of 2200 - 1500 cm⁻¹. The band marked with an asterisk (*) originates from the solvent due to incomplete background correction.

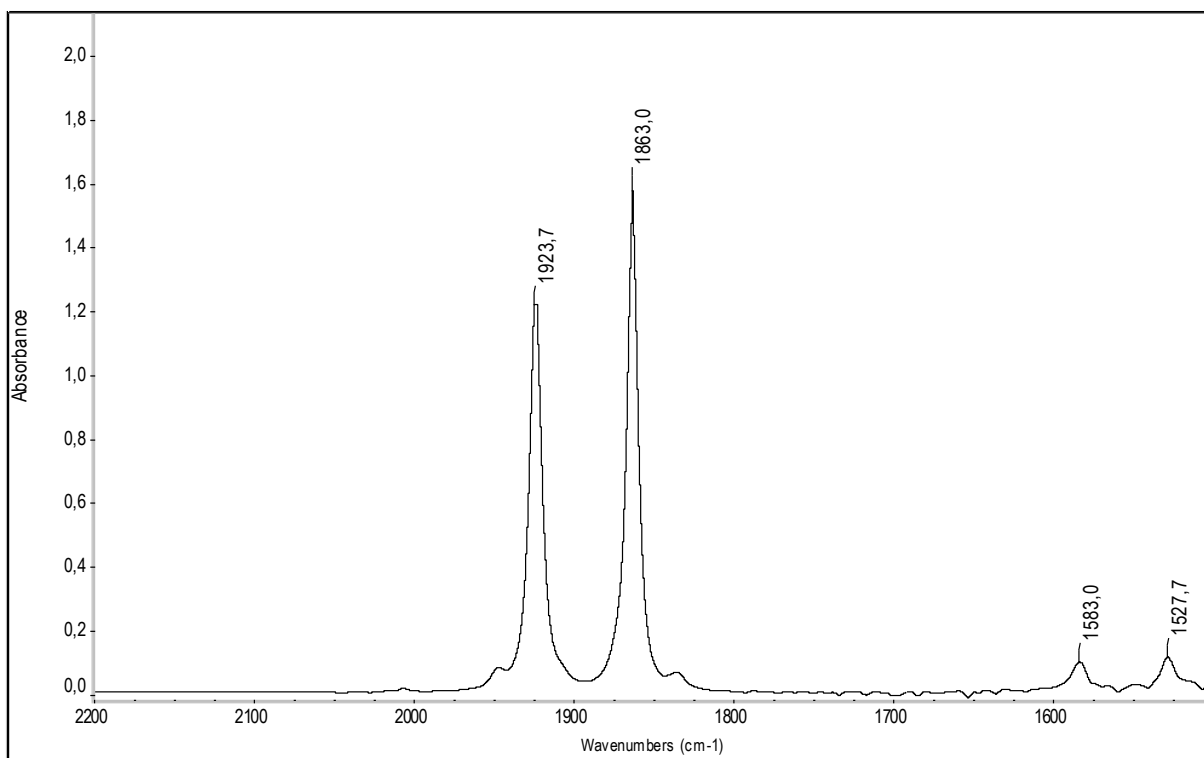


Figure S4. FT-IR spectrum of **1-Mo** in *n*-hexane in the spectral range of 2200 - 1500 cm^{-1} .

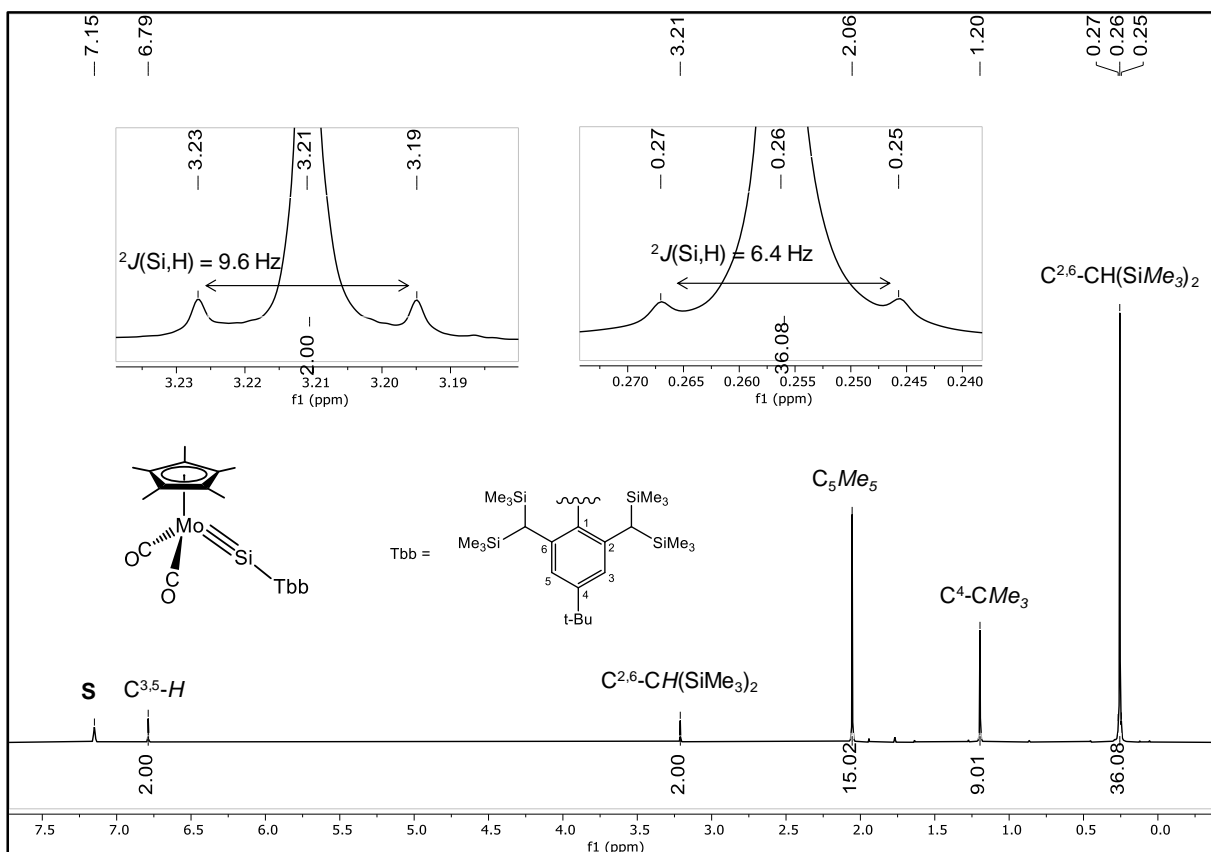


Figure S5. ^1H NMR spectrum (300.1 MHz) of **1-Mo** in (D_6) benzene at 298 K; the residual proton signal of the deuterated solvent is marked with the letter **S**. Two signals with their ^{29}Si satellites are shown in the insets.

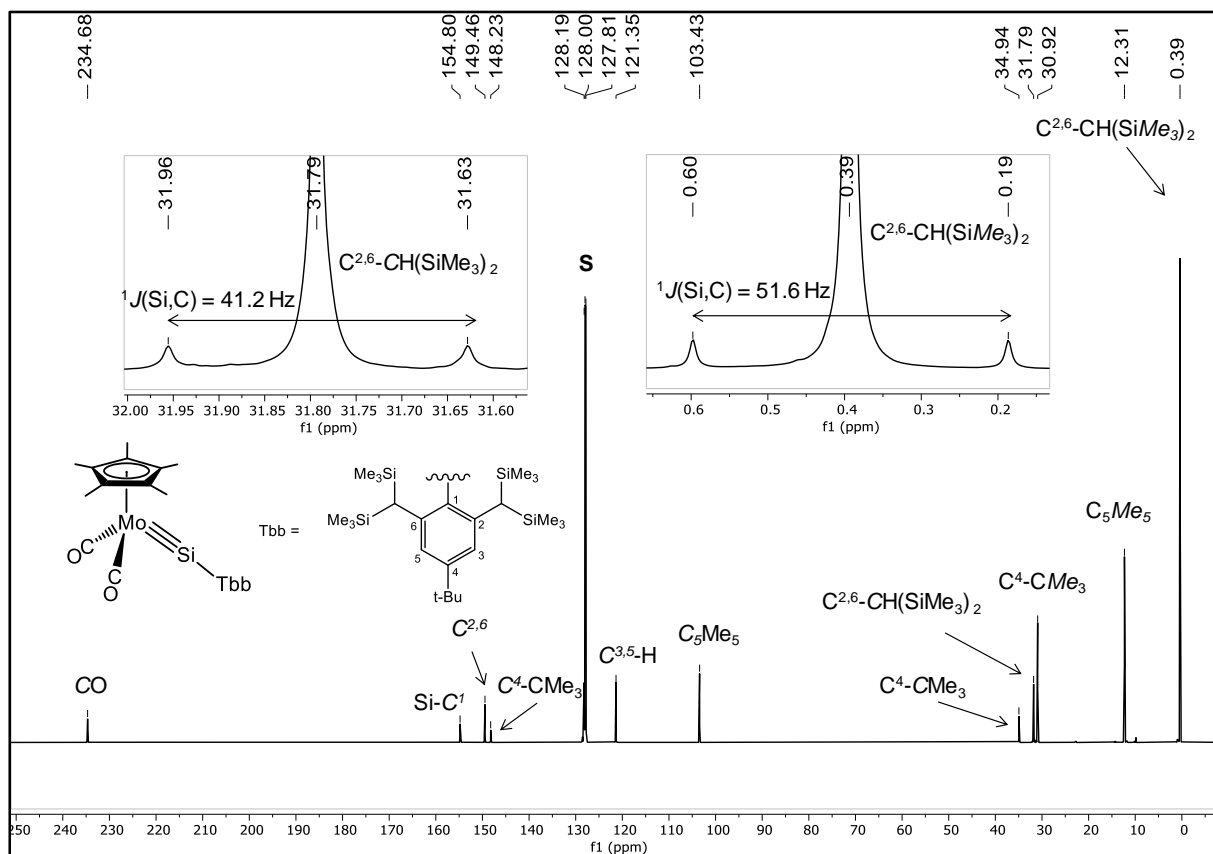


Figure S6. $^{13}\text{C}\{^1\text{H}\}$ NMR spectrum (125.8 MHz) of **1-Mo** in (D_6) benzene at 298 K; the signal of the deuterated solvent is marked with the letter **S**. Two signals with their ^{29}Si satellites are shown in the insets.

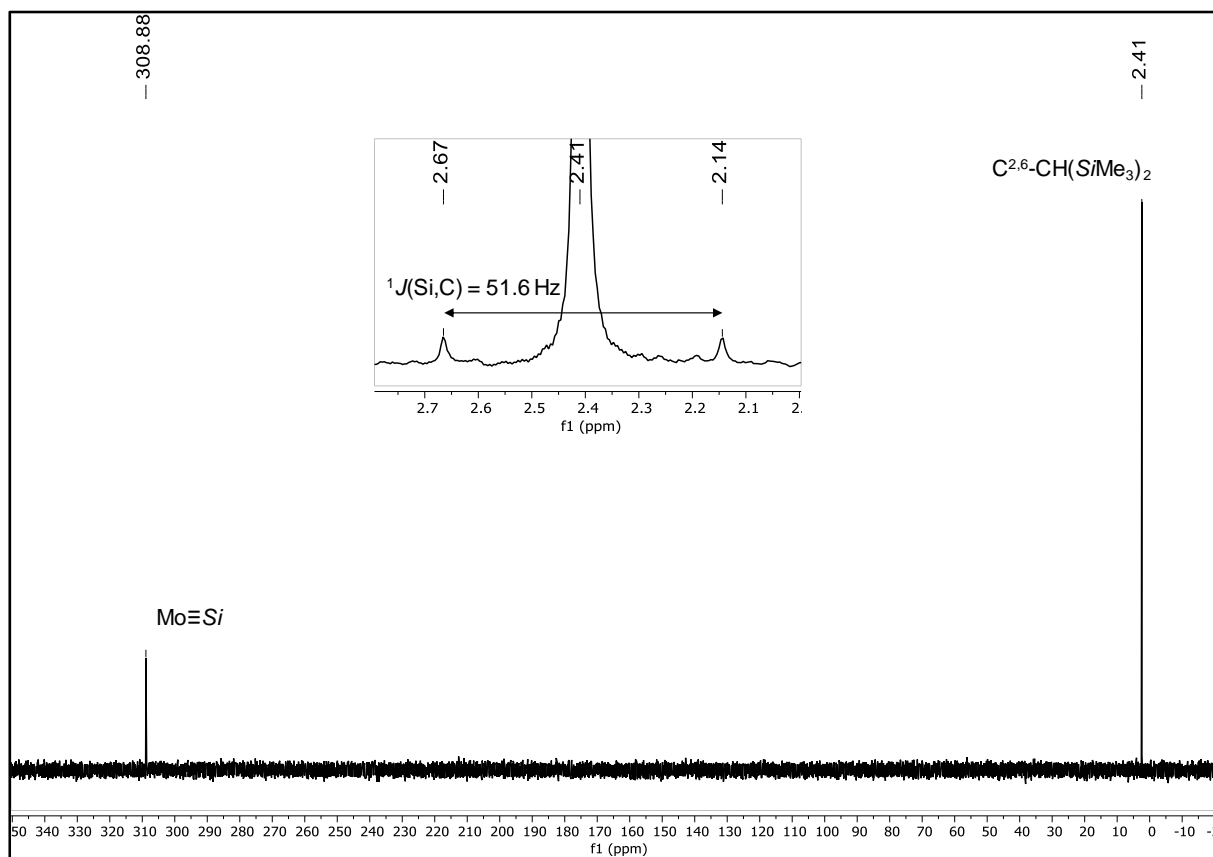
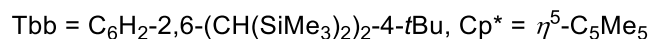
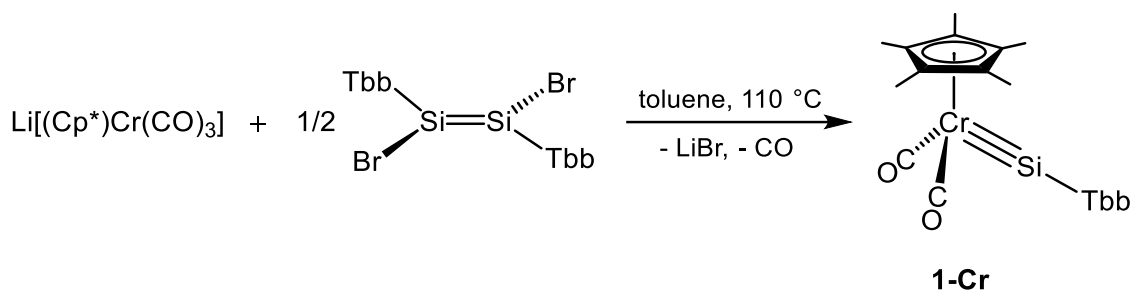


Figure S7. $^{29}\text{Si}\{^1\text{H}\}$ (zgig) NMR (99.36 MHz) spectrum of **1-Mo** in (D_6) benzene at 298 K. The SiMe_3 signal with its ^{13}C satellites is shown in the inset.

2.1.2 Synthesis from (*E*)-Tbb(Br)Si=Si(Br)Tbb and Li[Cp*Mo(CO)₂(PMe₃)₂]

A mixture of (*E*)-Tbb(Br)Si=Si(Br)Tbb (2.00 g, 1.79 mmol, 1.00 equiv.) and Li[Cp*Mo(CO)₃(PMe₃)₂] (1.34 g, 3.62 mmol, 2.02 equiv.) was suspended in 100 mL of toluene, and the yellow suspension was heated at 110 °C under static vacuum for 25 minutes. During this time all disilene dissolved and the color of the solution changed to orange-red. ¹H NMR spectroscopic analysis of an aliquot of the reaction solution showed the selective formation of silylidyne complex **1-Mo** and [Cp*(CO)(PMe₃)Mo≡Si-Tbb] (**1-Mo-PMe₃**) in a 10 : 1 molar ratio. The reaction mixture was evaporated to dryness under reduced pressure at 50 °C and the red-brown, sticky residue obtained was extracted with *n*-pentane (2 × 10 mL). The combined extracts were concentrated to approximately 4 mL under reduced pressure and stored at –30 °C for 24 hours. The crystallized red solid (987 mg) was isolated after filtration at –30 °C and dried in a fine vacuum at 50 °C for 30 minutes. ¹H NMR and IR spectroscopic analysis of the solid revealed the presence of **1-Mo** and **1-Mo-PMe₃**^[S8] in the approximate molar ratio of 12 : 1. After two more crystallizations from *n*-pentane, complex **1-Mo** was isolated in spectroscopically pure form. Yield: 320 mg (0.418 mmol, 23% from (*E*)-(Tbb)BrSi=SiBr(Tbb)).

[S8] Selected spectroscopic data obtained for **1-Mo-PMe₃** after IR and NMR spectroscopic analysis of the isolated solid: IR (toluene, 298 K): $\tilde{\nu}$ (cm⁻¹) = 1815 (s) [ν (CO)]; ¹H NMR (300.1 MHz, (D₆)benzene, 298 K): δ (ppm) = 0.29 (s, 18H, C^{2,6}-CH(SiMe₃)_A(SiMe₃)_B), 0.31 (s, 18H, C^{2,6}-CH(SiMe₃)_A(SiMe₃)_B), 1.25 (s, 9H, C⁴-CMe₃), 1.44 (d, 9H, ²J(³¹P, ¹H) = 7.4 Hz, PMe₃), 2.12 (s, 15H, C₅Me₅), 3.53 (s, ²J(²⁹Si, ¹H) = 9.7 Hz, 2H, C^{2,6}-CH(SiMe₃)₂), 6.82 (s, 2H, C^{3,5}-H). ³¹P{¹H} NMR (202.5 MHz, (D₆)benzene, 298 K): δ (ppm) = 16.6 (s, 1P, PMe₃).

2.2 [Cr(Cp*)(CO)₂(SiTbb)] (**1-Cr**)

A mixture of (*E*)-Tbb(Br)Si=Si(Br)Tbb (500 mg, 0.448 mmol, 1.00 equiv.) and Li[Cp*Cr(CO)₃] (249 mg, 0.895 mmol, 2.00 equiv.) was suspended in 35 mL of toluene and the resulting yellow-brown suspension was heated at 110 °C under static vacuum for 6 hours. During this time all disilene dissolved and the color of the solution changed to dark-brown. ¹H NMR spectroscopic analysis of an aliquot of the reaction mixture showed a complete conversion of the starting materials and the selective formation of **1-Cr**. The reaction mixture was evaporated to dryness under reduced pressure at 50 °C, and the red-brown, sticky residue obtained was extracted with *n*-pentane (2 × 5 mL). The combined extracts were concentrated to approximately 3 mL under reduced pressure and stored at –60 °C for 24 hours. The dark-brown, crystalline precipitate was isolated by filtration at –60 °C and dried in a fine vacuum at 50 °C for 30 minutes. Yield: 425 mg (0.589 mmol, 65% from (*E*)-(Tbb)BrSi=SiBr(Tbb)).

Elemental analysis calcd (%) for C₃₆H₆₄CrO₂Si₅ (721.32 g/mol): C 59.94, H 8.94; found: C 59.63, H 9.01%.

Complex **1-Cr** is a highly air sensitive, dark-brown solid that melts at 168 °C. It is highly soluble in *n*-pentane, diethyl ether, benzene and toluene.

Spectroscopy:

ATR-IR (solid, 298 K, *Figure S8* and *Figure S9*): $\tilde{\nu}$ (cm⁻¹) = 2951 (m), 2901 (w), 2868 (vw), 1902 (s) [$\nu(\text{CO})$], 1842 (s) [$\nu(\text{CO})$], 1581 (w), 1527 (w), 1478 (vw), 1459 (vw), 1448 (vw) 1425 (vw), 1395 (m), 1382 (w), 1379 (vw), 1362 (vw), 1258 (m, sh), 1246 (s), 1170 (m), 1140 (vw), 1045 (vw), 1026 (w), 1017 (w), 960 (m), 937 (w), 888 (m), 835 (vs), 770 (m), 762 (m), 743 (w), 723 (w), 696 (sh, w), 686 (m), 656 (w), 643 (m), 613 (w), 583 (m), 559 (w), 525 (w), 511 (w), 503 (w), 465 (w), 417 (m).

IR (toluene, 298 K, *Figure S10*): $\tilde{\nu}$ (cm⁻¹) = 1906 (s) [$\nu(\text{CO})$], 1847 (vs) [$\nu(\text{CO})$], 1583 (w) and 1526 (w) [$\nu(\text{C}=\text{C})_{\text{Tbb}}$].

IR (*n*-hexane, 298 K, *Figure S11*): $\tilde{\nu}$ (cm⁻¹) = 1913 (s) [$\nu(\text{CO})$], 1856 (vs) [$\nu(\text{CO})$], 1583 (w) and 1527 (w) [$\nu(\text{C}=\text{C})_{\text{Tbb}}$].

^1H NMR (500.1 MHz, (D_6) benzene, 298 K, *Figure S12*): δ (ppm) = 0.26 (s, $^2J(^{29}\text{Si}, ^1\text{H}) = 6.4$ Hz, 36H, $\text{C}^{2,6}\text{-CH}(\text{SiMe}_3)_2$), 1.19 (s, 9H, $\text{C}^4\text{-CMe}_3$), 1.98 (s, 15H, C_5Me_5), 3.19 (s, $^2J(^{29}\text{Si}, ^1\text{H}) = 9.4$ Hz, 2H, $\text{C}^{2,6}\text{-CH}(\text{SiMe}_3)_2$), 6.78 (s, 2H, $\text{C}^{3,5}\text{-H}$).

$^{13}\text{C}\{^1\text{H}\}$ NMR (125.8 MHz, (D_6) benzene, 298 K, *Figure S13*): δ (ppm) = 0.42 (s, $^1J(^{29}\text{Si}, ^{13}\text{C}) = 51.7$ Hz, 12C, $\text{C}^{2,6}\text{-CH}(\text{SiMe}_3)_2$), 12.4 (s, 5C, C_5Me_5), 30.9 (s, 3C, $\text{C}^4\text{-CMe}_3$), 31.9 (s, $^1J(^{29}\text{Si}, ^{13}\text{C}) = 41.2$ Hz, 2C, $\text{C}^{2,6}\text{-CH}(\text{SiMe}_3)_2$), 34.9 (s, 1C, $\text{C}^4\text{-CMe}_3$), 99.7 (s, 5C, C_5Me_5), 121.2 (s, 2C, $\text{C}^{3,5}\text{-H}$), 149.20 (s, 1C, Si-C^1), 149.25 (s, 2C, $\text{C}^{2,6}\text{-CH}(\text{SiMe}_3)_2$), 154.5 (s, 1C, $\text{C}^4\text{-CMe}_3$), 244.0 (s, 2C, $2 \times \text{CO}$).

$^{29}\text{Si}\{^1\text{H}\}$ NMR (99.36 MHz, (D_6) benzene, 298 K, *Figure S14*): δ (ppm) = 2.5 (s, $^1J(^{29}\text{Si}, ^{13}\text{C}) = 51.7$ Hz, 4Si, $\text{C}^{2,6}\text{-CH}(\text{SiMe}_3)_2$), 299.9 (s, 1Si, $\text{Cr}\equiv\text{Si}$).

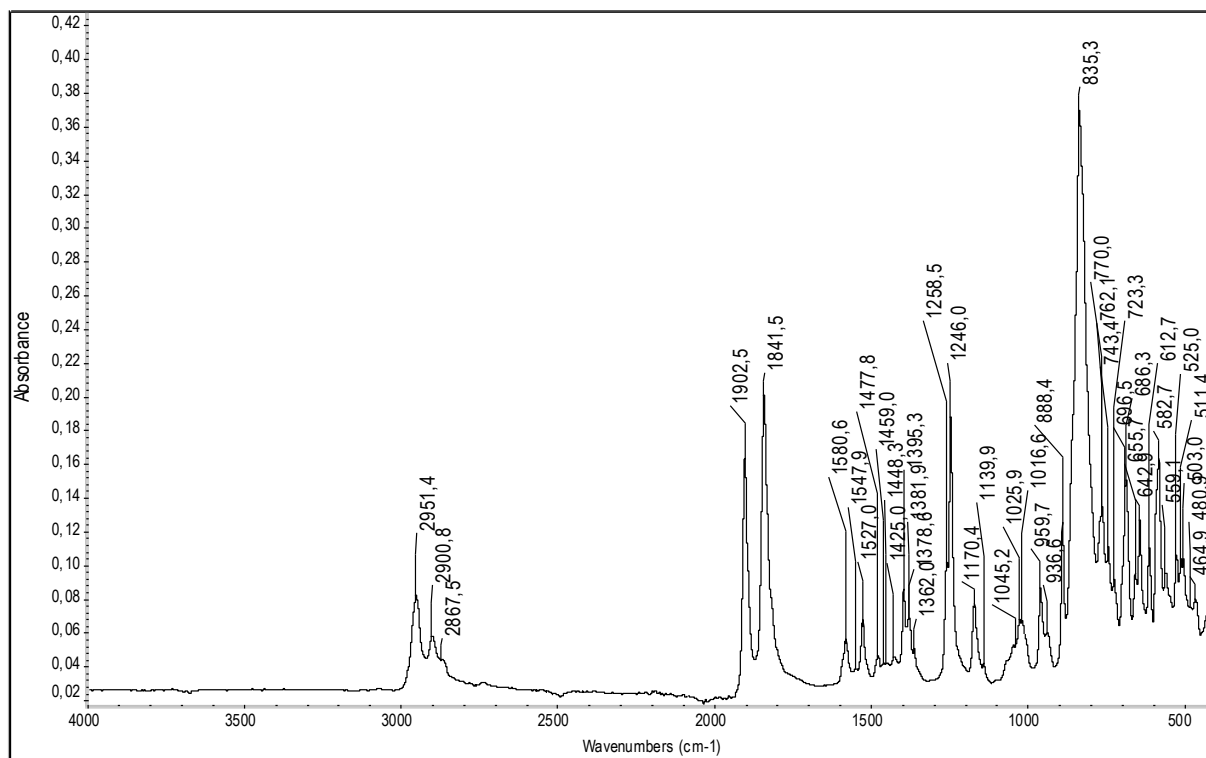


Figure S8. ATR-IR spectrum of **1-Cr** in the solid state in the spectral range of 4000 - 400 cm^{-1} .

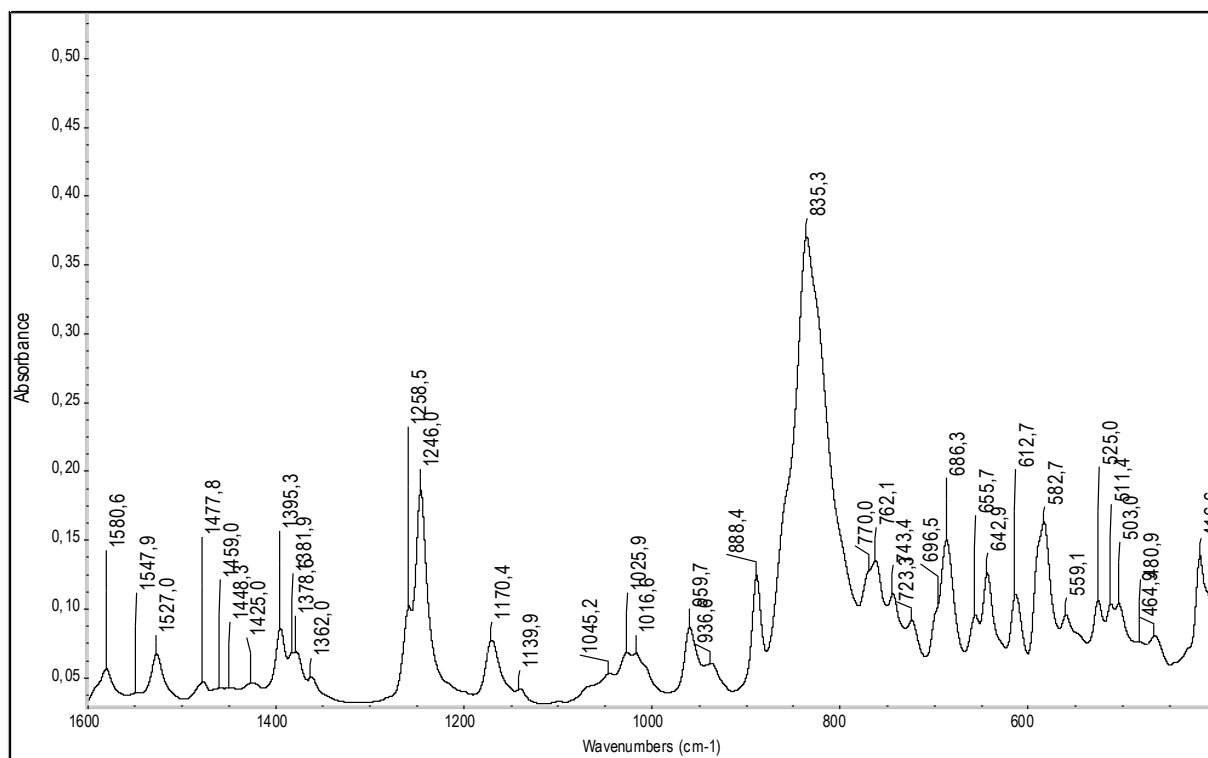


Figure S9. Excerpt of the ATR-IR spectrum of **1-Cr** in the solid state (spectral range: 1600 - 400 cm⁻¹).

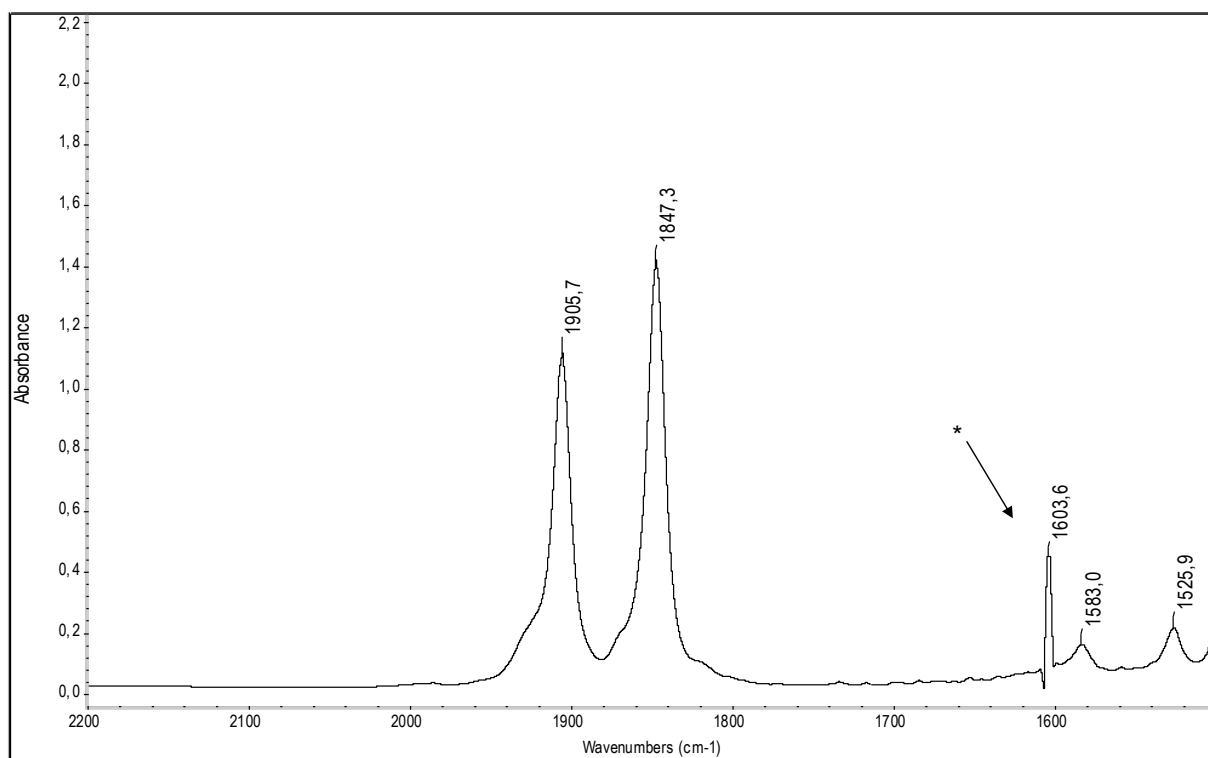


Figure S10. FT-IR spectrum of **1-Cr** in toluene in the spectral range of 2200 - 1500 cm⁻¹. The band marked with an asterisk (*) originates from the solvent due to incomplete background correction.

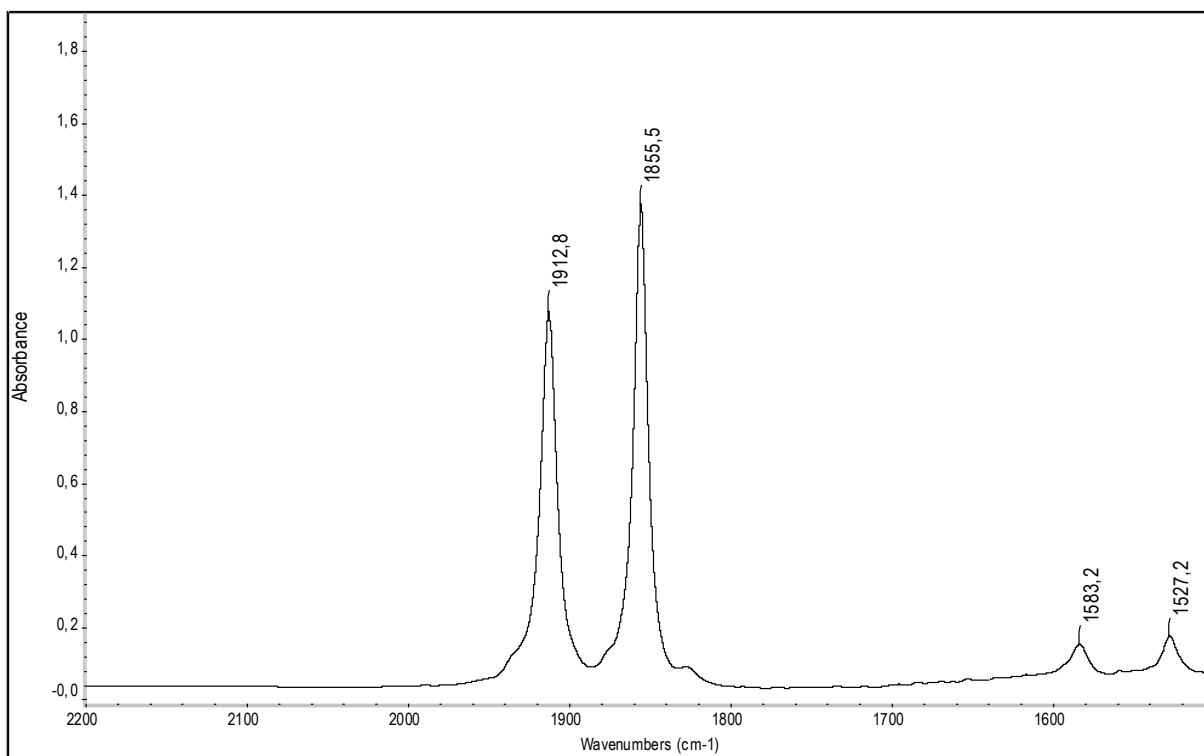


Figure S11. FT-IR spectrum of **1-Cr** in *n*-hexane in the spectral range of 2200 - 1500 cm^{-1} .

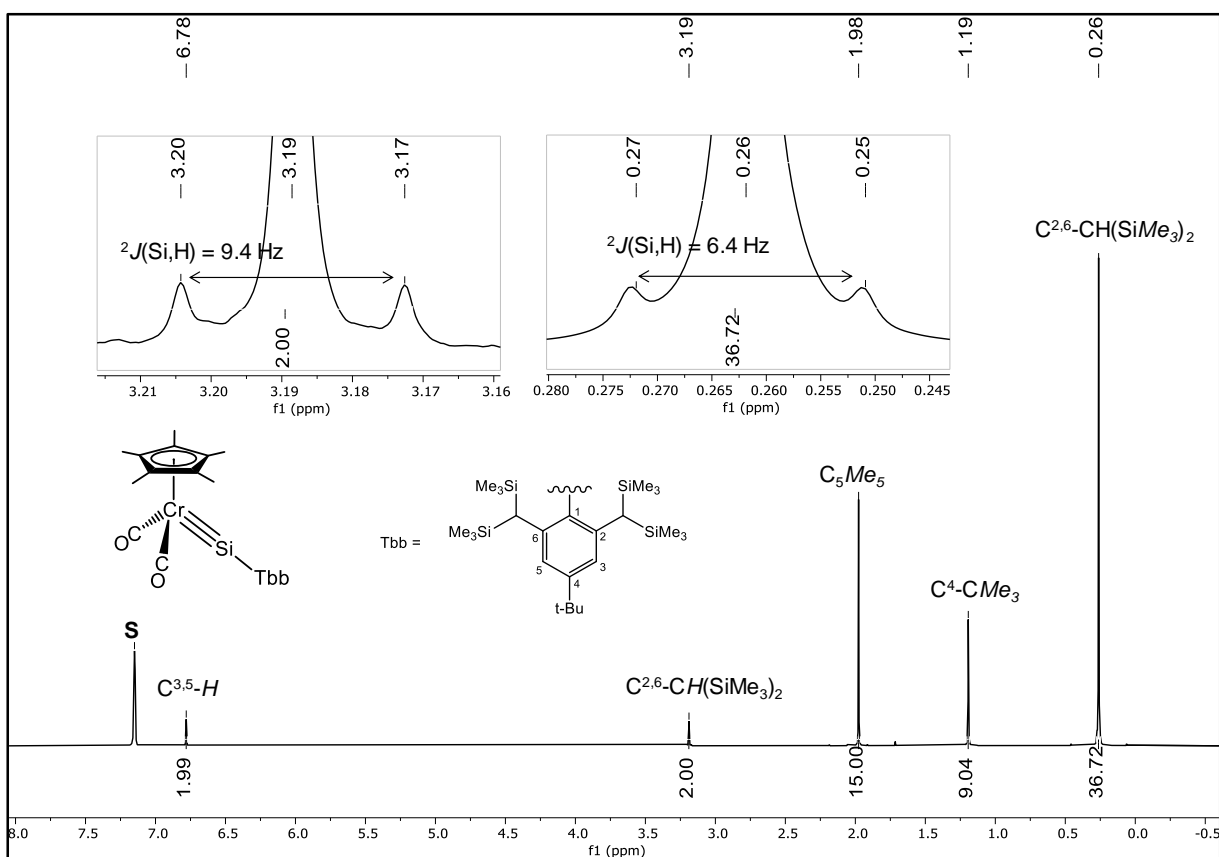


Figure S12. ^1H NMR spectrum (300.1 MHz) of **1-Cr** in (D_6) benzene at 298 K; the residual proton signal of the deuterated solvent is marked with the letter **S**. Two signals with their ^{29}Si satellites are shown in the insets.

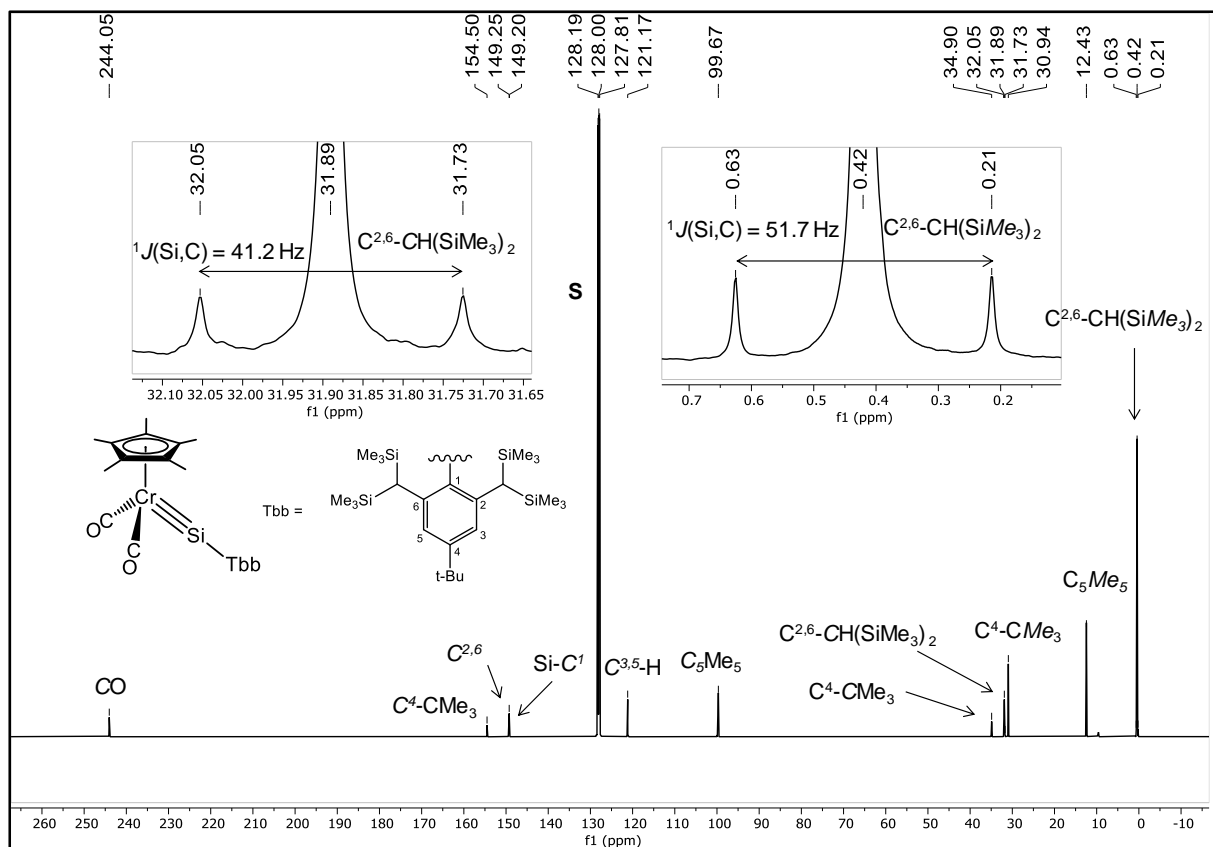


Figure S13. $^{13}\text{C}\{^1\text{H}\}$ NMR spectrum (125.8 MHz) of **1-Cr** in (D_6) benzene at 298 K; the signal of the deuterated solvent is marked with the letter **S**. Two signals with their ^{29}Si satellites are shown in the insets.

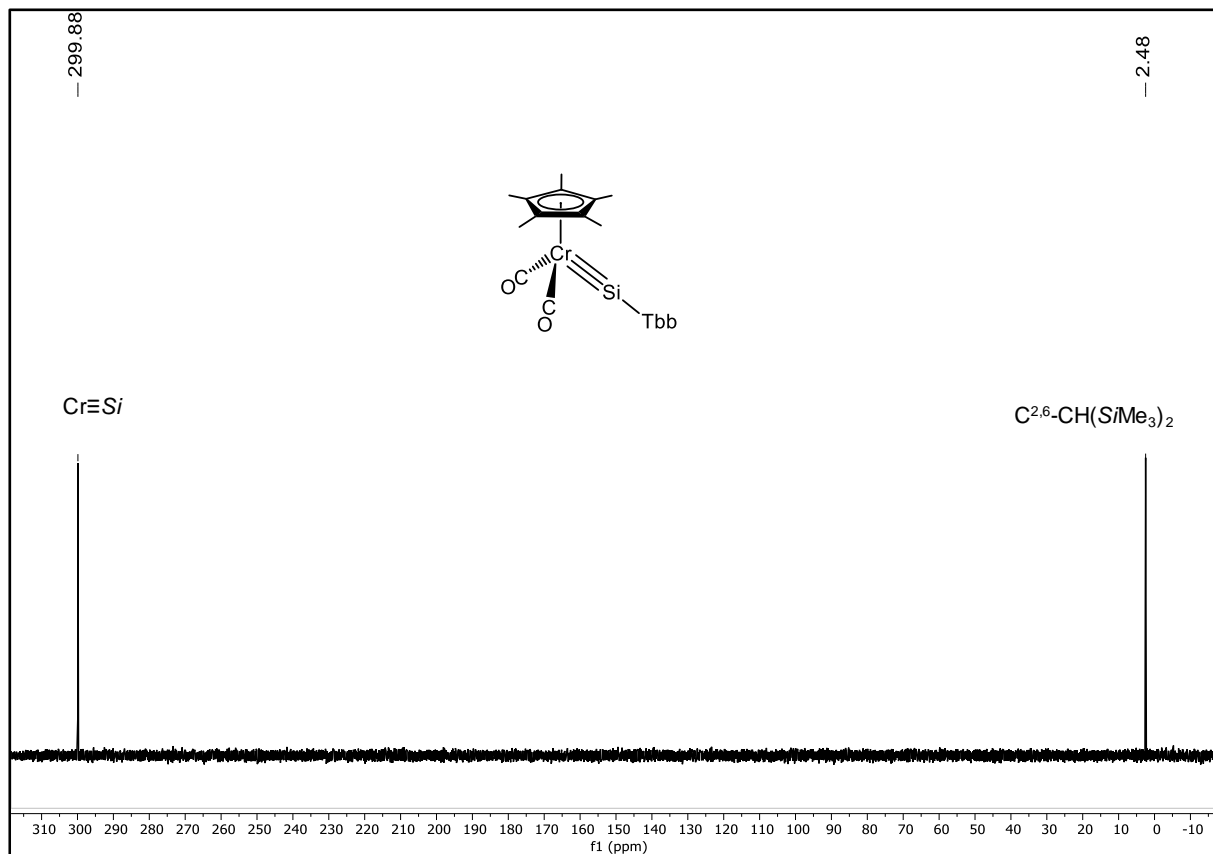
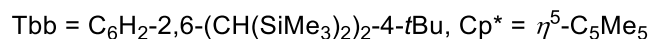
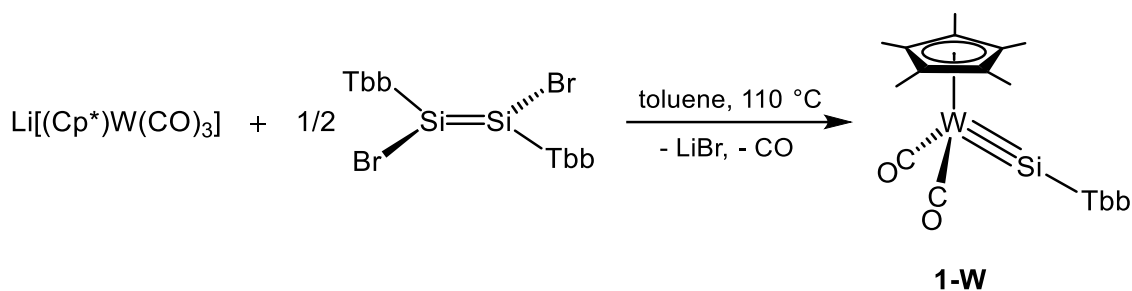


Figure S14. $^{29}\text{Si}\{^1\text{H}\}$ (zgig) NMR (99.36 MHz) spectrum of **1-Cr** in (D_6) benzene at 298 K.

2.3 [W(Cp*)(CO)₂(SiTbb)] (**1-W**)

A mixture of (*E*)-Tbb(Br)Si=Si(Br)Tbb (500 mg, 0.448 mmol, 1.00 equiv.) and Li[Cp*W(CO)₃] (368 mg, 0.897 mmol, 2.00 equiv.) was suspended in 25 mL of toluene and the resulting yellow suspension was heated at 110 °C under static vacuum for 6 hours. During this time all disilene dissolved and the color of the solution changed to orange-red. ¹H NMR spectroscopic analysis of an aliquot of the reaction mixture showed a complete conversion of the starting materials and the selective formation of **1-W**. The reaction mixture was evaporated to dryness under reduced pressure at 50 °C and the red-brown, sticky residue obtained was extracted with *n*-pentane (2 × 5 mL). The combined extracts were concentrated to approximately 1.5 mL under reduced pressure and stored at –30 °C for 24 hours. The crystallized orange-red solid was filtered at –30 °C and dried in a fine vacuum at 50 °C for 30 minutes. Yield: 428 mg (0.502 mmol, 56% from (*E*)-Tbb(Br)Si=Si(Br)Tbb).

Elemental analysis calcd (%) for C₃₆H₆₄O₂Si₅W (853.16 g/mol): C 50.68, H 7.56; found: C 49.92, H 7.57%.

Complex **1-W** is a highly air sensitive, orange-red solid that melts at 182 °C. It is highly soluble in *n*-pentane, diethyl ether, benzene and toluene.

Spectroscopy:

ATR-IR (solid, 298 K, *Figure S15* and *Figure S16*): $\tilde{\nu}$ (cm⁻¹) = 2953 (m), 2903 (w), 2869 (vw), 2738 (vw), 1934 (w), 1907 (vs) [ν (CO)], 1839 (vs) [ν (CO)], 1583 (w), 1530 (w), 1476 (vw), 1463 (vw), 1426 (vw), 1397 (w), 1384 (w), 1362 (vw), 1258 (m, sh), 1247 (s), 1173 (w), 1167 (w), 1143 (vw), 1069 (vw), 1049 (vw), 1018 (m), 959 (w), 936 (vw), 890 (m), 835 (vs), 772 (sh w), 764 (w), 745 (w), 725 (w), 688 (m), 657 (w), 646 (w), 611 (w), 592 (w), 586 (w), 560 (w), 541 (w), 513 (w), 479 (m), 417 (m).

IR (toluene, 298 K, *Figure S17*): $\tilde{\nu}$ (cm⁻¹) = 1911 (s) [ν (CO)], 1848 (vs) [ν (CO)], 1582 (w) and 1529 (w) [ν (C=C)_{Tbb}].

IR (*n*-hexane, 298 K, *Figure S18*): $\tilde{\nu}$ (cm⁻¹) = 1919 (s) [ν (CO)], 1857 (vs) [ν (CO)], 1583 (w) and 1529 (w) [ν (C=C)_{Tbb}].

^1H NMR (300.1 MHz, (D_6) benzene, 298 K, *Figure S19*): δ (ppm) = 0.25 (s, $^2J(^{29}\text{Si}, ^1\text{H}) = 6.4$ Hz, 36H, $\text{C}^{2,6}\text{-CH}(\text{SiMe}_3)_2$), 1.20 (s, 9H, $\text{C}^4\text{-CMe}_3$), 2.16 (s, 15H, C_5Me_5), 3.26 (s, $^2J(^{29}\text{Si}, ^1\text{H}) = 9.6$ Hz, 2H, $\text{C}^{2,6}\text{-CH}(\text{SiMe}_3)_2$), 6.82 (s, 2H, $\text{C}^{3,5}\text{-H}$).

$^{13}\text{C}\{^1\text{H}\}$ NMR (125.8 MHz, (D_6) benzene, 298 K, *Figure S20*): δ (ppm) = 0.36 (s, $^1J(^{29}\text{Si}, ^{13}\text{C}) = 51.6$ Hz, 12C, $\text{C}^{2,6}\text{-CH}(\text{SiMe}_3)_2$), 12.3 (s, 5C, C_5Me_5), 30.9 (s, 3C, $\text{C}^4\text{-CMe}_3$), 31.7 (s, $^1J(^{29}\text{Si}, ^{13}\text{C}) = 41.2$ Hz, 2C, $\text{C}^{2,6}\text{-CH}(\text{SiMe}_3)_2$), 35.0 (s, 1C, $\text{C}^4\text{-CMe}_3$), 101.7 (s, 5C, C_5Me_5), 121.9 (s, 2C, $\text{C}^{3,5}\text{-H}$), 149.2 (s, 2C, $\text{C}^{2,6}\text{-CH}(\text{SiMe}_3)_2$), 150.6 (s, 1C, Si-C^1), 154.7 (s, 1C, $\text{C}^4\text{-CMe}_3$), 224.9 (s, 2C, $^1J(^{183}\text{W}, ^{13}\text{C}) = 183.3$ Hz, $2 \times \text{CO}$).

$^{29}\text{Si}\{^1\text{H}\}$ NMR (99.36 MHz, (D_6) benzene, 298 K, *Figure S21*): δ (ppm) = 2.3 (s, $^1J(^{29}\text{Si}, ^{13}\text{C}) = 51.6$ Hz, 4Si, $\text{C}^{2,6}\text{-CH}(\text{SiMe}_3)_2$), 314.0 (s, $^1J(^{183}\text{W}, ^{29}\text{Si}) = 316.0$ Hz, 1Si, $\text{W}=\text{Si}$).

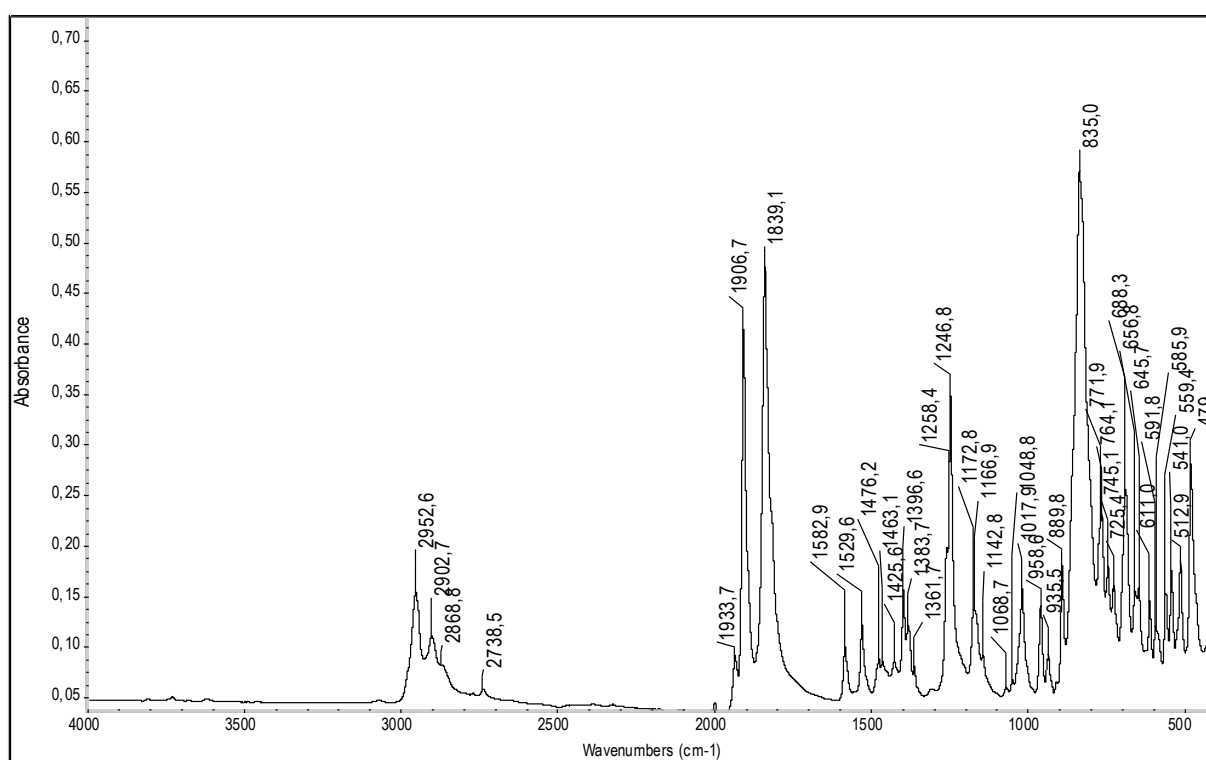


Figure S15. ATR-IR spectrum of **1-W** in the solid state in the spectral range of 4000 - 400 cm^{-1} .

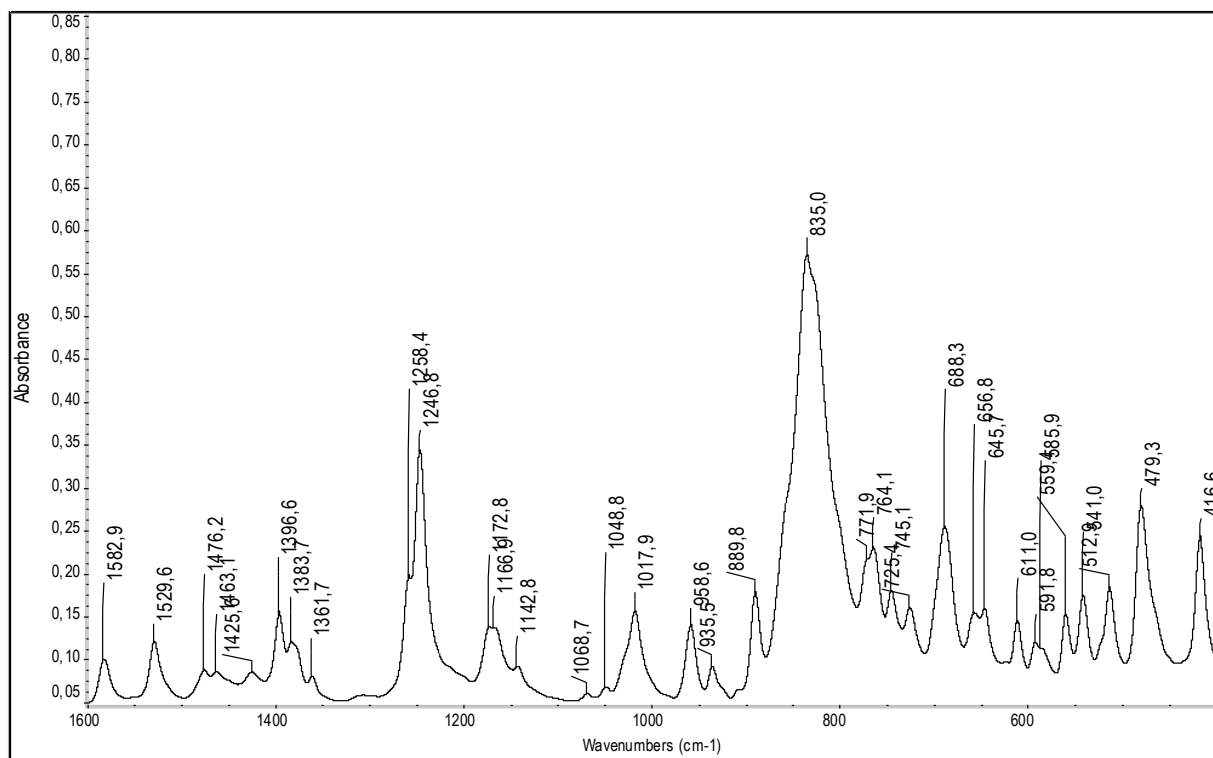


Figure S16. Excerpt of the ATR-IR spectrum of **1-W** in the solid state (spectral range: 1600 - 400 cm⁻¹).

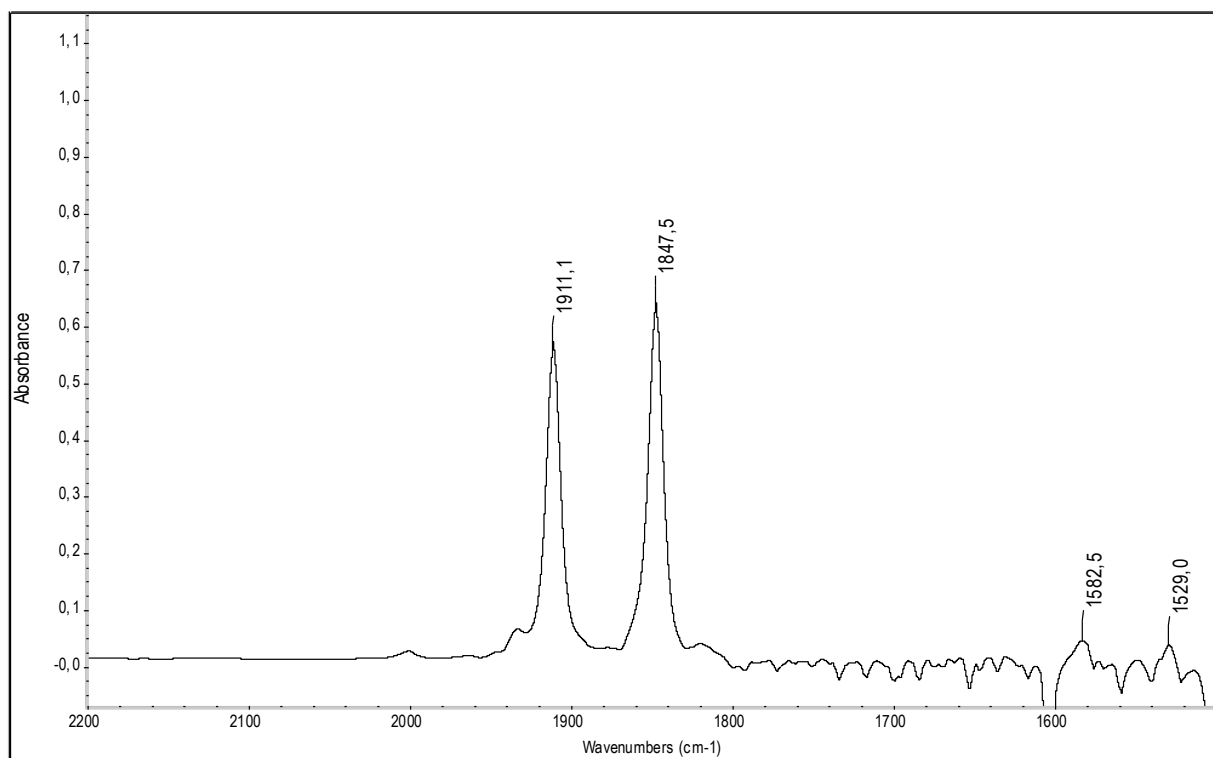


Figure S17. FT-IR spectrum of **1-W** in toluene in the spectral range of 2200 - 1500 cm⁻¹. The band marked with an asterisk (*) originates from the solvent due to incomplete background correction.

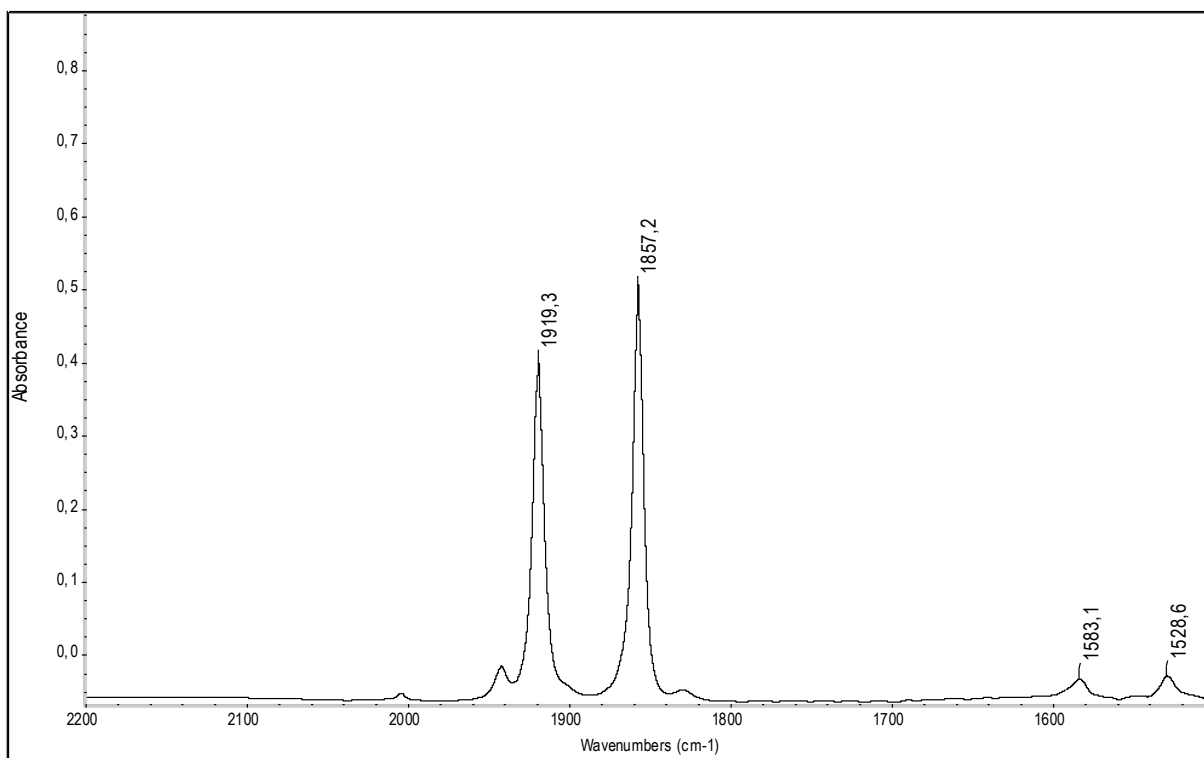


Figure S18. FT-IR spectrum of **1-W** in *n*-hexane in the spectral range of 2200 - 1500 cm^{-1} .

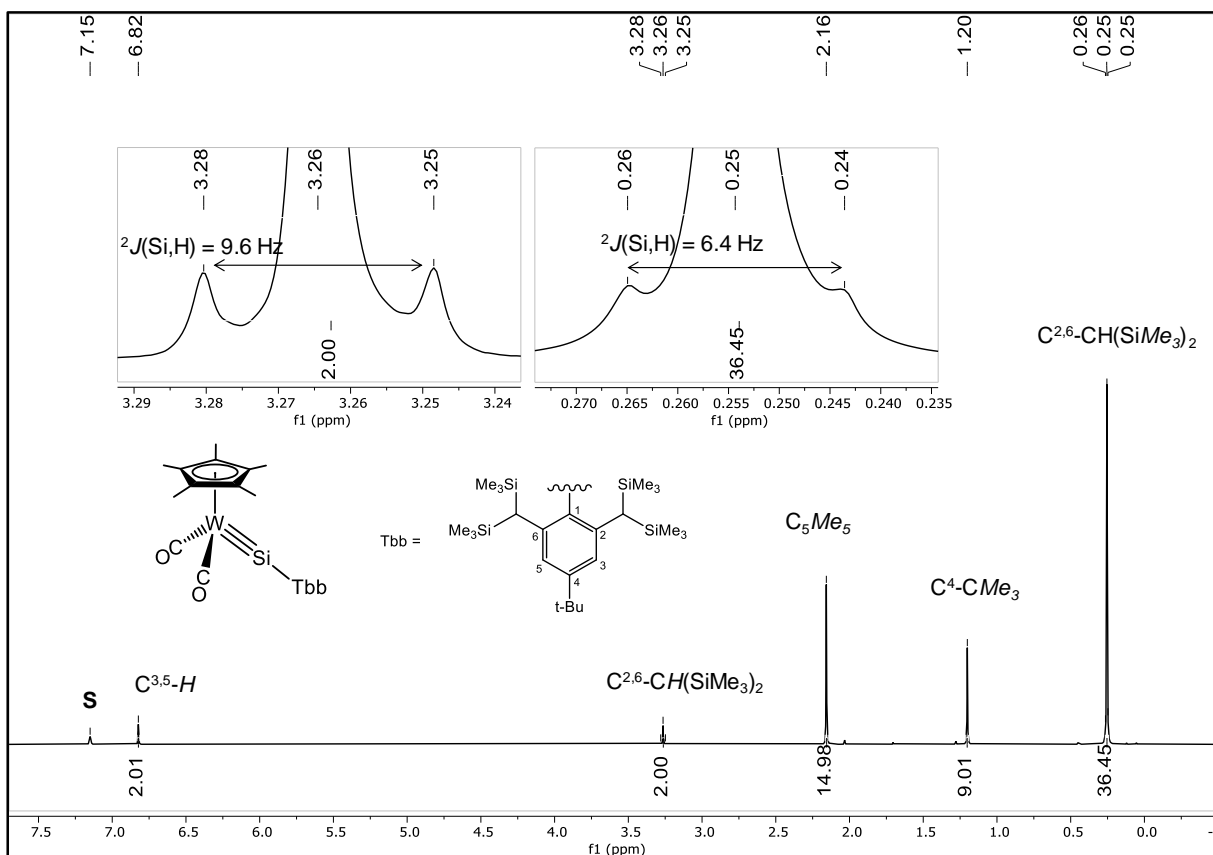


Figure S19. ^1H NMR spectrum (300.1 MHz) of **1-W** in (D_6) benzene at 298 K; the residual proton signal of the deuterated solvent is marked with the letter **S**. Two signals with their ^{29}Si satellites are shown in the insets.

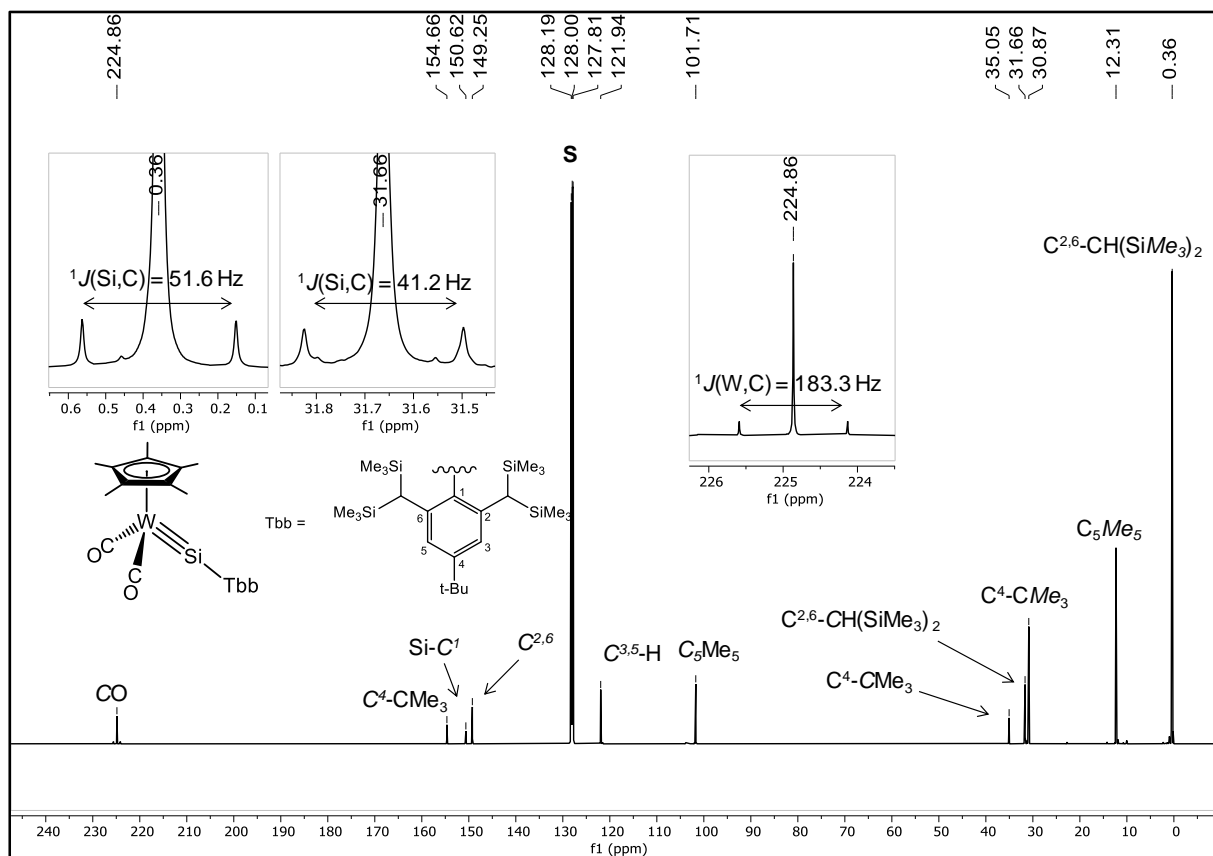


Figure S20. $^{13}\text{C}\{^1\text{H}\}$ NMR spectrum (125.8 MHz) of **1-W** in (D_6) benzene at 298 K; the signal of the deuterated solvent is marked with the letter **S**. Three signals with their ^{29}Si satellites are shown in the insets.

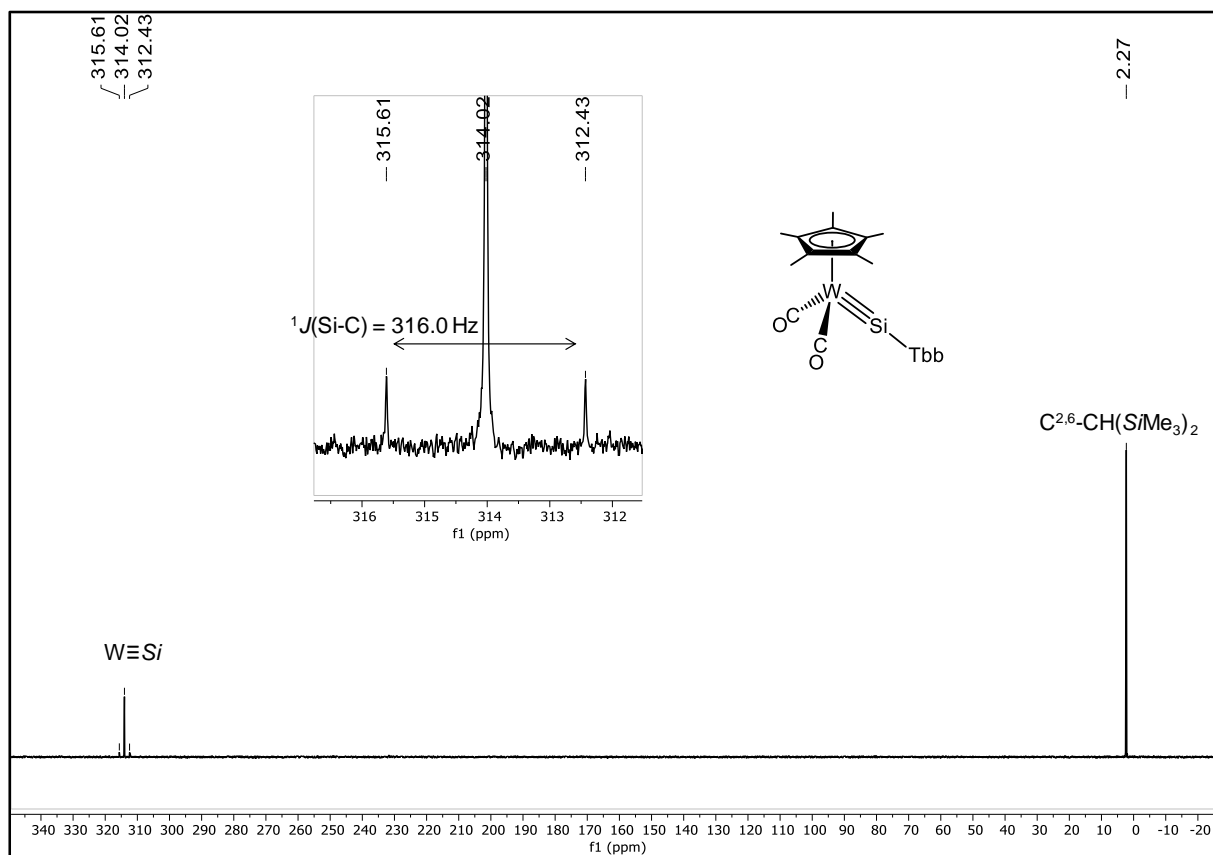
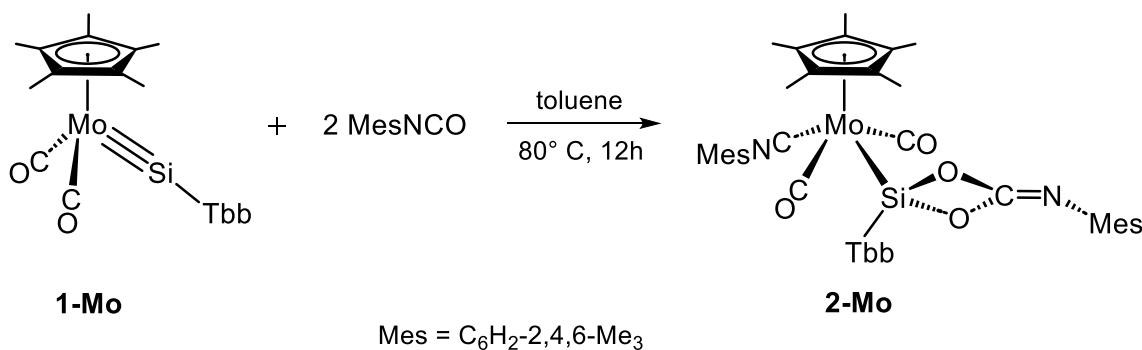


Figure S21. $^{29}\text{Si}\{^1\text{H}\}$ (zgig) NMR (99.36 MHz) spectrum of **1-W** in (D_6) benzene at 298 K. The $\text{W}=\text{Si}$ signal with its ^{183}W satellites is shown in the inset.

2.4 [Mo(Cp*)(CO)₂(CNMes){Si(Tbb)(κ²O,O'-O₂CNMes)}] (**2-Mo**)



A mixture of the silylidyne complex **1-Mo** (130 mg, 0.170 mmol, 1.00 equiv.) and mesityl isocyanate (55 mg, 0.34 mmol, 2.0 equiv.) was treated with 3 mL of toluene at room temperature and the orange-red reaction solution was heated at 80 °C for 12 hours. During this time, the colour of the solution changed to yellow-brown. ¹H NMR and IR spectroscopic analysis of an aliquot of the reaction solution showed the selective formation of complex **2-Mo**. The reaction solution was evaporated to dryness under reduced pressure and the yellow-brown residue was washed with *n*-hexane (3 × 2 mL). The creamy white solid obtained was dried in a fine vacuum at 60 °C for 30 minutes. Yield: 157 mg (0.144 mmol, 85% from **1-Mo**).

Elemental analysis calcd (%) for C₅₆H₈₆MoN₂O₄Si₅ (1087.66 g/mol): C 61.84, H 7.97, N 2.58; found: C 61.49, H 8.23, N 2.46%.

Complex **2-Mo** is an air sensitive, creamy white solid that melts with decomposition at 227 °C. It is sparingly soluble in *n*-pentane, *n*-hexane and good soluble in Et₂O, benzene and toluene.

Spectroscopy:

The ¹H, ¹³C and ²⁹Si NMR spectra of **2-Mo** were recorded in (D₈)THF at 243 K ((D₈)toluene was not suitable as a solvent due to the limited solubility of **2-Mo** at this temperature) and in (D₆)benzene at 298 K and 343 K. The compound **2-Mo** is C₁ symmetric and contains a stereogenic Si center due to the fixed orientation of the N_{imino}-bonded mesityl group. This is evidenced by the ¹³C{¹H} NMR spectrum of **2-Mo** at 243 K, which shows two singlets for the diastereotopic, *trans*-coordinated CO ligands (Figure S26 and Figure S28). In addition, rotation of the Tbb substituent about the Si-C_{Tbb} bond is frozen out at 243 K leading to diastereotopic C² and C⁶ and C³ and C⁵ positions of the Tbb substituent and to separate signals for these nuclei and the attached groups. For example, the ¹H NMR spectrum of **2-Mo** at 243 K shows two singlets for the C³- and C⁵-bonded aryl protons and two singlets for the C²- and C⁶-bonded methine protons (CH) of the diastereotopic disyl (CH(SiMe₃)₂) substituents (Figure S25). Similarly, four singlets are observed in the ¹H, ¹³C{¹H} and ²⁹Si{¹H} NMR spectra for the SiMe₃ groups, as each of the diastereotopic disyl substituent bears two diastereotopic SiMe₃ groups (Figure S25, Figure S27 and Figure S29). All signals were fully assigned by 2D NMR spectroscopy at 243 K. The aryl carbon atom carrying the Dsi group with the most shielded

SiMe₃ protons was denominated as the C² atom and the other carbon atoms (C³, C⁵ and C⁶) of the Tbb substituent assigned by 2D correlation NMR spectroscopy. The subscript letter A was used for the more shielded protons of the two diastereotopic SiMe₃ groups in each of the diastereotopic Dsi substituents.

With increasing temperature a dynamic process sets on leading to a broadening of the two CO ligands at 298 K (*Figure S35*) and their merging to one signal at 348 K (*Figure S40*). As shown by a comparison of the ¹H and ¹³C{¹H} NMR spectra of **2-Mo** at 243, 298 and 348 K, this process leads concomitantly to a site exchange of the diastereotopic C² and C⁶ and C³ and C⁵ positions of the Tbb substituent, and most likely involves a racemization of **2-Mo** via inversion of the N_{imino}-bonded mesityl group. The Gibbs energy of activation (ΔG^\ddagger (298 K)) was calculated to be approximately 60 kJ·mol⁻¹ and compares well with those found for the N-aryl iminocarbonates (MeO)₂C=N(*p*-C₆H₄X) (X = H, Cl, Me) (*E_a* (in acetone) = 56.1 – 69.5 kJ·mol⁻¹).^[S9] It should be noted, that neither a Berry-type pseudorotation of the square-pyramidal complex **2-Mo** nor a rotation of the Tbb substituent alone can explain the observed changes in the NMR spectra of **2-Mo** with increasing temperature.

ATR-IR (solid, 298 K, *Figure S22* and *Figure S23*): $\tilde{\nu}$ (cm⁻¹) = 2961 (w), 2947 (w), 2900 (w), 2859 (vw), 2096 (s) [ν (CN)], 1963 (m) [ν (CO)], 1900 (vs) [ν (CO)], 1709 (s) [ν (NCO₂)], 1693 (s) [ν (NCO₂)], 1607 (vw), 1589 (vw), 1524 (vw), 1477 (w), 1395 (w), 1381 (w), 1262 (w, sh), 1249 (m), 1178 (vw), 1162 (vw), 1147 (vw), 1045 (vw), 1033 (vw), 996 (w), 975 (m), 949 (m), 938 (w, sh), 878 (m, sh), 843 (vs), 788 (vw), 772 (vw), 764 (vw), 751 (vw), 736 (w), 718 (m), 681 (w), 663 (s), 645 (vw), 634 (vw), 613 (vw), 592 (m), 570 (s), 558 (m, sh), 547 (m, sh), 505 (m), 486 (w), 474 (m), 461 (s), 426 (m), 414 (m).

IR (toluene, 298 K, *Figure S24*): $\tilde{\nu}$ (cm⁻¹) = 2103 (s) [ν (CN)], 1962 (m) [ν (CO)], 1901 (vs) [ν (CO)], 1710 (m) [ν (NCO₂)], 1692 (m) [ν (NCO₂)].

¹H NMR (500.1 MHz, (D₈)THF, 243 K, *Figure S25*): δ (ppm) = -0.43 (s, 9H, C²-CH(SiMe₃)_A(SiMe₃)_B, Tbb), -0.12 (s, 9H, C²-CH(SiMe₃)_A(SiMe₃)_B, Tbb), 0.17 (s, 9H, C⁶-CH(SiMe₃)_A(SiMe₃)_B, Tbb), 0.28 (s, 9H, C⁶-CH(SiMe₃)_A(SiMe₃)_B, Tbb), 1.24 (s, 9H, C⁴-CMe₃, Tbb), 1.50 (s, ²*J*(²⁹Si, ¹H) = 9.1 Hz, 1H, C²-CH(SiMe₃)₂, Tbb), 1.82 (s, ²*J*(²⁹Si, ¹H) = 9.1 Hz, 1H, C⁶-CH(SiMe₃)₂, Tbb), 2.14 (s, 3H, C⁴-Me, Mes_A), 2.21 (s, 15H, C₅Me₅), ~2.20* (br, 6H, C^{2,6}-Me, Mes_A), 2.30 (s, 3H, C⁴-Me, Mes_B), 2.39 (s, 6H, C^{2,6}-Me, Mes_B), 6.59 (d, ⁴*J*(¹H, ¹H) = 1.7 Hz, 1H, C³-H, Tbb), 6.63 (br s, $\Delta\nu_{1/2}$ = 6.1 Hz, 2H, C^{3,5}-H, Mes_A), 6.76 (d, ⁴*J*(¹H, ¹H) = 1.7 Hz, 1H, C⁵-H, Tbb), 7.05 (s, 2H, C^{3,5}-H, Mes_B). *The position of the very broadened signal at ca. 2.20 ppm was deduced from the integral ratio of the ¹H NMR signals and was verified by ¹H-¹³C HMBC NMR spectroscopy.

[S9] N. P. Marullo, E. H. Wagener, *J. Am. Chem. Soc.*, **1966**, *88*, 5034–5035.

$^{13}\text{C}\{^1\text{H}\}$ NMR (125.8 MHz, (D_8)THF, 243 K, *Figure S26*, *Figure S27* and *Figure S28*): δ (ppm) = 1.2 (s, $^1J(^{29}\text{Si}, ^{13}\text{C}) = 51.7$ Hz, 3C, $\text{C}^2\text{-CH}(\text{SiMe}_3)_\text{A}(\text{SiMe}_3)_\text{B}$, Tbb), 1.3 (s, $^1J(^{29}\text{Si}, ^{13}\text{C}) = 50.6$ Hz, 3C, $\text{C}^2\text{-CH}(\text{SiMe}_3)_\text{A}(\text{SiMe}_3)_\text{B}$, Tbb), 2.0 (s, $^1J(^{29}\text{Si}, ^{13}\text{C}) = 51.7$ Hz, 3C, $\text{C}^6\text{-CH}(\text{SiMe}_3)_\text{A}(\text{SiMe}_3)_\text{B}$, Tbb), 3.2 (s, $^1J(^{29}\text{Si}, ^{13}\text{C}) = 50.6$ Hz, 3C, $\text{C}^6\text{-CH}(\text{SiMe}_3)_\text{A}(\text{SiMe}_3)_\text{B}$, Tbb), 11.9 (s, 5C, C_5Me_5), 18.7 (s, 2C, $\text{C}^{2,6}\text{-Me}$, Mes_B), 20.4 (s, 2C, $\text{C}^{2,6}\text{-Me}$, Mes_A), 20.9 (s, 1C, $\text{C}^4\text{-Me}$, Mes_A), 21.3 (s, 1C, $\text{C}^4\text{-Me}$, Mes_B), 28.5 (s, $^1J(^{29}\text{Si}, ^{13}\text{C}) = \sim 42.0$ Hz, 1C, $\text{C}^6\text{-CH}(\text{SiMe}_3)_2$, Tbb), 28.8 (s, $^1J(^{29}\text{Si}, ^{13}\text{C}) = \sim 40.0$ Hz, 1C, $\text{C}^2\text{-CH}(\text{SiMe}_3)_2$, Tbb), 31.6 (s, 3C, $\text{C}^4\text{-CMe}_3$, Tbb), 35.0 (s, 1C, $\text{C}^4\text{-CMe}_3$, Tbb), 105.9 (s, 5C, C_5Me_5), 121.3 (s, 1C, $\text{C}^5\text{-H}$, Tbb), 121.8 (s, 1C, $\text{C}^3\text{-H}$, Tbb), 126.5 (s, 1C, C^1 , Mes_B), 128.7 (br s, $\Delta\nu_{1/2} = 11.6$ Hz, 2C, $\text{C}^{3,5}\text{-H}$, Mes_A), 129.7 (s, 2C, $\text{C}^{3,5}\text{-H}$, Mes_B), 130.5 (s, 1C, C^4 , Mes_A), $\sim 130.8^*$ (br, 2C, $\text{C}^{2,6}$, Mes_A), 135.4 (s, 2C, $\text{C}^{2,6}$, Mes_B), 138.0 (s, 1C, C^1 , Tbb), 140.3 (s, 1C, C^4 , Mes_B), 142.3 (s, 1C, C^1 , Mes_A), 148.0 (s, 1C, C^6 , Tbb), 149.0 (s, 1C, C^2 , Tbb), 149.9 (s, 1C, $\text{O}_2\text{CN}(\text{Mes})_\text{A}$), 151.6 (s, 1C, $\text{C}^4\text{-CMe}_3$, Tbb), 183.1 (s, 1C, $\text{Mo-CN}(\text{Mes})_\text{B}$), 231.6 (s, 1C, CO), 234.0 (s, 1C, CO). * The signal of the $\text{C}^{2,6}$ carbon atoms of the Mes_A group at ca. 130.8 ppm appears as a hump due to hindered rotation.

$^{29}\text{Si}\{^1\text{H}\}$ NMR (99.36 MHz, (D_8)THF, 243 K, *Figure S29* and *Figure S30*): δ (ppm) = 1.1 (s, 1Si, $\text{C}^6\text{-CH}(\text{SiMe}_3)_\text{A}(\text{SiMe}_3)_\text{B}$, Tbb), 1.3 (s, 1Si, $\text{C}^2\text{-CH}(\text{SiMe}_3)_\text{A}(\text{SiMe}_3)_\text{B}$, Tbb), 4.2 (s, 1Si, $\text{C}^2\text{-CH}(\text{SiMe}_3)_\text{A}(\text{SiMe}_3)_\text{B}$, Tbb), 4.5 (s, 1Si, $\text{C}^6\text{-CH}(\text{SiMe}_3)_\text{A}(\text{SiMe}_3)_\text{B}$, Tbb), 108.0 (s, 1Si, MoSi).

^1H NMR (500.1 MHz, (D_6)benzene, 298 K, *Figure S31* and *Figure S32*): δ (ppm) = -0.02 (br s, $\Delta\nu_{1/2} = 26.3$ Hz, 9H, $\text{C}^{2/6}\text{-CH}(\text{SiMe}_3)_\text{A}(\text{SiMe}_3)$, Tbb), 0.10 (br s, $\Delta\nu_{1/2} = 28.8$ Hz, 9H, $\text{C}^{2/6}\text{-CH}(\text{SiMe}_3)_\text{A}(\text{SiMe}_3)_\text{B}$, Tbb), 0.49 (br s, $\Delta\nu_{1/2} = 35.0$ Hz, 18H, $\text{C}^{2/6}\text{-CH}(\text{SiMe}_3)_2$, Tbb), 1.28 (s, 9H, $\text{C}^4\text{-CMe}_3$, Tbb), ~ 1.88 (br s, $\Delta\nu_{1/2} = \sim 23$ Hz, 1H, $\text{C}^{2/6}\text{-CH}(\text{SiMe}_3)_2$, Tbb), 1.89 (s, 3H, $\text{C}^4\text{-Me}$, Mes_B), 1.99 (s, 15H, C_5Me_5), ~ 2.09 (br s, $\Delta\nu_{1/2} = \sim 23$ Hz, 1H, $\text{C}^{2/6}\text{-CH}(\text{SiMe}_3)_2$, Tbb), 2.21 (s, 6H, $\text{C}^{2,6}\text{-Me}$, Mes_B), 2.27 (s, 3H, $\text{C}^4\text{-Me}$, Mes_A), 2.70 (s, 6H, $\text{C}^{2,6}\text{-Me}$, Mes_A), 6.47 (s, 2H, $\text{C}^{3,5}\text{-H}$, Mes_B), 6.88 (br s, $\Delta\nu_{1/2} = 31.0$ Hz, 1H, $\text{C}^3\text{-H}$, Tbb), 6.97 (s, 2H, $\text{C}^{3,5}\text{-H}$, Mes_A), 7.01 (br s, $\Delta\nu_{1/2} = 31.0$ Hz, 1H, $\text{C}^5\text{-H}$, Tbb).

$^{13}\text{C}\{^1\text{H}\}$ NMR (125.8 MHz, (D_6)benzene, 298 K, *Figure S33*, *Figure S34* and *Figure S35*): δ (ppm) = 1.3 and 1.4 (br s each, 3C each, $\text{C}^{2/6}\text{-CH}(\text{SiMe}_3)_2$, Tbb), 2.1 (br s, $\Delta\nu_{1/2} = \sim 27$ Hz, 3C, $\text{C}^{2/6}\text{-CH}(\text{SiMe}_3)_2$, Tbb), 3.3 (br s, $\Delta\nu_{1/2} = \sim 27$ Hz, 3C, $\text{C}^{2/6}\text{-CH}(\text{SiMe}_3)_2$, Tbb), 11.6 (s, 5C, C_5Me_5), 18.4 (s, 2C, $\text{C}^{2,6}\text{-Me}$, Mes_B), 20.4 (s, 2C, $\text{C}^{2,6}\text{-Me}$, Mes_A), 20.9 (s, 2C, $\text{C}^4\text{-Me}$, Mes_A & Mes_B), 28.9 (br s, $\Delta\nu_{1/2} = 22.5$ Hz, 2C, $\text{C}^{2,6}\text{-CH}(\text{SiMe}_3)_2$, Tbb), 31.3 (s, 3C, $\text{C}^4\text{-CMe}_3$, Tbb), 34.5 (s, 1C, $\text{C}^4\text{-CMe}_3$, Tbb), 105.1 (s, 5C, C_5Me_5), 121.3 (br s, $\Delta\nu_{1/2} = 28.1$ Hz, 1C, $\text{C}^5\text{-H}$, Tbb), 121.6 (br s, $\Delta\nu_{1/2} = 31$ Hz, 1C, $\text{C}^3\text{-H}$, Tbb), 126.2 (s, 1C, C^1 , Mes_B), 128.8 (s, 2C, $\text{C}^{3,5}\text{-H}$, Mes_A), 129.0 (s, 2C, $\text{C}^{3,5}\text{-H}$, Mes_B), 130.7 (s, 1C, C^4 , Mes_A), 130.8 (s, 2C, $\text{C}^{2,6}$, Mes_A), 134.4 (s, 2C, $\text{C}^{2,6}$, Mes_B), 137.5 (s, 1C, C^1 , Tbb), 139.1 (s, 1C, C^4 , Mes_B), 142.0 (s, 1C, C^1 , Mes_A), 147.9 (br s, $\Delta\nu_{1/2} = 27.4$ Hz, 1C, $\text{C}^{2/6}$, Tbb), 148.9 (br s, $\Delta\nu_{1/2} = 29.5$ Hz, 1C, $\text{C}^{2/6}$, Tbb), 149.3 (s, 1C, $\text{O}_2\text{CN}(\text{Mes})_\text{A}$), 151.6 (s, 1C, $\text{C}^4\text{-CMe}_3$, Tbb), 184.8 (s, 1C, $\text{Mo-CN}(\text{Mes})_\text{B}$), 231.4 (br s, $\Delta\nu_{1/2} = 25.2$ Hz, 1C, CO), 233.5 (br s, $\Delta\nu_{1/2} = 34.1$ Hz, 1C, CO).

$^{29}\text{Si}\{^1\text{H}\}$ NMR (99.36 MHz, (D_6) benzene, 298 K, *Figure S36*): δ (ppm) = 1.4 and 4.5 (s each, 2Si each, $\text{C}^{2,6}\text{-CH}(\text{SiMe}_3)_2$), 105.8 (s, 1Si, MoSi).

^1H NMR (500.1 MHz, (D_6) benzene, 348 K, *Figure S37*): δ (ppm) = 0.26 (br s, $\Delta\nu_{1/2}$ = 48.5 Hz, 36H, $\text{C}^{2,6}\text{-CH}(\text{SiMe}_3)_2$ Tbb), 1.29 (s, 9H, $\text{C}^4\text{-CMe}_3$, Tbb), 1.92 (s, 3H, $\text{C}^4\text{-Me}$, Mes_B), 1.97 (br s, $\Delta\nu_{1/2}$ = 12.6 Hz, 2H, $\text{C}^{2,6}\text{-CH}(\text{SiMe}_3)_2$, Tbb), 2.03 (s, 15H, C_5Me_5), 2.24 (s, 6H, $\text{C}^{2,6}\text{-Me}$, Mes_B), 2.25 (s, 3H, $\text{C}^4\text{-Me}$, Mes_A), 2.64 (s, 6H, $\text{C}^{2,6}\text{-Me}$, Mes_A), 6.53 (s, 2H, $\text{C}^{3,5}\text{-H}$, Tbb), 6.93 (s, 4H, $2 \times \text{C}^{3,5}\text{-H}$, Mes_{A+B}), 7.01 (br s, $\Delta\nu_{1/2}$ = 31.0 Hz, 1H, $\text{C}^5\text{-H}$, Tbb).

$^{13}\text{C}\{^1\text{H}\}$ NMR (125.8 MHz, (D_6) benzene, 348 K, *Figure S38*, *Figure S39* and *Figure S40*): δ (ppm) = -0.86 – 5.31 (br s each, 3C each, $\text{C}^{2,6}\text{-CH}(\text{SiMe}_3)_2$, Tbb), 2.1 (br s, $\Delta\nu_{1/2}$ = ~ 27 Hz, 3C, $\text{C}^{2,6}\text{-CH}(\text{SiMe}_3)_2$, Tbb), 3.3 (br s, $\Delta\nu_{1/2}$ = 10.4 – 168.4 Hz, 12C, $\text{C}^{2,6}\text{-CH}(\text{SiMe}_3)_2$, Tbb), 11.6 (s, 5C, C_5Me_5), 18.4 (s, 2C, $\text{C}^{2,6}\text{-Me}$, Mes_B), 20.4 (s, 2C, $\text{C}^{2,6}\text{-Me}$, Mes_A), 20.8 and 20.9 (s, 2C, $\text{C}^4\text{-Me}$, Mes_A & Mes_B), 29.3 (s, 2C, $\text{C}^{2,6}\text{-CH}(\text{SiMe}_3)_2$, Tbb), 31.4 (s, 3C, $\text{C}^4\text{-CMe}_3$, Tbb), 34.5 (s, 1C, $\text{C}^4\text{-CMe}_3$, Tbb), 105.4 (s, 5C, C_5Me_5), 121.7 (s, 2C, $\text{C}^{3,5}\text{-H}$, Tbb), 126.5 (s, 1C, C^1 , Mes_B), 128.8 (s, 2C, $\text{C}^{3,5}\text{-H}$, Mes_A), 129.1 (s, 2C, $\text{C}^{3,5}\text{-H}$, Mes_B), 130.76 (s, 1C, C^4 , Mes_A), 130.85 (s, 2C, $\text{C}^{2,6}$, Mes_A), 134.5 (s, 2C, $\text{C}^{2,6}$, Mes_B), 137.8 (s, 1C, C^1 , Tbb), 139.1 (s, 1C, C^4 , Mes_B), 142.1 (s, 1C, C^1 , Mes_A), 148.6 (br s, $\Delta\nu_{1/2}$ = 15.3 Hz, 2C, $\text{C}^{2,6}$, Tbb), 149.1 (s, 1C, $\text{O}_2\text{CN}(\text{Mes})_A$), 151.7 (s, 1C, $\text{C}^4\text{-CMe}_3$, Tbb), 185.6 (s, 1C, Mo-CN(Mes)_B), 232.6 (br s, $\Delta\nu_{1/2}$ = 42.9 Hz, 2C, $2 \times \text{CO}$).

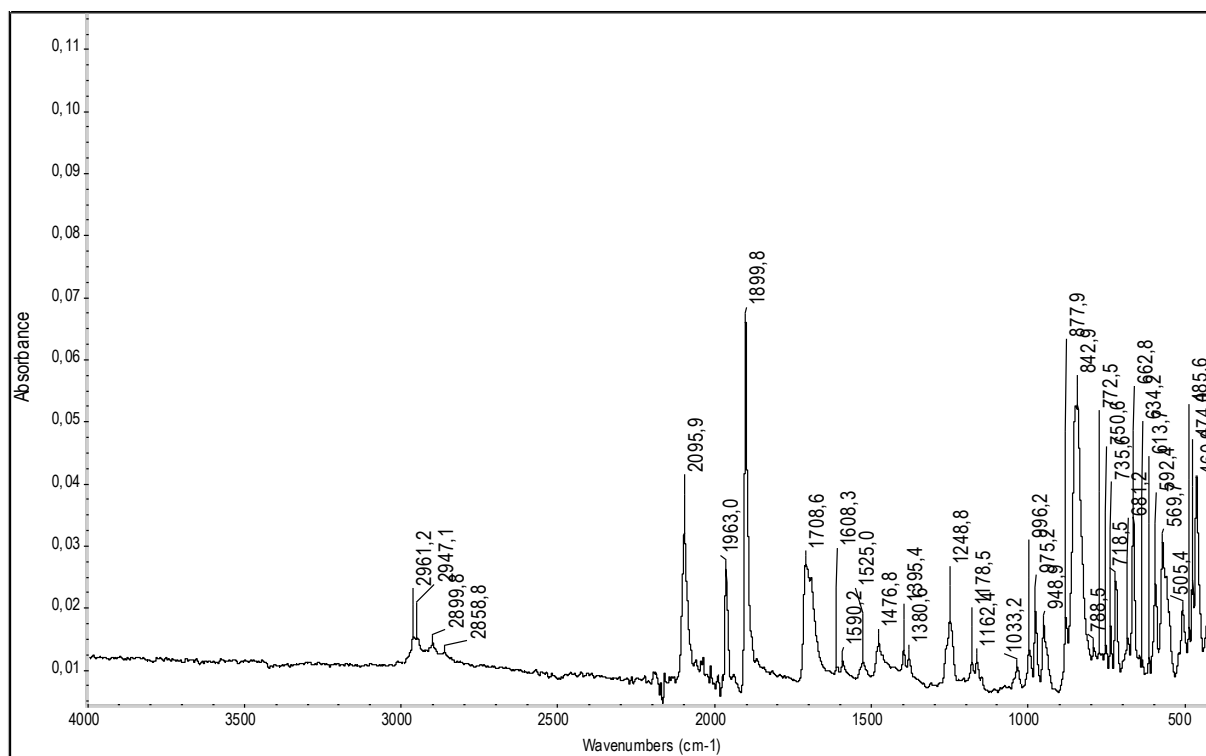


Figure S22. ATR-IR spectrum of **2-Mo** in the solid state in the spectral range of 4000 - 400 cm^{-1} .

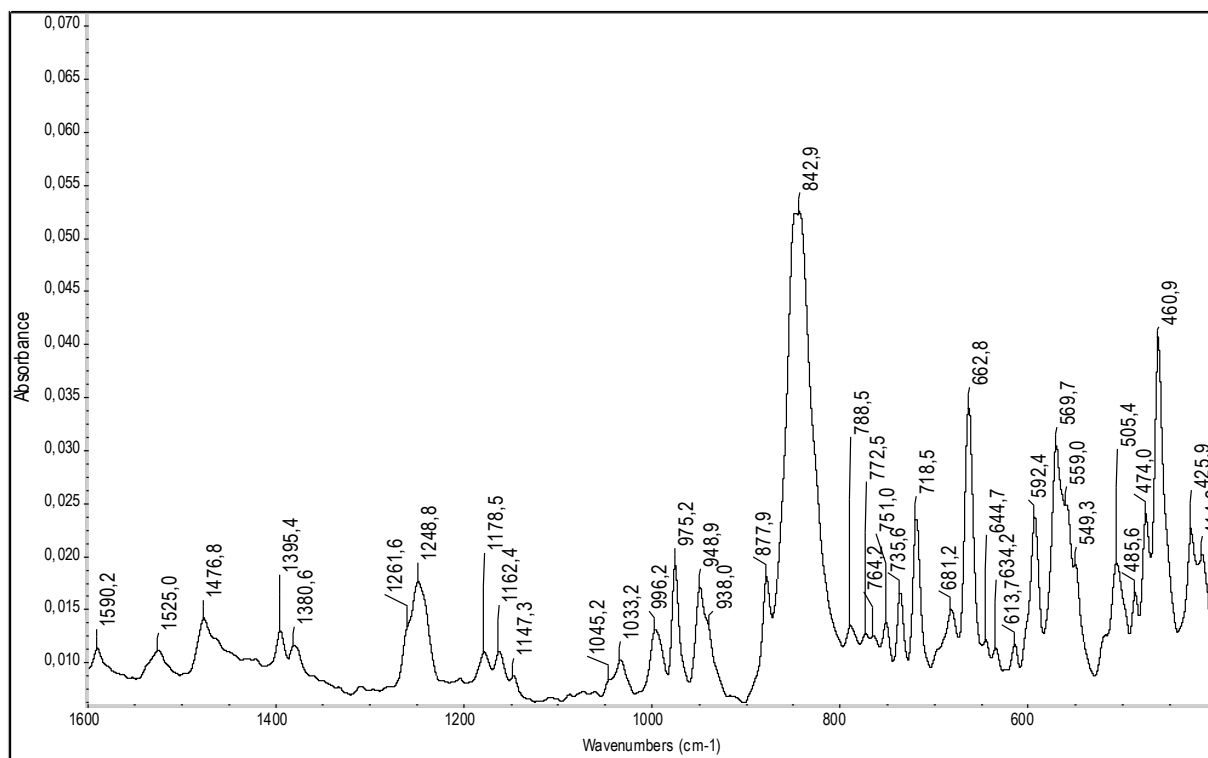


Figure S23. Excerpt of the ATR-IR spectrum of **2-Mo** in the solid state (spectral range: 1600 - 400 cm⁻¹).

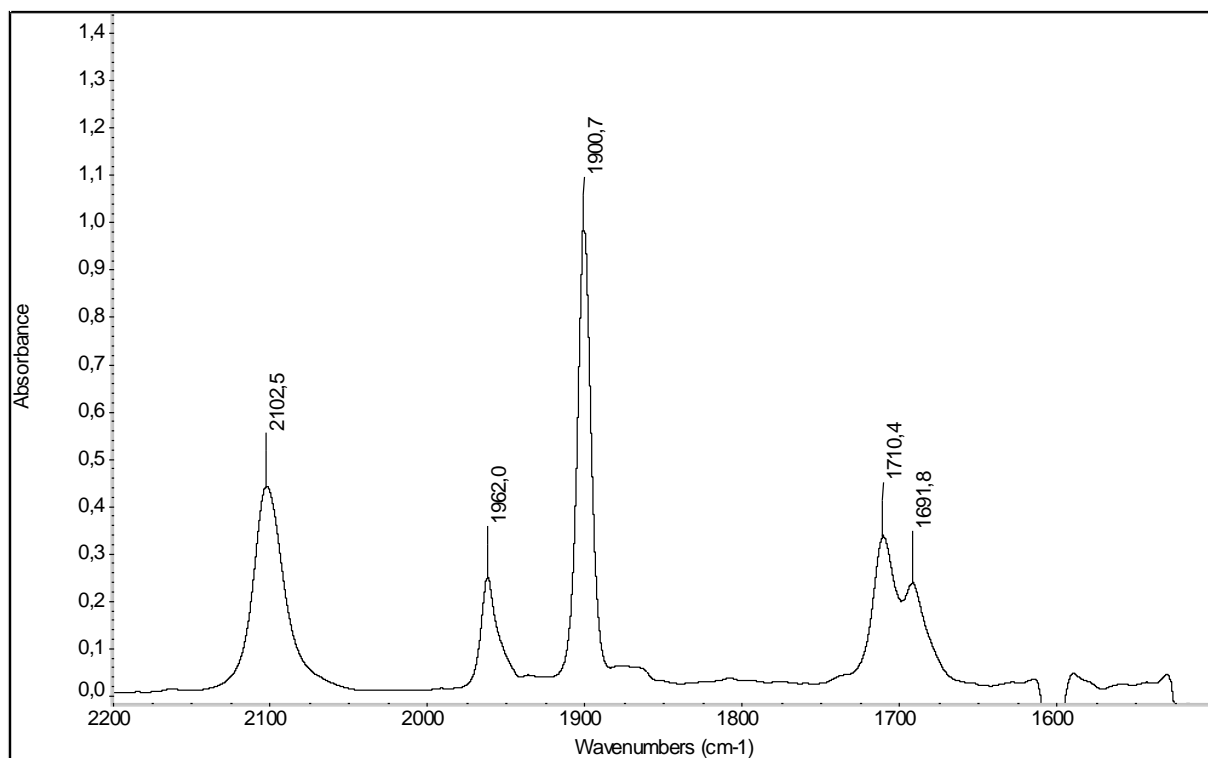


Figure S24. FT-IR spectrum of **2-Mo** in toluene in the spectral range of 2200 - 1500 cm⁻¹.

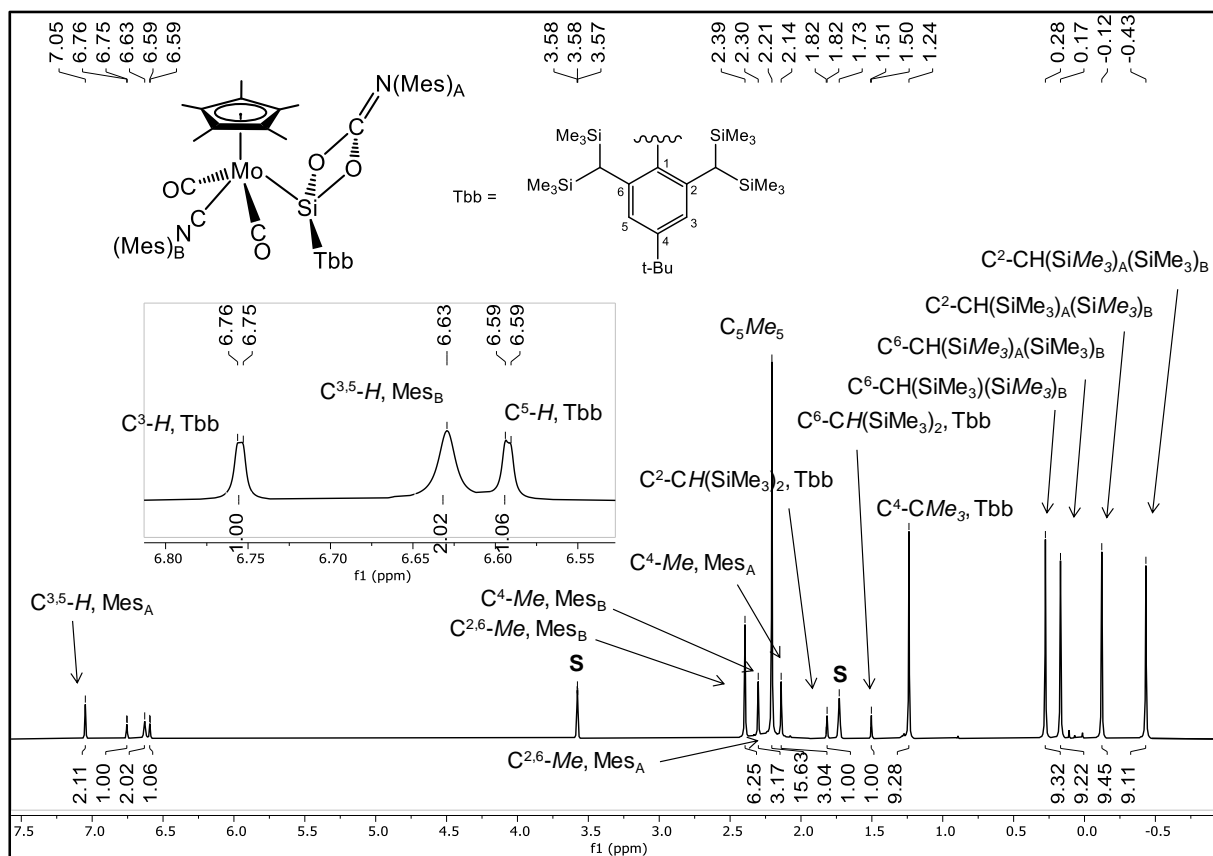


Figure S25. 1H NMR spectrum (500.1 MHz) of **2-Mo** in $(D_8)THF$ at 243 K; the residual proton signal of the deuterated solvent is marked with the letter **S**.

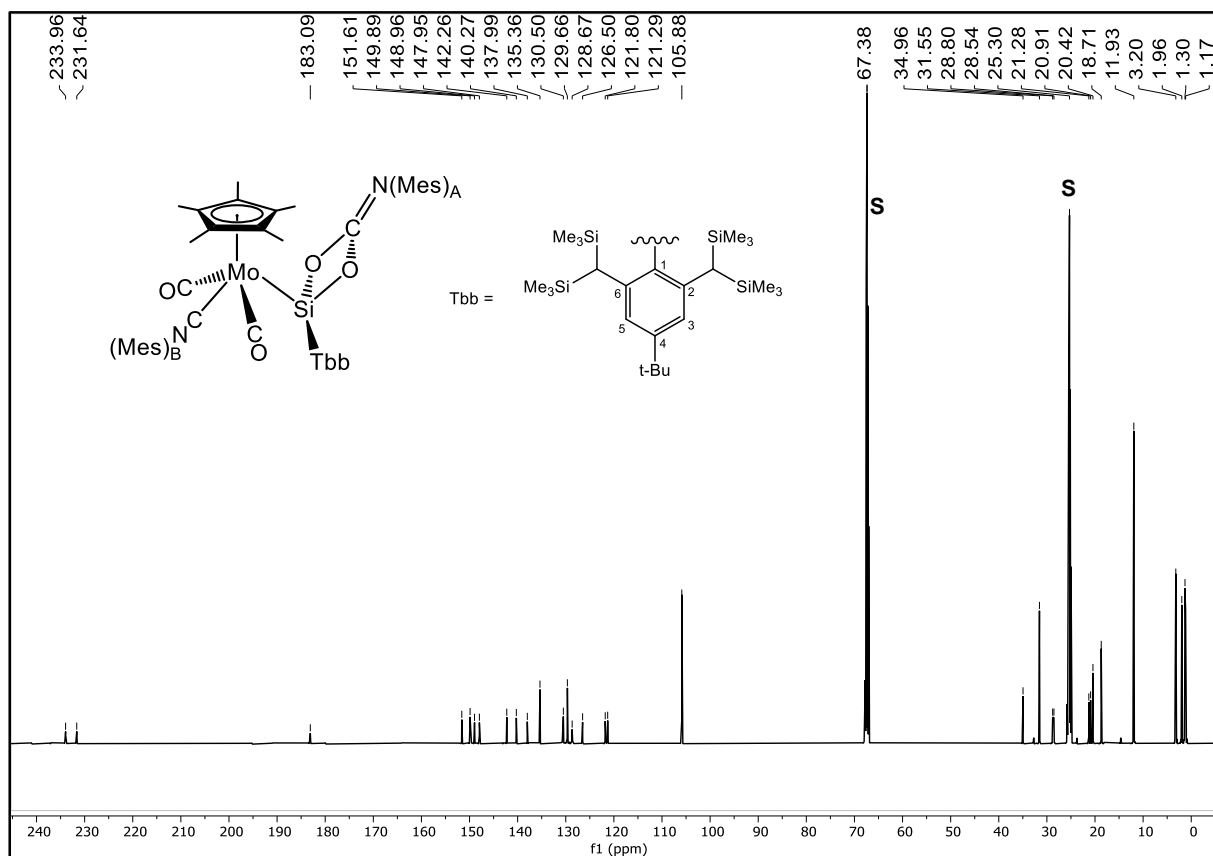


Figure S26. $^{13}C\{^1H\}$ NMR spectrum (125.8 MHz) of **2-Mo** in $(D_8)THF$ at 243 K; the signals of the deuterated solvent are marked with the letter **S**.

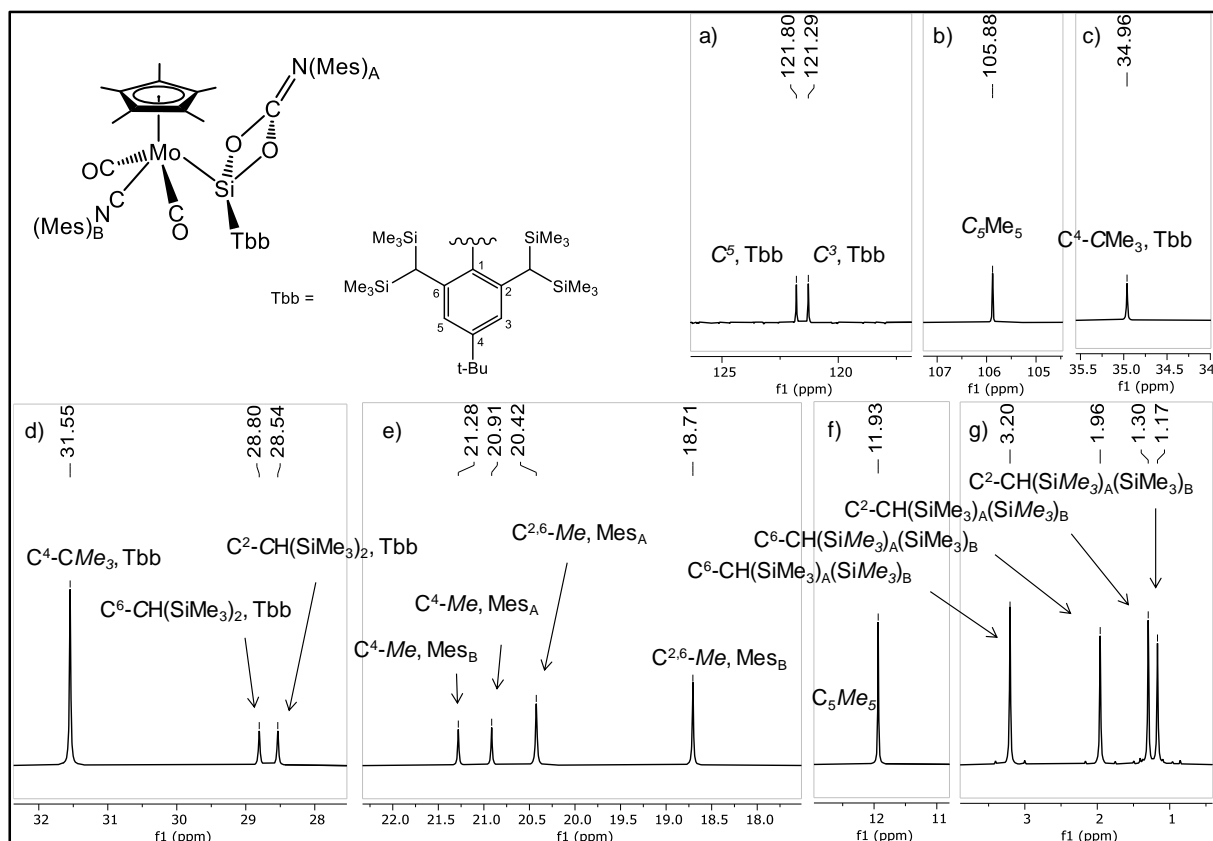


Figure S27. Seven excerpts (a - g) of the $^{13}\text{C}\{^1\text{H}\}$ NMR spectrum (125.8 MHz) of **2-Mo** in $(\text{D}_8)\text{THF}$ at 243 K.

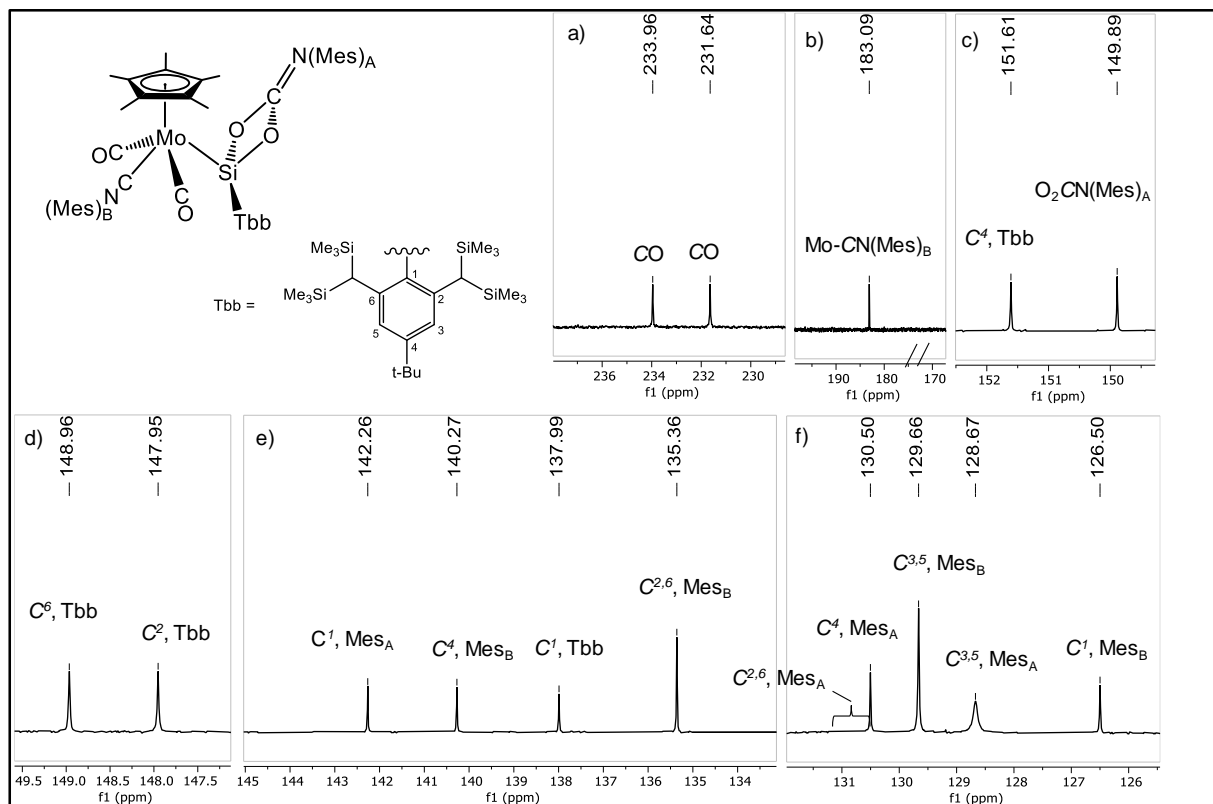


Figure S28. Six excerpts (a - f) of the $^{13}\text{C}\{^1\text{H}\}$ NMR spectrum (125.8 MHz) of **2-Mo** in $(\text{D}_8)\text{THF}$ at 243 K.

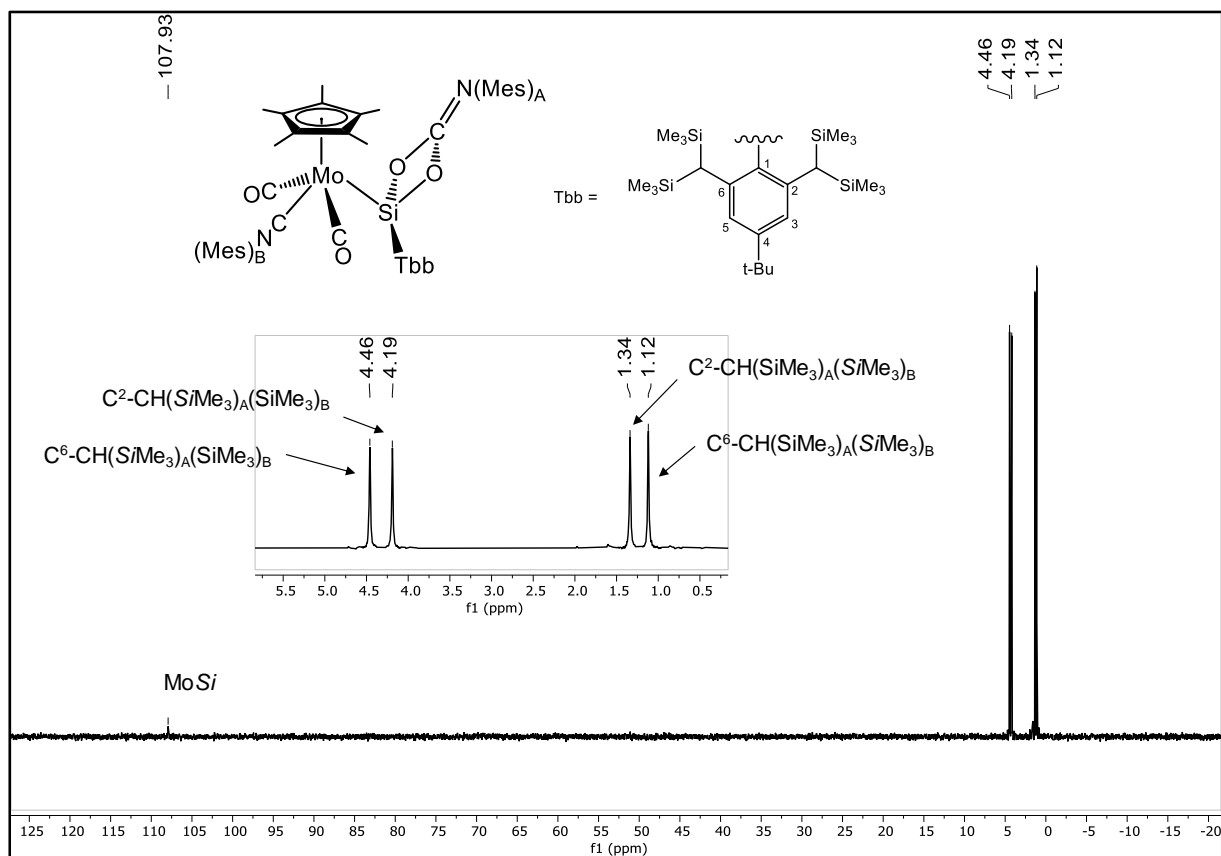


Figure S29. $^{29}\text{Si}\{^1\text{H}\}$ (dept20) NMR (99.36 MHz) spectrum of **2-Mo** in $(\text{D}_8)\text{THF}$ at 243 K. The SiMe_3 signals are also depicted in the inset.

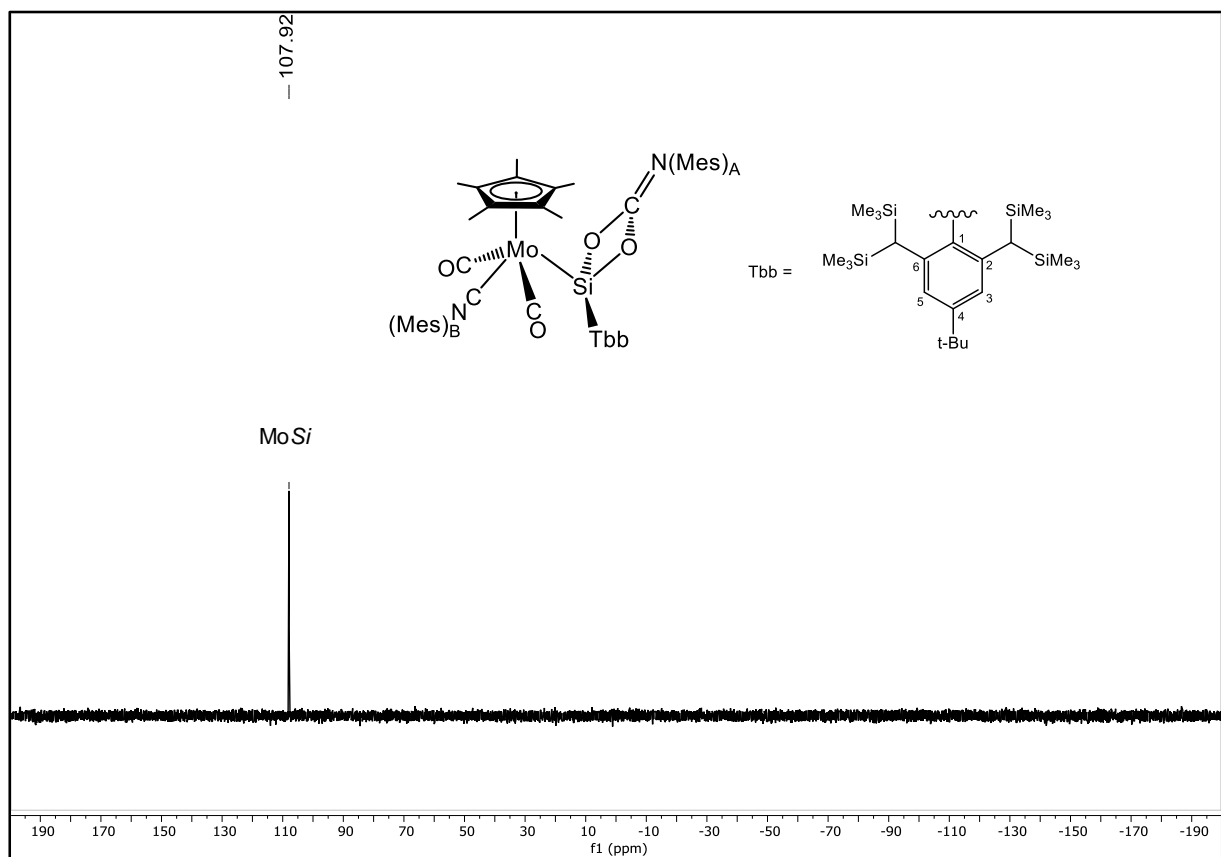


Figure S30. $^{29}\text{Si}\{^1\text{H}\}$ (zgig) NMR (99.36 MHz) spectrum of **2-Mo** in $(\text{D}_8)\text{THF}$ at 243 K.

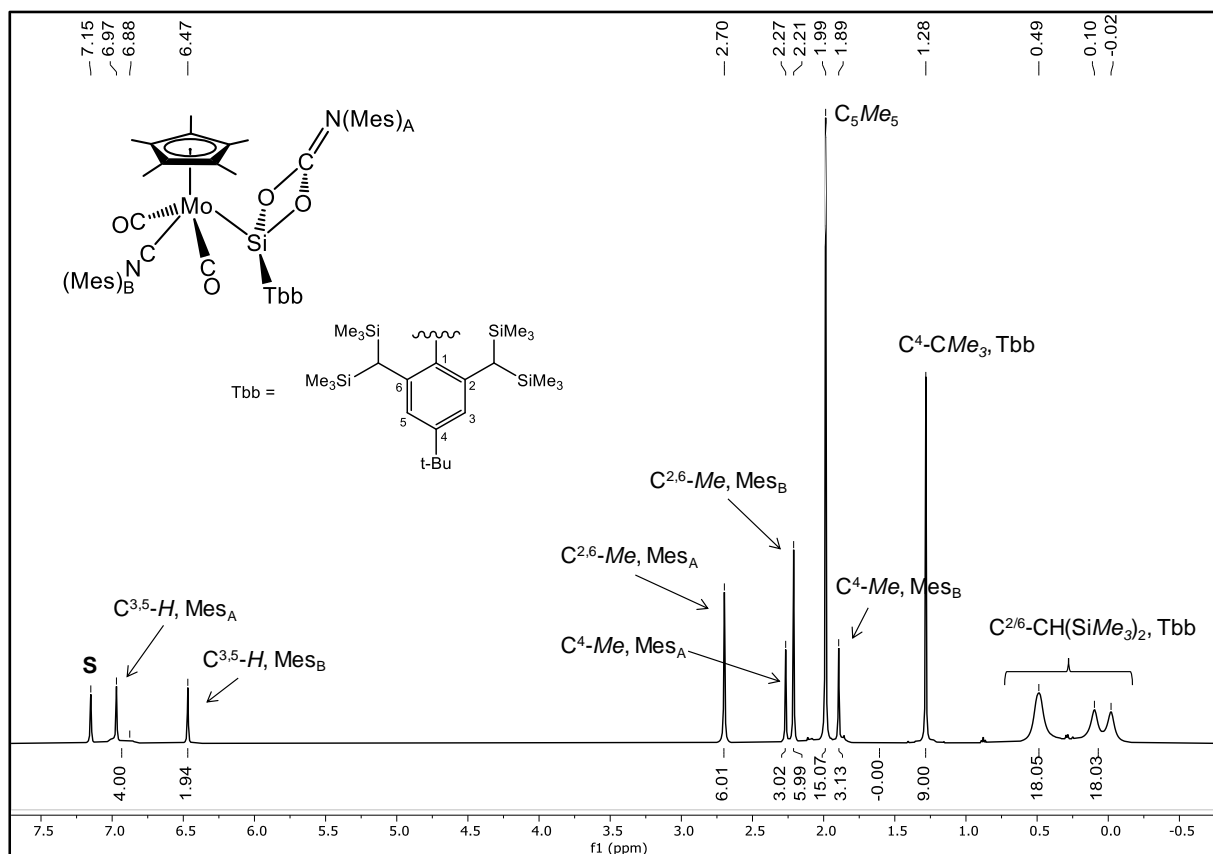


Figure S31. ^1H NMR spectrum (500.1 MHz) of **2-Mo** in (D_6) benzene at 298 K; the residual proton signal of the deuterated solvent is marked with the letter **S**.

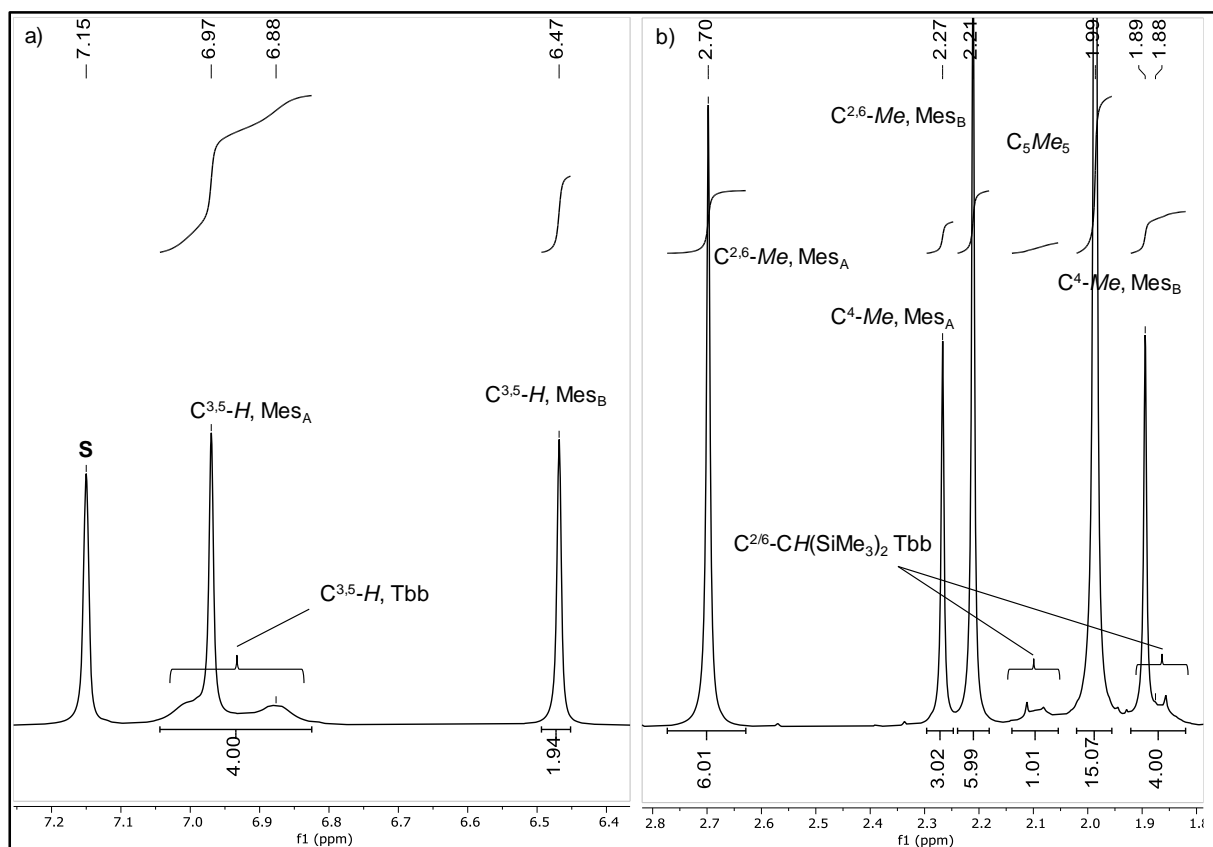


Figure S32. Two excerpts (a, b) of the ^1H NMR spectrum (500.1 MHz) of **2-Mo** in (D_6) benzene at 298 K; the residual proton signal of the deuterated solvent is marked with the letter **S**.

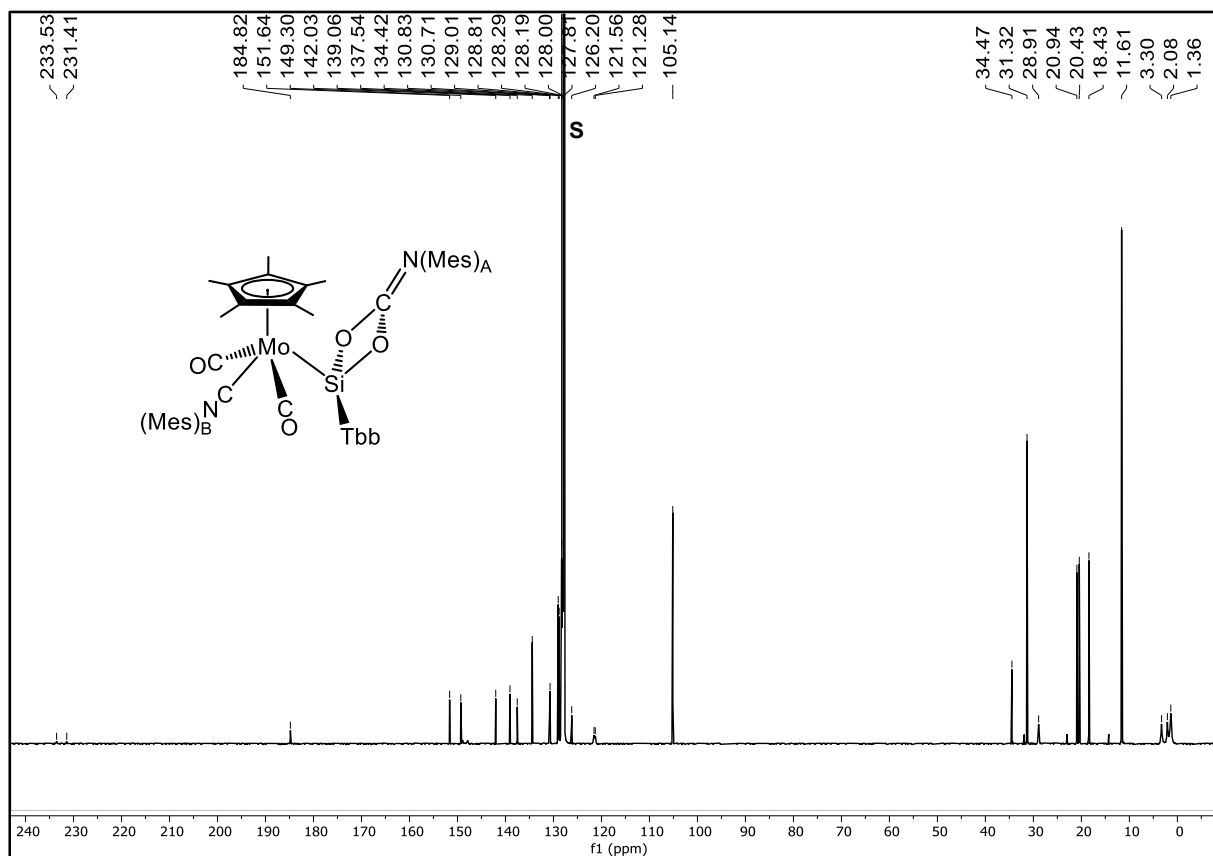


Figure S33. $^{13}\text{C}\{^1\text{H}\}$ NMR spectrum (125.8 MHz) of **2-Mo** in (D_6) benzene at 298 K; the signal of the deuterated solvent is marked with the letter **S**.

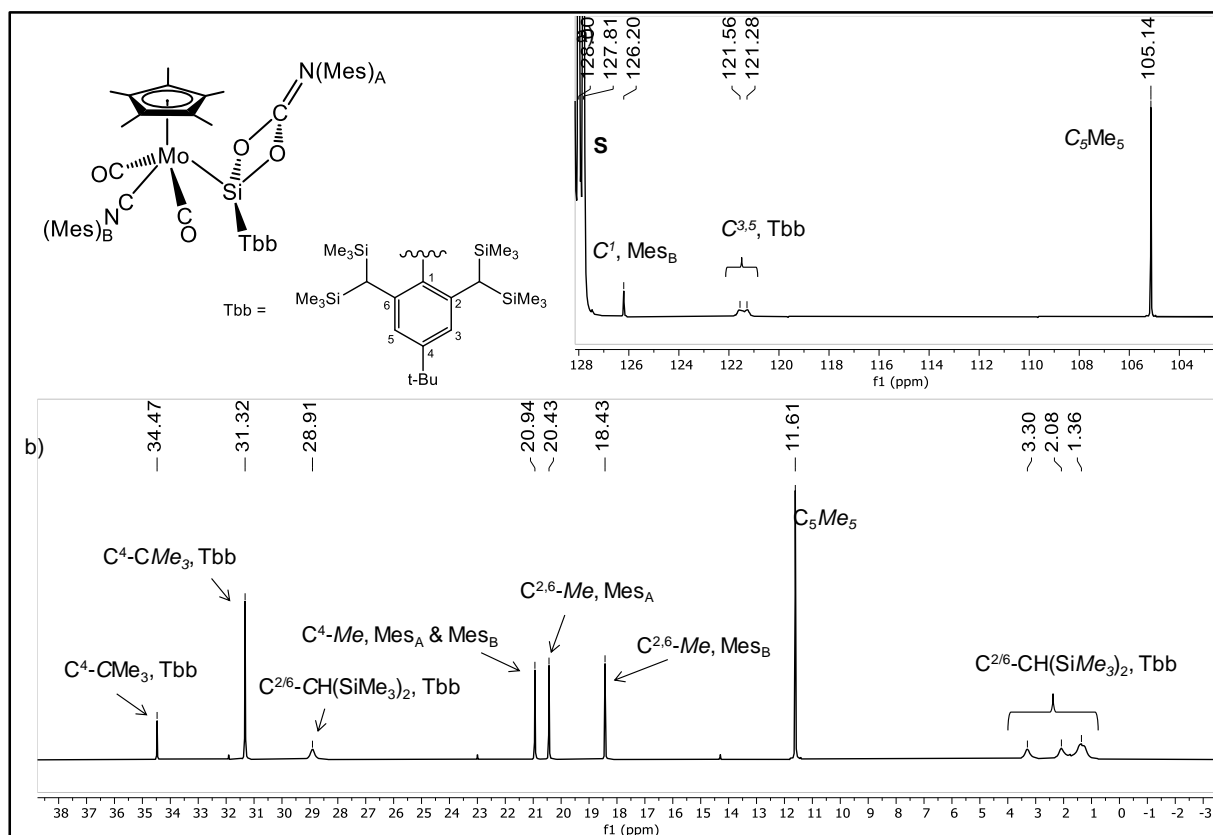


Figure S34. Two excerpts (a, b) of the $^{13}\text{C}\{^1\text{H}\}$ NMR spectrum (125.8 MHz) of **2-Mo** in (D_6) benzene at 298 K.

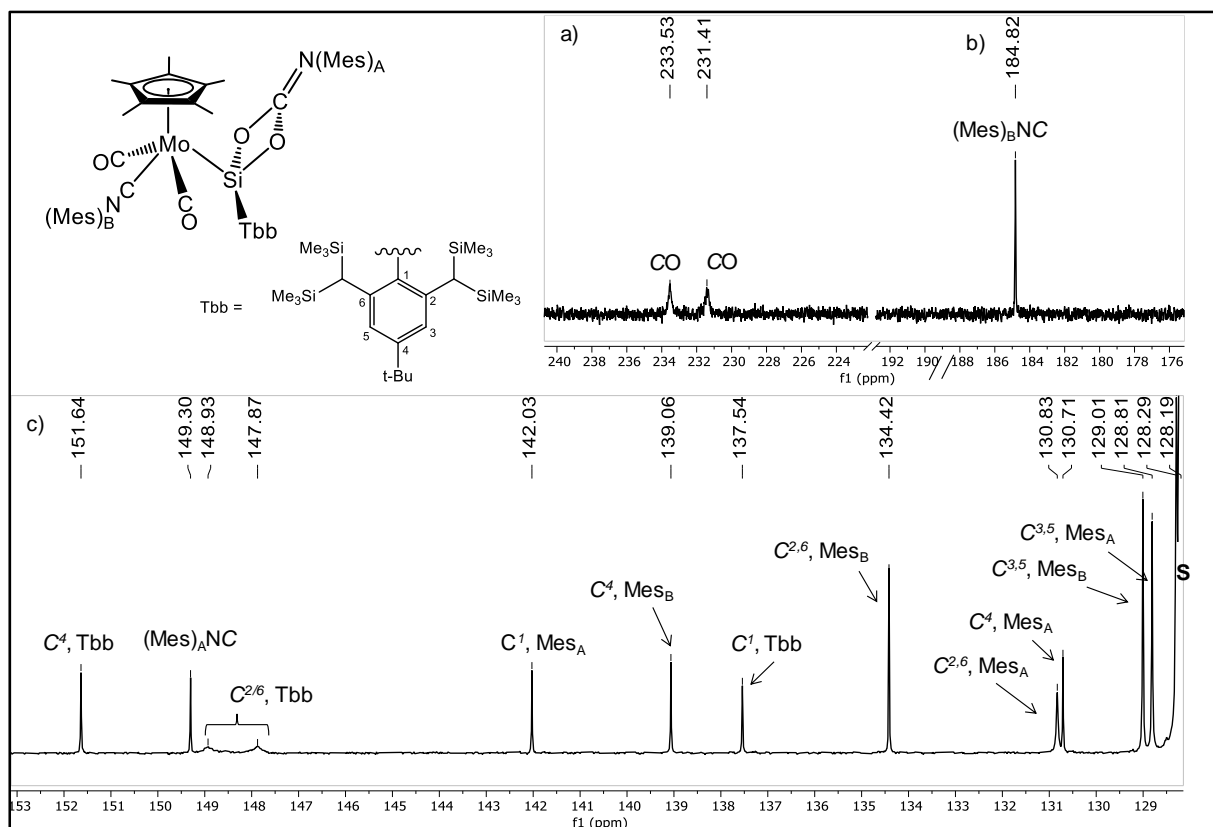


Figure S35. Three excerpts (a - c) of the $^{13}\text{C}\{^1\text{H}\}$ NMR spectrum (125.8 MHz) of **2-Mo** in (D_6) benzene at 298 K.

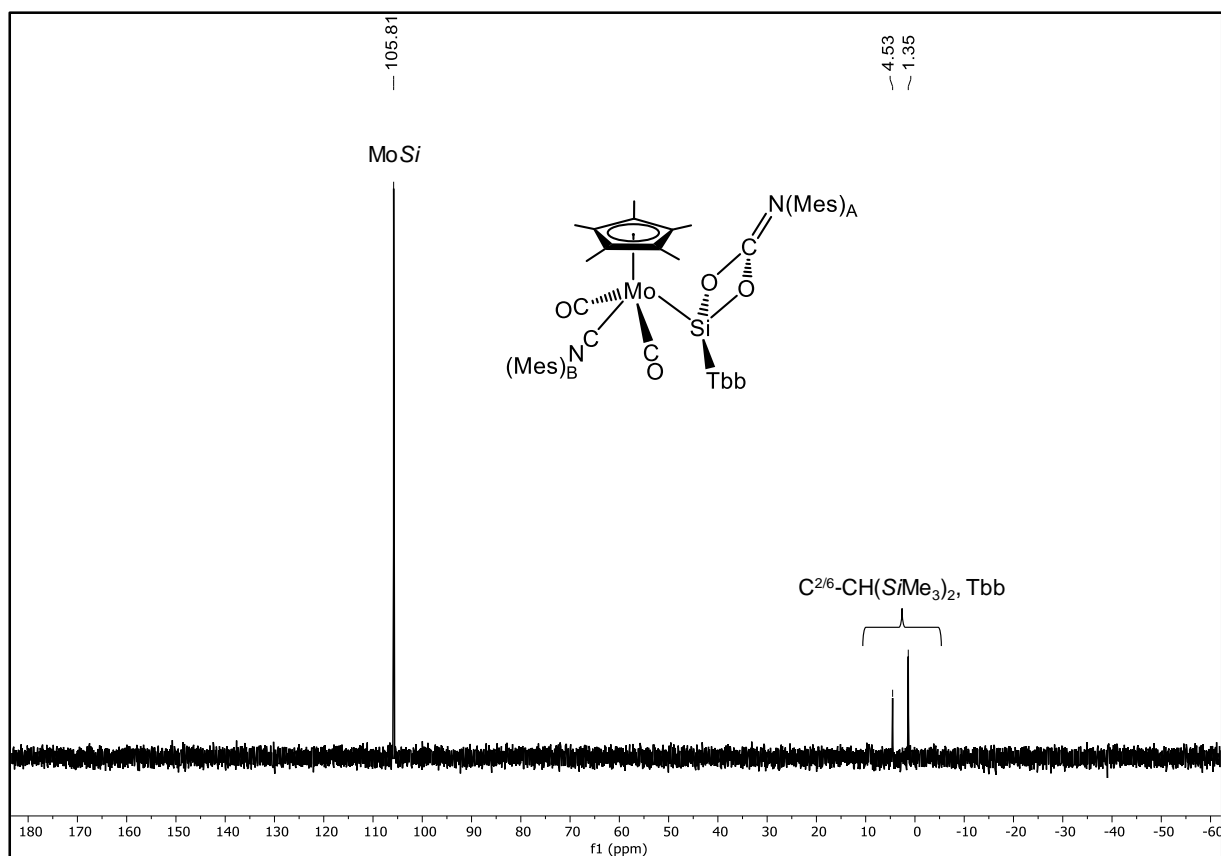


Figure S36. $^{29}\text{Si}\{^1\text{H}\}$ (zgig) NMR (99.36 MHz) spectrum of **2-Mo** in (D_6) benzene at 298 K.

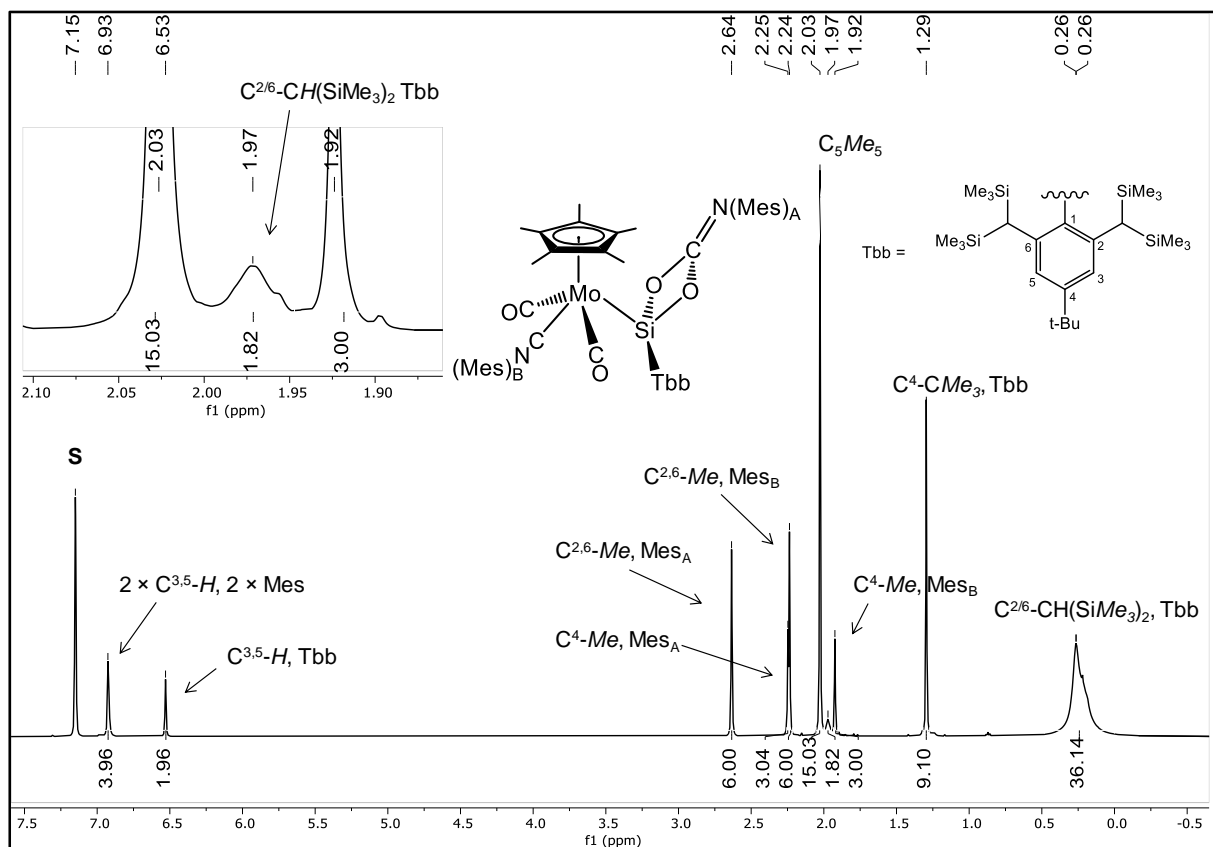


Figure S37. ^1H NMR spectrum (500.1 MHz) of **2-Mo** in (D_6) benzene at 348 K; the residual proton signal of the deuterated solvent is marked with the letter **S**. An excerpt of the spectrum is shown in inset.

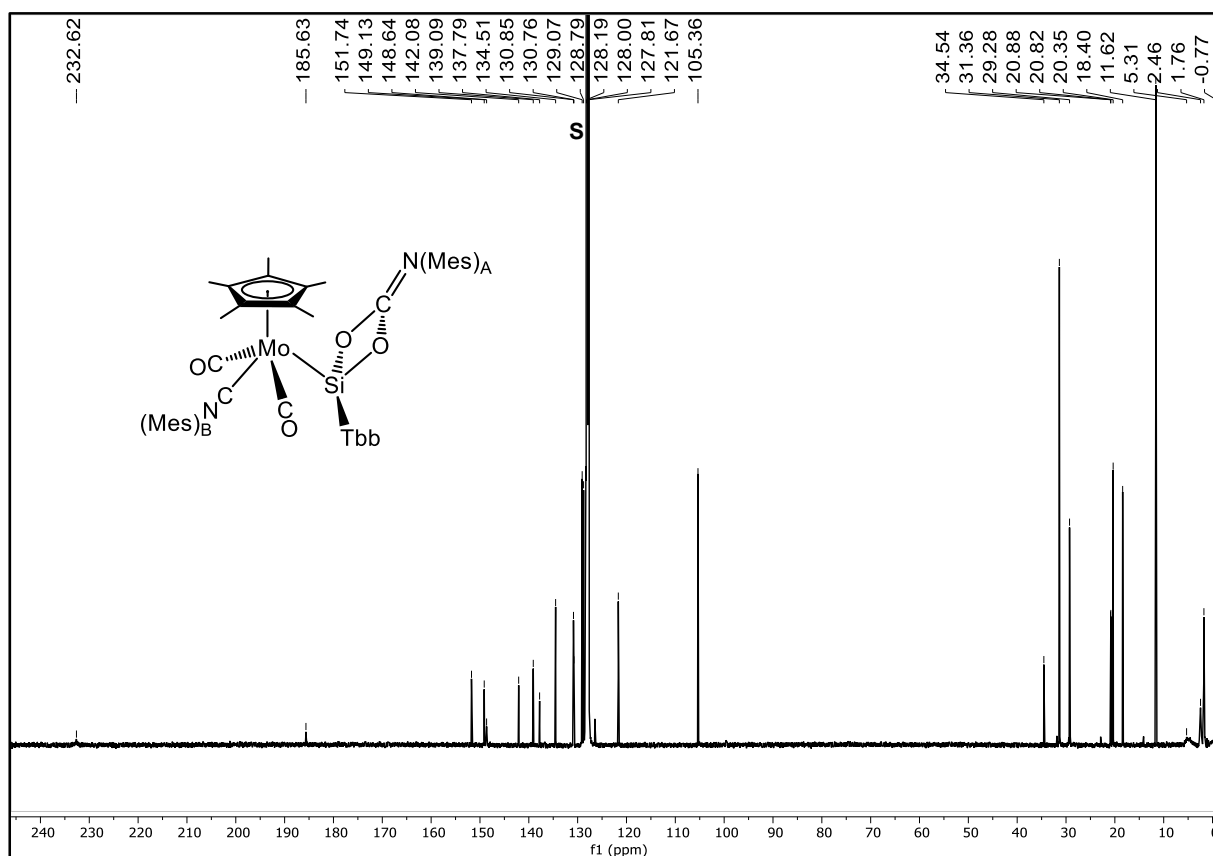


Figure S38. $^{13}\text{C}\{^1\text{H}\}$ NMR spectrum (125.8 MHz) of **2-Mo** in (D_6) benzene at 348 K; the signal of the deuterated solvent is marked with the letter **S**.

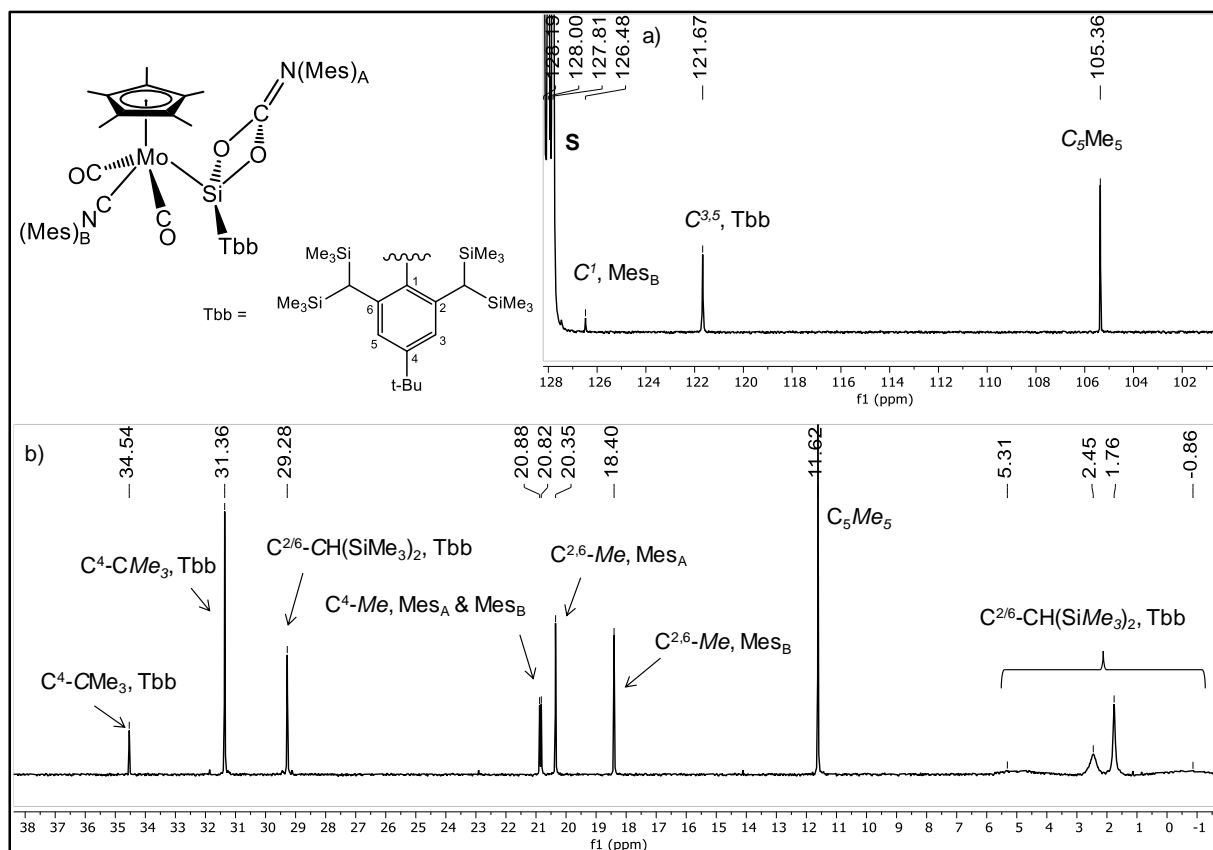


Figure S39. Two excerpts (a, b) of the $^{13}\text{C}\{^1\text{H}\}$ NMR spectrum (125.8 MHz) of **2-Mo** in (D_6) benzene at 348 K.

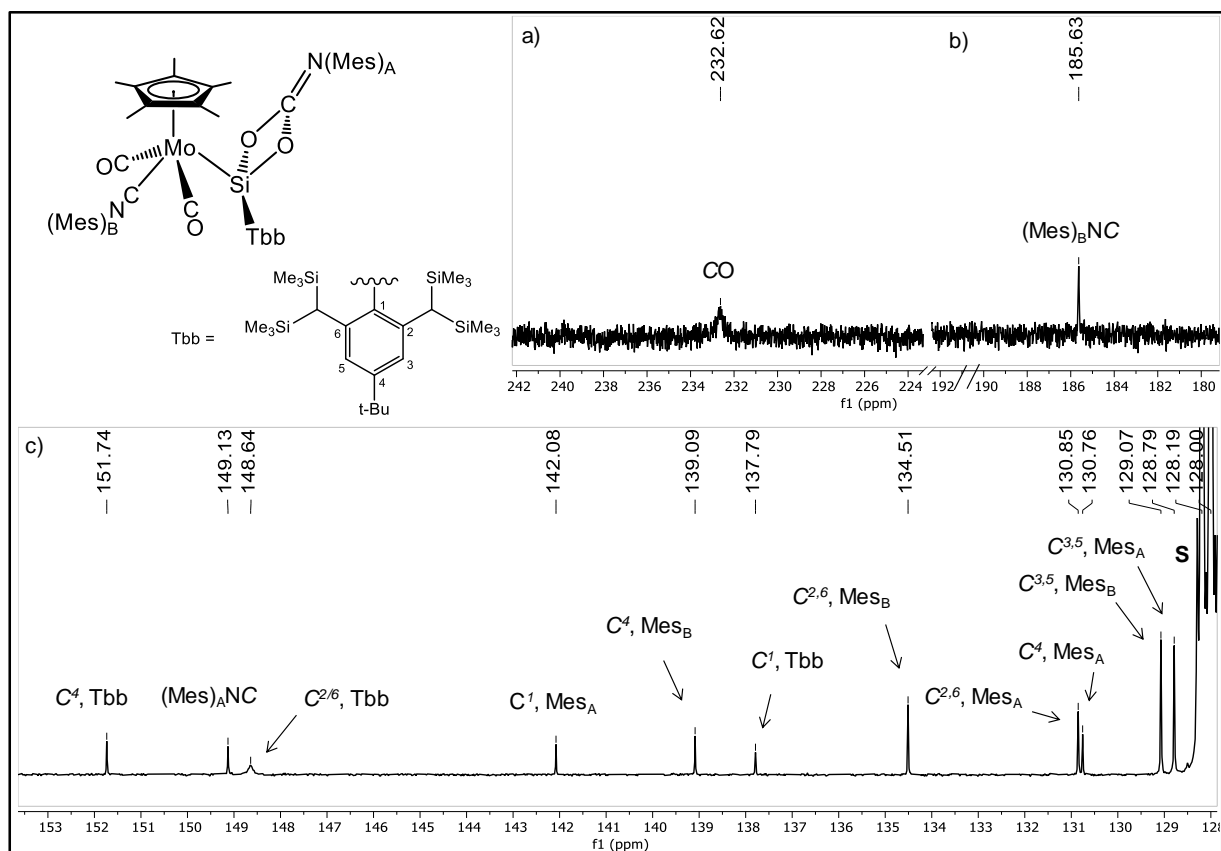
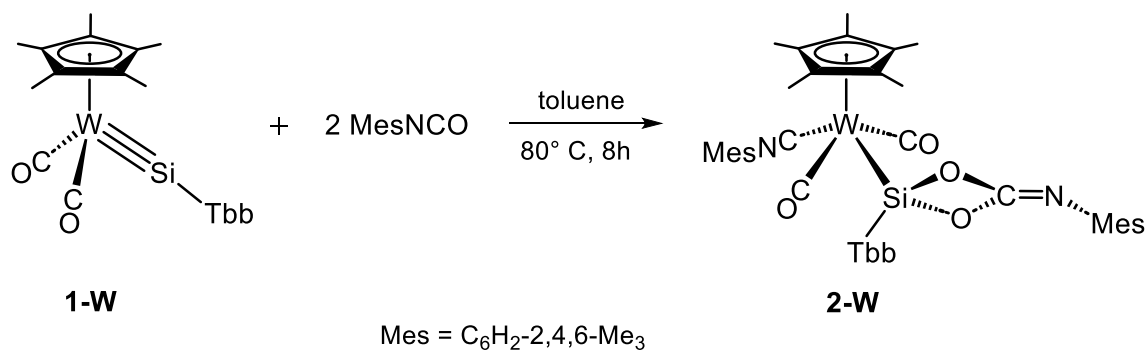


Figure S40. Three excerpts (a - c) of the $^{13}\text{C}\{^1\text{H}\}$ NMR spectrum (125.8 MHz) of **2-Mo** in (D_6) benzene at 348 K.

2.5 [W(Cp*)(CO)₂(CNMes){Si(Tbb)(κ²O,O'-O₂CNMes)}] (**2-W**)



A mixture of the silylidyne complex **1-W** (150 mg, 0.176 mmol, 1.00 equiv.) and mesityl isocyanate (57 mg, 0.35 mmol, 2.0 equiv.) was dissolved in 5 mL of toluene at room temperature and the orange-red reaction solution was heated at 80 °C for 8 hours. During this time, the colour of the solution changed to yellow-brown. ¹H NMR and IR spectroscopic analysis of an aliquot of the reaction solution showed the selective formation of complex **2-W**. The reaction solution was evaporated to dryness under reduced pressure and the yellow-brown residue was washed with *n*-pentane (3 × 2 mL). The creamy white solid obtained was dried in a fine vacuum at 40 °C for 1 hour. Yield: 185 mg (0.157 mmol, 89% from **1-W**).

Elemental analysis calcd (%) for C₅₆H₈₆N₂O₄Si₅W (1175.56 g/mol): C 57.22, H 7.37, N 2.38; found: C 56.80, H 7.42, N 2.30%.

Complex **2-W** is an air sensitive, creamy white solid that melts with decomposition at 228 °C. It is sparingly soluble in *n*-pentane, *n*-hexane and good soluble in Et₂O, benzene and toluene.

Spectroscopy:

The ¹H, ¹³C{¹H} NMR spectra of compound **2-W** in (D₆)benzene at 298 K show the same features as those of **2-Mo**. A similar dynamic process can be assumed as proposed for **2-Mo** in Section 2.4, page S21 to explain the broadening of individual signals.

ATR-IR (solid, 298 K, *Figure S41* and *Figure S42*): $\tilde{\nu}$ (cm⁻¹) = 2960 (w), 2947 (w), 2902 (w), 2862 (vw), 2091 (s) [ν (CN)], 1955 (m) [ν (CO)], 1891 (vs) [ν (CO)], 1708 (s) [ν (NCO₂)], 1692 (s) [ν (NCO₂)], 1609 (vw), 1591 (vw), 1527 (vw), 1477 (w), 1431 (w), 1396 (w), 1381 (w), 1262 (w, sh), 1247 (m), 1180 (vw), 1163 (vw), 1148 (vw), 1074 (vw), 1034 (vw), 996 (w), 976 (m), 949 (m), 939 (sh), 878 (m, sh), 839 (vs), 787 (w), 773 (w), 757 (vw), 736 (w), 719 (m), 682 (w), 662 (s), 645 (vw), 636 (vw), 614 (vw), 593 (m), 573 (s), 554 (m, sh), 542 (m, sh), 519 (vw), 501 (vw), 490 (w), 477 (m, sh), 462 (s), 425 (m).

IR (toluene, 298 K, *Figure S43*): $\tilde{\nu}$ (cm⁻¹) = 2097 (s) [ν (CN)], 1954 (m) [ν (CO)], 1894 (vs) [ν (CO)], 1710 (m) [ν (NCO₂)], 1694 (m) [ν (NCO₂)].

¹H NMR (500.1 MHz, (D₆)benzene, 298 K, *Figure S44* and *Figure S45*): δ (ppm) = -0.01 (br s, $\Delta\nu_{1/2}$ = 24.8 Hz, 9H, C^{2/6}-CH(SiMe₃)_A(SiMe₃), Tbb), 0.11 (br s, $\Delta\nu_{1/2}$ = 26.0 Hz, 9H, C^{2/6}-CH(SiMe₃)(SiMe₃)_B, Tbb), 0.49 (br s, $\Delta\nu_{1/2}$ = 33.2 Hz, 18H, C^{2/6}-CH(SiMe₃)₂, Tbb), 1.29 (s, 9H,

C^4-CMe_3 , Tbb), 1.87 (br s, $\Delta\nu_{1/2} = \sim 20$ Hz, 1H, $C^{2/6}-CH(SiMe_3)_2$, Tbb), 1.91 (s, 3H, C^4-Me , Mes_B), 2.06 (s, 15H, C_5Me_5), 2.09 (br s, $\Delta\nu_{1/2} = \sim 20$ Hz, 1H, $C^{2/6}-CH(SiMe_3)_2$, Tbb), 2.22 (s, 6H, $C^{2,6}-Me$, Mes_B), 2.27 (s, 3H, C^4-Me , Mes_A), 2.70 (s, 6H, $C^{2,6}-Me$, Mes_A), 6.49 (q, $^4J(^1H, ^1H) = 0.7$ Hz, 2H, $C^{3,5}-H$, Mes_B), 6.88 (br s, $\Delta\nu_{1/2} = 23.0$ Hz, 1H, C^3-H , Tbb), 6.98 (s, 2H, $C^{3,5}-H$, Mes_A), 7.00 (br s, $\Delta\nu_{1/2} = \sim 30$ Hz, 1H, C^5-H , Tbb).

$^{13}C\{^1H\}$ NMR (125.8 MHz, (D₆)benzene, 298 K, Figure S46, Figure S47 and Figure S48): δ (ppm) = 1.4 (br s, 6C, $\Delta\nu_{1/2} = 45.9$ Hz, $C^{2/6}-CH(SiMe_3)_2$, Tbb), 2.1 (br s, $\Delta\nu_{1/2} = 27.9$ Hz, 3C, $C^{2/6}-CH(SiMe_3)_2$, Tbb), 3.3 (br s, $\Delta\nu_{1/2} = 25$ Hz, 3C, $C^{2/6}-CH(SiMe_3)_2$, Tbb), 11.6 (s, 5C, C_5Me_5), 18.4 (s, 2C, $C^{2,6}-Me$, Mes_B), 20.4 (s, 2C, $C^{2,6}-Me$, Mes_A), 20.92 & 20.94 (s, 2C, C^4-Me , Mes_A & Mes_B), 28.8 (br s, $\Delta\nu_{1/2} = 42.2$ Hz, 2C, $C^{2/6}-CH(SiMe_3)_2$, Tbb), 31.3 (s, 3C, C^4-CMe_3 , Tbb), 34.5 (s, 1C, C^4-CMe_3 , Tbb), 103.6 (s, 5C, C_5Me_5), 121.2 (br s, $\Delta\nu_{1/2} = 24.0$ Hz, 1C, C^5-H , Tbb), 121.6 (br s, $\Delta\nu_{1/2} = 29.4$ Hz, 1C, C^3-H , Tbb), 126.4 (s, 1C, C^1 , Mes_B), 128.8 (s, 2C, $C^{3,5}-H$, Mes_A), 129.0 (s, 2C, $C^{3,5}-H$, Mes_B), 130.7 (s, 1C, C^4 , Mes_A), 130.9 (s, 2C, $C^{2,6}$, Mes_A), 134.5 (s, 2C, $C^{2,6}$, Mes_B), 137.3 (s, 1C, C^1 , Tbb), 139.0 (s, 1C, C^4 , Mes_B), 142.0 (s, 1C, C^1 , Mes_A), 148.0 (br s, $\Delta\nu_{1/2} = 28.9$ Hz, 1C, $C^{2/6}$, Tbb), 149.0 (br s, $\Delta\nu_{1/2} = 27.1$ Hz, 1C, $C^{2/6}$, Tbb), 149.4 (s, 1C, $O_2CN(Mes)_A$), 151.6 (s, 1C, C^4-CMe_3 , Tbb), 171.2 (s, 1C, $W-CN(Mes)_B$), 223.2 (br s, $\Delta\nu_{1/2} = 37.1$ Hz, 1C, CO), 225.1 (br s, $\Delta\nu_{1/2} = 28.0$ Hz, 1C, CO).

$^{29}Si\{^1H\}$ NMR (99.36 MHz, (D₆)benzene, 298 K, Figure S49): δ (ppm) = 1.3 (s, 2Si, $C^{2/6}-CH(SiMe_3)_2$), 4.5 (br s, $\Delta\nu_{1/2} = 18.2$ Hz, 2Si, $C^{2/6}-CH(SiMe_3)_2$), 88.6 (s, $^1J(^{183}W, ^{29}Si) = 79.6$ Hz, 1Si, WS).

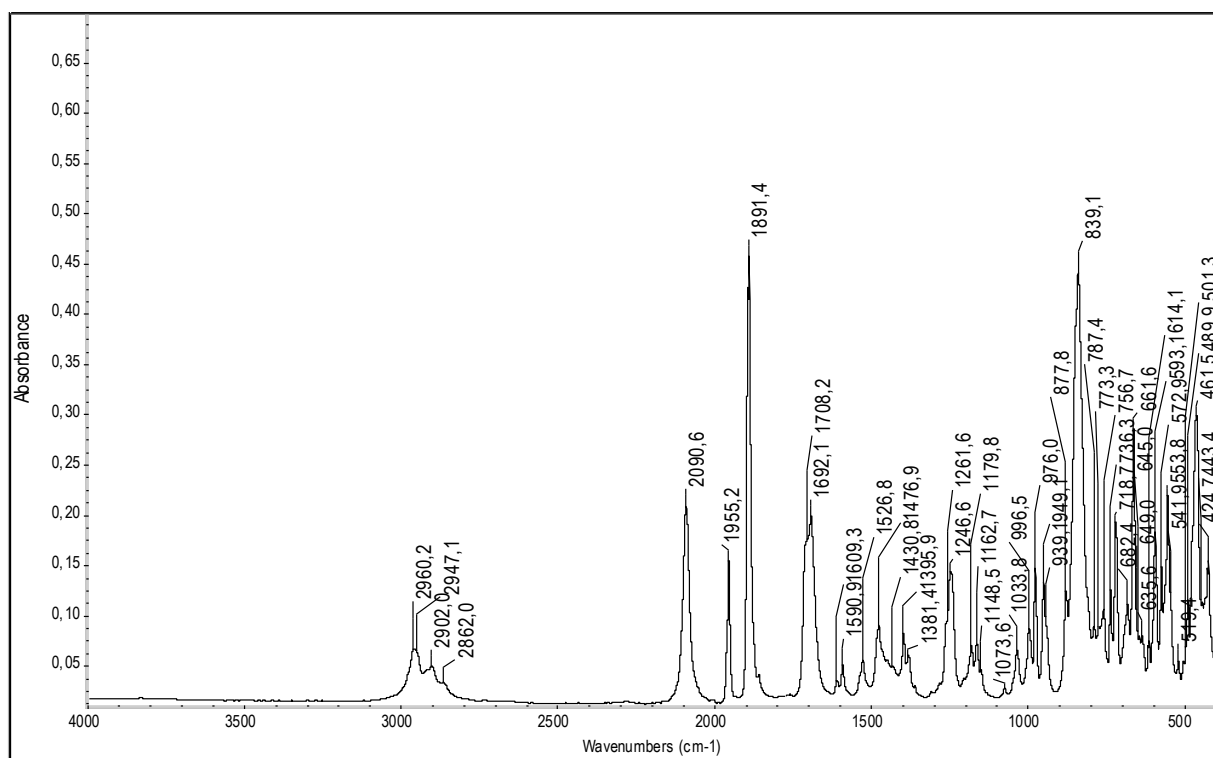


Figure S41. ATR-IR spectrum of **2-W** in the solid state in the spectral range of 4000 - 400 cm^{-1} .

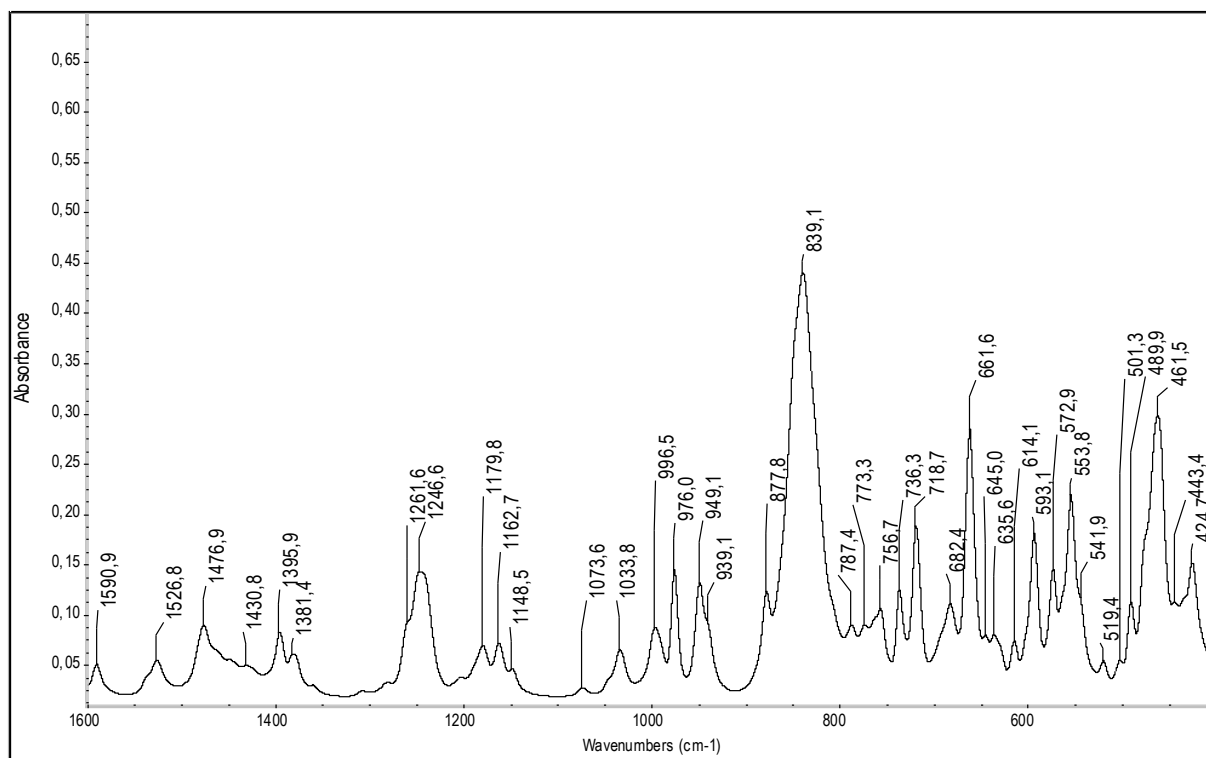


Figure S42. Excerpt of the ATR-IR spectrum of 2-W in the solid state (spectral range: 1600 - 400 cm⁻¹).

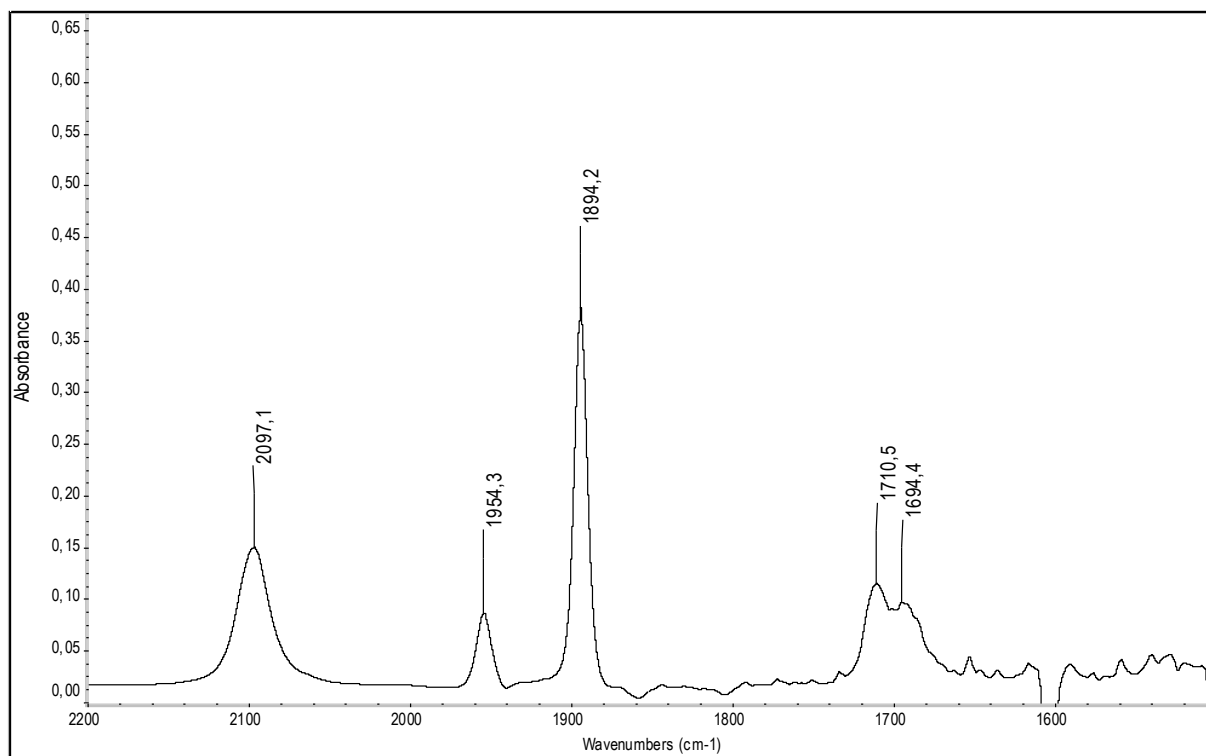


Figure S43. FT-IR spectrum of 2-W in toluene in the spectral range of 2200 - 1500 cm⁻¹.

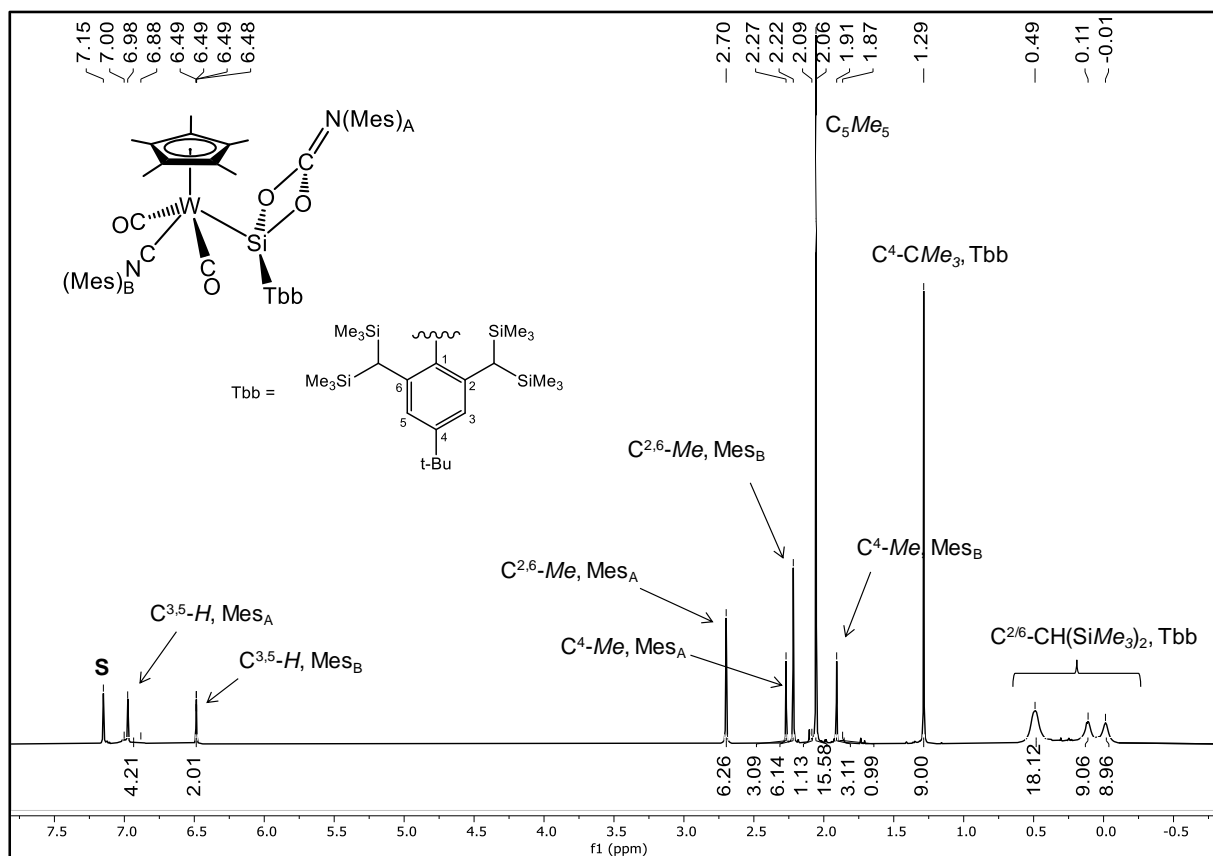


Figure S44. ^1H NMR spectrum (500.1 MHz) of **2-W** in (D_6) benzene at 298 K; the residual proton signal of the deuterated solvent is marked with the letter **S**.

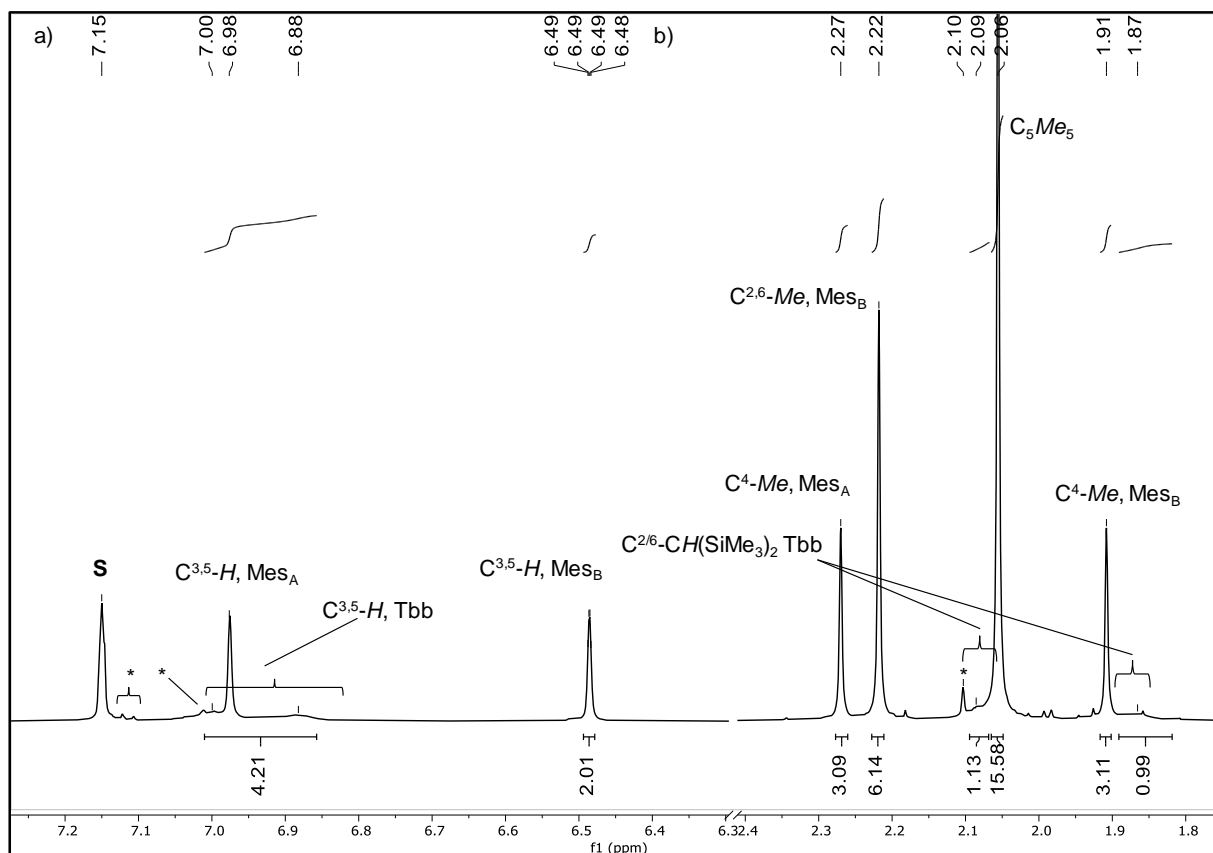


Figure S45. Two excerpts (a, b) of the ^1H NMR spectrum (500.1 MHz) of **2-W** in (D_6) benzene at 298 K; the residual proton signal of the deuterated solvent is marked with the letter **S** and the signal of traces of toluene marked with an asterisk (*)

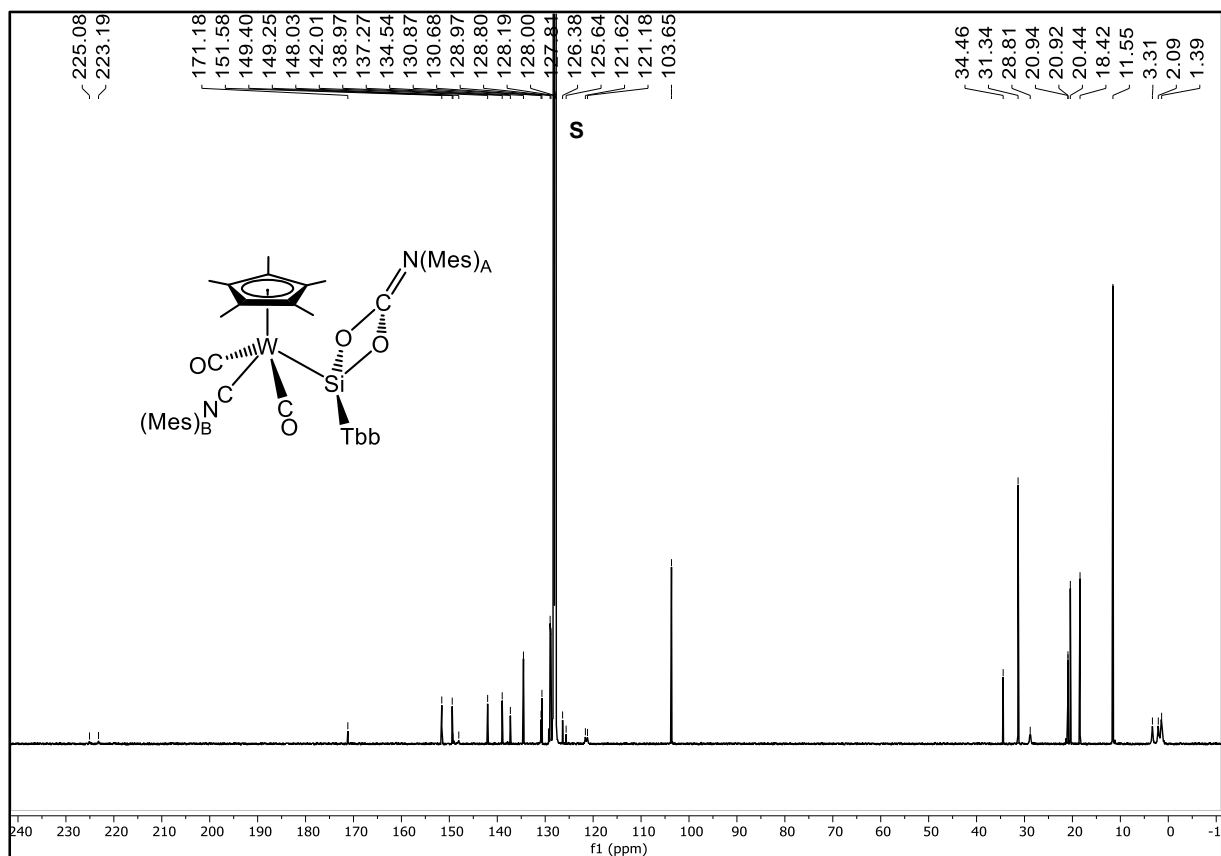


Figure S46. $^{13}\text{C}\{^1\text{H}\}$ NMR spectrum (125.8 MHz) of **2-W** in (D_6) benzene at 298 K; the signal of the deuterated solvent is marked with the letter **S**.

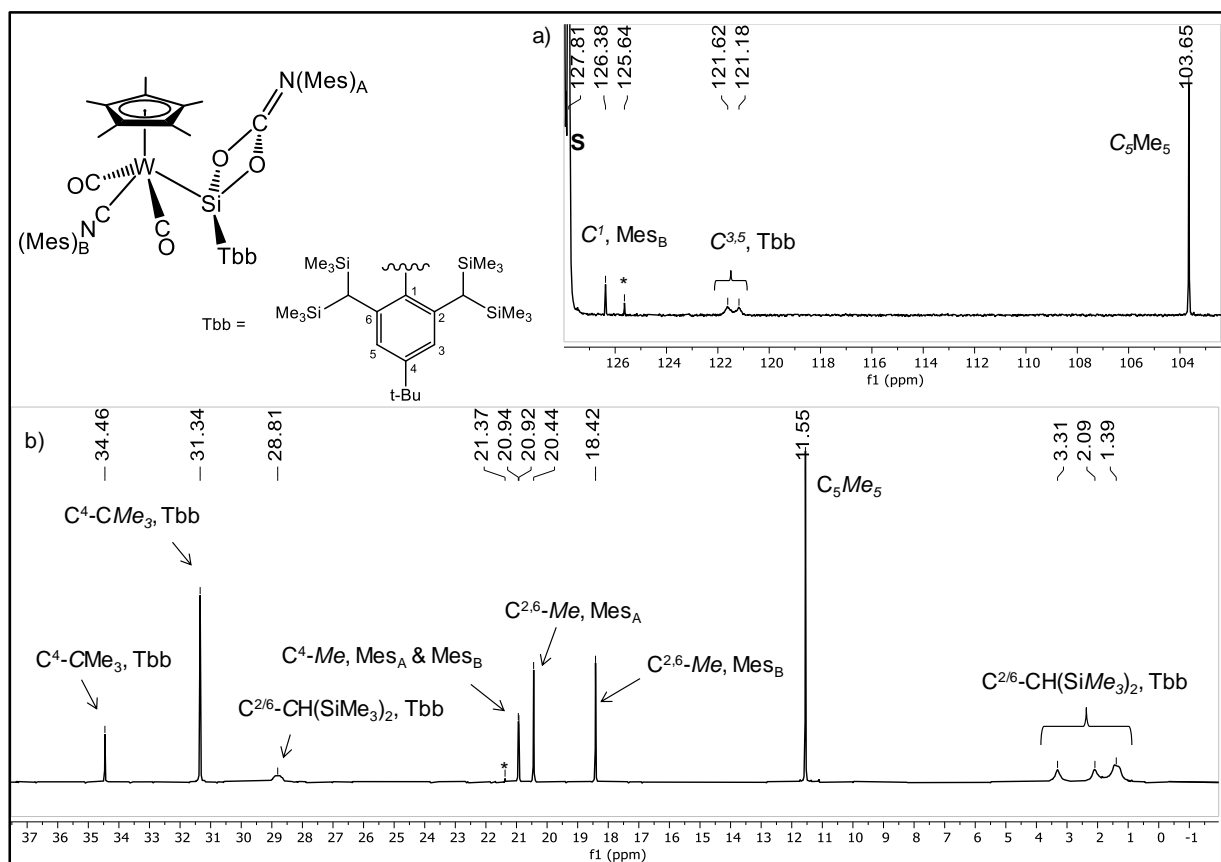


Figure S47. Two excerpts (a, b) of the $^{13}\text{C}\{^1\text{H}\}$ NMR spectrum (125.8 MHz) of **2-W** in (D_6) benzene at 298 K. The signals of traces of toluene are marked with an asterisk (*).

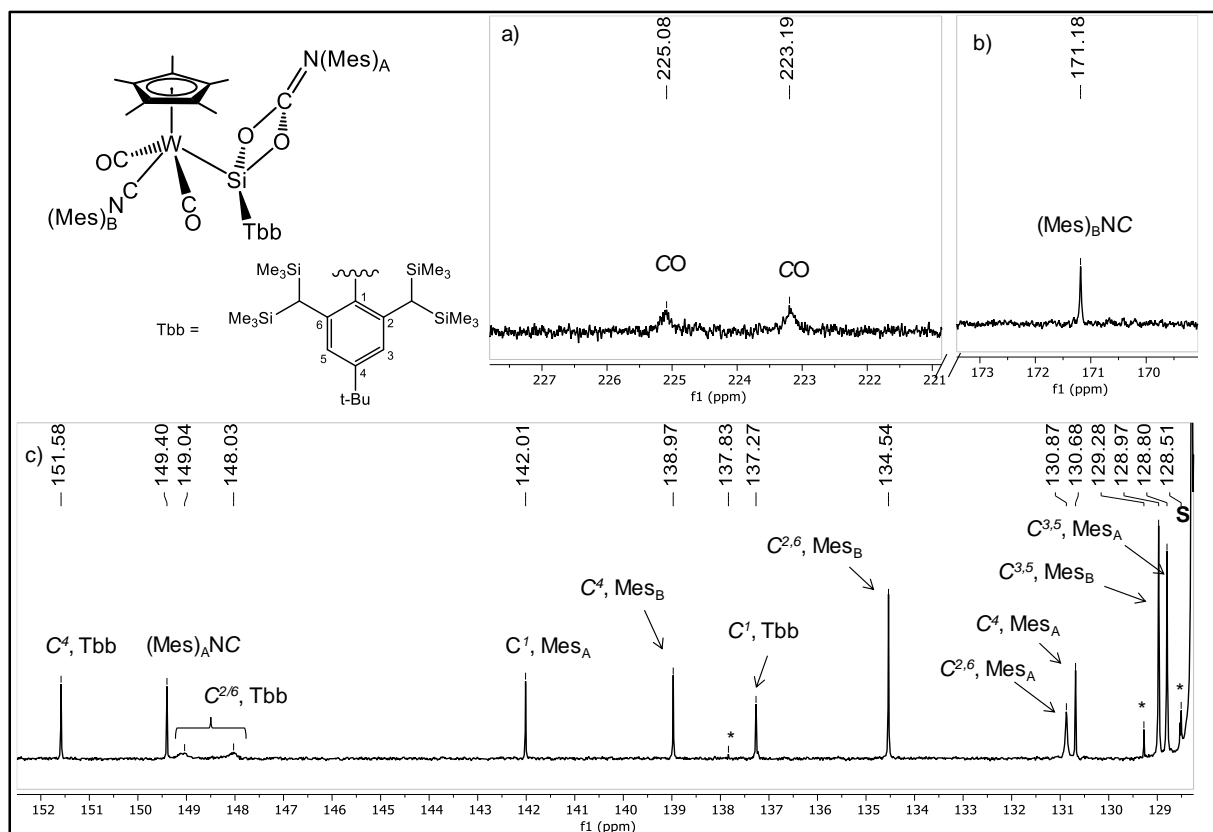


Figure S48. Three excerpts (a - c) of the $^{13}\text{C}\{^1\text{H}\}$ NMR spectrum (125.8 MHz) of **2-W** in (D_6) benzene at 298 K. The signals of traces of toluene are marked with an asterisk (*).

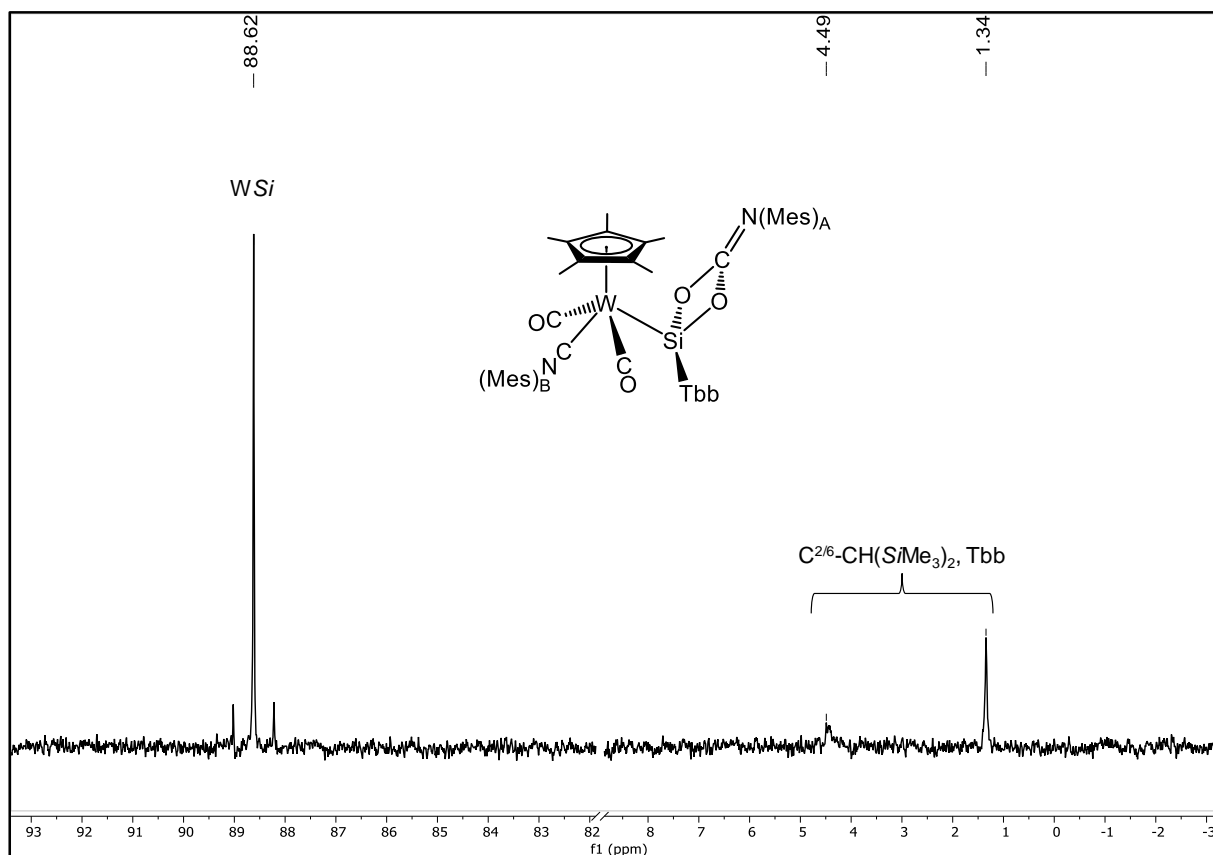
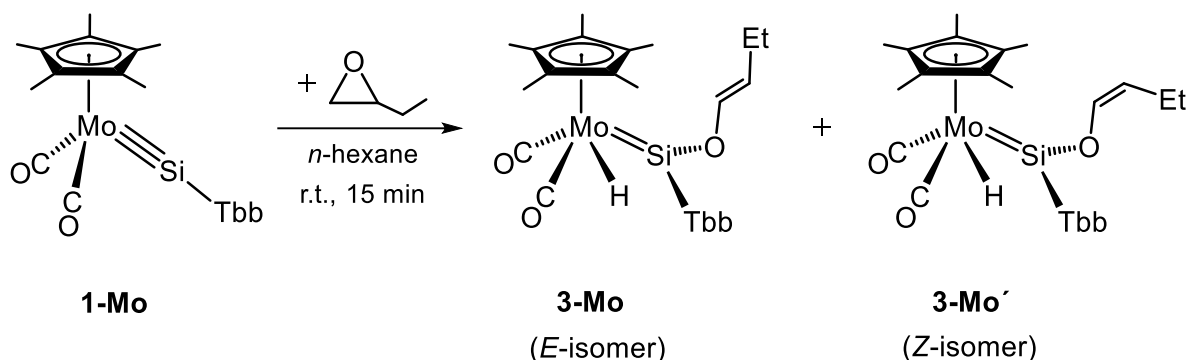


Figure S49. $^{29}\text{Si}\{^1\text{H}\}$ (zgig) NMR (99.36 MHz) spectrum of **2-W** in (D_6) benzene at 298 K.

2.6 $[\text{Mo}(\text{Cp}^*)(\text{H})(\text{CO})_2\{\text{Si}(\text{Tbb})(\text{OCH}=\text{CH}\text{Et})\}]$ (**3-Mo**)

A 0.057 M stock solution of ethyloxirane (6.84 mL, 0.390 mmol, 1.00 equiv.) in *n*-hexane was added dropwise to an orange-red solution of the silyldiylidene complex **1-Mo** (300 mg, 0.392 mmol, 1.00 equiv.) in 10 mL of *n*-hexane. A rapid color change was observed and the resulting brownish yellow reaction solution was stirred at room temperature for 15 minutes. ^1H NMR and IR spectroscopic analysis of an aliquot of the reaction solution showed the formation of the butenenolatosilylidene complex **3-Mo** (*E*-isomer) as the major product along with a second Cp* and Tbb containing product, which on the basis of its ^1H NMR spectroscopic data is presumed to be the *Z*-isomer **3-Mo'**.^[S10] The ratio of the two isomers *E/Z* was calculated as 7:3 using the integral ratio of the NMR signals of the Cp* protons. The reaction solution was concentrated to approximately 1.5 mL and stored at $-20\text{ }^\circ\text{C}$ overnight. The crystallized solid was filtered at $-20\text{ }^\circ\text{C}$ and dried in a fine vacuum at ambient temperature for one hour. ^1H NMR spectroscopic analysis of the solid showed that it was exclusively the *E*-isomer. Yield: 140 mg (0.167 mmol, 43% from **1-Mo**).

Elemental analysis calcd (%) for $\text{C}_{40}\text{H}_{72}\text{MoO}_3\text{Si}_5$ (837.36 g/mol): C 57.37, H 8.67; found: C 57.01, H 8.69%.

Complex **3-Mo** is a very air sensitive, pale-yellow solid that melts with decomposition at $165\text{ }^\circ\text{C}$. It is good soluble in *n*-pentane, *n*-hexane, benzene and toluene.

Spectroscopy:

The IR spectrum of **3-Mo** in *n*-hexane solution shows three $\nu(\text{CO})$ bands at 1956, 1882 and 1872 cm^{-1} as well as a shoulder on the low frequency side of the band at 1956 cm^{-1} suggesting the presence of two isomers in solution. In comparison, the NMR spectra of **3-Mo** shows only

[S10] The following ^1H NMR signals of **3-Mo'** were extracted from the ^1H NMR spectrum of the mixture (300.1 MHz, (D_6) benzene, 298 K) of the reaction mixture: δ (ppm) = 0.26 (s, 18H, $\text{C}^{2,6}\text{-CH}(\text{SiMe}_3)_A(\text{SiMe}_3)_B$, Tbb), 0.31 (s, 18H, $\text{C}^{2,6}\text{-CH}(\text{SiMe}_3)_A(\text{SiMe}_3)_B$, Tbb), 0.99 (t, $^3J(^1\text{H},^1\text{H}) = 7.3\text{ Hz}$, 3H, $\text{OCH}=\text{CHCH}_2\text{CH}_3$), 1.30 (s, 9H, $\text{C}^4\text{-CMe}_3$, Tbb), 1.93 (s, 15H, C_5Me_5), 2.28 (s, $^2J(^{29}\text{Si},^1\text{H}) = 9.2\text{ Hz}$, 2H, $\text{C}^{2,6}\text{-CH}(\text{SiMe}_3)_2$, Tbb), 4.66 (dt, $^3J(^1\text{H},^1\text{H}) = 7.3\text{ Hz}$, $^3J(^1\text{H},^1\text{H}) = 6.3\text{ Hz}$, 1H, $\text{OCH}=\text{CHCH}_2\text{CH}_3$), 6.87 (s, 2H, $\text{C}^{3,5}\text{-H}$, Tbb), 6.97 (dt, $^3J(^1\text{H},^1\text{H}) = 6.3\text{ Hz}$, $^4J(^1\text{H},^1\text{H}) = 1.6\text{ Hz}$, 1H, $\text{OCH}=\text{CHCH}_2\text{CH}_3$).

one set of signals, the number and multiplicity of which indicate a time-averaged C_s -symmetric structure. For example, one Mo-H resonance is observed in the ^1H NMR spectrum at $\delta = -7.42$ ppm flanked by ^{29}Si satellites ($J(^{29}\text{Si}, ^1\text{H}) = 22$ Hz) (Figure S54), only one ^{13}C NMR signal for the two carbonyl ligands at $\delta = 235.0$ ppm (Figure S56) and one ^{29}Si NMR signal for the Mo=Si group at 215.8 ppm (Figure S57). The IR and NMR spectroscopic features of **3-Mo** in solution were rationalized in combination with quantum chemical studies. In solution two *cis* isomers *cis*_{anti} and *cis*_{syn} are in equilibrium. Interconversion of the two *cis* isomers proceeds via a C_s -symmetric transition state with a *trans* geometry and is too fast on the NMR spectroscopic time scale. Details of the quantum chemical studies, the geometries and electronic structures of the two *cis* isomers and their dynamics are presented in Section 4.2.

ATR-IR (solid, 298 K, Figure S50 and Figure S51): $\tilde{\nu}$ (cm^{-1}) = 2957 (m), 2900 (w), 2856 (w, br), 2773 (vw), 1931 (s) [$\nu(\text{CO})$], 1851 (vs) [$\nu(\text{CO})$], 1739 (w) [$\nu(\text{Mo-H})$], 1663 (w) [$\nu(\text{C}=\text{C})_{\text{OCH}=\text{CH}}]$], 1589 (w), 1533 (w), 1477 (vw), 1454 (w), 1429 (vw), 1396 (w), 1384 (vw), 1360 (vw), 1258 (m), 1245 (s), 1176 (w), 1166 (w), 1141 (m), 1134 (m), 1096 (w), 1068 (vw), 1030 (vw), 1008 (w), 996 (w), 959 (w), 929 (w), 910 (vw), 883 (m), 860 (m, sh), 835 (vs), 803 (s), 772 (m), 746 (w), 722 (w), 687 (m), 663 (vw), 645 (w), 625 (vw), 605 (w), 559 (w), 544 (w), 507 (m, sh), 497 (m), 478 (m), 424 (m).

IR (*n*-hexane, 298 K, Figure S52): $\tilde{\nu}$ (cm^{-1}) = 1956 (vs) [$\nu(\text{CO})$], 1882 (s) [$\nu(\text{CO})$], 1872 (s) [$\nu(\text{CO})$], 1662 (w) [$\nu(\text{C}=\text{C})_{\text{OCH}=\text{CH}}]$], 1590 (w) and 1532 (w) [$\nu(\text{C}=\text{C})_{\text{Tbb}}$].

^1H NMR (500.1 MHz, (D_6)benzene, 298 K, Figure S53 and Figure S54): δ (ppm) = -7.42 (s, $J(^{29}\text{Si}, ^1\text{H}) = 22$ Hz, 1H, Mo-H), 0.25 (s, 18H, $\text{C}^{2,6}\text{-CH}(\text{SiMe}_3)_\text{A}(\text{SiMe}_3)_\text{B}$, Tbb),^[S11] 0.32 (s, 18H, $\text{C}^{2,6}\text{-CH}(\text{SiMe}_3)_\text{A}(\text{SiMe}_3)_\text{B}$, Tbb), 1.00 (t, $^3J(^1\text{H}, ^1\text{H}) = 7.4$ Hz, 3H, $\text{OCH}=\text{CHCH}_2\text{CH}_3$), 1.30 (s, 9H, $\text{C}^4\text{-CMe}_3$, Tbb), 1.95 (s, 15H, C_5Me_5), 2.01 (quintd, $^3J(^1\text{H}, ^1\text{H}) = 7.4$ Hz, $^3J(^1\text{H}, ^1\text{H}) = 1.4$ Hz, 2H, $\text{OCH}=\text{CHCH}_2\text{CH}_3$), 2.23 (s, $^2J(^{29}\text{Si}, ^1\text{H}) = 9.2$ Hz, 2H, $\text{C}^{2,6}\text{-CH}(\text{SiMe}_3)_2$, Tbb), 5.36 (dt, $^3J(^1\text{H}, ^1\text{H}) = 12.1$ Hz, $^3J(^1\text{H}, ^1\text{H}) = 7.4$ Hz, 1H, $\text{OCH}=\text{CHCH}_2\text{CH}_3$), 6.87 (s, 2H, $\text{C}^{3,5}\text{-H}$, Tbb), 7.01 (dt, $^3J(^1\text{H}, ^1\text{H}) = 12.1$ Hz, $^4J(^1\text{H}, ^1\text{H}) = 1.3$ Hz, 1H, $\text{OCH}=\text{CHCH}_2\text{CH}_3$).

$^{13}\text{C}\{^1\text{H}\}$ NMR (125.8 MHz, (D_6)benzene, 298 K, Figure S55 and Figure S56): δ (ppm) = 1.1 (s, $^1J(^{29}\text{Si}, ^{13}\text{C}) = 51.1$ Hz, 6C, $\text{C}^{2,6}\text{-CH}(\text{SiMe}_3)_\text{A}(\text{SiMe}_3)_\text{B}$, Tbb), 1.2 (s, $^1J(^{29}\text{Si}, ^{13}\text{C}) = 51.4$ Hz, 6C, $\text{C}^{2,6}\text{-CH}(\text{SiMe}_3)_\text{A}(\text{SiMe}_3)_\text{B}$, Tbb), 11.9 (s, 5C, C_5Me_5), 15.3 (s, 1C, $\text{OCH}=\text{CHCH}_2\text{CH}_3$), 21.6 (s, 1C, $\text{OCH}=\text{CHCH}_2\text{CH}_3$), 31.2 (s, 3C, $\text{C}^4\text{-CMe}_3$, Tbb), 31.6 (s, 2C, $^1J(^{29}\text{Si}, ^{13}\text{C}) = 41.9$ Hz, $\text{C}^{2,6}\text{-CH}(\text{SiMe}_3)_2$, Tbb), 34.5 (s, 1C, $\text{C}^4\text{-CMe}_3$, Tbb), 103.2 (s, 5C, C_5Me_5), 114.5 (s, 1C,

[S11] The diastereotopic SiMe_3 groups of the $\text{C}^{2,6}$ -bonded Dsi substituents were labeled with the subscript letters A and B, respectively. The letter A was used for the more shielded ^1H NMR signal of the SiMe_3 groups, and the SiMe_3 signals in the $^{13}\text{C}\{^1\text{H}\}$ and $^{29}\text{Si}\{^1\text{H}\}$ NMR spectra were assigned by $^1\text{H}\text{-}^{13}\text{C}$ HSQC, $^1\text{H}\text{-}^{13}\text{C}$ HMBC and $^1\text{H}\text{-}^{29}\text{Si}\text{-HMBC}$ experiments.

OCH=CH_{Et}), 121.3 (s, 2C, C^{3,5}-H, Tbb), 140.7 (s, 1C, OCH=CH_{Et}), 141.0 (s, 1C, Si-C¹, Tbb), 146.9 (s, 2C, C^{2,6}, Tbb), 151.8 (s, 1C, C⁴, Tbb), 235.0 (s, 2C, 2 × CO).

²⁹Si{¹H} NMR (99.36 MHz, (D₆)benzene, 298 K, Figure S57): δ (ppm) = 2.8 (s, 2Si, C^{2,6}-CH(SiMe₃)_A(SiMe₃)_B, Tbb), 2.9 (s, 2Si, C^{2,6}-CH(SiMe₃)_A(SiMe₃)_B, Tbb), 215.8 (s, 1Si, Mo=Si).

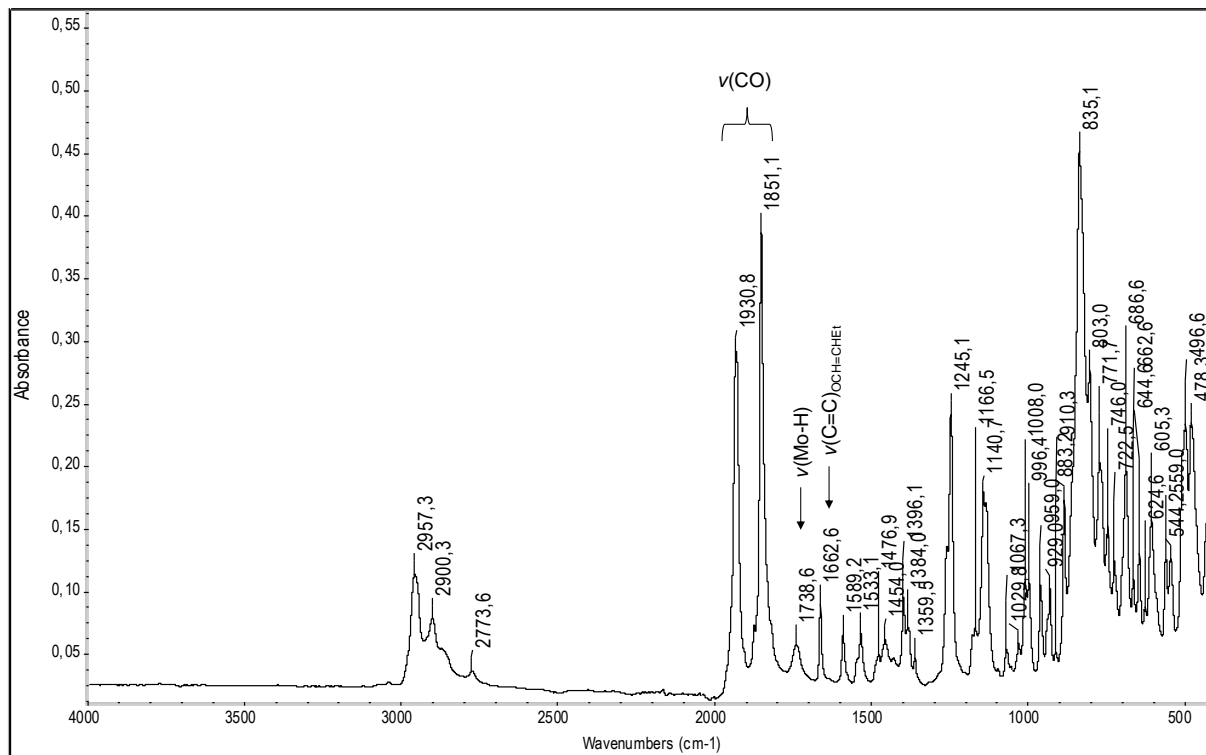


Figure S50. ATR-IR spectrum of **3-Mo** in the solid state in the spectral range of 4000 - 400 cm⁻¹.

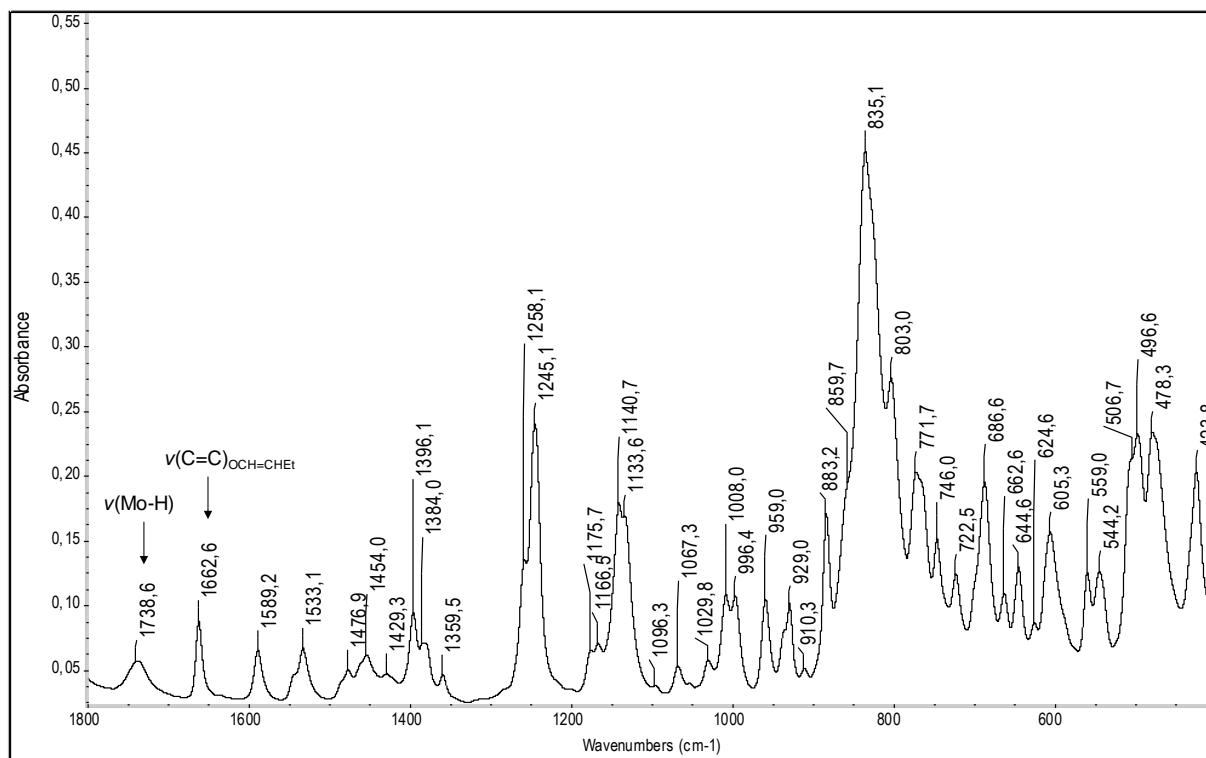


Figure S51. Excerpt of the ATR-IR spectrum of **3-Mo** in the solid state (spectral range: 1800 - 400 cm⁻¹).

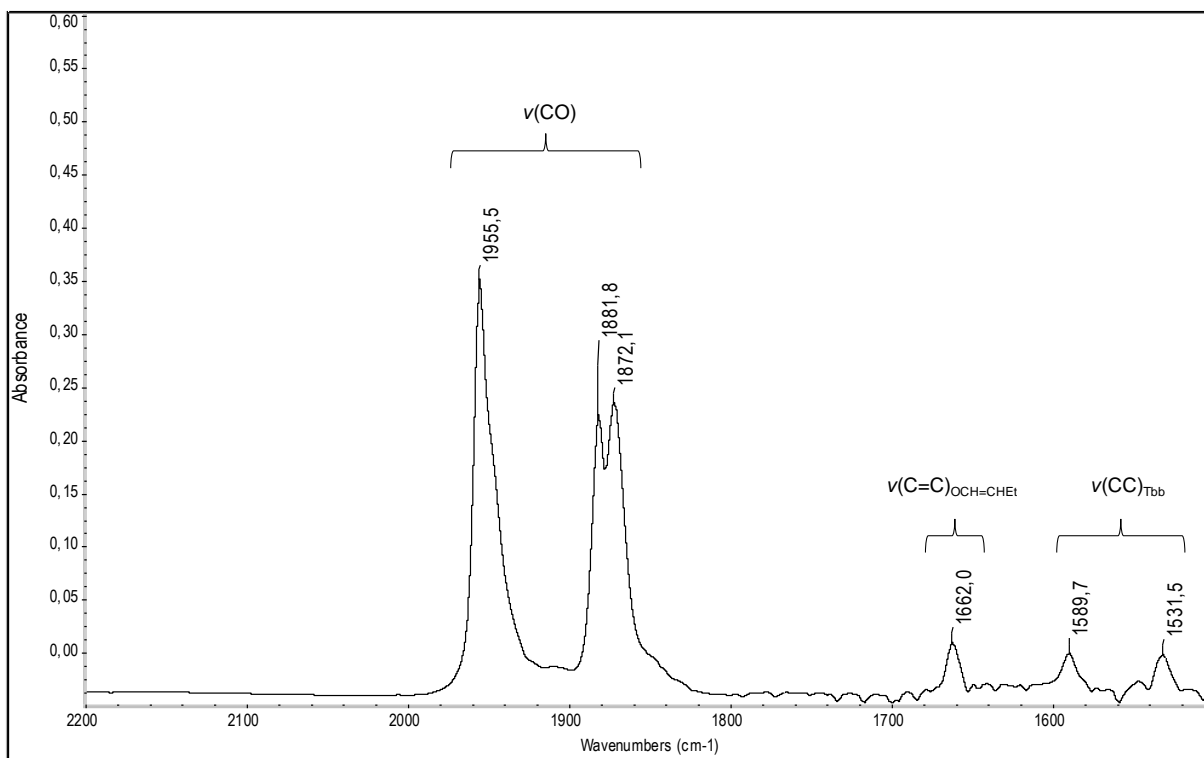


Figure S52. FT-IR spectrum of **3-Mo** in *n*-hexane in the spectral range of 2200 - 1500 cm^{-1} .

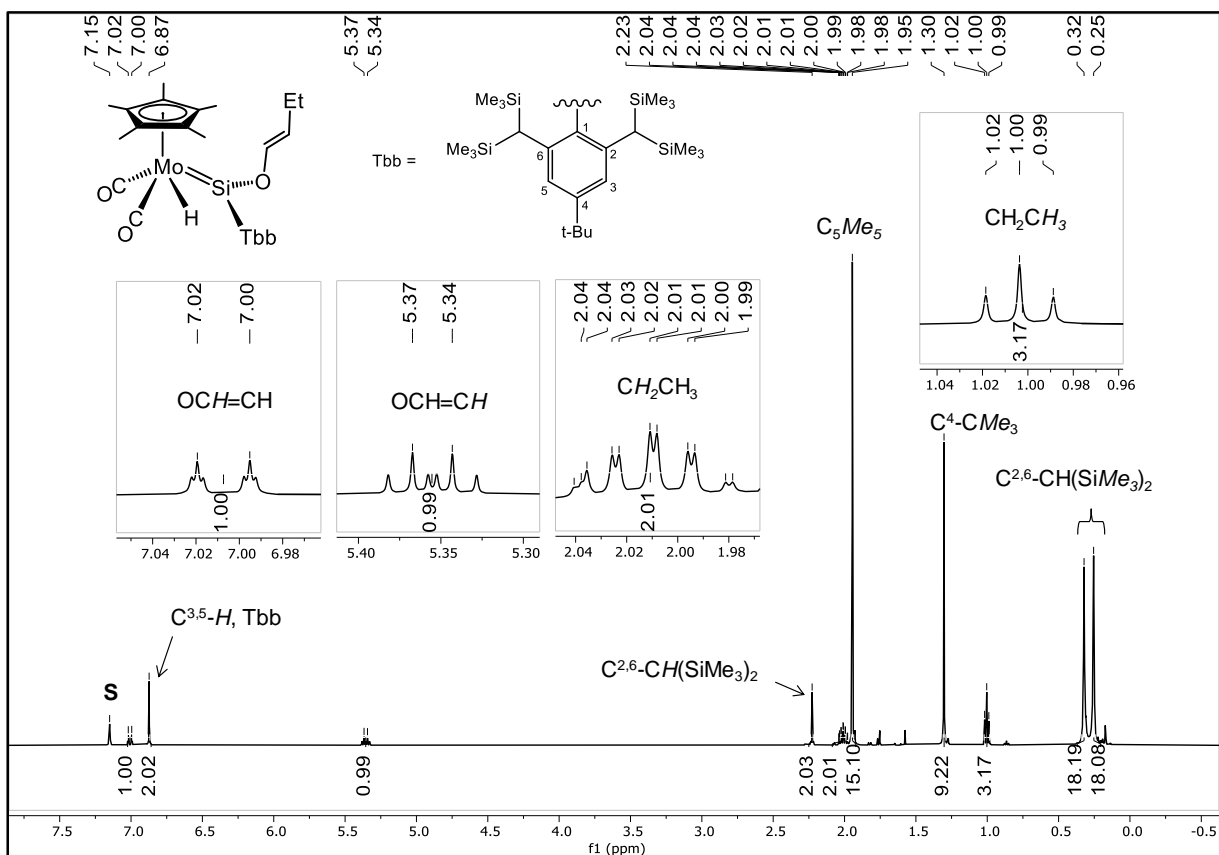


Figure S53. ^1H NMR spectrum (500.1 MHz) of **3-Mo** in (D_6) benzene at 298 K; the residual proton signal of the deuterated solvent is marked with the letter **S**. Four excerpts of the spectrum are shown in the insets.

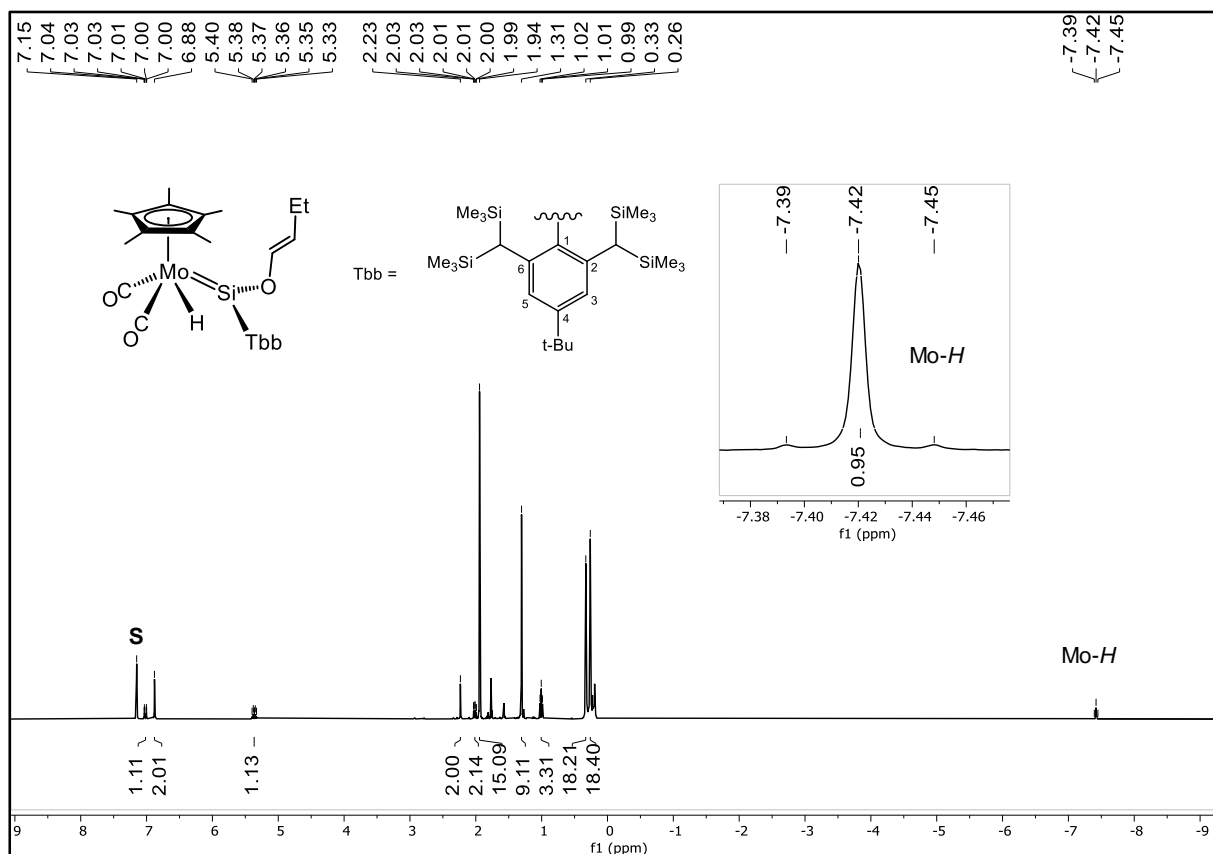


Figure S54. ^1H NMR spectrum (400.1 MHz) of another batch of **3-Mo** in (D_6) benzene at 298 K in the chemical shift range $\delta = 9 - (-9)$ ppm including the Mo-H signal. The residual proton signal of the deuterated solvent is marked with the letter **S**. The Mo-H signal is depicted in an inset.

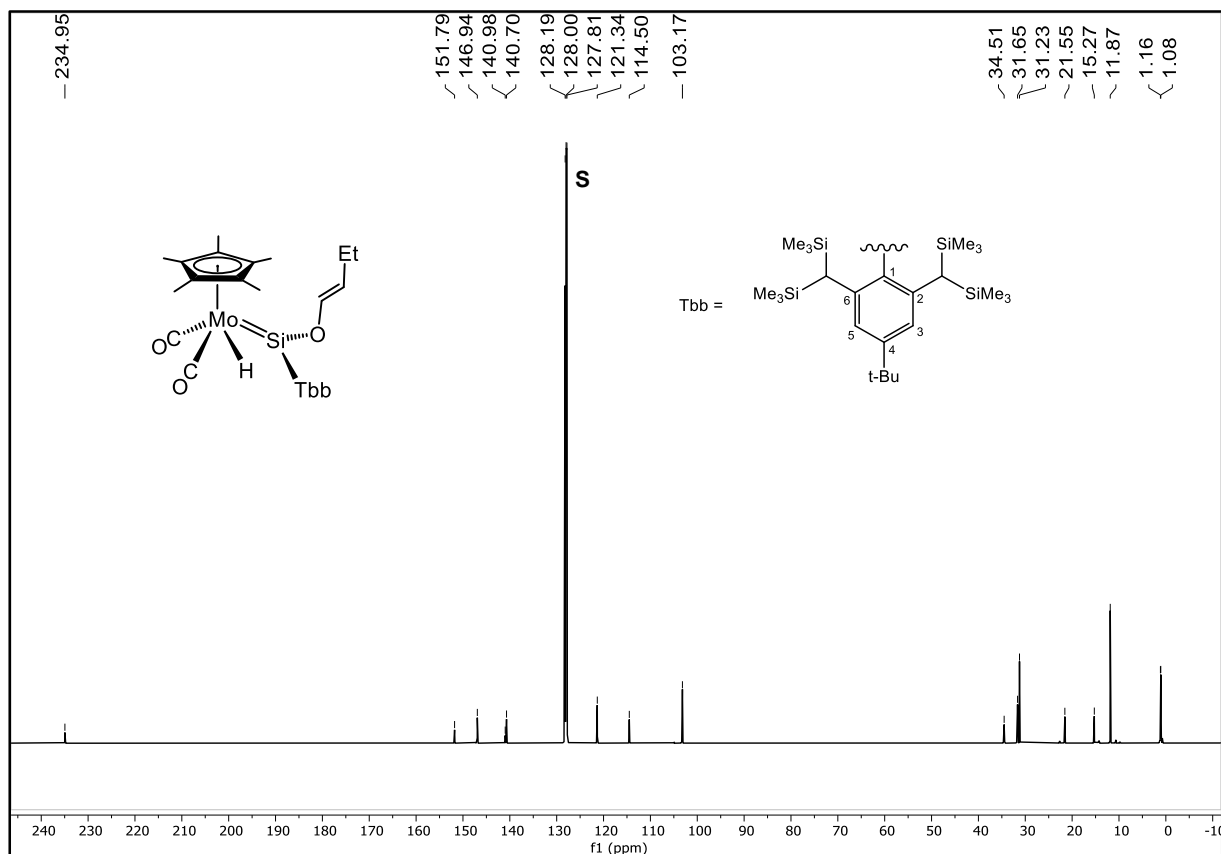


Figure S55. $^{13}\text{C}\{^1\text{H}\}$ NMR spectrum (125.8 MHz) of **3-Mo** in (D_6) benzene at 298 K; the signal of the deuterated solvent is marked with the letter **S**.

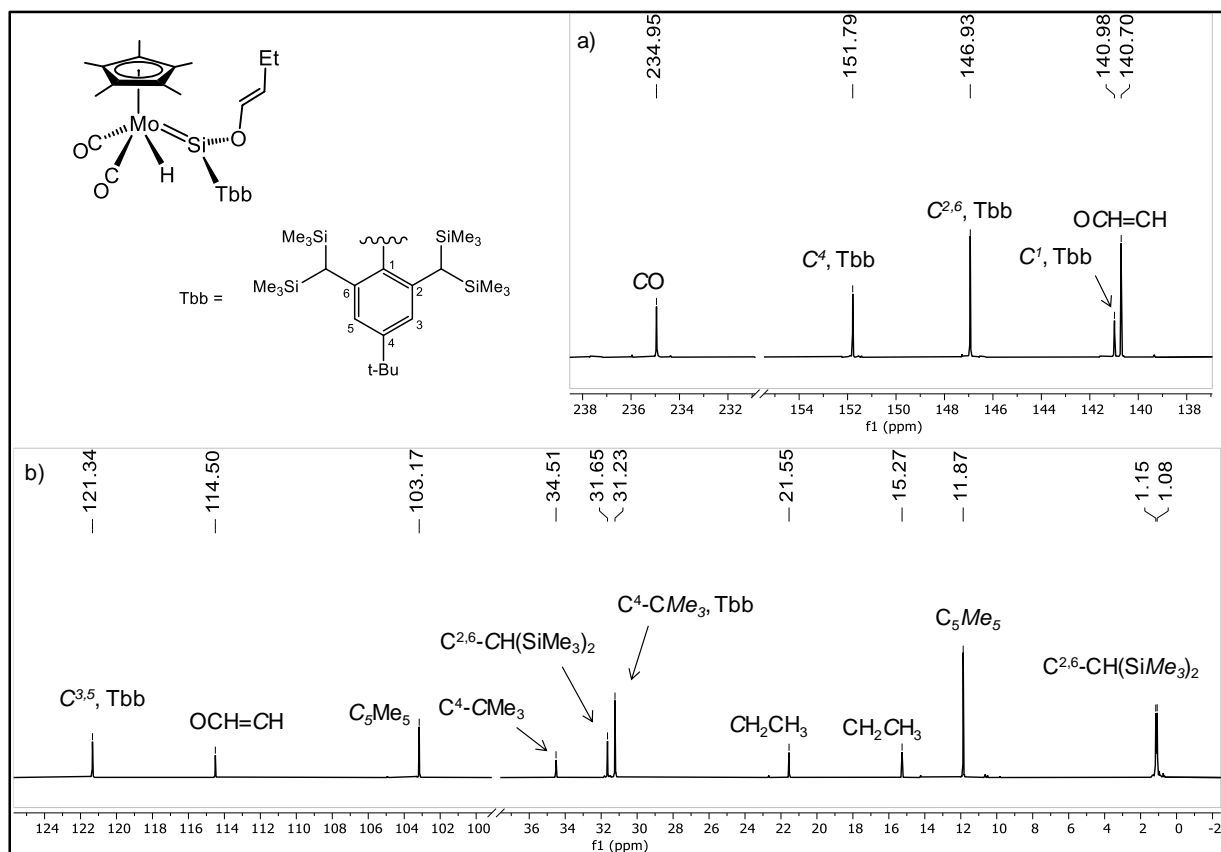


Figure S56. Two excerpts (a, b) of the $^{13}\text{C}\{^1\text{H}\}$ NMR spectrum (125.8 MHz) of **3-Mo** in (D_6) benzene at 298 K; the signal of the deuterated solvent is marked with the letter **S**.

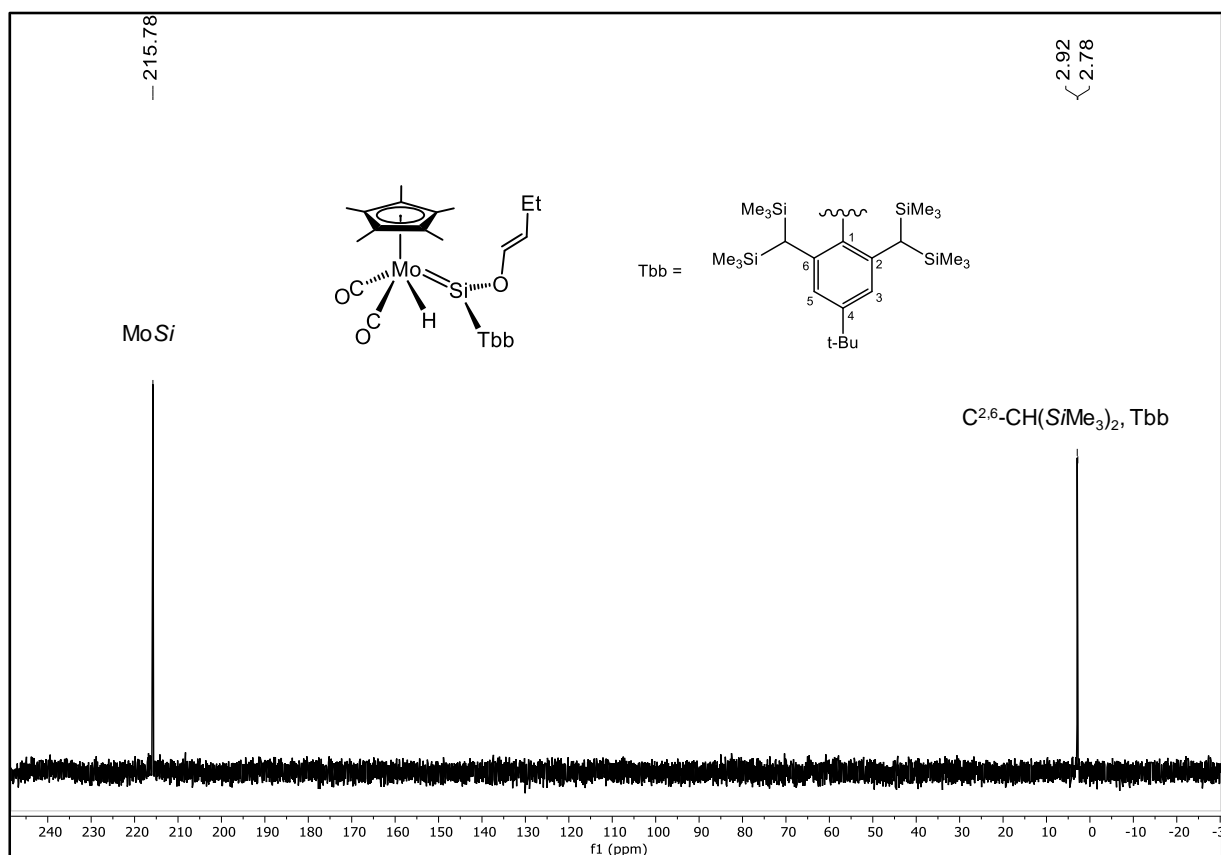
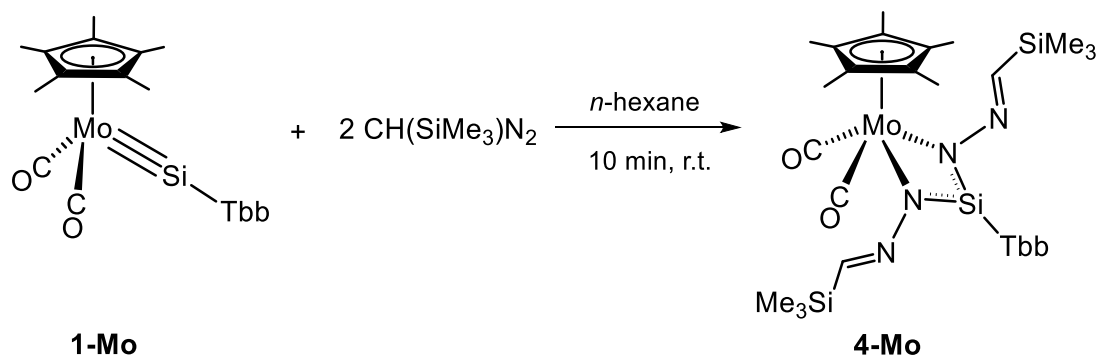


Figure S57. $^{29}\text{Si}\{^1\text{H}\}$ (zgig) NMR (99.36 MHz) spectrum of **3-Mo** in (D_6) benzene at 298 K.

2.7 **[Mo(Cp*)(CO)₂{κ²N,N'-(N₂CHSiMe₃)₂Si(Tbb)}] (4-Mo)**

A 2.0 M stock solution of trimethylsilyldiazomethane (0.39 mL, 0.78 mmol, 2.0 equiv.) in *n*-hexane was added dropwise to an orange-red solution of the silyldiynyl complex **1-Mo** (300 mg, 0.392 mmol, 1.00 equiv.) in 10 mL of *n*-hexane. The reaction solution turned brown immediately. It was stirred at room temperature for 10 minutes. ¹H NMR and IR spectroscopic analysis of an aliquot of the reaction solution showed a selective formation of complex **4-Mo**. The reaction solution was concentrated to approximately 2 mL and stored at –30 °C overnight. The crystallized, orange-red solid was isolated after filtration at –30 °C and dried in a fine vacuum at 35 °C for 30 minutes. Yield: 158 mg (0.159 mmol, 41% from **1-Mo**).

Elemental analysis calcd (%) for C₄₄H₈₄MoN₄O₂Si₇ (993.70 g/mol): C 53.18, H 8.52, N 5.64; found: C 53.02, H 8.65, N 5.47%.

Complex **4-Mo** is a highly air sensitive, orange-red solid that melts with decomposition at 141 °C. It is good soluble in *n*-pentane, *n*-hexane, diethyl ether, benzene and toluene. Handling of **4-Mo** in a Schlenk line under argon flow is accompanied by some decomposition due to its very high air-sensitivity.

Spectroscopy:

Complex **4-Mo** is C_s-symmetric with the plane of symmetry passing through the atoms Mo, C_g and Si (C_g denotes the Cp* ring centroid). Therefore, only one set of signals is observed for the two N=CH(SiMe₃) arms of the silaamidinato ligand in the ¹H and ¹³C{¹H} NMR spectra. The Tbb substituent is orthogonally oriented to the four-membered metallacycle MoN₂Si and its rotation about the Si-C_{Tbb} bond is frozen out in solution on the NMR time scale. This leads to diastereotopic C² and C⁶ or C³ and C⁵ atoms in the Tbb substituent with each of the diastereotopic C² and C⁶ bonded CH(SiMe₃)₂ (Dsi) substituents containing a pair of enantiotopic SiMe₃ groups. Evidence for this is provided for example by the two ¹H NMR doublet signals with the intensity ratio of 1:1 observed for the C³ and C⁵ bonded hydrogen atoms or the two ¹H NMR singlet signals with the intensity ratio of 18:18 observed for the SiMe₃ groups (see *Figure S62*). The *ortho*-carbon atom carrying the Dsi group with the more shielded SiMe₃ protons was denominated as C² carbon atom and the other carbon atoms (C³, C⁵ and C⁵) and the groups attached to them assigned by 2D NMR correlation spectroscopy.

ATR-IR (solid, 298 K, *Figure S58* and *Figure S59*): $\tilde{\nu}$ (cm^{-1}) = 2952 (m), 2900 (w), 2745 (vw), 1914 (s) [$\nu(\text{CO})$], 1820 (s) [$\nu(\text{CO})$], 1582 (w), 1567 (w), 1528 (m), 1478 (vw), 1396 (m), 1380 (w), 1362 (vw), 1287 (vw), 1245 (m), 1188 (w), 1179 (w), 1123 (m), 1051 (vw), 1029 (vw), 1000 (w), 970 (w), 939 (w), 885 (w), 856 (s, sh), 832 (vs), 763 (w), 746 (w), 722 (m), 688 (m), 665 (w), 647 (vw), 620 (w), 591 (vw), 557 (vw), 539 (vw), 518 (w), 479 (m), 438 (w), 417 (m).

IR (toluene, 298 K, *Figure S60*): $\tilde{\nu}$ (cm^{-1}) = 1917 (vs), 1826 (s) [$\nu(\text{CO})$], 1584 (w) and 1533 (w) [$\nu(\text{C}=\text{C})_{\text{Tbb}}$], 1522 (w).

IR (*n*-hexane, 298 K, *Figure S61*): $\tilde{\nu}$ (cm^{-1}) = 1924 (vs), 1836 (s) [$\nu(\text{CO})$], 1584 (w) and 1534 (w) [$\nu(\text{C}=\text{C})_{\text{Tbb}}$], 1523 (w).

^1H NMR (500.1 MHz, (D_6) benzene, 298 K, *Figure S62*): δ (ppm) = 0.13 (s, $^2J(^{29}\text{Si}, ^1\text{H}) = 6.5$ Hz, 18H, $\text{C}^2\text{-CH}(\text{SiMe}_3)_2$, Tbb), 0.27 (s, $^2J(^{29}\text{Si}, ^1\text{H}) = 6.7$ Hz, 18H, $\text{C}^6\text{-CH}(\text{SiMe}_3)_2$, Tbb), 0.30 (s, $^2J(^{29}\text{Si}, ^1\text{H}) = 6.4$ Hz, 18H, 2 \times NCH(SiMe_3)), 1.21 (s, 9H, $\text{C}^4\text{-CMe}_3$, Tbb), 1.33 (s, 1H, $\text{C}^2\text{-CH}(\text{SiMe}_3)_2$, Tbb), 1.77 (s, 15H, C_5Me_5), 2.24 (s, 1H, $\text{C}^6\text{-CH}(\text{SiMe}_3)_2$, Tbb), 6.87 (d, $^4J(^1\text{H}, ^1\text{H}) = 1.6$ Hz, 1H, $\text{C}^3\text{-H}$, Tbb), 6.90 (d, $^4J(^1\text{H}, ^1\text{H}) = 1.6$ Hz, 1H, $\text{C}^5\text{-H}$, Tbb), 7.55 (s, $^2J(^{29}\text{Si}, ^1\text{H}) = 14.6$ Hz, 2H, 2 \times NCH(SiMe_3)).

$^{13}\text{C}\{^1\text{H}\}$ NMR (125.8 MHz, (D_6) benzene, 298 K, *Figure S63* and *Figure S64*): δ (ppm) = -1.0 (s, $^1J(^{29}\text{Si}, ^{13}\text{C}) = 52.6$ Hz, 6C, 2 \times NCH(SiMe_3)), 0.85 (s, $^1J(^{29}\text{Si}, ^{13}\text{C}) = 51.8$ Hz, 6C, $\text{C}^6\text{-CH}(\text{SiMe}_3)_2$, Tbb), 0.88 (s, $^1J(^{29}\text{Si}, ^{13}\text{C}) = 51.8$ Hz, 6C, $\text{C}^2\text{-CH}(\text{SiMe}_3)_2$, Tbb), 11.0 (s, 5C, C_5Me_5), 31.0 (s, 3C, $\text{C}^4\text{-CMe}_3$, Tbb), 34.8 (s, 1C, $\text{C}^4\text{-CMe}_3$, Tbb), 37.1 (s, $^1J(^{29}\text{Si}, ^{13}\text{C}) = 40.2$ Hz, 1C, $\text{C}^2\text{-CH}(\text{SiMe}_3)_2$, Tbb), 39.1 (s, $^1J(^{29}\text{Si}, ^{13}\text{C}) = 40.2$ Hz, 1C, $\text{C}^6\text{-CH}(\text{SiMe}_3)_2$, Tbb), 106.4 (s, 5C, C_5Me_5), 120.0 (s, 1C, $\text{C}^5\text{-H}$, Tbb), 120.4 (s, 1C, $\text{C}^3\text{-H}$, Tbb), 128.4 (s, 1C, Si- C^1 , Tbb), 150.3 (s, 1C, C^6 , Tbb), 152.2 (s, 1C, C^2 , Tbb), 155.7 (s, 1C, $\text{C}^4\text{-CMe}_3$, Tbb), 156.4 (s, 2C, 2 \times NCH(SiMe_3)), 263.4 (s, 2C, 2 \times CO).

$^{29}\text{Si}\{^1\text{H}\}$ NMR (99.36 MHz, (D_6) benzene, 298 K, *Figure S66* and *Figure S67*): δ (ppm) = -9.5 (s, $^1J(^{29}\text{Si}, ^{13}\text{C}) = 52.6$ Hz, 2Si, 2 \times NCH(SiMe_3), Tbb), 3.0 (s, $^1J(^{29}\text{Si}, ^{13}\text{C}) = 51.8$ Hz, 2Si, $\text{C}^6\text{-CH}(\text{SiMe}_3)_2$, Tbb), 3.1 (s, $^1J(^{29}\text{Si}, ^{13}\text{C}) = 51.8$ Hz, 2Si, $\text{C}^2\text{-CH}(\text{SiMe}_3)_2$, Tbb), 31.9 (s, 1Si, NS/N).

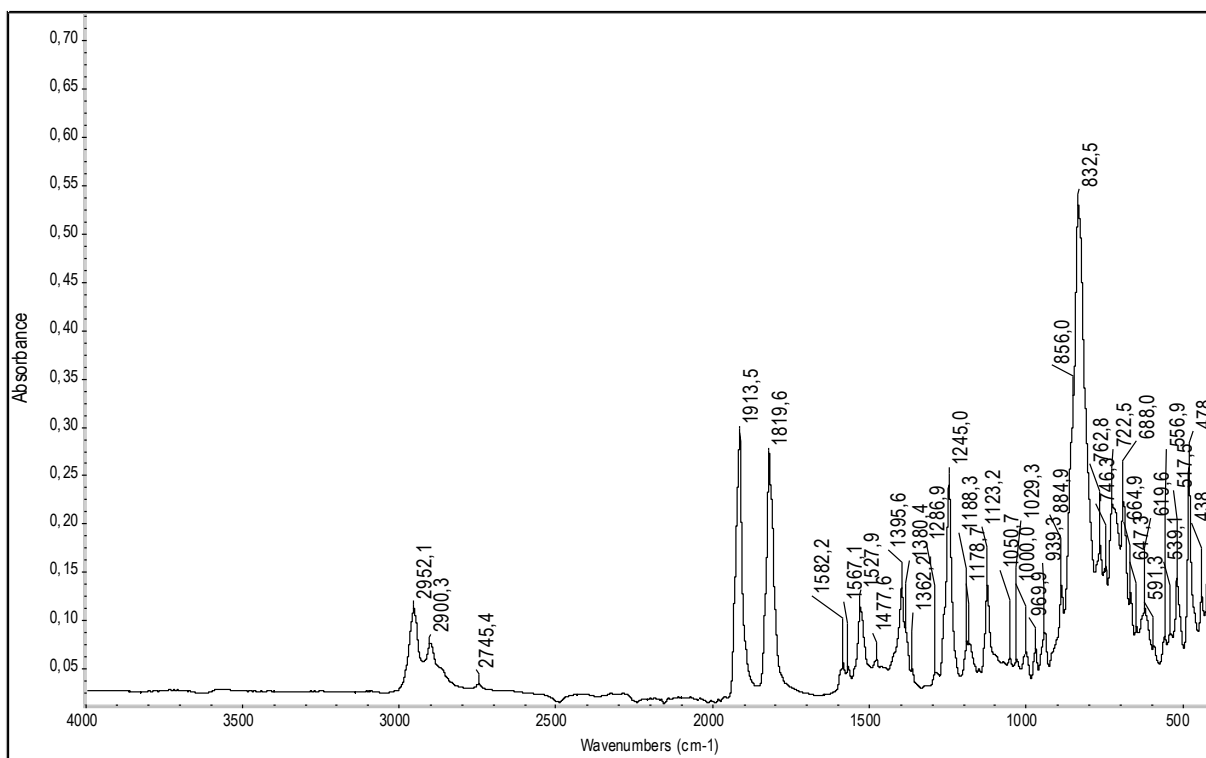


Figure S58. ATR-IR spectrum of 4-Mo in the solid state in the spectral range of 4000 - 400 cm⁻¹.

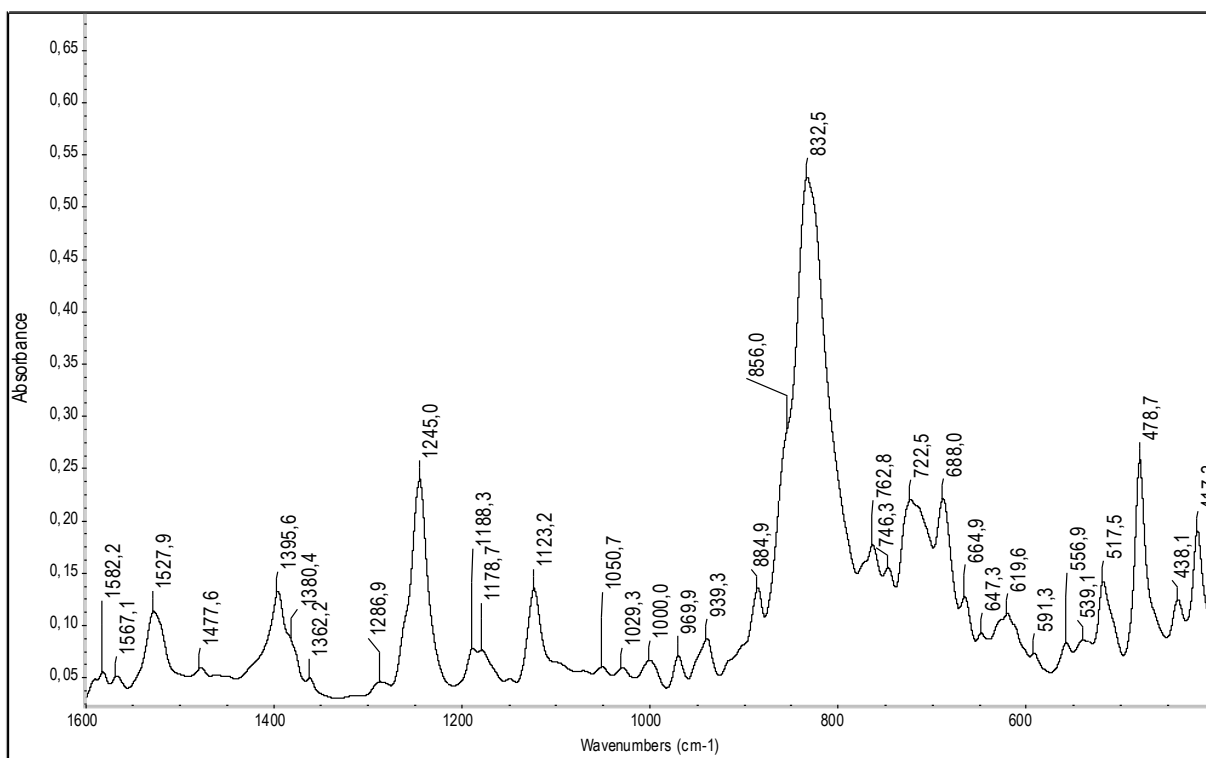


Figure S59. Excerpt of the ATR-IR spectrum of 4-Mo in the solid state (spectral range: 1600 - 400 cm⁻¹).

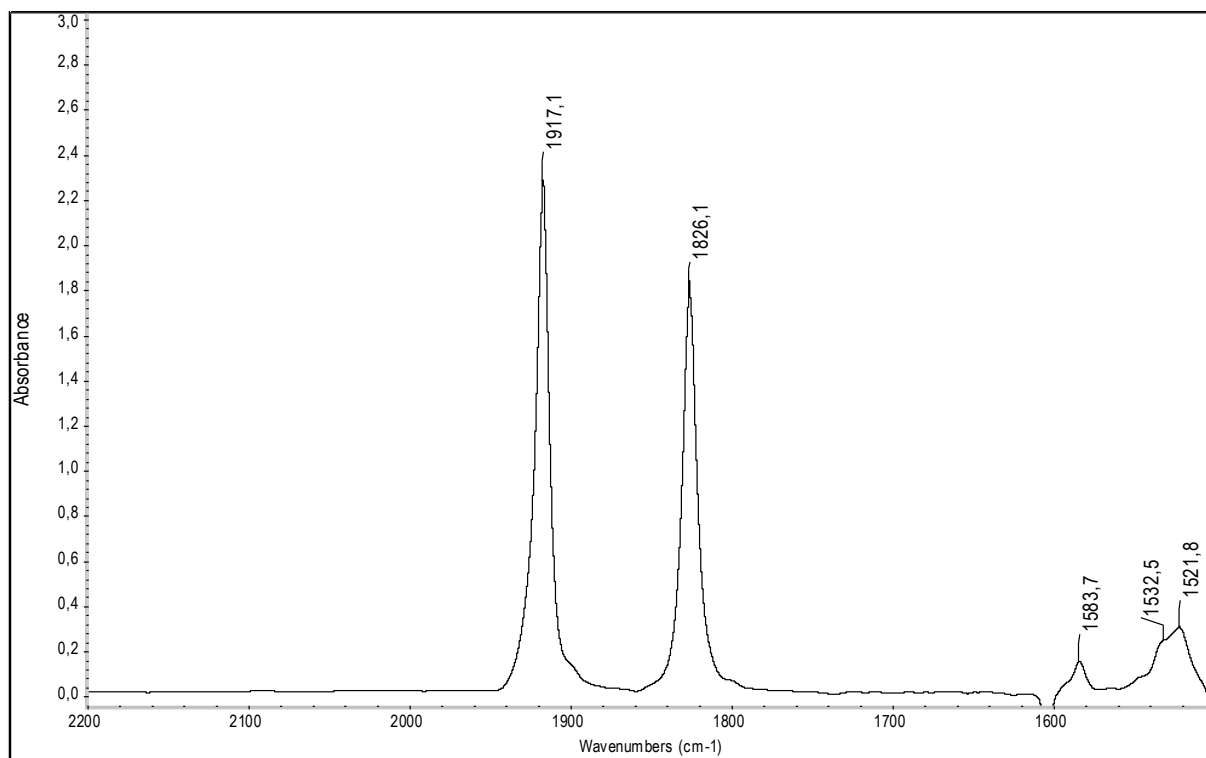


Figure S60. FT-IR spectrum of **4-Mo** in toluene in the spectral range of 2200 - 1500 cm⁻¹.

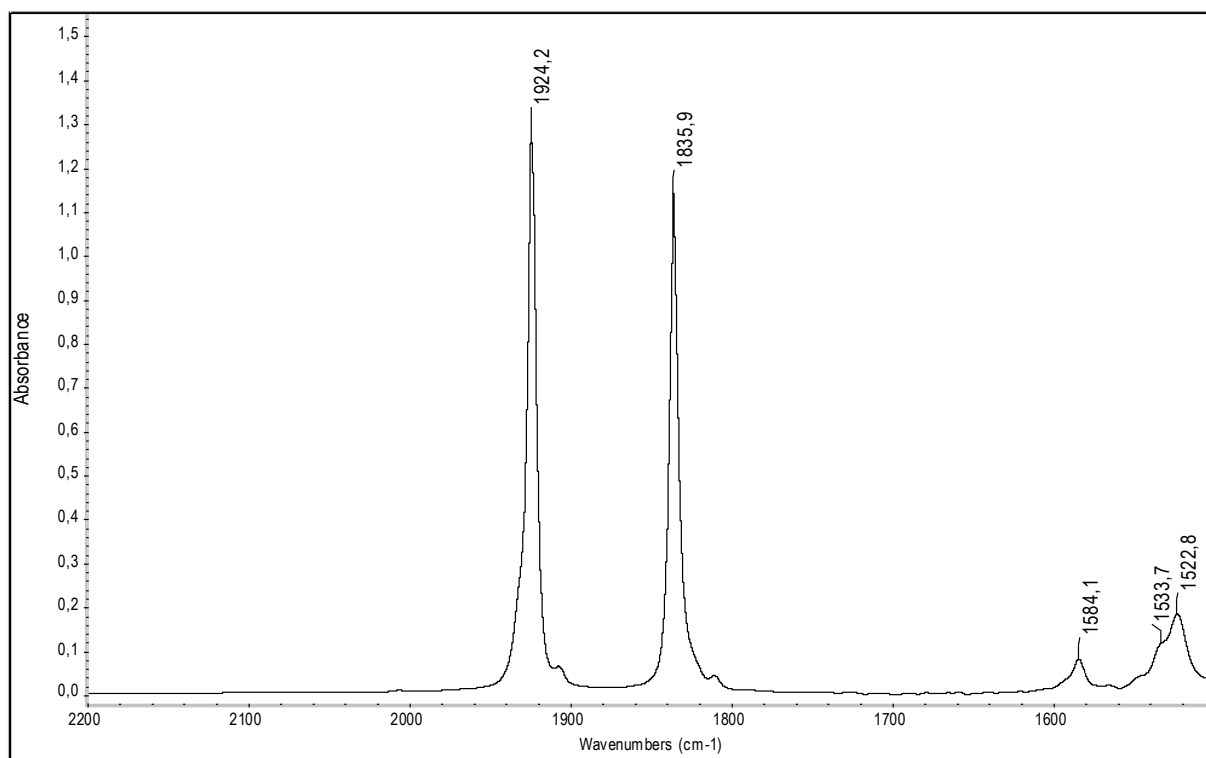
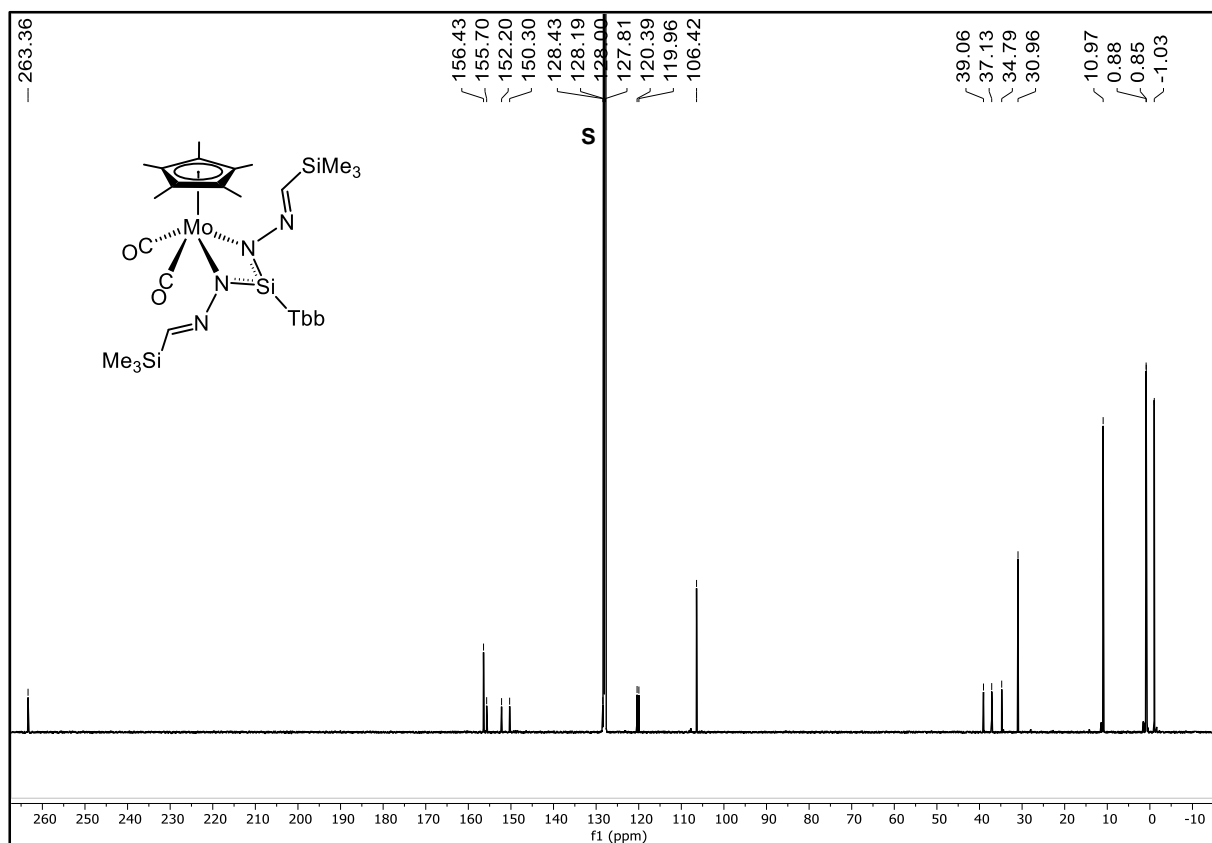
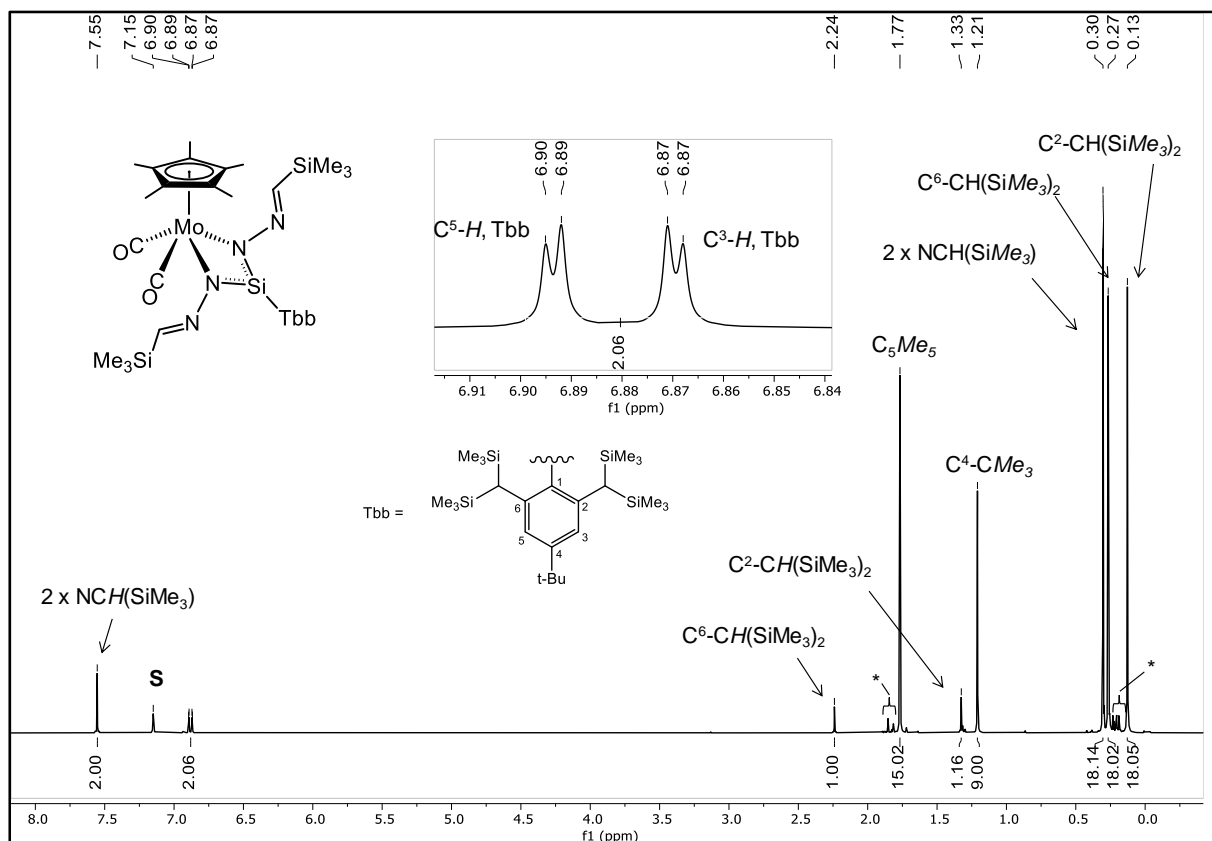


Figure S61. FT-IR spectrum of **4-Mo** in *n*-hexane in the spectral range of 2200 - 1500 cm⁻¹.



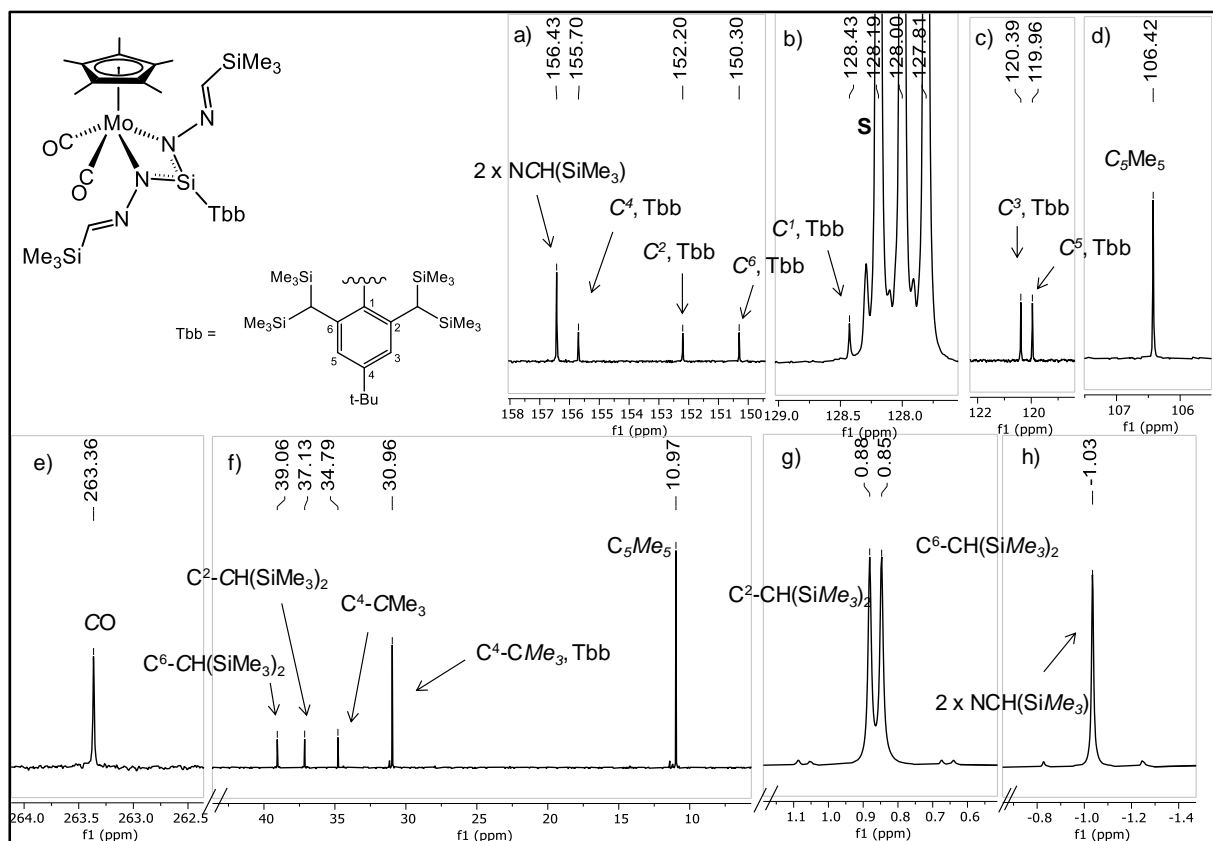


Figure S64. Eight excerpts (a - h) of the $^{13}\text{C}\{^1\text{H}\}$ NMR spectrum (125.8 MHz) of **4-Mo** in (D_6) benzene at 298 K; the signal of the deuterated solvent is marked with the letter S.

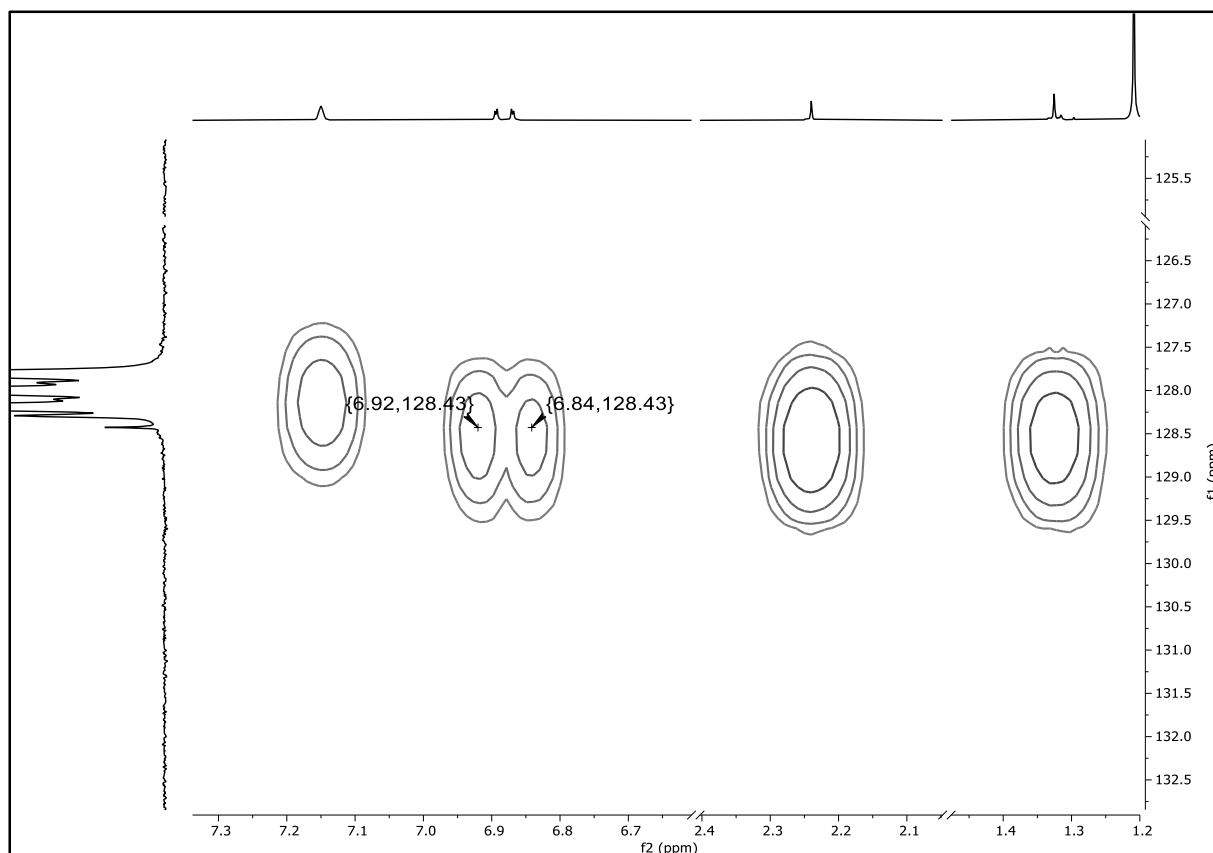


Figure S65. Excerpt of the ^1H - ^{13}C HMBC spectrum (500.1 MHz, 125.8 MHz) of **4-Mo** in (D_6) benzene at 298 K.

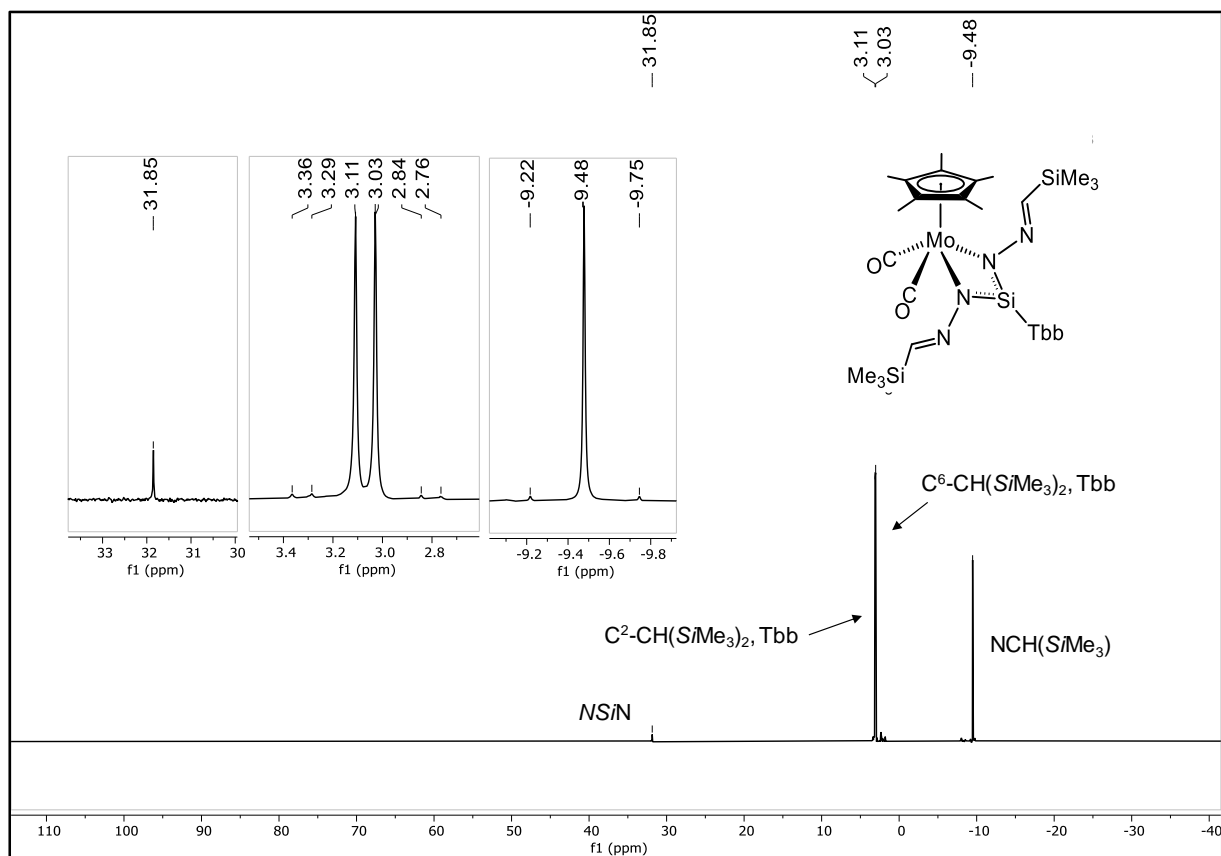


Figure S66. $^{29}\text{Si}\{^1\text{H}\}$ (dept20) NMR (99.36 MHz) spectrum of **4-Mo** in (D_6) benzene at 298 K. Three excerpts of the spectrum are shown in the insets.

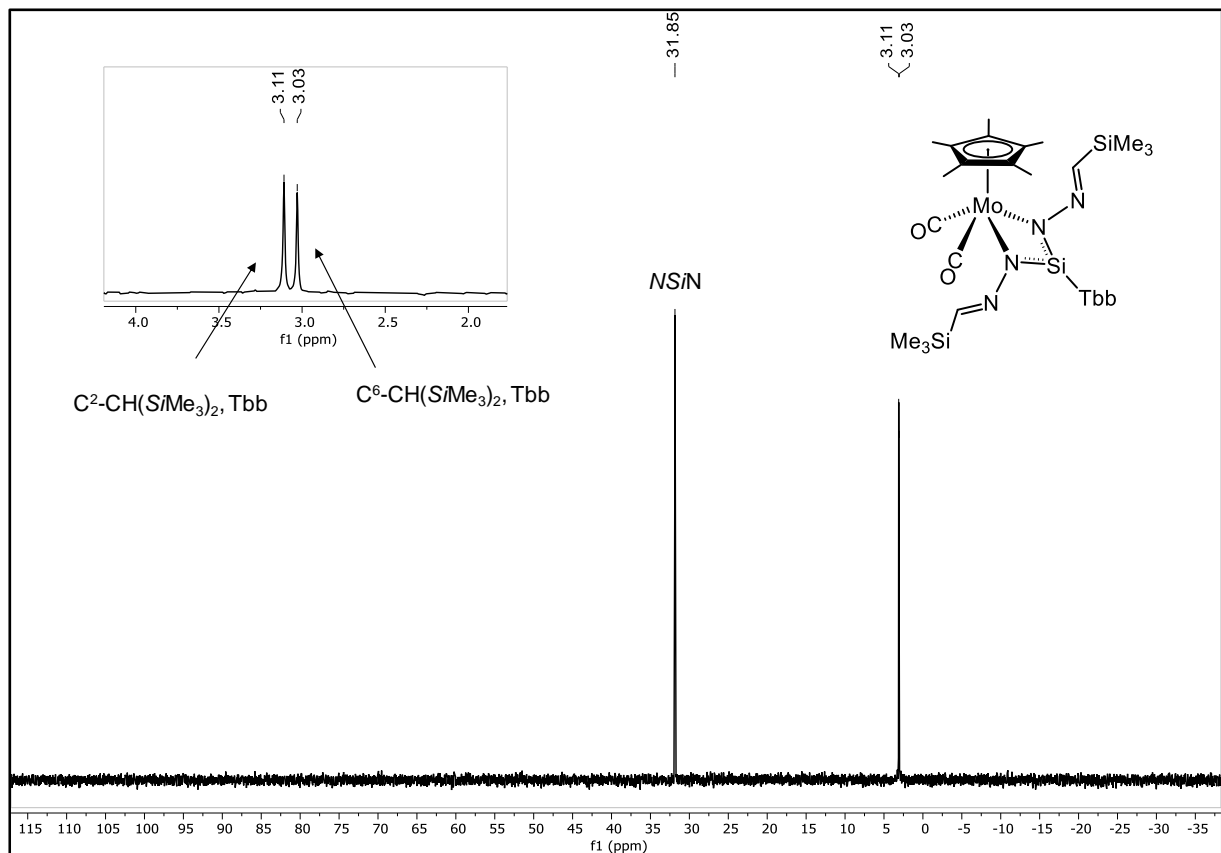
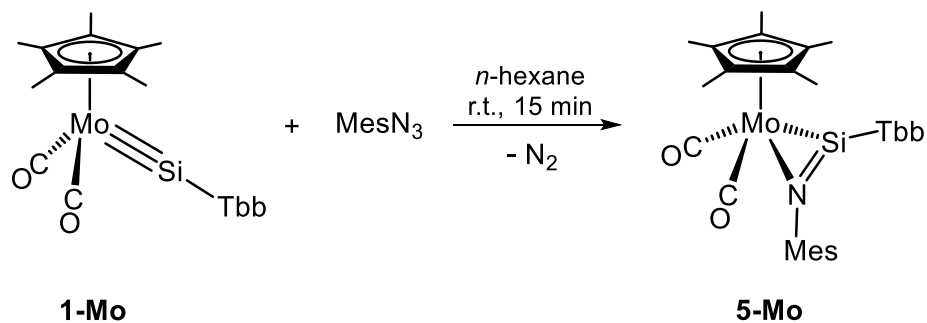


Figure S67. $^{29}\text{Si}\{^1\text{H}\}$ (zsig) NMR (99.36 MHz) spectrum of **4-Mo** in (D_6) benzene at 298 K. An excerpt of the spectrum is shown in the inset.

2.8 $[\text{Mo}(\text{Cp}^*)(\text{CO})_2\{\eta^2\text{-Si}(\text{Tbb})\text{N}(\text{Mes})\}]$ (**5-Mo**)

A solution of mesityl azide (55 mg, 0.34 mmol, 1.0 equiv.) in 2 mL of *n*-hexane was added dropwise to an orange-red solution of the silylidyne complex **1-Mo** (258 mg, 0.337 mmol, 1.00 equiv.) in 5 mL of *n*-hexane. The reaction solution turned black-brown immediately. It was stirred at room temperature for 15 minutes. ^1H NMR and IR spectroscopic analysis of an aliquot of the reaction solution showed the selective formation of compound **5-Mo**. The reaction solution was stored at $-30\text{ }^\circ\text{C}$ for 16 hours. The crystallized black solid was filtered at $-30\text{ }^\circ\text{C}$ and dried in a fine vacuum at $40\text{ }^\circ\text{C}$ for 2 hours. Yield: 140 mg (0.156 mmol, 46% from **1-Mo**).

Elemental analysis calcd (%) for $\text{C}_{45}\text{H}_{75}\text{MoNO}_2\text{Si}_5$ (898.45 g/mol): C 60.16, H 8.41, N 1.56; found: C 60.10, H 8.44, N 1.55%.

Complex **5-Mo** is an air sensitive, black solid that melts with decomposition at $176\text{ }^\circ\text{C}$. It is good soluble in *n*-pentane, *n*-hexane, diethyl ether, benzene and toluene.

Spectroscopy:

The ^1H and $^{13}\text{C}\{^1\text{H}\}$ NMR spectra of complex **5-Mo** show a single set of signals for the *ortho*- and *meta* positions of the Mes and Tbb substituent indicating a rapid rotation of the Mes and Tbb group around the N-C_{Mes} and Si-C_{Tbb} bonds, respectively. In addition, only a single ^{13}C NMR signal is observed for the diastereotopic CO ligands and a single ^1H and ^{13}C NMR signal for the diastereotopic SiMe_3 groups of the Dsi substituents indicating that complex **5-Mo** is not stereochemically rigid in solution on the NMR time scale (see *Figure S72* and *Figure S74*). The dynamic process presumably involves a 180° rotation of the silaiiminoacyl ligand about an axis connecting the Mo atom with the midpoint of the $\text{Si}=\text{N}$ bond and leads to the enantiomer of **5-Mo**, in which the Si and N atoms have swapped coordination sites. The enantiomerization proceeds presumably via a C_s symmetric Cp^* capped trigonal-bipyramidal intermediate (or transition state) with the CO ligands occupying the equatorial positions. Notably, the same stereomutation process was proposed for the iminoacyl complexes $[\text{Mo}(\eta^5\text{-C}_5\text{R}_5)(\text{CO})_2(\eta^2\text{C},\text{N-})$

(C(R¹)NEt)] (R = H, Me; R¹ = Me, Et), the carbon homologues of **5-Mo**, based on VT NMR experiments.^[S12]

ATR-IR (solid, 298 K, *Figure S68* and *Figure S69*): $\tilde{\nu}$ (cm⁻¹) = 2953 (m), 2903 (w), 2871 (vw, sh), 1919 (s) [$\nu(\text{CO})$], 1845 (s) [$\nu(\text{CO})$], 1588 (w), 1527 (w), 1470 (m), 1419 (m), 1395 (w), 1383 (w), 1362 (vw), 1336 (m), 1290 (vw), 1261 (m, sh), 1246 (s), 1177 (vw, sh) 1164 (w), 1138 (vw), 1048 (vw), 1017 (m), 952 (m), 942 (m, sh), 888 (m), 836 (vs), 772 (w), 761 (m), 742 (w), 734 (w), 724 (w), 685 (m), 663 (m), 645 (vw), 627 (w), 601 (w), 578 (vw), 561 (vw), 533 (m), 516 (m), 482 (m), 470 (m), 455 (m), 428 (m).

IR (toluene, 298 K, *Figure S70*): $\tilde{\nu}$ (cm⁻¹) = 1925 (s), 1844 (s) [$\nu(\text{CO})$], 1587 (w) and 1528 (w) [$\nu(\text{C}=\text{C})_{\text{Tbb}}$].

IR (*n*-hexane, 298 K, *Figure S71*): $\tilde{\nu}$ (cm⁻¹) = 1945 (w), 1931 (s), 1856 (s), 1838 (w) [$\nu(\text{CO})$], 1587 (w) and 1527 (w) [$\nu(\text{C}=\text{C})_{\text{Tbb}}$].

¹H NMR (500.1 MHz, (D₆)benzene, 298 K, *Figure S72*): δ (ppm) = 0.17 (s, $^2J(^{29}\text{Si}, ^1\text{H}) = 6.4$ Hz, 36H, C^{2,6}-CH(SiMe₃)₂, Tbb), 1.25 (s, 9H, C⁴-CMe₃, Tbb), 1.76 (s, 15H, C₅Me₅), 2.18 (s, 3H, C⁴-Me, Mes), 2.21 (s, 6H, C^{2,6}-Me, Mes), 2.67 (s, $^2J(^{29}\text{Si}, ^1\text{H}) = 8.9$ Hz, 2H, C^{2,6}-CH(SiMe₃)₂, Tbb), 6.80* (br s, 2H, C^{3,5}-H, Mes), 6.94 (s, 2H, C^{3,5}-H, Tbb). *Broadening of the signal at $\delta = 6.80$ ppm results from the unresolved coupling with the methyl protons of the mesityl group (see inset in *Figure S72*).

¹³C{¹H} NMR (125.8 MHz, (D₆)benzene, 298 K, *Figure S73* and *Figure S74*): δ (ppm) = 0.9 (s, $^1J(^{29}\text{Si}, ^{13}\text{C}) = 51.5$ Hz, 12C, C^{2,6}-CH(SiMe₃)₂, Tbb), 11.4 (s, 5C, C₅Me₅), 20.8 (s, 1C, C⁴-Me, Mes), 23.0 (s, 2C, C^{2,6}-Me, Mes), 31.0 (s, 3C, C⁴-CMe₃, Tbb), 31.4 (s, $^1J(^{29}\text{Si}, ^{13}\text{C}) = 40.6$ Hz, 2C, C^{2,6}-CH(SiMe₃)₂, Tbb), 34.7 (s, 1C, C⁴-CMe₃, Tbb), 106.0 (s, 5C, C₅Me₅), 122.4 (s, 2C, C^{3,5}-H, Tbb), 127.9 (s, 1C, C¹, Tbb), 128.6 (s, 1C, C⁴, Mes), 129.4 (s, 2C, C^{3,5}-H, Mes), 132.6 (s, 2C, C^{2,6}, Mes), 142.3 (s, 1C, C¹, Mes), 152.6 (s, 2C, C^{2,6}, Tbb), 154.6 (s, 1C, C⁴-CMe₃, Tbb), 249.9 (s, 2C, 2 × CO).

²⁹Si{¹H} NMR (99.36 MHz, (D₆)benzene, 298 K, *Figure S76*): δ (ppm) = 2.7 (s, 4Si, C^{2,6}-CH(SiMe₃)₂), 142.9 (s, 1Si, MoSi).

[S12] a) A. C. Filippou, E. O. Fischer, W. Grünleitner, *J. Organomet. Chem.* **1990**, 386, 333; b) A. C. Filippou, W. Grünleitner, C. Völkl, P. Kiprof, *J. Organomet. Chem.* **1991**, 413, 181.

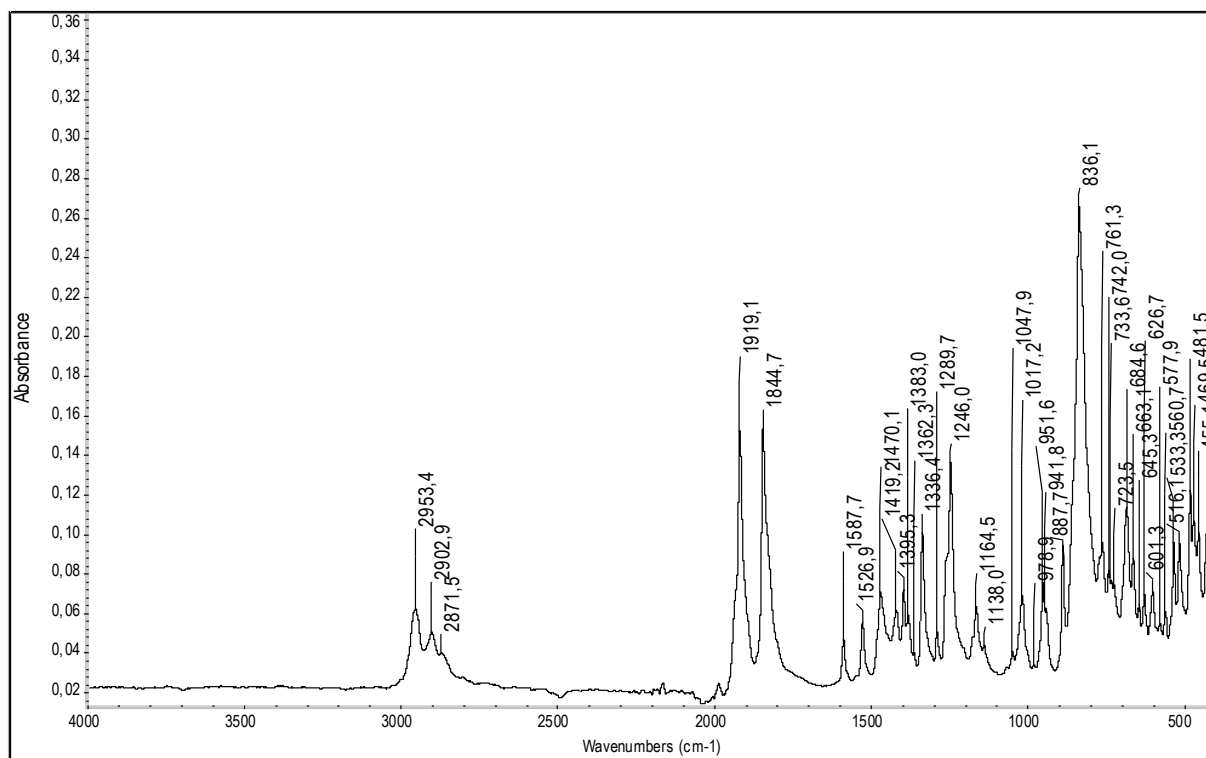


Figure S68. ATR-IR spectrum of **5-Mo** in the solid state in the spectral range of 4000 - 400 cm⁻¹.

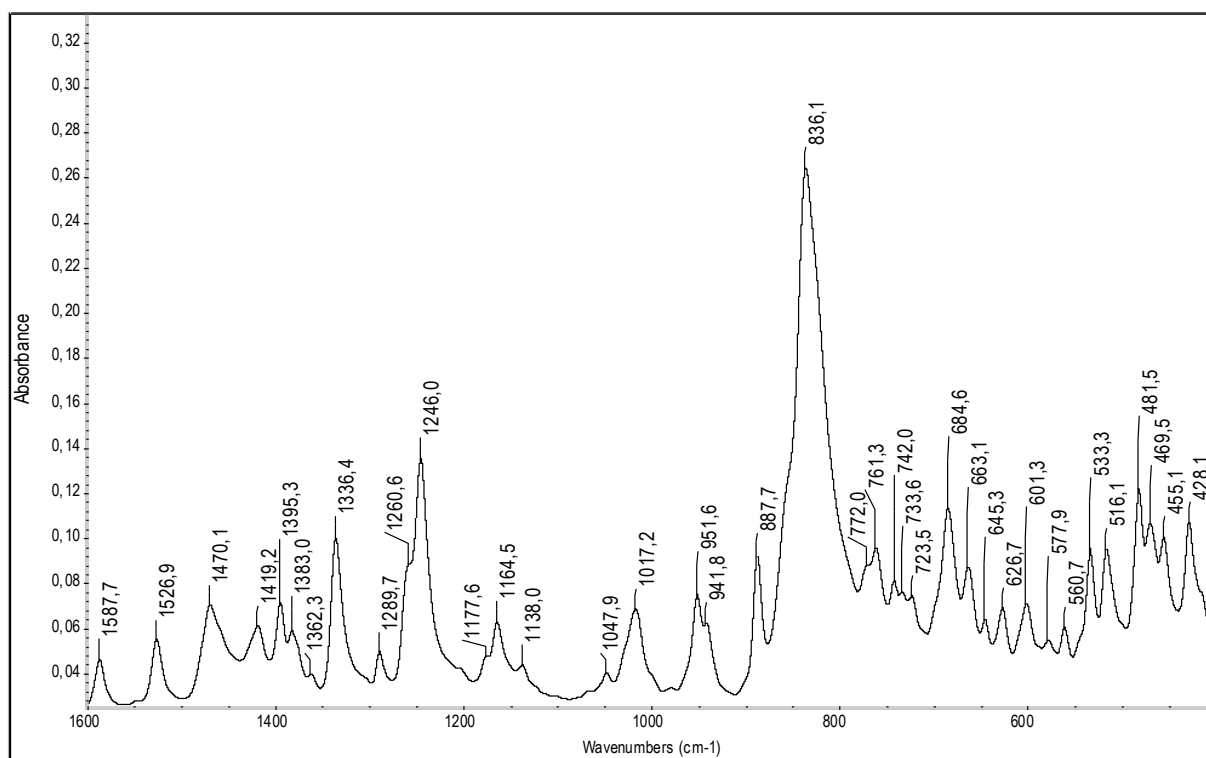


Figure S69. Excerpt of the ATR-IR spectrum of **5-Mo** in the solid state (spectral range: 1600 - 400 cm⁻¹).

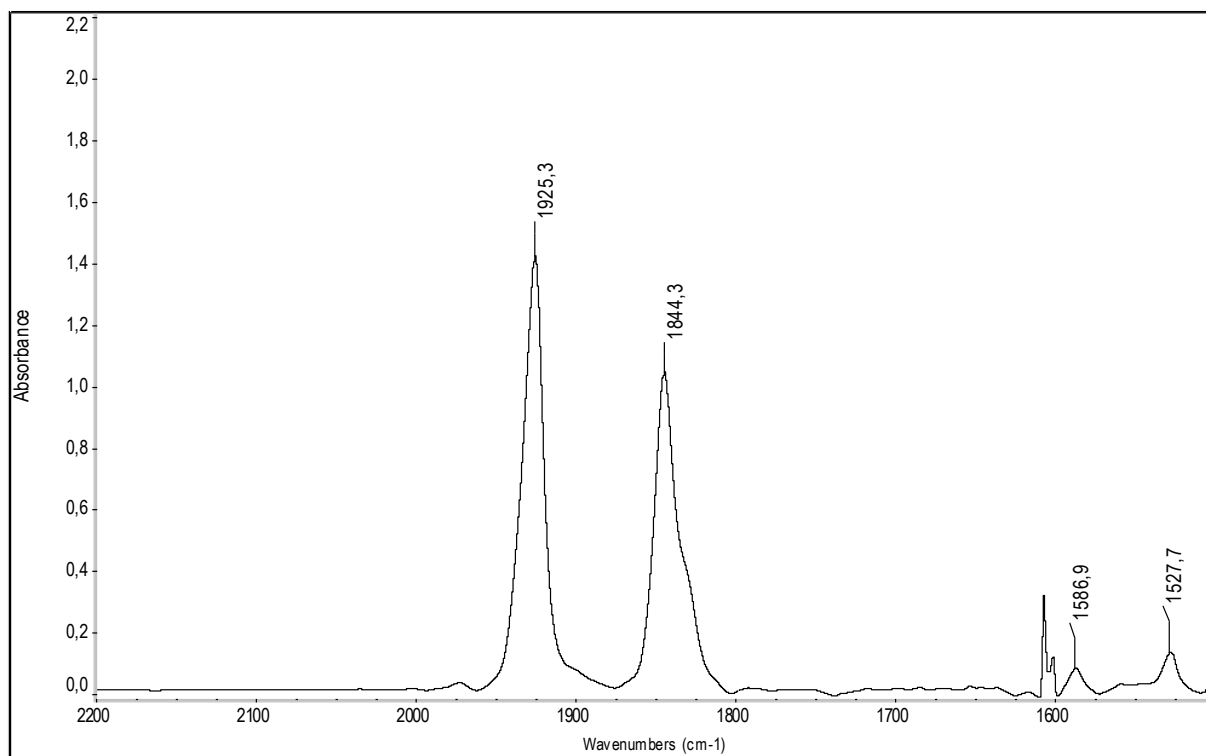


Figure S70. FT-IR spectrum of **5-Mo** in toluene in the spectral range of 2200 - 1500 cm⁻¹.

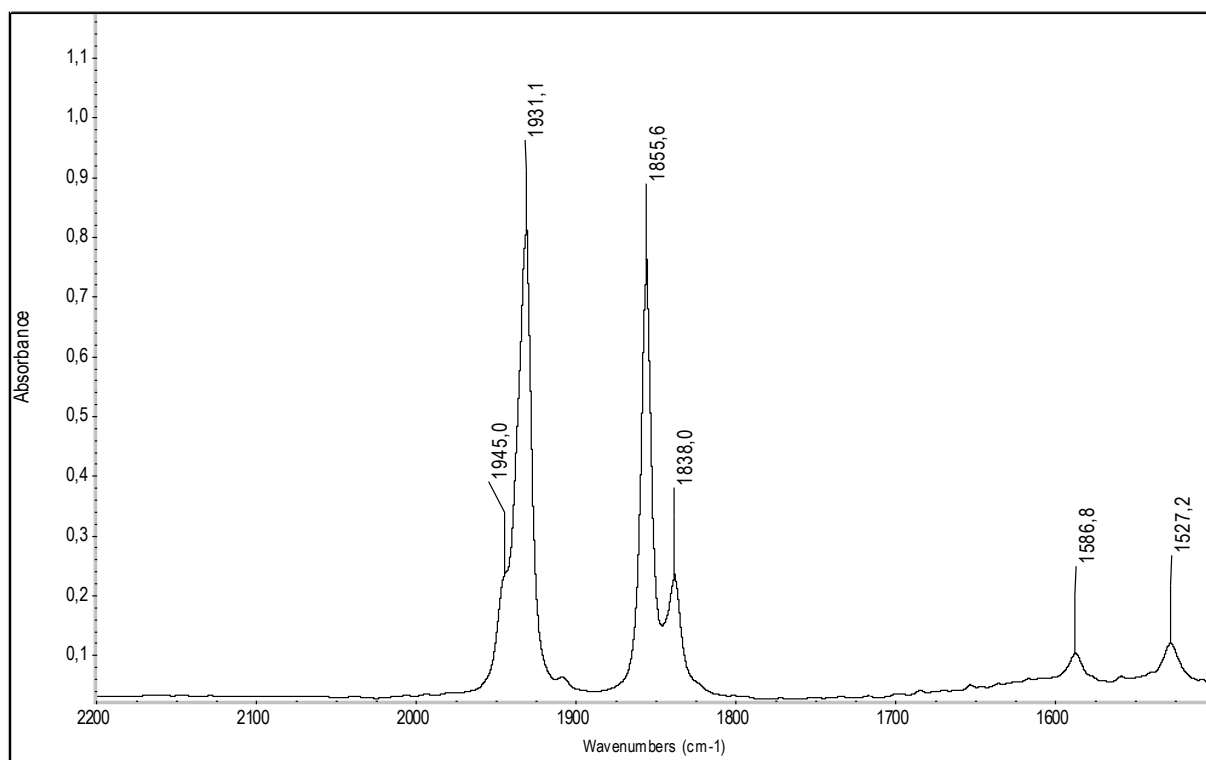


Figure S71. FT-IR spectrum of **5-Mo** in *n*-hexane in the spectral range of 2200 - 1500 cm⁻¹.

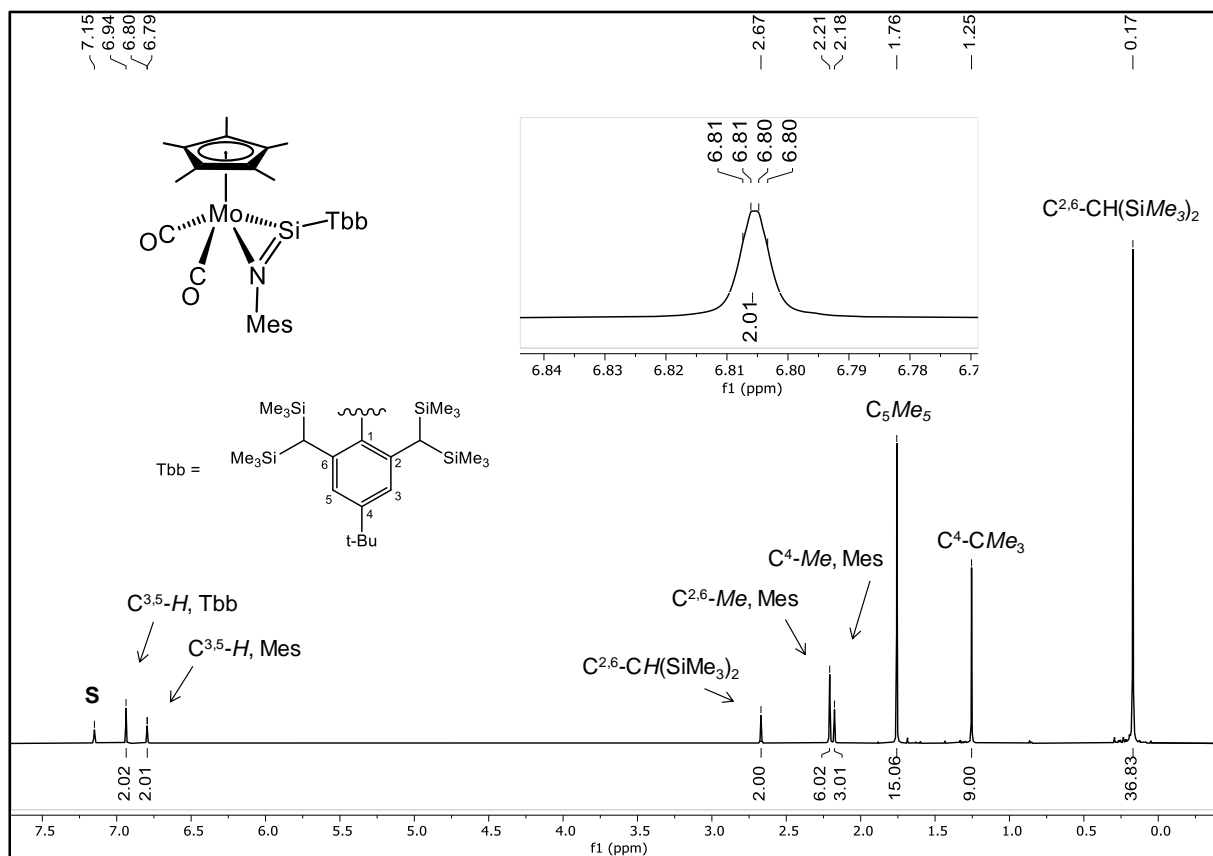


Figure S72. ¹H NMR spectrum (500.1 MHz) of **5-Mo** in (D₆)benzene at 298 K; the residual proton signal of the deuterated solvent is marked with the letter **S**. The C^{3,5}-H signal of the Mes group is shown in the inset.

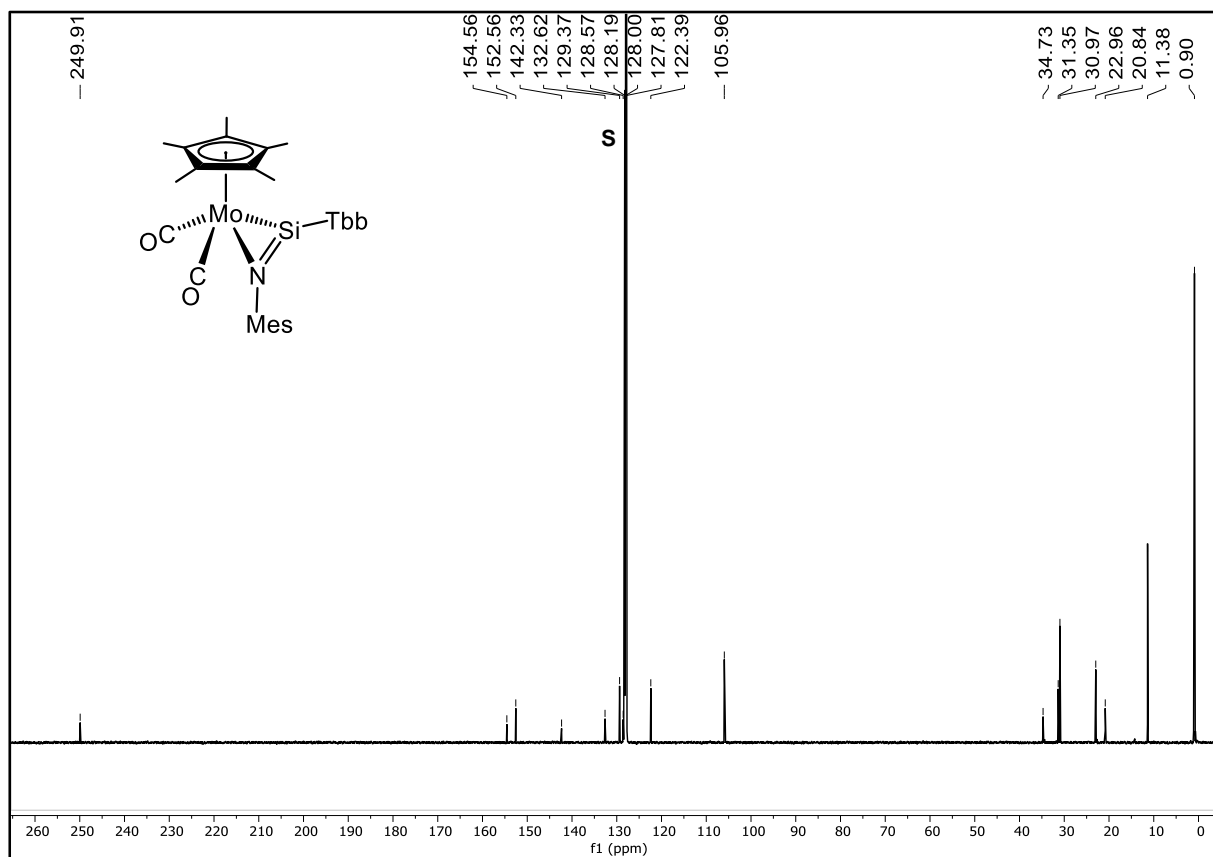


Figure S73. ¹³C{¹H} NMR spectrum (125.8 MHz) of **5-Mo** in (D₆)benzene at 298 K; the signal of the deuterated solvent is marked with the letter **S**.

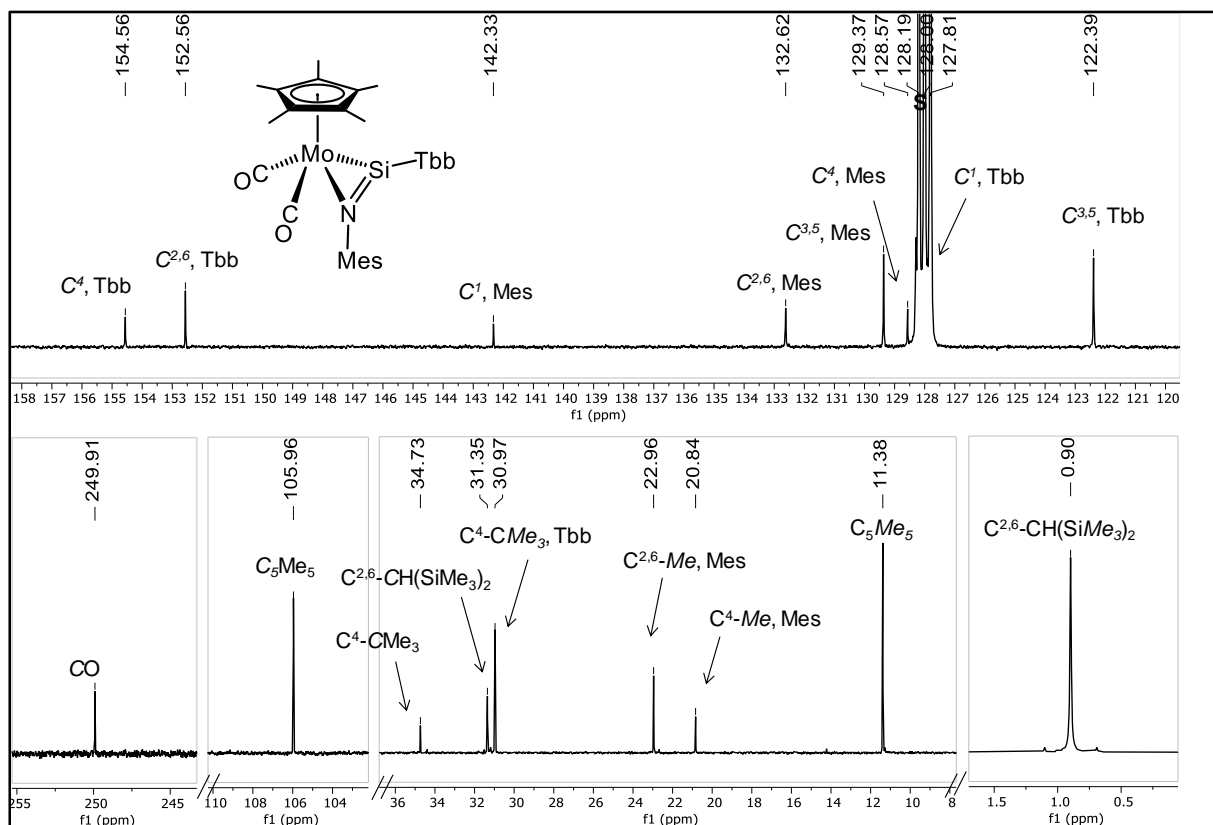


Figure S74. Five excerpts (a - e) of the $^{13}\text{C}\{^1\text{H}\}$ NMR spectrum (125.8 MHz) of **5-Mo** in (D_6) benzene at 298 K; the signal of the deuterated solvent is marked with the letter **S**.

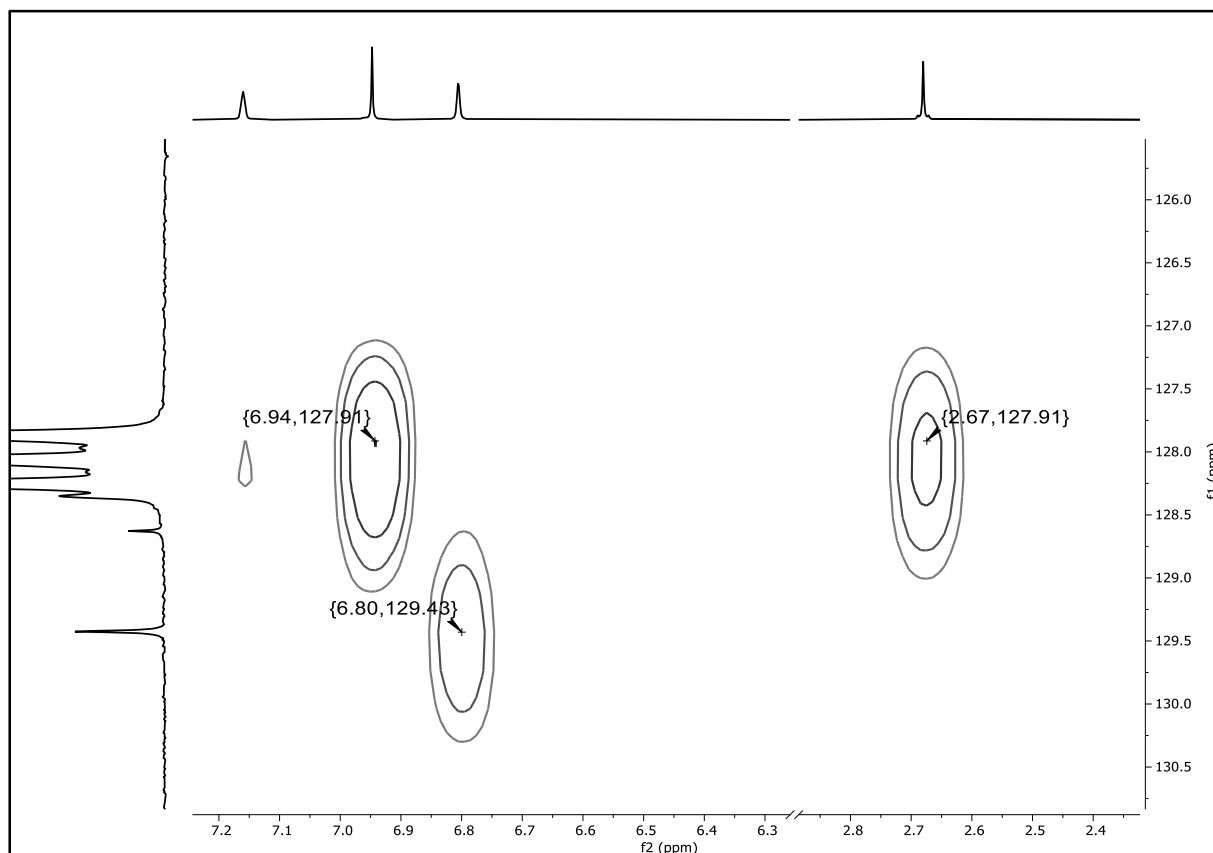


Figure S75. ^1H - ^{13}C HMBC spectrum (500.1 MHz, 125.8 MHz) of **5-Mo** in (D_6) benzene at 298 K.

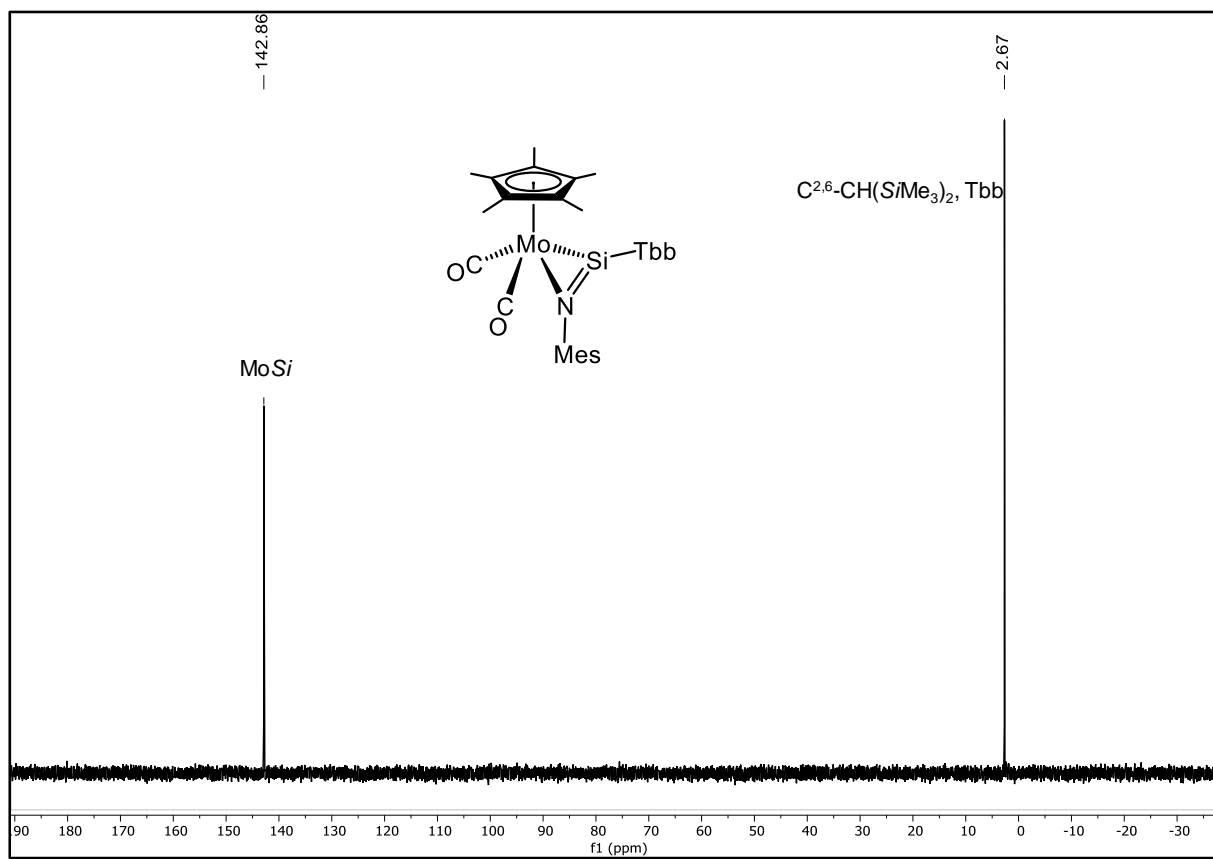


Figure S76. $^{29}\text{Si}\{^1\text{H}\}$ (zgig) NMR (99.36 MHz) spectrum of **5-Mo** in (D_6) benzene at 298 K.

3 Crystal structure determination of **1-Cr – 5-Mo**

3.1 Crystal data and structure refinement parameters of **1-Cr – 5-Mo**

Suitable single crystals of **1-Cr – 5-Mo** for the X-ray diffraction analyses were grown as follows: Dark brown crystals of **1-Cr** were obtained upon slow evaporation of a *n*-pentane solution at ambient temperature. Orange-red crystals of **1-Mo** and red crystals of **1-W** were formed after storage of saturated *n*-hexane solutions at $-30\text{ }^{\circ}\text{C}$. Light yellow crystals of **2-Mo** were obtained upon very slow evaporation of a saturated Et₂O solution at ambient temperature, and colorless crystals of **2-W•(toluene)** upon slow diffusion of *n*-pentane into a saturated toluene solution at $-30\text{ }^{\circ}\text{C}$. Light yellow crystals of **3-Mo**, red crystals of **4-Mo** and dark brown crystals of **5-Mo** were formed after storage of saturated *n*-pentane solutions at $-10\text{ }^{\circ}\text{C}$ (**3-Mo**) and $-30\text{ }^{\circ}\text{C}$ (**4-Mo**, **5-Mo**) overnight. Data collection of **1-Cr** and **1-Mo** was performed on a Bruker D8 Venture and a Bruker X8-KappaApexII diffractometer, respectively, using graphite monochromated Mo-K_α radiation ($\lambda = 0.71073\text{ \AA}$). Data collections of **2-Mo – 5-Mo** were performed on a STOE IPDS-2T diffractometer using graphite monochromated Mo-K_α radiation ($\lambda = 0.71073\text{ \AA}$). The diffractometers were equipped with low-temperature devices (Bruker D8 Venture diffractometer: Cryostream 1000 and 1000 Plus (Oxford Cryosystems); BRUKER X8-KappaApexII diffractometer: Kryoflex, Bruker AXS GmbH, 100(2)K; STOE IPDS-2T: Cryostream 700 series, Oxford Cryosystems, 123(2) K)). Intensities were measured by fine-slicing φ - and ω -scans and corrected for background, polarization and Lorentz effects.

An empirical absorption correction^[S13] was applied for **1-Mo** and a semi-empirical absorption correction by scaling of reflection intensities with a subsequent spherical absorption correction was performed with LANA for compounds **2-Mo – 5-Mo**.^[S14] Structure solution was done using intrinsic phasing methods included in the SHELXT program system and refined by full matrix least-squares/difference Fourier syntheses with SHELXL-2018/4.^[S15] All non-hydrogen atoms were refined anisotropically; hydrogen atoms were placed in geometrically calculated positions and included using a riding model on the bound carbon atoms and relative isotropic displacement parameters unless otherwise stated. DIAMOND (version 2.1c) was used for the ellipsoid representations of the molecular structures.^[S16]

1-Cr showed particular problems in the refinement, since the crystallographic mirror plane of the space group intersects the molecule in such a way that the ring carbon atoms of the Tbb group and the Si_{silyldyne} atom lie in the crystallographic mirror plane but not the Cr atom, which leads to two different side positions for the Cr atom and thus to different positions of the Cp*

[S13] SADABS, 2009/2, AXS, 2009.

[S14] J. Koziskova, F. Hahn, J. Richter, J. Kozisek, *Acta Chim. Slovaca*, **2016**, 9, 136.

[S15] G. M. Sheldrick, *Acta Crystallogr. A*, **2015**, 71, 3; G. M. Sheldrick, *Acta Crystallogr. C*, **2015**, 71, 3.

[S16] K. Brandenburg, *Diamond Version 2.1c*, 1999.

ring and the CO groups. A two-fold azimuthal disorder of the Cp* ring leads therefore (with the mirror plane of the space group) to 4 different Cp* layers around the Cr atoms; 4 individual positions summing up to 1 carbonyl group give rise to the 8 positions of the two CO groups with respect to the mirror plane. Since the interatomic distances between closely spaced side positions are well below the atomic resolution of the diffraction experiment (0.81 Å), Cr-CO, Cr-Cp* as well as intra- and interligand distances of these groups cannot be reliably discussed, although the crystallographic quality parameters (R_{int} , R_1 , wR_2 , GOOF, and $I/\sigma(I)$) ensure a reasonable model quality.

The Mo-bonded hydrogen atom in **3-Mo** was located in the difference density plot and freely refined in subsequent difference Fourier syntheses using a 1.2-fold isotropic displacement parameter relative to Mo. A disordered *tert*-butyl group in **3-Mo** (side occupation of 38%) and a disordered Me₃Si group in **4-Mo** (side occupation of 39%) were refined using an atomistic disorder model together with SHELXL-DFIX/SIMU restraints (if needed) according to standard procedures, whose details can be found in the respective deposited CIF file.

CCDC numbers CCDC-2421358 (**1-Cr**), CCDC-2421359 (**1-Mo**), CCDC-2421360 (**1-W**), CCDC-2421361 (**2-Mo**), CCDC-2421362 (**2-W(toluene)**), CCDC-2421363 (**3-Mo**), CCDC-2421364 (**4-Mo**) and CCDC-2421365 (**5-Mo**) contain the supplementary crystallographic data for this paper, which can be obtained free of charge from the Cambridge Crystallographic Data Centre via http://www.ccdc.cam.ac.uk/data_request/cif.

Table S1. Crystal data and structure refinement parameters of **1-Cr** and **1-Mo**

	1-Cr	1-Mo
Device Type	Bruker D8 Venture	Bruker X8-KappaApexII
Empirical formula	C ₃₆ H ₆₄ CrO ₂ Si ₅	C ₃₆ H ₆₄ MoO ₂ Si ₅
Moiety formula	C ₃₆ H ₆₄ CrO ₂ Si ₅	C ₃₆ H ₆₄ MoO ₂ Si ₅
Formula weight	721.32	765.26
Temperature/K	100	100
Crystal system	monoclinic	Triclinic
Space group	<i>P2₁/m</i>	<i>P</i> $\bar{1}$
<i>a</i> /Å	12.061(3)	11.5351(7)
<i>b</i> /Å	15.143(4)	12.8114(7)
<i>c</i> /Å	12.602(3)	15.6333(9)
α /°	90	75.707(3)
β /°	97.363(6)	73.035(3)
γ /°	90	83.321(3)
Volume/Å ³	2282.7(9)	2138.9(2)
Z	2	2
ρ_{calc}	1.049	1.188 g/cm ³
μ /mm ⁻¹	0.407	0.474
F(000)	780.0	816.0
Crystal size/mm ³	0.6 × 0.6 × 0.5	0.12 × 0.09 × 0.08
Absorption correction	multi-scan	empirical
Tmin; Tmax	0.6073; 0.7457	0.6219; 0.7459
Radiation	MoK α (λ = 0.71073)	MoK α (λ = 0.71073)
2 θ range for data collection/°	3.404 to 51.998°	4.826 to 56°
Completeness to theta	0.995	0.991
Index ranges	-14 ≤ <i>h</i> ≤ 14, -18 ≤ <i>k</i> ≤ 14, -15 ≤ <i>l</i> ≤ 13	-15 ≤ <i>h</i> ≤ 15, -16 ≤ <i>k</i> ≤ 16, -20 ≤ <i>l</i> ≤ 20
Reflections collected	22149	50959
Independent reflections	4642 [R _{int} = 0.0478, R _{sigma} = 0.0412]	10127 [R _{int} = 0.0735, R _{sigma} = 0.0763]
Data/restraints/parameters	4642/1063/469	10127/0/417
Goodness-of-fit on F ²	1.017	1.052
Final R indexes [<i>I</i> ≥ 2 σ (<i>I</i>)]	R ₁ = 0.0830, wR ₂ = 0.2292	R ₁ = 0.0510, wR ₂ = 0.1132
Final R indexes [all data]	R ₁ = 0.1195, wR ₂ = 0.2696	R ₁ = 0.0835, wR ₂ = 0.1231
Largest diff. peak/hole / e Å ⁻³	0.62/-0.53	0.89/-0.74

Table S2. Crystal data and structure refinement parameters of **1-W** and **2-Mo**

	1-W	2-Mo
Device Type	Bruker X8-KappaApexII	STOE IPDS 2T
Empirical formula	C ₃₆ H ₆₄ O ₂ Si ₅ W	C ₅₆ H ₈₆ MoN ₂ O ₄ Si ₅
Moiety formula	C ₃₆ H ₆₄ O ₂ Si ₅ W	C ₅₆ H ₈₆ MoN ₂ O ₄ Si ₅
Formula weight	853.17	1087.65
Temperature/K	100	123(2)
Crystal system	triclinic	monoclinic
Space group	<i>P</i> $\bar{1}$	<i>P</i> 2 ₁ / <i>c</i>
<i>a</i> /Å	11.5444(3)	14.6764(3)
<i>b</i> /Å	12.8236(4)	15.6767(3)
<i>c</i> /Å	15.6549(5)	26.4415(4)
α /°	75.7391(15)	90
β /°	73.0022(15)	93.7959(16)
γ /°	83.4120(15)	90
Volume/Å ³	2145.74(11)	6070.28(17)
Z	2	4
ρ_{calc}	1.320	1.190
μ/mm^{-1}	2.859	0.357
F(000)	880.0	2320.0
Crystal size/mm ³	0.1 × 0.06 × 0.05	0.36 × 0.24 × 0.2
Absorption correction	empirical	Integration
Tmin; Tmax	0.6558; 0.7460	0.6822; 0.8123
Radiation	MoK α (λ = 0.71073)	MoK α (λ = 0.71073)
2 θ range for data collection/°	6.96 to 56°	4.016 to 51°
Completeness to theta	0.992	1.000
Index ranges	-15 ≤ <i>h</i> ≤ 13, -16 ≤ <i>k</i> ≤ 16, -20 ≤ <i>l</i> ≤ 20	-16 ≤ <i>h</i> ≤ 17, -18 ≤ <i>k</i> ≤ 18, -32 ≤ <i>l</i> ≤ 32
Reflections collected	24355	40392
Independent reflections	10267 [R _{int} = 0.0320, R _{sigma} = 0.0464]	11285 [R _{int} = 0.0745, R _{sigma} = 0.0774]
Data/restraints/parameters	10267/0/417	11285/0/639
Goodness-of-fit on F ²	1.012	1.011
Final R indexes [<i>I</i> ≥ 2 σ (<i>I</i>)]	R ₁ = 0.0261, wR ₂ = 0.0488	R ₁ = 0.0374, wR ₂ = 0.0782
Final R indexes [all data]	R ₁ = 0.0328, wR ₂ = 0.0508	R ₁ = 0.0660, wR ₂ = 0.0848
Largest diff. peak/hole / e Å ⁻³	0.74/-0.69	0.35/-0.39

Table S3. Crystal data and structure refinement parameters of **2-W•(toluene)** and **3-Mo**

	2-W•(toluene)	3-Mo
Device Type	STOE IPDS 2T	STOE IPDS-2T
Empirical formula	C ₆₃ H ₉₄ N ₂ O ₄ Si ₅ W	C ₄₀ H ₇₂ MoO ₃ Si ₅
Moiety formula	C ₅₆ H ₈₆ N ₂ O ₄ Si ₅ W, C ₇ H ₈	C ₄₀ H ₇₂ MoO ₃ Si ₅
Formula weight	1267.70	837.36
Temperature/K	123(2)	123
Crystal system	monoclinic	orthorhombic
Space group	<i>P2₁/c</i>	<i>Pbca</i>
a/Å	13.4410(2)	17.438(3)
b/Å	14.4060(2)	16.527(3)
c/Å	34.6694(5)	33.683(10)
α/°	90	90
β/°	99.3260(10)	90
γ/°	90	90
Volume/Å ³	6624.34(17)	9707(4)
Z	4	8
ρ _{calc}	1.271	1.146
μ/mm ⁻¹	1.878	0.425
F(000)	2648.0	3584.0
Crystal size/mm ³	0.48 × 0.3 × 0.02	0.16 × 0.12 × 0.06
Absorption correction	integration	integration
Tmin; Tmax	0.6871; 0.7818	0.8207; 0.9300
Radiation	MoKα (λ = 0.71073)	MoKα (λ = 0.71073)
2θ range for data collection/°	5.046 to 53.958°	4.97 to 50.494°
Completeness to theta	0.998	0.996
Index ranges	-15 ≤ h ≤ 17, -18 ≤ k ≤ 16, -42 ≤ l ≤ 42	-20 ≤ h ≤ 18, -13 ≤ k ≤ 19, -34 ≤ l ≤ 40
Reflections collected	98885	46377
Independent reflections	13967 [R _{int} = 0.0878, R _{sigma} = 0.0794]	8747 [R _{int} = 0.1425, R _{sigma} = 0.1150]
Data/restraints/parameters	13967/138/748	8747/149/497
Goodness-of-fit on F ²	0.876	1.046
Final R indexes [I ≥ 2σ (I)]	R ₁ = 0.0393, wR ₂ = 0.0773	R ₁ = 0.0894, wR ₂ = 0.1756
Final R indexes [all data]	R ₁ = 0.0819, wR ₂ = 0.0856	R ₁ = 0.1427, wR ₂ = 0.1954
Largest diff. peak/hole / e Å ⁻³	0.91/-1.49	0.81/-0.59

Table S4. Crystal data and structure refinement parameters of **4-Mo** and **5-Mo**

	4-Mo	5-Mo
Device Type	STOE IPDS-2T	STOE IPDS-2T
Empirical formula	C ₄₄ H ₈₄ MoN ₄ O ₂ Si ₇	C ₄₅ H ₇₅ MoNO ₂ Si ₅
Moiety formula	C ₄₄ H ₈₄ MoN ₄ O ₂ Si ₇	C ₄₅ H ₇₅ MoNO ₂ Si ₅
Formula weight	993.72	898.45
Temperature/K	123(2)	123
Crystal system	monoclinic	monoclinic
Space group	P2 ₁ /n	P2 ₁ /n
a/Å	12.1671(3)	13.2535(4)
b/Å	42.6785(10)	22.9327(8)
c/Å	12.6572(4)	16.6254(5)
α/°	90	90
β/°	118.635(2)	98.153(2)
γ/°	90	90
Volume/Å ³	5768.7(3)	5002.0(3)
Z	4	4
ρ _{calc} /cm ³	1.144	1.193
μ/mm ⁻¹	0.407	0.416
F(000)	2128.0	1920.0
Crystal size/mm ³	0.27 × 0.22 × 0.13	0.17 × 0.12 × 0.05
Absorption correction	integration	integration
Tmin; Tmax	0.7942; 0.9062	0.6463; 0.9338
Radiation	MoKα (λ = 0.71073)	MoKα (λ = 0.71073)
2θ range for data collection/°	4.266 to 50.498°	5.12 to 55.996°
Completeness to theta	0.999	0.999
Index ranges	-14 ≤ h ≤ 14, -51 ≤ k ≤ 51, -15 ≤ l ≤ 14	-17 ≤ h ≤ 17, -30 ≤ k ≤ 29, -21 ≤ l ≤ 21
Reflections collected	43029	83409
Independent reflections	10458 [R _{int} = 0.0264, R _{sigma} = 0.0213]	12051 [R _{int} = 0.1453, R _{sigma} = 0.0759]
Data/restraints/parameters	10458/674/578	12051/0/510
Goodness-of-fit on F ²	1.031	1.065
Final R indexes [I ≥ 2σ (I)]	R ₁ = 0.0761, wR ₂ = 0.1797	R ₁ = 0.0544, wR ₂ = 0.1089
Final R indexes [all data]	R ₁ = 0.0863, wR ₂ = 0.1874	R ₁ = 0.0818, wR ₂ = 0.1179
Largest diff. peak/hole / e Å ⁻³	2.63/-0.97	0.66/-1.01

3.2 Molecular structures of 1-Cr – 5-Mo with selected bonding parameters

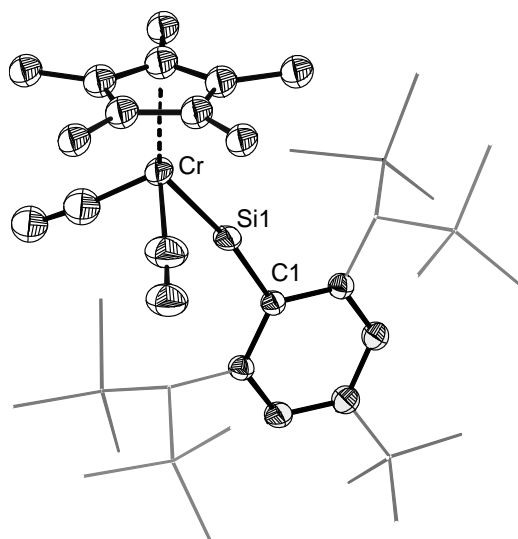


Figure S77. DIAMOND plot of the molecular structure of **1-Cr**. Thermal ellipsoids are set at 30% probability, hydrogen atoms were omitted and the substituents of the Tbb group are presented as a wireframe for the sake of clarity. Selected bond lengths (pm) and bond angles (°): Cr–Si1 210.4(2), Si–C1 184.9(5); Cr–Si1–C1 170.4(2). Due to the particular problems encountered in the refinement of **1-Cr**, no reliable Cr–CO or C–O bond lengths can be given.

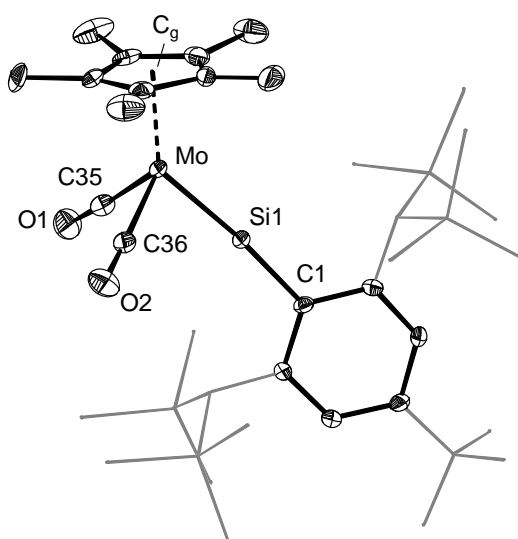


Figure S78. DIAMOND plot of the molecular structure of **1-Mo**. Thermal ellipsoids are set at 50% probability, hydrogen atoms were omitted and the substituents of the Tbb group are presented as a wireframe for the sake of clarity. Selected bond lengths (pm) and bond angles (°): Mo–Si1 223.2(1), Mo–C35 197.0(4), Mo–C36 196.2(4), Si1–C1 185.6(3); Mo–Si1–C1 174.3(1), Si1–Mo–C35 89.1(1), Si1–Mo–C36 86.8(1), C35–Mo–C36 87.9(2), Si1–Mo–C_g 135.86(7), C35–Mo–C_g 122.2(1), C36–Mo–C_g 121.2(1); C_g denotes the Cp* ring centroid.

S67

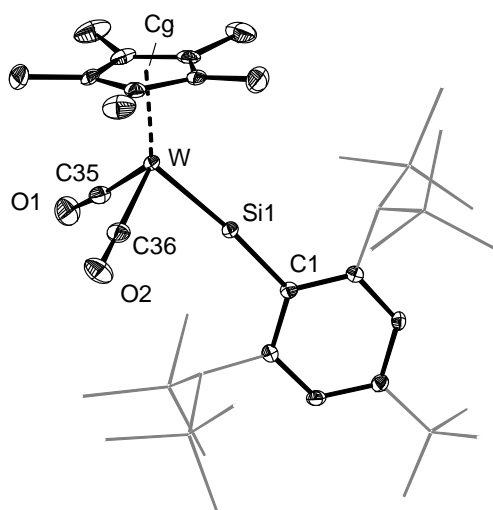


Figure S79. DIAMOND plot of the molecular structure of **1-W**. Thermal ellipsoids are set at 50% probability, hydrogen atoms were omitted and the substituents of the Tbb group are presented as a wireframe for the sake of clarity. Selected bond lengths (pm) and bond angles ($^{\circ}$): W–Si1 224.55(6), W–C35 195.7(3), W–C36 196.7(3), Si1–C1 185.1(2); W–Si1–C1 174.88(8), Si1–W–C35 89.42(7), Si1–W–C 86.97(7), C35–W–C36 88.5(1), Si1–W–C_g 135.86(2), C35–W–C_g 120.74(7), C36–W–C_g 120.98(7); C_g denotes the Cp* ring centroid.

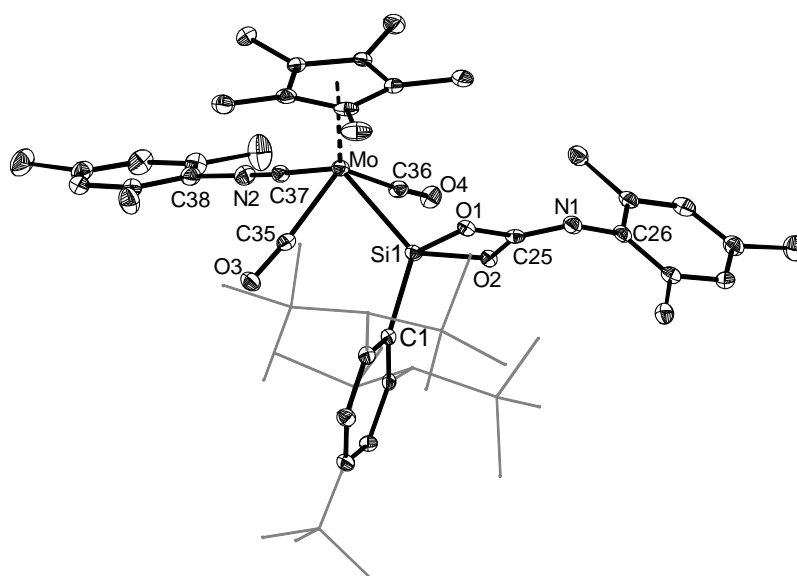


Figure S80. DIAMOND plot of the molecular structure of **2-Mo**. Thermal ellipsoids are set at 30% probability, hydrogen atoms were omitted and the substituents of the Tbb group are presented as a wireframe for the sake of clarity. Selected bond lengths (pm) and bond angles ($^{\circ}$): Mo–Si1 253.01(7), Mo–C35 198.8(3), Mo–C36 197.8(3), Mo–C37 204.2(3), Si1–O1 174.8(2), Si1–O2 176.0(2), Si1–C1 188.8(2), O1–C25 135.9(3), O2–C25 136.0(3), N1–C25 125.9(3), N1–C26 142.3(3), O3–C35 115.0(3), O4–C36 115.3(3), N2–C37 116.3(3), N2–C38 140.2(3); Si1–Mo–C35 74.11(7), Si1–Mo–C36 73.47(7), Si1–Mo–C37 127.7(1), C35–Mo–C36 110.3(1), C35–Mo–C37 76.2(1), C36–Mo–C37 78.0(1), Mo–Si1–C1 123.93(8), Mo–Si1–O1 115.17(6), Mo–Si1–O2 117.13(6), O1–Si1–C1 108.6(1), O2–Si1–C1 106.1(1), O1–Si1–O2 75.69(8), O1–C25–O2 104.6(2), Si1–O1–C25 90.1(1), Si1–O2–C25 89.5(1), C25–N1–C26 122.4(2), Mo–C35–O3 174.4(2), Mo–C36–O4 174.5(2), Mo–C37–N2 177.6(2), C37–N2–C38 164.9(3).

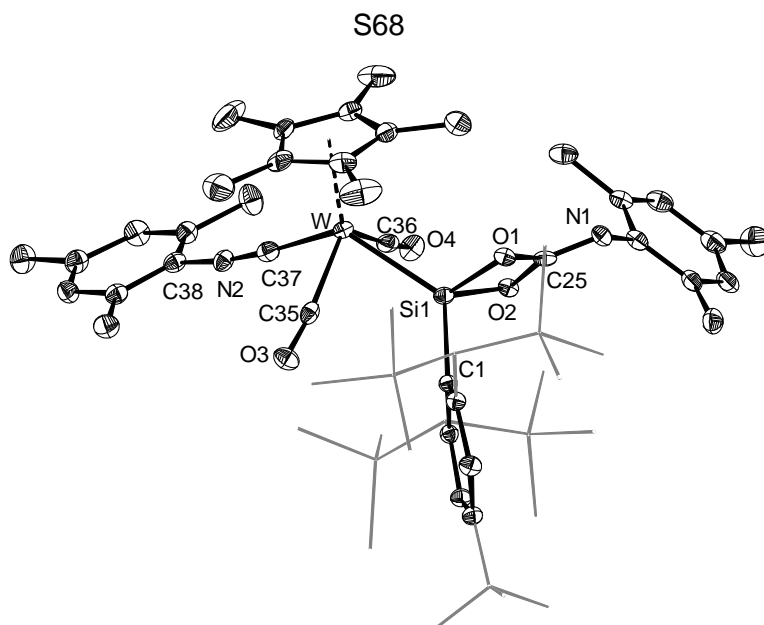


Figure S81. DIAMOND plot of the molecular structure of **2-W**. Thermal ellipsoids are set at 30% probability, hydrogen atoms were omitted and the substituents of the Tbb group are presented as a wireframe for the sake of clarity. Selected bond lengths (pm) and bond angles ($^{\circ}$): W–Si1 253.5(1), W–C35 198.8(5), W–C36 197.2(5), W–C37 204.2(5), Si1–O1 175.4(3), Si1–O2 175.9(3), Si1–C1 187.9(4), O1–C25 135.6(5), O2–C25 136.6(5), N1–C25 125.7(5), N1–C26 143.7(5), O3–C35 114.5(5), O4–C36 117.0(5), N2–C37 116.1(5), N2–C38 140.8(5); Si1–W–C35 75.2(1), Si1–W–C36 72.9(1), Si1–W–C37 128.4(1), C35–W–C36 111.6(2), C35–W–C37 77.9(2), C36–W–C37 77.4(2), W–Si1–C1 127.2(1), W–Si1–O1 116.2(1), W–Si1–O2 116.3(1), O1–Si1–C1 105.2(2), O2–Si1–C1 104.0(2), O1–Si1–O2 75.7(1), O1–C25–O2 104.8(3), Si1–O1–C25 90.0(2), Si1–O2–C25 89.5(2), C25–N1–C26 118.9(4), W–C35–O3 174.3(3), W–C36–O4 175.6(4), W–C37–N2 176.4(4), C37–N2–C38 170.0(5).

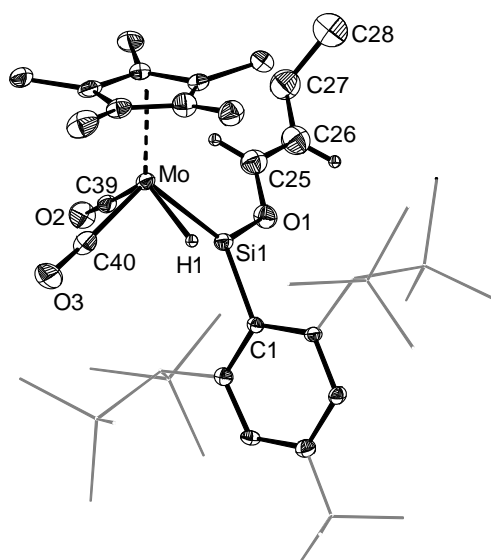


Figure S82. DIAMOND plot of the molecular structure of **3-Mo**. Thermal ellipsoids are set at 30% probability, hydrogen atoms except those bonded to the Mo, C25 and C26 atoms were omitted and the substituents of the Tbb group are presented as a wireframe for the sake of clarity. Selected bond lengths (pm), interatomic distances (pm) (indicated by a dotted line) and bond angles ($^{\circ}$) and distances (pm): Mo–Si1 235.8(2), Mo–H1 181(7), Mo–C39 196.1(8), Mo–C40 197.8(8), Si1–C1 188.2(6), Si1–O1 164.7(5), O1–C25 138(1), C25–C26 133(1), C26–C27 148.0(8), C27–C28 153(1), O2–C39 116.3(8), O3–C40 113.9(9); Si1...H1 208(6); Si1–Mo–C39 75.4(2), Si1–Mo–C40 106.4(2), Si1–Mo–H 58.1(19), C39–Mo–C40 84.9(3), Mo–Si1–C1 135.4(2), Mo–Si1–O1 124.6(2), O1–Si1–C1 100.0(3), O1–C25–C26 121.3(8), C25–C26–C27 124.3(9), C26–C27–C28 113.1(9), Mo–C39–O2 177.7(6), Mo–C40–O3 176.6(7).

S69

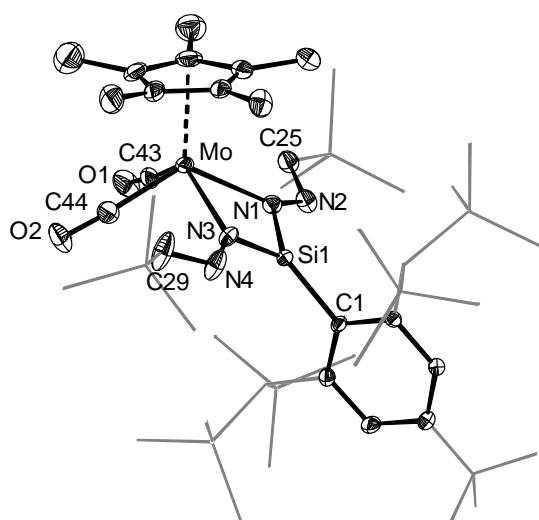


Figure S83. DIAMOND plot of the molecular structure of **4-Mo**. Thermal ellipsoids are set at 30% probability, hydrogen atoms were omitted and the substituents of the Tbb group are presented as a wireframe for the sake of clarity. Selected bond lengths (pm), interatomic distances (pm) (indicated by a dotted line) and bond angles ($^{\circ}$): Mo–N1 224.5(4), Mo–N3 222.7(4), Mo–C43 195.0(5), Mo–C44 195.4(5), Si1–N1 165.8(4), Si1–N3 165.1(4), Si1–C1 183.6(4), N1–N2 138.2(6), N2–C25 129.2(7), N3–N4 137.4(6), N4–C29 129.0(8), O1–C43 116.3(7), O2–C44 115.8(7); Mo \cdots Si1 296.1(1); N1–Mo–N3 67.0(1), N1–Mo–C43 85.4(2), N1–Mo–C44 124.1(2), N3–Mo–C43 127.2(2), N3–Mo–C44 85.5(2), Mo–N1–Si1 97.6(2), Mo–N1–N2 138.8(3), Si1–N1–N2 122.9(3), Mo–N3–Si1 98.4(2), Mo–N3–N4 136.8(3), Si1–N3–N4 124.2(3), N1–Si1–N3 96.4(2), N1–Si1–C1 130.8(2), N3–Si1–C1 132.6(2), N1–N2–C25 117.3(5), N3–N4–C29 117.7(5), N2–C25–Si6 121.0(5), N4–C29–Si7 124.0(5), Mo–C43–O1 176.3(5), Mo–C44–O2 175.7(5).

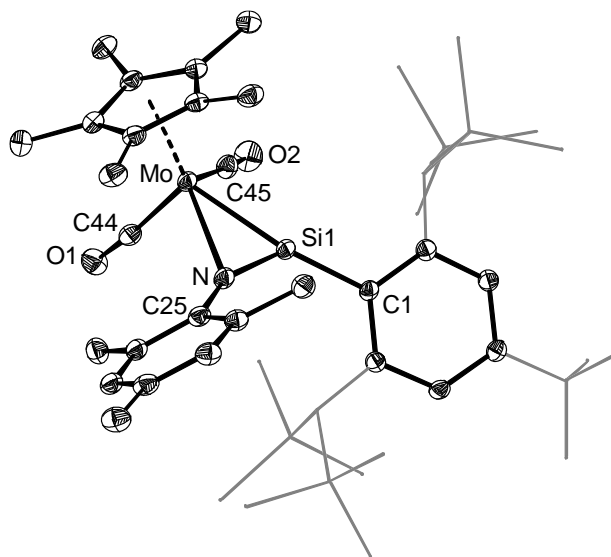


Figure S84. DIAMOND plot of the molecular structure of **5-Mo**. Thermal ellipsoids are set at 30% probability, hydrogen atoms were omitted and the substituents of the Tbb group are presented as a wireframe for the sake of clarity. Selected bond lengths (pm) and bond angles ($^{\circ}$): Mo–Si1 2.3977(8), Mo–N 239.1(2), Mo–C44 196.3(3), Mo–C45 195.0(3), Si1–N 161.5(3), Si1–C1 187.0(3), N–C25 140.2(4), O1–C44 116.2(4), O2–C45 116.1(4); Si1–Mo–N 39.41(7), Si1–Mo–C44 104.65(9), Si1–Mo–C45 83.05(9), N–Mo–C44 93.0(1), N–Mo–C45 117.2(1), C44–Mo–C45 76.7(1), Mo–Si1–C1 161.92(9), Mo–Si1–N 70.07(8), N–Si1–C1 126.4(1), Mo–N–Si1 70.52(9), Mo–N–C25 135.5(2), Si1–N–C25 151.8(2), Mo–C44–O1 173.8(3), Mo–C45–O2 177.1(3).

4 Electronic structure calculations

4.1 General methodology

Electronic structure calculations were carried out in the gas phase using the ORCA 5.0.3 program.^[S17] All calculations were performed using the DFT method B97-D3(BJ)-ATM/def2-TZVP, which consists of the GGA functional B97-D3(BJ)^[S18] in combination with the three body dispersion energy correction functional (ATM)^[S19], the triple- ζ quality basis set def2-TZVP^[S20] for all atoms and the auxiliary basis set of the type def2/J for the RI-JS^[S21] approximation of the Coulomb integral (J) using ORCA's standard convergence settings (method I).

To obtain high-level electronic energies, single-point energy calculations were performed on top of the calculated structures using the PWPB95-D3(BJ)-ATM/def2-QZVPP level of theory, consisting of the double-hybrid functional set PWPB95^[S22] with the D3(BJ)-ATM dispersion treatment and the quadruple- ζ basis set def2-QZVPP^[S20a] (method II). Thermochemical quantities on the level of theory "II" were obtained by adding the thermodynamic corrections obtained on the level of theory "I" to the electronic energies obtained on the level of theory "II". All optimized structures were verified as stationary points on the potential energy surface (PES) by analytical frequency calculations to obtain harmonic vibrations of the following classes – no significant imaginary frequency (minimum), one significant imaginary frequency (first-order saddle point or transition state). Transition states were localised using initial structures from relaxed potential energy surface scans or with the help of the NEB method.^[S23]

Bader's Atoms-in-molecules analyses were carried out using AIM2000, version 2.^[S24] The Si-H-coupling constants were calculated using the ORCA 5.0.3 program and therein implemented methods.^[S17,S25] NPA partial charges were calculated with NBO7.0.^[S26] The graphical

[S17] F. Neese, *WIREs Comput. Mol. Sci.* **2018**, 8, e1327.

[S18] (a) S. Grimme, J. Antony, S. Ehrlich, H. Krieg, *J. Chem. Phys.* **2010**, 132, 154104. (b) S. Grimme, S. Ehrlich, L. Goerigk, *J. Comput. Chem.* **2011**, 32, 1456.

[S19] (a) B. M. Axilrod, E. Teller, *J. Chem. Phys.* **1943**, 11, 299. (b) Y. Muto, *Proc. Phys. Math. Soc. Jpn.* **1943**, 17, 629.

[S20] (a) F. Weigend, R. Ahlrichs, *Phys. Chem. Chem. Phys.* **2005**, 7, 3297. (b) F. Weigend, *Phys. Chem. Chem. Phys.* **2006**, 8, 1057.

[S21] O. Vahtras, J. Almlöf, M. W. Feyereisen, *Chem. Phys. Lett.* **1993**, 213, 514.

[S22] L. Goerigk, S. Grimme, *J. Chem. Theory Comput.* **2011**, 7, 291.

[S23] G. Henkelman, B. P. Uberuaga, H. Jónsson, *J. Chem. Phys.* **2000**, 113, 9901.

[S24] F. Biegler-König, J. Schönbohm, *J. Comput. Chem.* **2002**, 23, 1489.

[S25] T. Helgaker, M. Jaszuński, K. Ruud, *Chem. Rev.* **1999**, 99, 293.

[S26] *NBO 7.0*. E. D. Glendening, J. K. Badenhoop, A. E. Reed, J. E. Carpenter, J. A. Bohmann, C. M. Morales, P. Karafiloglou, C. R. Landis, and F. Weinhold, Theoretical Chemistry Institute, University of Wisconsin, Madison (**2018**).

representations of the calculated structures were created using the program Olex2 (Version 1.3.0).^[S27]

4.2 Quantum chemical and experimental studies of the stereoisomerism and dynamics of **3-Mo**

A thorough analysis of the potential energy surface (PES) of **3-Mo** was performed by quantum chemical calculations to explain the IR and NMR spectroscopic features of **3-Mo** in solution. In fact, the molecular structure of **3-Mo** in the solid-state shows one isomer with two *cis*-ligated CO ligands. If one assumes, that only this *cis* isomer would be present in solution, then only two $\nu(\text{CO})$ bands of similar intensity would be expected in the IR spectrum of **3-Mo**, one at higher frequency arising from the in-phase stretching mode of the CO ligands and one at lower frequency originating from the out-of-phase stretching mode of the CO ligands.^[S28] However, the IR spectrum of **3-Mo** in *n*-hexane shows three clearly visible $\nu(\text{CO})$ bands at 1956, 1882 and 1872 cm^{-1} as well as a shoulder on the low-frequency side of the band at 1956 cm^{-1} , indicating that an additional isomer of **3-Mo** must be present in solution (*Figure S52*). This observation is in line with the results of quantum chemical studies suggesting the presence of two diastereomers of similar low energy, termed as *cis*_{anti} and *cis*_{syn}, respectively. Both isomers are *cis*-configured, i.e. have *cis*-ligated CO ligands, and are each present in solution as a racemic mixture of the *C* (clockwise) and *A* (anticlockwise) enantiomers (*Figure S85*).^[S29, S30, S31] Both display a tilted conformation of the silylidene ligand, with the Si-bonded OR

-
- [S27] O. V. Dolomanov, L. J. Bourhis, R. J. Gildea, J. A. K. Howard, H. Puschmann, *J. Appl. Cryst.*, **2009**, *42*, 339.
- [S28] A. C. Filippou, J. G. Winter, M. Feist, G. Kociok-Köhn, I. Hinz, *Polyhedron*, **1998**, *17*, 7, 1103 and references therein.
- [S29] N. G. Connelly, T. Damhus, R. M. Hartshorn and A. T. Hutton, *Nomenclature of inorganic chemistry: IUPAC recommendations 2005, IUPAC Red Book, IR-9*, Royal society of chemistry, Cambridge, ISBN: 978-0-85404-438-2, 2005.
- [S30] According to the IUPAC rules for the description of the configuration of coordination compounds (ref. S29), the two *cis*-isomers *C/A-cis*_{anti} and *C/A-cis*_{syn} are referred to as *C/A-SPY-5-13* isomers. *C* (*C*: clockwise) and *A* (*A*: anticlockwise) are the symbols for the absolute configuration of the isomers, *SPY-5* is the polyhedral symbol assuming that the closest idealized geometry of the isomers is square pyramidal with the Cp* ligand located at the apex of the square pyramid, and 13 is the configuration index, if the Cp* ligand at the apex of the square pyramid is considered to be the ligand of highest priority (priority number 1) and the hydrido ligand in the basal plane of the pyramid is considered to be the ligand of lowest priority (priority number 4). Similarly, the *trans*-isomer *trans* is denoted as the *SPY-5-12* isomer according to the same rules.
- [S31] In the present work, we have omitted the polyhedral symbol *SPY-5*, since all isomers have the same coordination geometry (square-pyramidal) and have decided to use the symbols *cis* and *trans* instead of the configuration index 13, as has been often done in the literature for complexes of the type $[(\eta^5\text{-C}_5\text{R}_5)\text{M}(\text{CO})_2\text{LX}]$ (*M* = Cr – W; *L* = 2e-donor ligand; *X* = 1e-donor ligand) (ref. S28).

substituent pointing towards the Cp* ring, as evidenced by the dihedral angle $C_g\text{-Mo-Si-O}$ of $+48.7/-48.7^\circ$ (**C/A-cis_{anti}**) and $-55.8/+55.8^\circ$ (**C/A-cis_{syn}**), respectively, where C_g is the Cp* ring centroid.^[S32]

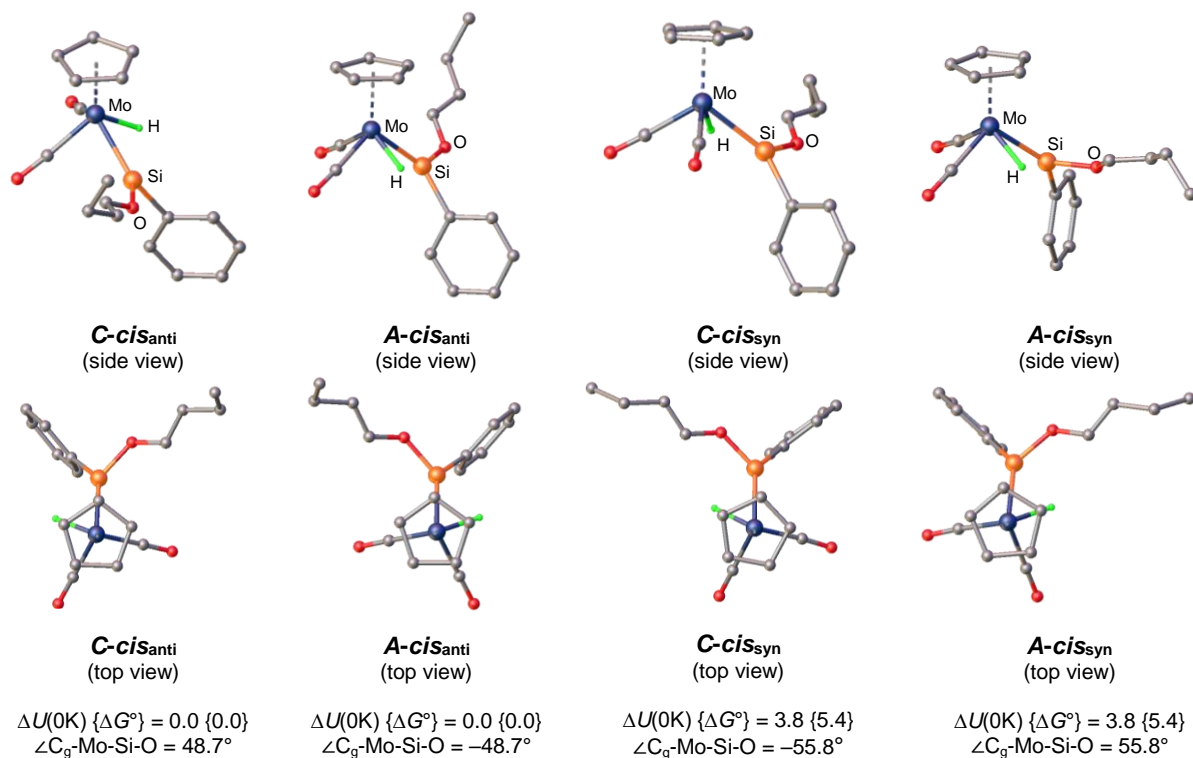


Figure S85. Side view (*top row*) and top view (*bottom row*) of the calculated structures (Olex plots) of the C and A enantiomers of the *cis* isomers **cis_{anti}** and **cis_{syn}** of **3-Mo** with their relative zero-point vibrational energy corrected inner energies $\Delta U(0K)$ (kJ·mol⁻¹), standard Gibbs energies ΔG° (kJ·mol⁻¹) (values in curly brackets) and the values of the dihedral angle $C_g\text{-Mo-Si-O}$, respectively. The methyl groups of the Cp* ligand and the substituents of the Tbb group were omitted for clarity.

The isomers **C/A-cis_{anti}** and **C/A-cis_{syn}** differ though in the relative orientation of the silylidyne and the hydrido ligand. A view along the Mo-Si bond shows, that in **A-cis_{anti}** the Mo-H and Si-OR groups are in *anticlinal* conformation ($\angle\text{H-Mo-Si-OR} = -157.1^\circ$), i.e. the Mo-H bond vector points almost in the opposite direction of the Si-OR bond vector, whereas in **A-cis_{syn}** the Mo-H and Si-OR groups have a *synclinal* conformation ($\angle\text{H-Mo-Si-OR} = -50.9^\circ$) (*Figure S86*). **cis_{anti}** is the most stable isomer with a slightly lower Gibbs energy of 5.4 kJ mol⁻¹ than the **cis_{syn}** isomer. In addition, a *trans*-configured isomer, labeled as **trans**, was found as a local minimum on the PES, whose Gibbs energy is 15.3 kJ/mol higher than that of the most stable isomer **cis_{anti}** (*Figure S86*). The calculated bonding parameters of the isomers **cis_{anti}**, **cis_{syn}** and **trans**, as well as the experimental values of **3-Mo** are summarized in *Tables S5* and *S6*. The calculated bond lengths and angles of **cis_{anti}** agree very well with the experimental bond

[S32] It should be mentioned that the rotamers with the Tbb substituents pointing towards the Cp* ligand were also identified as minima of the energy surface, but these appear at higher energy and are irrelevant in the context of the observed fluxionality and isomerism of **3-Mo** in solution.

lengths and bond angles of **3-Mo** and even the twist angles TA1 and TA2, which describe the twist of the silylidene ligand with respect to the Cp* ring and the hydrido ligand, respectively, or the C₉-Mo-Si-O dihedral angle, which describes the orientation of the OR substituent with respect to the Cp* ring, compare very well with the experimental values (Tables S5 and S6, Figure S86).

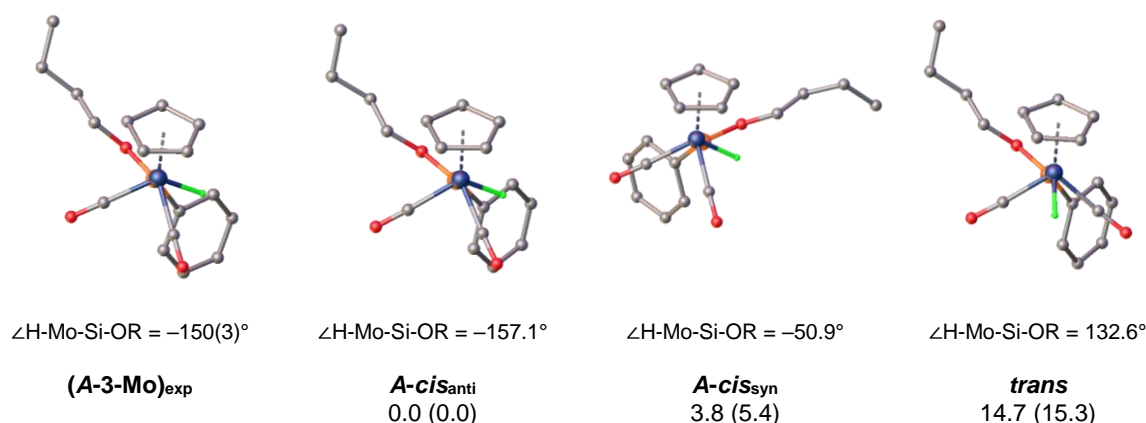


Figure S86. View along the Mo-Si bond of the experimental structure of **3-Mo** (A enantiomer) and the calculated structures of **A-cis_{anti}**, **A-cis_{syn}** and **trans** (Olex plots) with their relative zero-point vibrational energy corrected inner energies $\Delta U(0\text{K})$ (kJ·mol⁻¹) and standard Gibbs energies ΔG° (kJ·mol⁻¹) (values in parentheses). The methyl groups of the Cp* ligand and the substituents of the Tbb group were omitted for clarity.

The computed Mo-H bond lengths of **cis_{anti}** (173.1 pm) and **cis_{syn}** (175.0 pm) lie in the range of Mo-H 2c-2e bond lengths ($d(\text{Mo-H}) = 168.5(3) - 178.9(7)$) obtained from neutron diffraction studies.^[S33,S34] In comparison, the calculated Si-H distances of **cis_{anti}** (209.1 pm) and **cis_{syn}**

Table S5. Selected experimental and calculated bond lengths of the A enantiomer of **3-Mo** (**(A-3-Mo)_{exp}**: experimental values; **(A-3-Mo)_{th} = A-cis_{anti}**: calculated values), and calculated bond lengths of the isomers **A-cis_{syn}** and **trans**.

	Mo-Si	Mo-H	Mo-CO	Mo-C ₉	Si...H	Si-O	Si-C	C-O
(A-3-Mo)_{exp}	235.8(2)	181(7)	196.1(8) ^[a] 197.8(8) ^[b]	202.4(3)	208(6)	164.7(5)	188.2(6)	116.3(8) ^[a] 113.9(9) ^[b]
A-cis_{anti} (A-3-Mo)_{th}	236.1	173.1	195.8 ^[a] 196.1 ^[b]	204.9	209.1	168.6	188.3	117.1 ^[a] 116.3 ^[b]
A-cis_{syn}	236.6	175.0	194.9 ^[a] 197.1 ^[b]	203.8	195.9	168.3	188.8	116.7 ^[a] 116.3 ^[b]
trans	239.1	170.2	196.1 ^[c] 196.5 ^[d]	204.5	361.3	168.6	189.0	116.9 ^[c] 116.5 ^[d]

[a] CO located *trans* to H. [b] CO located *trans* to Si. [c] oriented towards the but-1-ene-1-olato group. [d] oriented towards the Tbb group.

[S33] (a) R. Bau, M. H. Drabnis, *Inorg. Chim. Acta.*, **1997**, *259*, 27.

[S34] (a) A. J. Schultz, K. L. Stearley, J. M. Williams, R. Mink, *Inorg. Chem.* **1977**, *16*, 3303; (b) L. Brammer, D. Zhao, R. M. Bullock, R. K. McMullan, *Inorg. Chem.*, **1993**, *32*, 4819; (c) Y.-C. Tsai, M. J. A. Johnson, D. J. Mindiola, C. C. Cummins, W. T. Klooster, T. F. Koetzle, *J. Am. Chem. Soc.* **1999**, *121*, 44, 10426; (d) M. Baya, J. Houghton, J.-C. Daran, R. Poli, L. Male, A. Albinati, M. Gutman, *Chem. Eur. J.* **2007**, *13*, 5347.

Table S6. Selected experimental and calculated bond angles, twist angles and dihedral angles (°) of the *A* enantiomer of **3-Mo** (**A-(3-Mo)**_{exp} : experimental values; **A-(3-Mo)**_{th} = **A-cis_{anti}**: calculated values), and calculated bond angles, twist angles and dihedral angles (°) of the isomers **A-cis_{syn}** and **trans**.

	CO-Mo-CO	H-Mo-Si	Mo-Si-O	Mo-Si-C	O-Si-C	C _g -Mo-H	C _g -Mo-Si	ΣSi ^[1]	TA1 ^[2]	TA2 ^[3]	DHA1 ^[4]	DHA2 ^[5]
(A-3-Mo) _{exp}	84.9(3)	58(2)	124.6(2)	135.4(2)	100.0(3)	120(2)	131.4(1)	360	45.2(2)	31(3)	-46.2(3)	-150(3)
A-cis_{anti} (A-(3-Mo)) _{th}	85.3	59.1	123.3	137.8	98.9	121.9	127.8	360	48.5	22.0	-48.7	-157.1
A-cis_{syn}	82.4	54.4	122.9	138.4	98.5	122.3	126.5	359.8	53.6	52.2	55.8	-50.9
trans	107.5	123.1	122.8	138.2	98.9	111.7	125.2	359.9	47.4	45.2	-48.8	132.6

[1] Sum of the bond angles at the Mo-bonded silicon atom (Si1); [2] twist angle (interplanar angle) between the (C_g,Mo,Si)-plane (C_g: Cp* ring centroid) and the (O,Si,C_{Tbb})-plane. [3] twist angle (interplanar angle) between the (H,Mo,Si)- plane and the (O,Si,C_{Tbb})-plane; [4] dihedral angle (torsion angle) C_g-Mo-Si-O. [5] dihedral angle (torsion angle) H-Mo-Si-O.

(195.9 pm) are considerably longer than those obtained for 2c-2e Si-H bonds by neutron diffraction ($d(\text{Si-H}) = 148.1(5) - 150.6(2)$).^[S35] The Si-H distances of **cis_{anti}** and **cis_{syn}** are much shorter than the sum of the van der Waals radii of Si and H (320 pm),^[S36] and appear in the range of distances for which non-classical M-H...Si interactions have been discussed.^[S37] A topological analysis of the electron density of both isomers was carried out using the AIM method^[S38] to address the question, whether a direct Si...H bonding interaction is present in **cis_{anti}** and **cis_{syn}**. For **cis_{anti}**, no bond path and no bond critical point was found between the Si and the H atom excluding any direct Si...H bonding interaction (*Figure S87, left*). The interatomic surfaces crossing the Mo-H and the Mo-Si paths do approach, but not meet each other in the charge concentration area between the Si and H atom (*Figure S87, left*). In comparison, for **cis_{syn}** a bond path with a bond critical point was found between the Si and the H atom. In this case, the interatomic surfaces crossing the Mo-H and the Mo-Si bond paths meet the interatomic surface, which crosses the Si-H bond path, at a ring critical point (rcp), that is closely located to the Si-H bond critical point (*Figure S87, right*). The proximity of the ring and bond critical point of the Si-H bond, as well as the similar values of the electron density

[S35] (a) J. A. K. Howard, P. A. Keller, T. Vogt, A. L. Taylor, N. D. Dix, J. L. Spencer, *Acta. Cryst.* **1992**, *B48*, 438; (b) P. P. Gasper, A. M. Beatty, T. Chen, T. Haile, D. Lei, W. R. Winchester, J. Braddock-Wilking, N. P. Rath, W. T. Klooster, T. F. Koetzle, S. A. Mason, A. Albinati, *Organometallics* **1999**, *18*, 3921; (c) I. Tanaka, T. Ohhara, N. Niimura, Y. Ohashi, Q. Jiang, D. H. Berry, R. Bau, *J. Chem. Res.* **1999**, *1*, 14; (d) M. Grellier, T. Ayed, J.-C. Barthelat, A. Albinati, S. Mason, L. Vendier, Y. Coppel, S. Sabo-Etienne, *J. Am. Chem. Soc.* **2009**, *131*, 7633; (e) E. Hupf, L. A. Malaspina, S. Holsten, F. Kleemiss, A. J. Edwards, J. R. Price, V. Kozich, K. Heyne, S. Mebs, S. Grabowsky, J. Beckmann, *Inorg. Chem.* **2019**, *58*, 16372.

[S36] (a) A. Bondi, *J. Phys. Chem.* **1964**, *68*, 441; (b) M. Mantina, A. C. Chamberlin, R. Valero, C. J. Cramer, D. G. Truhlar, *J. Phys. Chem. A* **2009**, *113*, 5806.

[S37] J. Y. Corey, *Chem. Rev.* **2011**, *111*, 863.

[S38] MORPHY98, a program written by P. L. A. Popelier with a contribution from R. G. A. Bone, UMIST, Manchester, England, EU 1998.

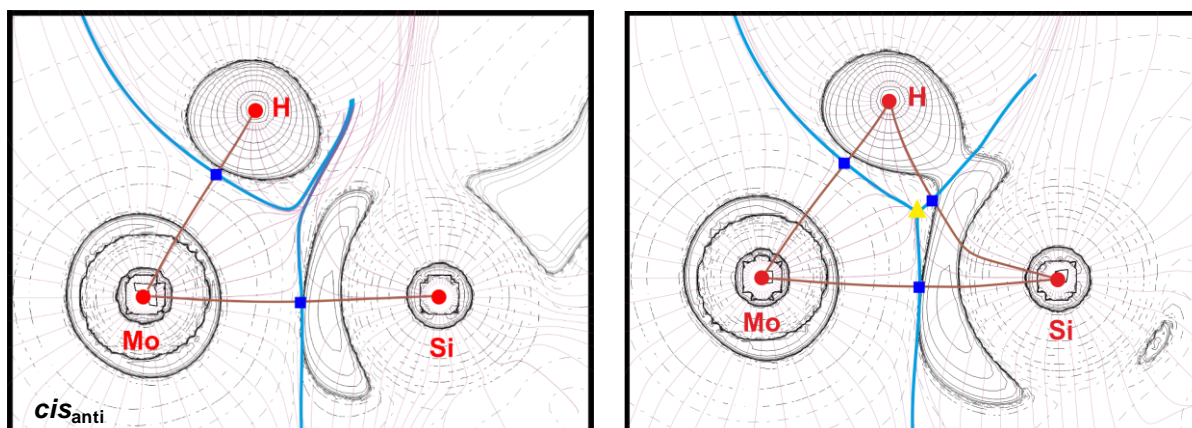


Figure S87. Molecular graph of *cis*_{anti} (left) and *cis*_{syn} (right) showing core critical points (red circles), bond critical points (dark blue squares), ring critical points (yellow triangles), bond paths (brown lines), gradient paths (mauve lines, projected into the given plane), areas of charge concentration (solid hairlines) and charge depletion (broken hairlines) as well as interatomic surfaces (blue lines).

Table S7. Results of the AIM analyses of *cis*_{anti} and *cis*_{syn}; values are given at the respective bond critical point (r_{bcp}) of each A-B bond and the ring critical point (rcp) of *cis*_{syn}: electron density (ρ), Laplacian of the electron density ($\nabla^2\rho$), relative kinetic energy density ($\frac{G}{\rho}$), relative total energy density ($\frac{H}{\rho}$) and bond ellipticity (ϵ); the position of the bcp is given in %, whereby a value larger than 50% means that the bcp is further away from atom A.

A-B	%A	%B	$\rho(r_{\text{bcp}})/\text{e}\text{\AA}^{-3}$	$\nabla^2\rho(r_{\text{bcp}})/\text{e}\text{\AA}^{-5}$	$\frac{G}{\rho}(r_{\text{bcp}})/\text{E}_\text{H}\text{e}^{-1}$	$\frac{H}{\rho}(r_{\text{bcp}})/\text{E}_\text{H}\text{e}^{-1}$	ϵ
<i>cis</i>_{anti}							
Mo-H	65	35	0.732	2.157	0.674	-0.468	0.115
Mo-Si	53	47	0.598	0.113	0.478	-0.465	0.279
<i>cis</i>_{syn}							
Mo-H	65	35	0.686	2.917	0.727	-0.429	0.185
Mo-Si	53	47	0.587	0.230	0.485	-0.458	0.028
Si-H	57	43	0.478	0.023	0.344	-0.341	1.267
rcp	17.8 pm ^a		0.474 ^b	1.508 ^b	0.516 ^b	-0.294 ^b	./.

^a: distance between the rcp and the bcp(Si-H); ^b: values at the rcp.

at these points indicate a very weak direct Si...H interaction, which is also reflected in the low value of the energy density (Table S7).

Further information on the Si...H interaction in *cis*_{anti} and *cis*_{syn} can be obtained from the sign and magnitude of the ²⁹Si,¹H spin-spin coupling constant. One bond Si,H coupling constants (¹J(Si,H)) have negative signs due to the negative gyromagnetic ratio of the ²⁹Si nucleus and range from ca. (-150) – (-400) Hz in silanes and transition metal hydrosilyl complexes, where only 2c-2e [TM-SiHRR'] interactions are present.^[S39,S40] In comparison, two-bond (geminal)

[S39] J. Schraml, J. M. Bellama, in *Determination of Organic Structures by Physical Methods*, F. C. Nachod, J. J. Zuckermann and E. W. Randall (Eds.), Academic Press, Vol 6 (Chapter 4), **1976**, pp. 203 – 269.

[S40] J. Y. Corey, J. Braddock-Wilking, *Chem. Rev.* **1999**, 99, 175.

coupling constants (${}^2J(\text{Si},\text{H})$) in silanes^[S39,S41] and transition metal silyl hydrides, as $[\text{Fe}(\text{H})(\text{SiCl}_3)(\text{CO})_4]$,^[S42] have usually positive signs^[S43] and much smaller values (ca. 5 – 25 Hz). The calculated ${}^{29}\text{Si},{}^1\text{H}$ coupling constant of **cis_{anti}** has a positive sign (+27.7 Hz), as expected for a ${}^2J(\text{Si},\text{H})$ coupling, and is in line with the AIM results excluding a direct Si...H interaction in **cis_{anti}**. In comparison, the calculated ${}^{29}\text{Si},{}^1\text{H}$ coupling constant of **cis_{syn}**, where the Si–H distance (195.9 pm) is shorter by 14 pm than in **cis_{anti}** has a negative value (-7.2 Hz). Notably, the same trend and a sign change of the $J(\text{Si},\text{H})$ coupling from plus to minus is observed in transition metal silyl hydride complexes upon decreasing the Si-H distance leading to an increased direct M-Si...H bonding interaction and finally to non classical hydrosilane complexes.^[S42b,S44] In case of **cis_{syn}** the negative sign of the $J(\text{Si},\text{H})$ coupling, as expected for a ${}^1J(\text{Si},\text{H})$ coupling, and its small absolute value suggests in combination with the AIM results a direct, weak Si...H bonding interaction.

A natural population analysis shows that a shortening of the Si-H distance by 14 pm and a strengthening of the Si...H interaction in **cis_{syn}** has only a small influence on the partial charges (Table S8). In all isomers the Si atom carries a high positive charge and the Mo atom a negative charge indicating a large polarization of the Mo=Si bond, whereas the metal-bonded H atom is almost electroneutral in **cis_{anti}** and **cis_{syn}** and slightly positive charged in the **trans** isomer.

Table S8. Charges of the given atoms and fragments obtained from Natural Population Analysis (NPA).

	Mo	Si	H	Mo(CO) ₂ Cp*	Si(OR)Tbb
cis_{anti}	-0.77	1.70	0.04	-0.68	0.64
cis_{syn}	-0.78	1.67	0.02	-0.63	0.61
trans	-0.79	1.67	0.12	-0.69	0.58

The IR spectrum of **3-Mo** in *n*-hexane solution shows three clearly visible $\nu(\text{CO})$ band maxima at 1956, 1882 and 1872 cm^{-1} as well as a shoulder on the low-frequency side of the band at 1956 cm^{-1} (Figure S88). Curve fitting and deconvolution of the IR spectrum using a Gaussian profile gave four bands peaking at 1956, 1950, 1883 and 1872 cm^{-1} (Figure S88) and their frequency integrated intensities, which are listed in Table S9.

[S41] W. McFarlane, *J. Chem. Soc. A* **1967**; 1275.

[S42] (a) D. L. Lichtenberger, *Organometallics* **2003**, *22*, 1599; (b) P. Meixner, K. Batke, A. Fischer, D. Schmitz, G. Eickerling, M. Kalter, K. Ruhland, K. Eichele, J. E. Barquera-Lozada, N. P. M. Casati, F. Montisci, P. Macchi, W. Scherer, *J. Phys. Chem. A* **2017**, *121*, 38, 7219.

[S43] An exception seems to be the vinyl silane $\text{Me}_3\text{SiCH}=\text{CH}_2$, for which a negative ${}^2J(\text{Si},\text{H})$ coupling constant was predicted by calculations: Y. Y. Rusakov, L. B. Krivdin, V. M. Nosova, A. V. Kisin, *Magn. Reson. Chem.* **2012**, *50*, 278.

[S44] W. Scherer, P. Meixner, K. Batke, J. E. Barquera-Lozada, K. Ruhland, A. Fischer, G. Eickerling, K. Eichele, *Angew. Chem. Int. Ed.* **2016**, *55*, 11673.

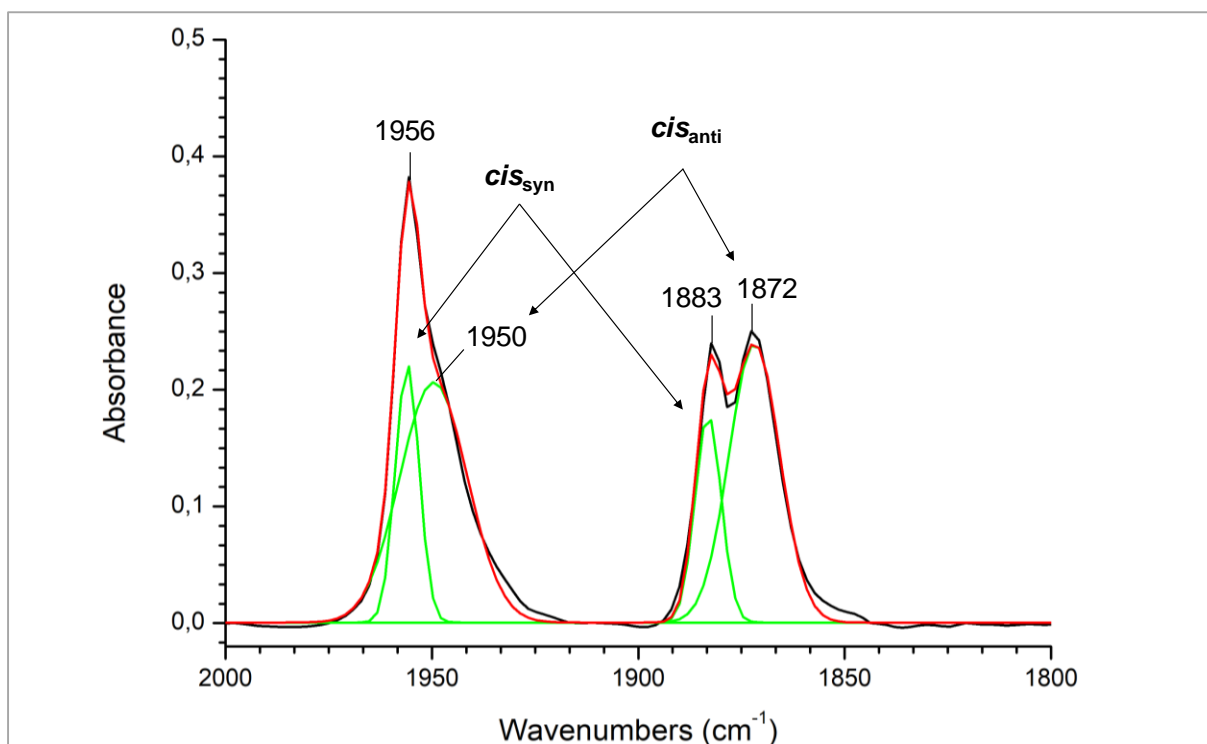


Figure S88. Experimental (black line), simulated (red line) and deconvoluted IR spectrum (green lines) of **3-Mo** in *n*-hexane solution using a Gaussian profile.

After comparison with the calculated harmonic frequencies of the ***cis*_{anti}** and ***cis*_{syn}** isomers (Table S9), the bands at 1950 and 1872 cm⁻¹ can be assigned to the in-phase and out-of-phase combination of the two CO stretching modes of the ***cis*_{anti}** isomer, and those at 1956 and 1883 cm⁻¹ to the in-phase and out-of-phase combination of the two CO stretching modes of the ***cis*_{syn}** isomer.

The equilibrium constant $K_{\text{exp}} = \frac{c(\textit{cis}_{\text{anti}})}{c(\textit{cis}_{\text{syn}})}$ and the Gibbs energy difference $\Delta G^{\circ}_{\text{exp}} (G^{\circ}(\textit{cis}_{\text{anti}}) - G^{\circ}(\textit{cis}_{\text{syn}}))$ at 298K can be estimated assuming that the sum of the frequency integrated intensities of the two $\nu(\text{CO})$ bands of the isomer ***cis*_{anti}** is equal to that of ***cis*_{syn}**.^[S45] The obtained values ($K_{\text{exp}} = 2.6$, $\Delta G^{\circ}_{\text{exp}} (298\text{K}) = -2.4 \text{ kJ mol}^{-1}$) are in reasonable agreement with the calculated values ($K_{\text{th}} = 8.8$, $\Delta G^{\circ}_{\text{th}} = -5.4 \text{ kJ mol}^{-1}$).

[S45] This assumption is based on the hypothesis that the Napierian molar absorption coefficient of the in-phase combination of the two CO stretching modes of ***cis*_{anti}** is equal to that of ***cis*_{syn}**, and analogously that the Napierian molar absorption coefficient of the out-of-phase combination of the two CO modes of ***cis*_{anti}** mode is equal to that of ***cis*_{syn}**, since the structure and bonding parameters of the M(CO)₂ fragment are very similar in the two isomers.

Table S9. Experimental $\nu(\text{CO})$, $\nu(\text{Mo-H})$ and $\nu(\text{C=C})$ frequencies of **3-Mo** and calculated values of the *cis*_{anti} and *cis*_{syn} and *trans* isomers of **3-Mo**.

Isomer	$\nu(\text{CO})$ (cm^{-1})	Frequency integrated intensity of $\nu(\text{CO})$ bands (cm^{-1})	Absolute intensity of $\nu(\text{CO})$ bands (km mol^{-1})	Relative intensity of $\nu(\text{CO})$ bands	$\nu(\text{Mo-H})^a$ (cm^{-1})	$\nu(\text{C=C})^a$ (cm^{-1})
Experimental						
3-Mo	1950	4.23	-	1	1739 ^b	1662
	1872	3.68		0.87		
3-Mo	1956	1.59	-	1		
	1883	1.42		0.89		
Calculated						
<i>cis</i> _{anti}	1946	-	766	1	1791	1675
	1877		603	0.79	[82;0.11]	[74;0.10]
<i>cis</i> _{syn}	1946	-	779	1	1735	1674
	1882		585	0.75	[93;0.12]	[65;0.09]
<i>trans</i>	1938	-	385	0.44	1838	1675
	1883		877	1	[10;0.01]	[68;0.08]

^a absolute intensities (km mol^{-1}) and relative intensities of the $\nu(\text{Mo-H})$ and the $\nu(\text{C=C})$ bands are given in square brackets; ^b $\nu(\text{Mo-H})$ obtained from the solid state ATR-IR spectrum of **3-Mo**.

Based on the calculated Gibbs energy difference $\Delta G_{\text{trans-cis}}$ between the *trans* isomer and the *cis*_{anti} isomer at 298 K of 15.3 kJ mol^{-1} , the molar ratio of $\frac{\text{trans}}{\text{cis}_{\text{anti}}}$ can be estimated at 298 K as 0.002. This value suggests that the *trans* isomer should be hardly visible in the IR spectrum of **3-Mo** due to its very low concentration.

The IR spectrum of **3-Mo** in *n*-hexane shows also one characteristic band arising from the C=C stretching mode of the but-1-ene-1-olato substituent at 1662 cm^{-1} (Figure S52), which compares well with the calculated value of the *cis*_{anti} (1675 cm^{-1}) and *cis*_{syn} isomer (1674 cm^{-1}). In comparison, no band could be observed for the Mo-H stretching mode in solution (Figure S52), which is however clearly visible in the ATR-IR spectrum of **3-Mo** at 1739 cm^{-1} (Figure S50). To rationalize this observation the relaxed potential energy surface around the minimum structure of *cis*_{anti} and *cis*_{syn} was calculated, varying the Mo-H distance from 1.6 to 2.0 \AA and the Si-H distance from $1.6 - 2.2 \text{ \AA}$ (Figure S89). The 2-dimensional surface plots show a shallow potential and an enhanced flexibility of the hydride around the respective minimum position. For example, a change of the Si-H distance from $1.9 - 2.2 \text{ \AA}$ and of the Mo-H distance from $1.7 - 1.8 \text{ \AA}$ leads to an increase of the electronic energy of *cis*_{anti} by maximal 2 kJ mol^{-1} .

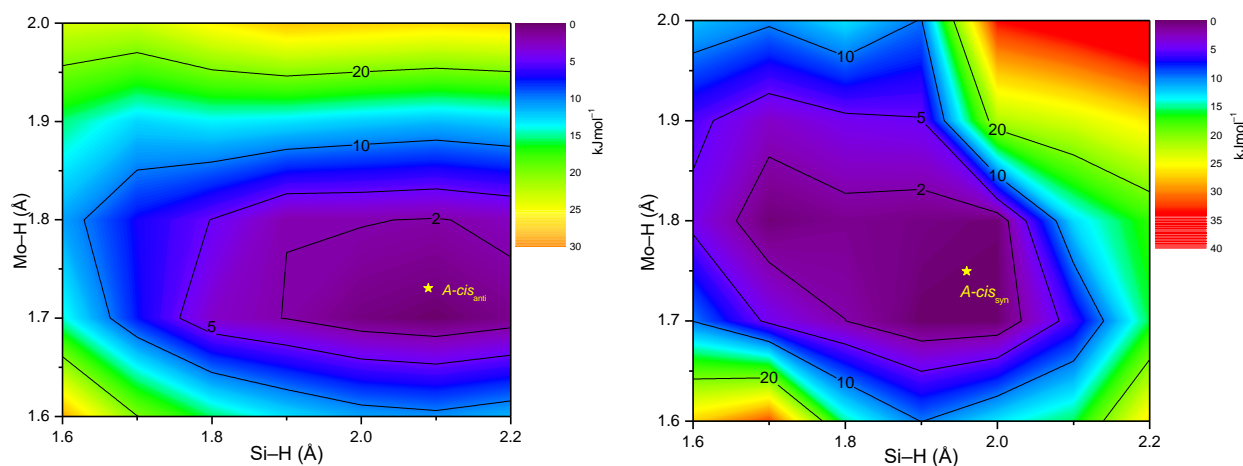


Figure S89. Two-dimensional representation of the relaxed potential energy surface *cis_{anti}* (left) and *cis_{syn}* (right) as a function of the Si–H and Mo–H distance in Å (mesh width: 5 pm). Electronic energies are given in kJ mol⁻¹. The global (fully optimized) minimum (set to 0.0 kJ mol⁻¹) is depicted with a yellow star. Iso-energy lines at 2, 5, 10, and 20 kJ mol⁻¹ are drawn as black lines .

Therefore, one may assume that several rapidly equilibrating species are present in solution. Their energy differ by less than 2 kJ mol⁻¹ from the minimum structures *cis_{anti}* and *cis_{syn}* and their Mo–H bond lengths and Si–H distances vary in a range of few pm around the values of the minimum structures of *cis_{anti}* and *cis_{syn}*, respectively. The positions of the $\nu(\text{CO})$ bands of these species are essentially the same as those of *cis_{anti}* and *cis_{syn}*, respectively, but their $\nu(\text{Mo–H})$ bands vary, as evidenced by a comparison of *cis_{anti}* and *cis_{syn}*, which shows that a shortening of the Mo–H bond by 2 pm (*cis_{syn}* (175.0 pm) \rightarrow *cis_{anti}* (173.1 pm)) leads to an increase of the $\nu(\text{Mo–H})$ frequency by 56 cm⁻¹ (*cis_{syn}* (1735 cm⁻¹) \rightarrow *cis_{anti}* (1791 cm⁻¹)). This suggests that the low intensity of the $\nu(\text{Mo–H})$ band of *cis_{anti}* and *cis_{syn}* is distributed over a larger range of wavenumbers around the respective band maximum in solution leading to a considerable broadening of the $\nu(\text{Mo–H})$ band. Notably, the Boltzmann corrected IR spectrum of the ensemble of structures covered by the two PES scans (Figure S89) is quite similar to the experimental spectrum of **3-Mo** in *n*-hexane solution verifying the above assumptions (Figure S52).

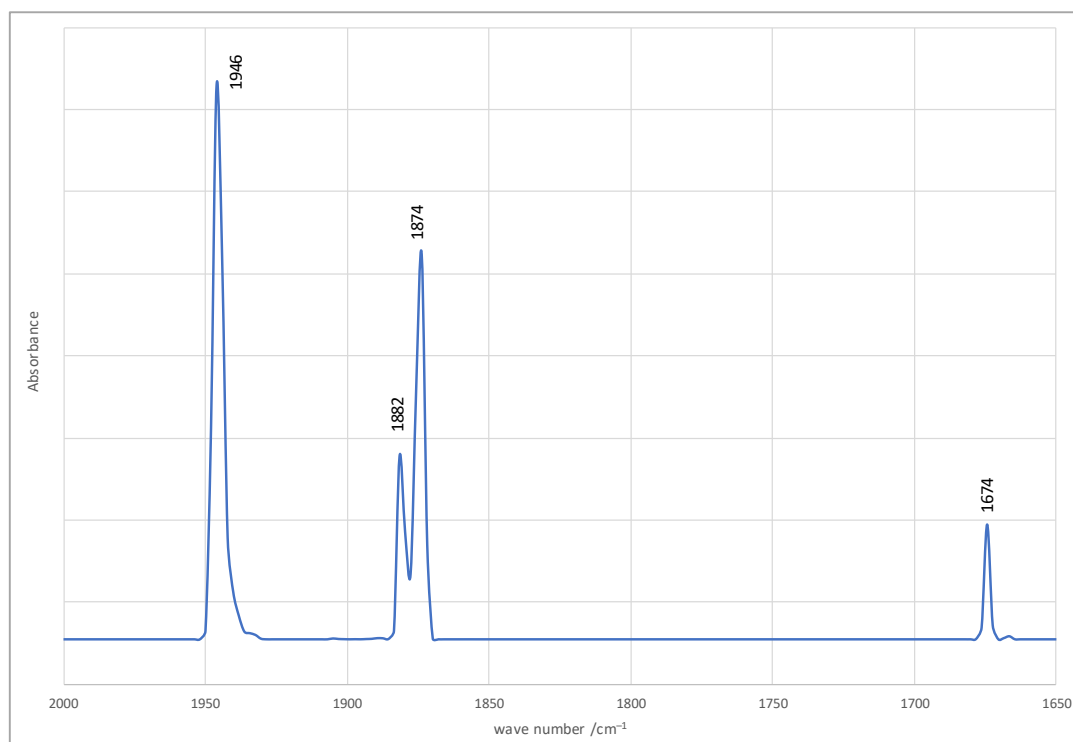


Figure S90. Simulated, Boltzmann-corrected IR spectrum of all species covered in the PES scans of **A-cis_{anti}** and **A-cis_{syn}** (see Figure S89). For all IR bands gaussian profiles were used with a full width at half maximum of 2 cm⁻¹; the individual IR spectra of the species were multiplied by the fraction of the species in the ensemble obtained using Boltzmann's partition function and then summed up to give the simulated spectrum.

As outlined above, the experimental and theoretical IR studies of **3-Mo** indicate the presence of two isomers (**cis_{anti}** and **cis_{syn}**) in solution. In comparison, the ¹H, ¹³C{¹H} and ²⁹Si{¹H} NMR spectra of **3-Mo** show only one set of signals, the number and multiplicity of which indicate a time-averaged C_s-symmetric structure in solution with the symmetry plane passing through the silylidene ligand plane and bisecting the Cp*Mo(CO)₂ fragment and the Tbb ring plane. For example, the ¹H NMR spectrum of **3-Mo** in (D₆)benzene at 298 K shows only one Mo-H resonance at δ = -7.42 ppm, which is flanked by ²⁹Si satellites with a ²⁹Si-¹H spin-spin coupling constant of 22 Hz (Figure S54). Notably, the experimental value of the J(Si,H) coupling constant compares well with the calculated value of J(Si,H)_{th} obtained from the following equation,

$$J(\text{Si}, \text{H})_{\text{th}} = x_1 \cdot J(\text{Si}, \text{H})_{\text{th}}(\text{cis}_{\text{anti}}) + x_2 \cdot J(\text{Si}, \text{H})_{\text{th}}(\text{cis}_{\text{syn}})$$

where x_1 and x_2 are the mole fractions of **cis_{anti}** and **cis_{syn}**, respectively, obtained from the IR spectrum of **3-Mo** ($K_{\text{exp}} = 2.6$, *vide supra*), $J(\text{Si}, \text{H})_{\text{th}}(\text{cis}_{\text{anti}})$ is the calculated Si,H coupling constant of **cis_{anti}**, and $J(\text{Si}, \text{H})_{\text{th}}(\text{cis}_{\text{syn}})$ is the calculated Si,H coupling constant of **cis_{syn}**. With $x_1 = 0.72$, $x_2 = 0.28$, $J(\text{Si}, \text{H})_{\text{th}}(\text{cis}_{\text{anti}}) = +27.7$ Hz and $J(\text{Si}, \text{H})_{\text{th}}(\text{cis}_{\text{syn}}) = -7.2$ Hz, a $J(\text{Si}, \text{H})_{\text{th}}$ value of 18 Hz is obtained.

Furthermore, the ¹³C{¹H} spectrum of **3-Mo** shows only one signal for the two CO ligands at δ = 235 ppm (Figure S56). This is quite different from what would be expected for the static structures of the C₁-symmetric isomers **cis_{anti}** and **cis_{syn}**, for which two singlets should be

observed for the diastereotopic CO ligands, respectively. Similarly, the $^{29}\text{Si}\{^1\text{H}\}$ NMR spectrum of **3-Mo** shows only one ^{29}Si resonance for the Mo=Si group at $\delta = 215.8$ ppm instead of the expected two resonances, and two ^{29}Si signals for the SiMe₃ groups instead of the four signals expected for each of the *cis* isomers in case of a hindered rotation of the Tbb substituent around the Si-C_{Tbb} bond (Figure S57).

All NMR features of **3-Mo** can be explained if one assumes that in solution, a rapid equilibration of the two *cis* isomers occurs, which proceeds via a C_s-symmetric state. This process is too fast to be resolved on the NMR time scale ($10^1 - 10^6$ s). The two *cis* isomers can be observed though by IR spectroscopy due to the faster time scale of this method ($10^{-11} - 10^{-14}$ s). This was verified by quantum chemical studies suggesting a reaction path via two enantiomeric *trans* intermediates for the interconversion of *cis*_{anti} and *cis*_{syn} (Figure S91).

4.2.1 Stereoisomerization pathways of 3-Mo

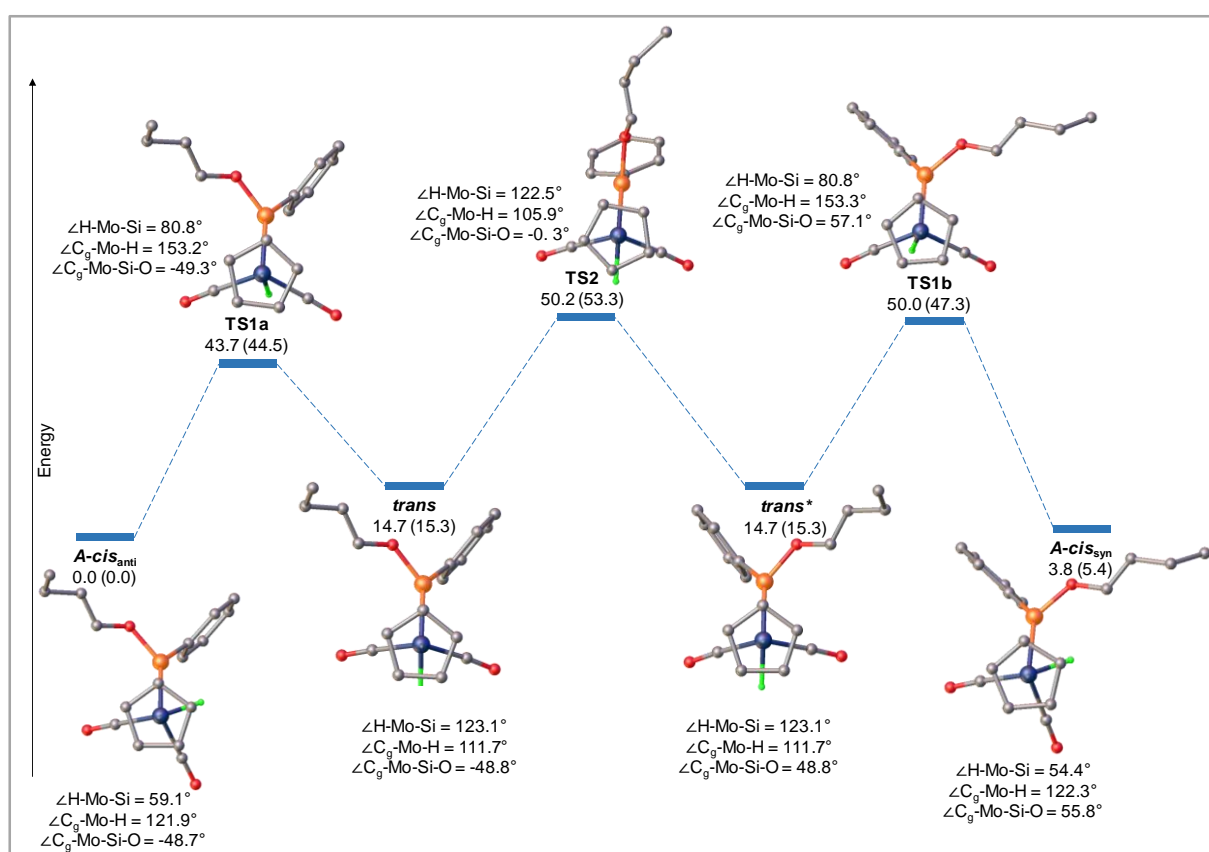


Figure S91. Reaction profile for the diastereomerization of **A-cis_{anti}** to **A-cis_{syn}**; Olex plots of the calculated structures of **A-cis_{anti}**, **A-cis_{syn}**, the transition states (**TS1a**, **TS2** and **TS1b**) and the intermediates **trans** and **trans*** (top views) with their relative zero-point vibrational energy corrected inner energies $\Delta U(0\text{K})$ (kJ·mol⁻¹) and standard Gibbs energies ΔG° (kJ·mol⁻¹) (values in parentheses).

In the first step **A-cis_{anti}** isomerizes to the *trans* diastereomer **trans** by migration of the H ligand from the *cis* to the *trans* position to the silylidene ligand (Figure S91). A closer look at the trajectory connecting **A-cis_{anti}** to **trans** via the transition state **TS1a** shows that the H-Mo-Si angle and the Si-H distance increase continuously along the path from **A-cis_{anti}** to **trans**, while

the C_g-Mo-H angle increases first from 121.9° (**A-cis_{anti}**) to a maximum value in a pseudo-trigonal-bipyramidal structure, in which the Cp* and H ligands occupy nearly the apical positions, and then decreases over 153° in the transition state **TS1a** to 111.7° in the product **trans** (Table S10). Remarkably, the tilted conformation of the silylidene ligand is maintained during the isomerization as shown by the twist angle TA1 making the **trans** product chiral. In the next step the isomer **trans** transforms to its conformational enantiomer **trans*** via the C_s symmetric transition state **TS2** (Figure S91). A look at the trajectory connecting **trans** to **trans*** shows that the reaction path involves a rotation of the silylidene ligand around the Mo=Si bond as shown by the change in the dihedral angle C_g-Mo-Si-O (DHA1) from -48.8° in **trans** to +48.8° in **trans***. The silylidene ligand adopts in the transition state **TS2** an upright conformation with the OR substituent pointing towards the Cp* group ($\angle(\text{C}_g\text{-Mo-Si-O}) = -0.3^\circ$). In the final step **trans*** converts to the *cis* diastereomer **A-cis_{syn}** by migration of the H ligand from the *trans* to the *cis* position relative to the silylidene ligand. The reaction path is similar to the one that leads the **trans** intermediate back to **A-cis_{anti}**. It is noteworthy, that the isomerization pathway leading to equilibration between **A-cis_{anti}** and its diastereomer **A-cis_{syn}** in solution (and in the same way between **C-cis_{anti}** and **C-cis_{syn}**) does not involve a change in the metal configuration. The calculated Gibbs energies of activation range from 32 to 44.5 kJ·mol⁻¹ for the forward reaction and from 29.2 to 41.9 kJ·mol⁻¹ for the backward reaction suggesting that the process may be detectable by NMR spectroscopy at low-temperature. However, the ¹H NMR (300.1 MHz) spectrum of **3-Mo** in (D₈)toluene showed no significant change up to 193 K and the ¹³C{¹H} NMR spectrum (75.47 MHz) of **3-Mo** at 193K only showed an incipient broadening of the CO signal at $\delta = 236.2$ ppm ($\Delta\nu_{1/2} = 10.3$ Hz) indicating that the process at 193 K is still too fast on the NMR time scale (Figure S92).

Table S10. Selected calculated bonding parameters of the transition states and the intermediates of the diastereomerization of **A-cis_{anti}** to **A-cis_{syn}**.

	Mo-Si	Mo-H	Si...H	H-Mo-CO ^a [1]	H-Mo-CO ^b [1]	CO-Mo-CO	H-Mo-Si	C _g -Mo-Si	C _g -Mo-H	TA1[2]	TA2[3]	DHA1[4]	DHA2[5]
A-cis_{anti} A-(3-Mo)_{th}	236.1	173.1	209.1	116.8	68.9	85.3	59.1	127.8	121.9	48.5	22.0	-48.7	-157.1
TS1a	236.6	173.1	269.9	63.2	49.3	109.4	80.8	124.8	153.2	48.9	38.9	-49.3	139.4
trans	239.1	170.2	361.3	71.2	63.8	107.5	123.1	125.2	111.7	47.4	45.2	-48.8	132.6
TS2	242.0	168.5	361.6	67.7	65.7	107.6	122.5	131.6	105.9	1.8	0.53	-0.3	-179.3
trans*	239.1	170.2	361.3	63.8	71.2	107.5	123.1	125.2	111.7	47.4	45.2	48.8	-132.6
TS1b	236.1	173.0	269.5	49.2	62.9	109.4	80.8	124.9	153.3	54.8	44.6	57.1	-130.9
A-cis_{syn}	236.6	175.0	195.9	116.2	72.0	82.4	54.4	126.5	122.3	126.4	52.2	55.8	-50.9

[1] CO^a = CO ligand located *trans* to hydride in **A-cis_{anti}** and **A-cis_{syn}**; CO^b = CO ligand located *cis* to hydride in **A-cis_{anti}** and **A-cis_{syn}**; [2] twist angle (interplanar angle) between the (C_g,Mo,Si)-plane (C_g: Cp* ring centroid) and the (O,Si,C_{Tbb})-plane; [3] twist angle (interplanar angle) between the (H,Mo,Si)- plane and the (O,Si,C_{Tbb})-plane; [4] dihedral angle (torsion angle) C_g-Mo-Si-O. [5] dihedral angle (torsion angle) H-Mo-Si-O.

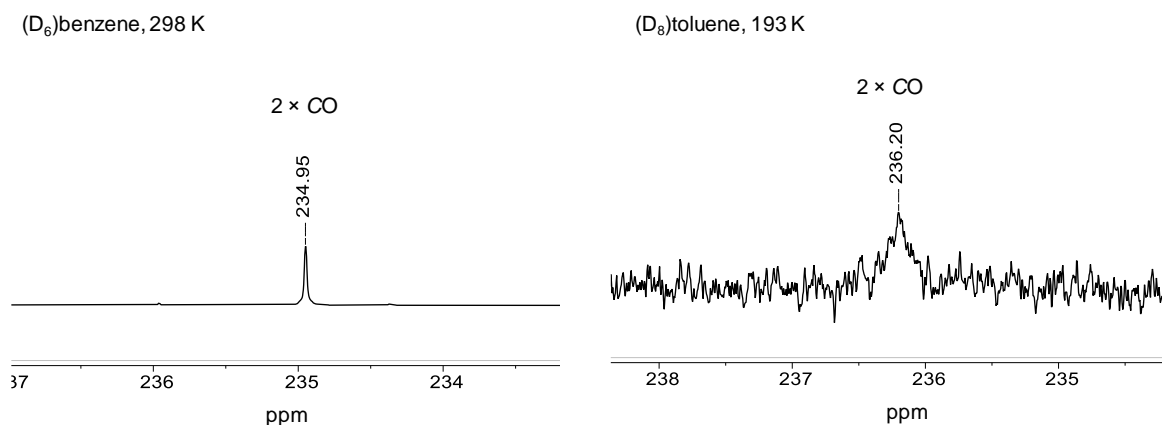


Figure S92. Carbonyl signal of **3-Mo** in the $^{13}\text{C}\{^1\text{H}\}$ NMR spectrum (125.8 MHz, (D_6) benzene) at 298 K (*left*) and the $^{13}\text{C}\{^1\text{H}\}$ NMR spectrum (75.47 MHz, (D_8) toluene) at 193 K (*right*).

A second diastereomerization pathway was found leading directly from **A-cis_{anti}** to **C-cis_{syn}** via the transition state **TS3** (*Figure S93*). In this case, the H ligand migrates from the one to the other *cis* coordination site relative to the silylidene ligand, i.e. the metal configuration changes from *A* to *C*. A look at the trajectory connecting **A-cis_{anti}** to **C-cis_{syn}** shows that the Mo-H bond moves around the silylidene ligand from the opposite site to the Cp* group (*Table S11*). This is evidenced by the increase in the C₉-Mo-H angle to 170° in the **TS3** transition state, which adopts a pseudotrigonal-bipyramidal structure with the Cp* and H ligands occupying the apical positions. During the H migration, the silylidene ligand retains its tilted conformation as

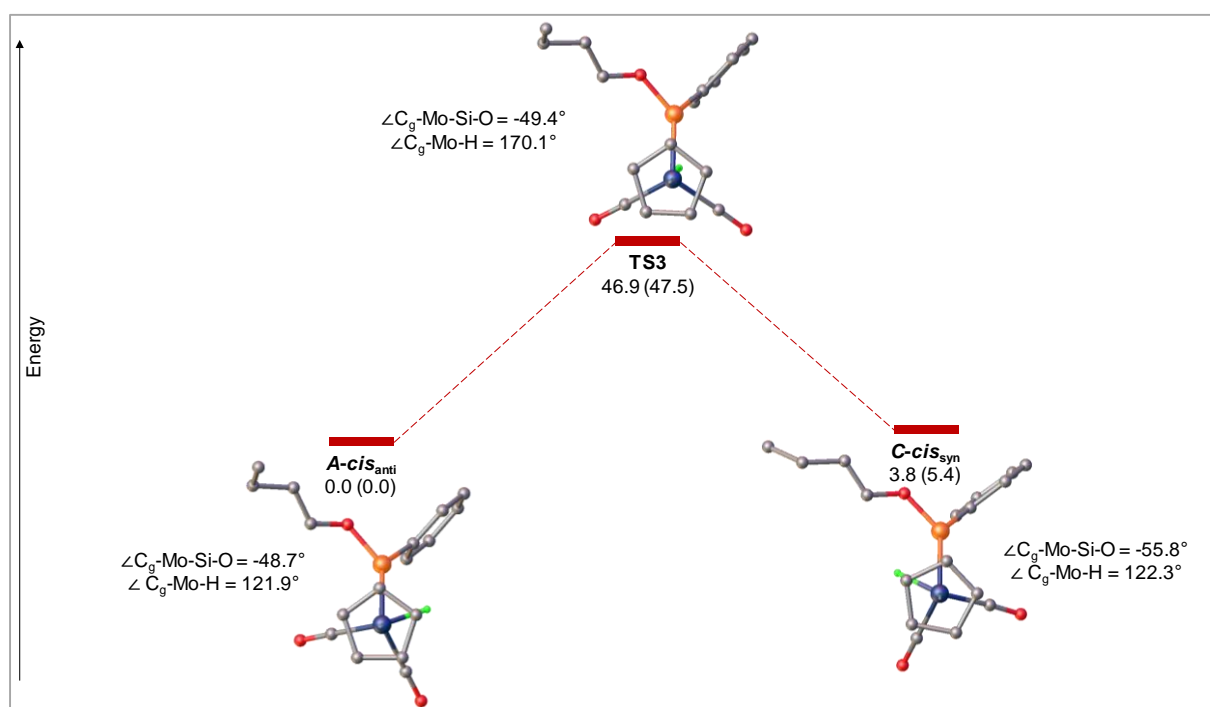


Figure S93. Reaction profile for the diastereomerization of **A-cis_{anti}** to **C-cis_{syn}**; Olex plots of the calculated structures of **A-cis_{anti}**, **C-cis_{syn}** and the transition state **TS3** (top views) with their relative zero-point vibrational energy corrected inner energies $\Delta U(0\text{K})$ ($\text{kJ}\cdot\text{mol}^{-1}$) and standard Gibbs energies ΔG° ($\text{kJ}\cdot\text{mol}^{-1}$) (values in parentheses).

shown by the slight change in the dihedral angle $C_g\text{-Mo-Si-O}$ (**A-cis_{anti}** → **TS3** → **C-cis_{syn}** : $-48.7^\circ \rightarrow -49.4^\circ \rightarrow -55.8^\circ$). However, this dynamic process, which has a similar barrier ($\Delta G^\ddagger = 47.5 \text{ kJ mol}^{-1}$) to the diastereomerization **A-cis_{anti}** → **A-cis_{syn}** (Figure S91), cannot explain the time averaged mirror-symmetric structure of **3-Mo** in solution observed by NMR spectroscopy.

Table S11. Selected calculated bonding parameters of **A-cis_{anti}**, **C-cis_{syn}** and the transition state **TS3** for the diastereomerization of **A-cis_{anti}** to **C-cis_{syn}**.

	Mo-Si	Mo-H	Si...H	H-Mo-CO ^a [1]	H-Mo-CO ^b [1]	CO-Mo-CO	H-Mo-Si	C _g -Mo-Si	C _g -Mo-H	TA1 ^[2]	TA2 ^[3]	DHA1 ^[4]	DHA2 ^[5]
A-cis_{anti} A-(3-Mo)_{th}	236.1	173.1	209.1	116.8	68.9	85.3	59.1	127.8	121.9	48.5	22.0	-48.7	-157.1
TS3	236.1	172.0	181.6	73.0	66.6	99.6	49.9	121.3	170.1	46.5	39.4	-49.4	135.9
C-cis_{syn}	236.6	175.0	195.9	72.0	116.2	82.4	54.4	126.5	122.3	53.6	52.2	-55.8	50.9

[1] CO^a = CO ligand located *trans* to hydride in **A-cis_{anti}** and *cis* to hydride in **C-cis_{syn}**; CO^b = CO ligand located *cis* to hydride in **A-cis_{anti}** and *trans* to hydride in **A-cis_{syn}**; [2] twist angle (interplanar angle) between the (C_g,Mo,Si)-plane (C_g: Cp* ring centroid) and the (O,Si,C_{Tbb})-plane. [3] twist angle (interplanar angle) between the (H,Mo,Si)-plane and the (O,Si,C_{Tbb})-plane; [4] dihedral angle (torsion angle) C_g-Mo-Si-O. [5] dihedral angle (torsion angle) H-Mo-Si-O.

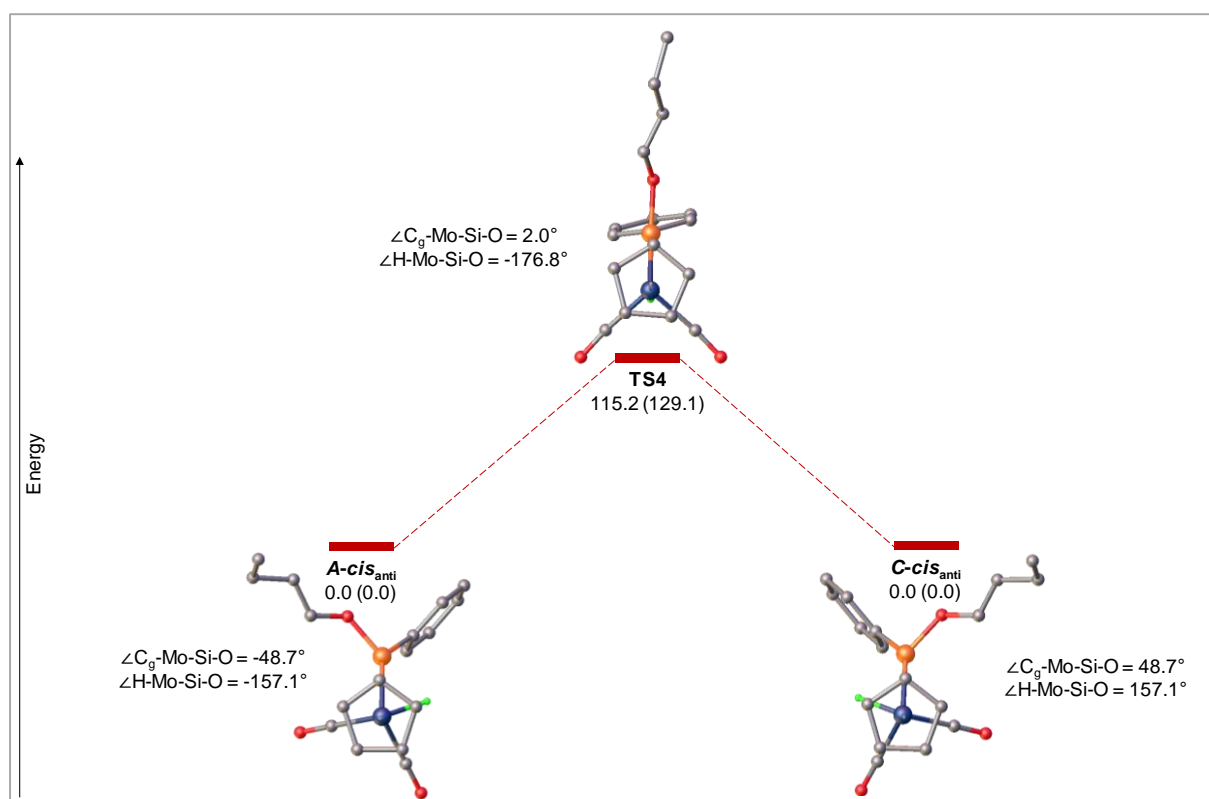


Figure S94. Reaction profile for the enantiomerization of **A-cis_{anti}** to **C-cis_{anti}**; Olex plots of the calculated structures of **A-cis_{anti}**, **C-cis_{anti}** and the transition state **TS4** (top views) with their relative zero-point vibrational energy corrected inner energies $\Delta U(0K)$ ($\text{kJ}\cdot\text{mol}^{-1}$) and standard Gibbs energies ΔG° ($\text{kJ}\cdot\text{mol}^{-1}$) (values in parentheses).

Finally, also a reaction path leading from **A-cis_{anti}** to **C-cis_{anti}** via the mirror-symmetric transition state **TS4** was uncovered by nudged elastic band (NEB) calculations (Figure S94, Table S12). However, the enantiomerization proceeds over a barrier ($\Delta G^\ddagger = 129.1 \text{ kJ mol}^{-1}$) that is too high for the dynamics of **3-Mo** in solution observed by NMR spectroscopy.

Table S12. Selected calculated bonding parameters of **A-cis_{anti}**, **C-cis_{anti}** and the transition state **TS4** of the enantiomerization of **A-cis_{anti}** to **C-cis_{anti}**

	Mo-Si	Mo-H	Si...H	H-Mo-CO ^a [1]	H-Mo-CO ^b [1]	CO-Mo-CO	H-Mo-Si	C _g -Mo-Si	C _g -Mo-H	TA1 ^[2]	TA2 ^[3]	DHA1 ^[4]	DHA2 ^[5]
A-cis_{anti} A-(3-Mo)_{th}	236.1	173.1	209.1	116.8	68.9	85.3	59.1	127.8	121.9	48.5	22.0	-48.7	-157.1
TS4	243.8	171.2	205.6	67.2	68.0	91.2	56.2	126.6	177.0	0.8	1.2	2.0	-176.8
C-cis_{anti}	236.1	173.1	209.1	68.9	116.8	85.3	59.1	127.8	121.9	48.5	22.0	48.7	157.1

[1] CO^a = CO ligand located *trans* to hydride in **A-cis_{anti}** and *cis* to hydride in **C-cis_{anti}**; CO^b = CO ligand *cis* located to hydride in **A-cis_{anti}** and *trans* to hydride in **C-cis_{anti}**; [2] twist angle (interplanar angle) between the (C_g,Mo,Si)-plane (C_g: Cp* ring centroid) and the (O,Si,C_{Tbb})-plane. [3] twist angle (interplanar angle) between the (H,Mo,Si)- plane and the (O,Si,C_{Tbb})-plane; [4] dihedral angle (torsion angle) C_g-Mo-Si-O. [5] dihedral angle (torsion angle) H-Mo-Si-O.